Supplementary Damping Control for Transient Stability Enhancement in Power Systems with High Share of Power Electronic Interfaced Wind Generation

Stelios Papadakis

Delft University of Technology

TU Delft Delft University of Technology

Challenge the future

Supplementary Damping Control for Transient Stability Enhancement in Power Systems with High Share of Power Electronic Interfaced Wind Generation

by

Stelios Papadakis

in partial fulfillment of the requirements for the degree of

Master of Science
in Electrical Engineering

at the Delft University of Technology,
to be defended publicly on Monday November 11, 2019 at 14:00 PM.

Supervisor:	Dr.ir. Jose Rueda Torres,	TU Delft
Thesis committee:	Prof.ir. Mart Van der Meijden,	TU Delft
	Dr.ir. Jose Rueda Torres,	TU Delft
	Dr. Jianning Dong,	TU Delft

TU Delft Delft University of Technology

Acknowledgements

I would like to express my deep gratitude, to all those people who helped me grow as a research engineer and contributed to the thesis completion. The final deliverable is a result, derived not only from my personal effort, but mainly can be considered as a collaborative attempt, since several people supported me.

First, I would like to thank, my daily supervisor, Dr. José Rueda, for giving me the opportunity to participate into such an interesting and challenging research topic. His relentless guidance and supervision regarding the progress of the thesis, was remarkable. Moreover, I am really grateful for his understanding and his positive attitude especially when difficult times arose. Due to the aforementioned reasons, it was literally a pleasure to work with him. Additionally, I would like to thank Prof. ir. Mart Van der Meijden for the trust he showed towards me and let me have a closer look on the way that big European projects are organized and functioning. The advice and knowledge, I got from him during our meetings, is well appreciated. Moreover, I thank Dr. Jianning Dong for his time and accepting being part of my thesis committee.

It is also necessary to express my gratitude to Arcadio Perilla, a TU Delft PhD candidate and now additionally a good friend. Without being obliged to, due to his main participation in other European projects, he willingly was helping me throughout this journey. I would like to really thank him, for all the discussions, proposed ideas, and the passion that he has and also transferred to me, especially in the difficult periods, when the project results were not the expected ones. I wish the best in his professional and personal life, and I am sure that he will thrive, because he is talented and one of the most determined persons, I have ever met.

Of course I could not omit mentioning Dr. Zameer Ahmad, for all his advice and feedback. Apart from being an excellent researcher and supervisor he is also a very optimistic person which made me really happy to collaborate with. Furthermore, I need to namely thank the following researchers for their given advice so as to overcome technical problems I may had all these months: Dr. Elyas Rakhshani, Dr. Jose Chavez Muro, Dr. Ebrahim Adabi, Dr. Mario Ndreko. The same also applies for the following PhD students: Nakisa Farrokhseresht and Digvijay Gusain.

Last but not least, I would like to thank my master student colleagues and friends in the University and in particular Nidarshan, Shubham and Christos for the good collaboration and all the good moments we had together.

Finally, this new experience for me to leave my country and study abroad, would not be achieved without the encouragement and great support that I had from my parents all these years. I would like to thank them for all the sacrifices they have made for my brother and me, without ever applying additional pressure to us, and we hope that one day we will make them proud.

To sum up, I am proud, to be a part of the IEPG group at TU Delft as a master student, and I hope that our paths will cross again in the future. Until then:

"Enjoy Life!"

Stelios Papadakis
Delft, October 2019

Abstract

During the last years, electric power generation was based mainly on large centralized fossil fuelled power plants. However, nowadays and in the future, efforts are made to increase the share from renewable sources, as a result of increasing environmental concern. Indeed, in some networks areas, wind generators gradually start to replace conventional synchronous generators, while the European Union has set a "20 - 20 - 20" target plan, which aims to achieve a 20% reduction in green house gas emissions compared to 1990 levels, have 20% of the energy on the basis of consumption coming from renewable sources and a 20% increase in energy efficiency by 2020.

Due to the increment of wind generator share, power system stability and reliability may be affected. This is attributed to the fact that the characteristics of wind turbines are different from the ones of conventional plants. Therefore different frequency, voltage and transient stability system performances arise which require different measures to be tackled.

This report, underlines the importance of rotor angle stability studies in power systems with high share of power electronic interfaced generation units. These studies are related to the ability of the synchronous generators to remain in synchronism when subjected to large disturbances (e.g. faults).

A supplementary damping control as a mitigation solution against rotor angle stability threats is studied in power systems dominated by full-scale power electronics wind generation units. This solution, as it is shown in this report, is cost-effective and is adopted for modification of the outer control of fully decoupled wind generators. Concerning related work reported in existing literature, several researchers have used the frequency deviation as input for power system stabilizer added to the grid side converter of a fully decoupled wind generator, whereas other researchers have used the terminal voltage. However, rotor angle remote signals for damping the Synchronous machines oscillations can also be used. Therefore, a supplementary damping control for fully decoupled wind generators, considering rotor angle deviations as input signal, is adopted in this report. The thesis report also provides a detailed overview of the adopted structure of supplementary damping control. Besides, a discussion, based on EMT and RMS simulations performed by using RSCAD and DIgSILENT PowerFactory tools respectively, is presented to address research gaps in existing literature, namely, identifying the most suitable wind generator locations for addition of supplementary damping control, the degree of improvement in damping performance due to the use of rotor angle deviation as input signal, the effectiveness of wind generator with the damping controller as affected by distance to reference generator, and the effectiveness of the controller when the distance between synchronous generator and wind generator is taken into account. Different indicators related to transient stability studies are used so as to evaluate the performance of the controllers, whereas optimization techniques are also utilized to find their appropriate settings.

For the rotor angle stability studies, different power systems were studied. In particular, faults were examined in a modified IEEE 9 Bus benchmark system as well as the test system of the Great Britain (GB) transmission power system. The aforementioned systems are used to examine the performance of wind generators with damping controller in systems with different dynamic behavior. For each system, different scenarios were applied, by simulating different fault locations (modified IEEE 9 Bus system/GB system), or different wind share level (GB system), different time delays due to data latencies (GB system) and different input signals in the proposed damping controllers (GB system). The selected cases include critical operational scenarios, i.e. fault locations in lines with high pre-fault apparent power dispatch, faults in prone to instability synchronous machines' terminals, high latency delays of 200ms. Faults with relatively high clearing time of 120ms are applied in the system, so the systems are examined close to their limits.

Contents

List of Tables

List of Figures

List of Abbreviations

$ACER$	Agency for the Cooperation of EnergyRegulators
AF	Asymmetry Factor
AVR	Automatic Voltage Regulator
BR	Breaking Resistor
CCT	Critical Clearing Time
$DFIG$	Doubly Fed Induction Generator
DTC	Direct Torque Control
$ENTSO-E$	European Network of Transmission System Operator
ESS	Energy System Storage
FCT	Fault Clearing Time
FIT	Feed-in Tariffs
FOC	Flux Oriented Control
FRT	Fault Ride Through
$FSCWG$	Full Scale Converter Wind Generator
FSM	Frequency Sensitivity Mode
GB	Great Britain
GSC	Grid Side Converter
KPI	Key Performance Indicator
$LFSM-O$	Limited Frequency Sensitivity Mode for Over-frequencies
$LFSM-U$	Limited Frequency Sensitivity Mode for Under-frequencies
$LVRT$	Low Voltage Ride Through
MMF	Magneto-Motive Force
$MPPT$	Maximum Power Point Tracking
$MTPA$	Maximum Torque per Ampere
$MVMO$	Mean Variance Mapping Optimization
$NCRfG$	Network Codes on Requirements for Grid Connection of Generators
NPC	Neutral Point Converter
PCC	Point of Common Coupling
PE	Power Electronics
$PEIWG$	Power Electronic Interfaced Wind Generation

PLL	Phase - Locked Loop
PMSG	Permanent Magnet Synchronous Generator
PPA	Power Purchasing Agreements
PSD	Power Spectral Density
PSS	Power System Stabilizer
PWM	Pulse Width Modulation
RES	Renewable Energy Source
RSC	Rotor Side Converter
SCIG	Squirrel Cage Induction Generator
SCMES	Super Conducting Magnetic Energy Storage
SDC	Supplementary Damping Control
SG	Synchronous Generator
SMIB	Single Machine Infinite Bus
SPWM	Sinusoidal Pulse Width Modulation
STATCOM	Static Synchronous Compensators
TSO	Transmission System Operator
VSC	Voltage Source Converter
VDAPI	Voltage Dependent Active Power Injection
WG	Wind Generator
WRIG	Wound Rotor Induction Generator

1

Introduction

The first chapter provides a general overview about the current and future tendency for utilizing wind energy sources, and the stability problems that contemporary power system face. Afterwards, the problem definition that the current thesis deals with, as well as limitations of existing methodologies to tackle it, are presented. Last, this chapter comprises the main objectives, followed by research questions and the thesis outline.

1.1. Background

Traditionally, over the past years, mainly synchronous generators were used to generate power. However, in the future, several changes are expected in the electrical power systems. In particular, due to Kyoto protocol, a series of incentive programs have been set in order to aid and encourage investors to associate in renewable energies. For instance, Feed- in Tariffs, (FIT) have been provided by system or market operators, often in the context of Power Purchasing Agreements (PPA). The payment of the FIT which is guaranteed for a certain period of time that is often related to the economic lifetime of the respective Renewable Energy Source (RES) infrastructure, (usually between 15-25 years), allows the RES investor to recover the different costs (capital, O&M) that are demanded. Some other supporting schemes, that guarantee preferential rates for RESs, are tax incentives and tradable green certificates (e.g. renewable portofolio standard) [1].

The aforementioned beneficiary policies, led the power system to undergo an evolutionary phase, since the traditional fossil-fuel plants are gradually decommissioned and at the same time RESs are increasing their penetrations in the energy mix. Among the different renewable technologies, wind energy is rapidly increasing its share in the generation mix. Figure 1.1 demonstrates the upward trend of the annual wind energy installation in a global aspect [2].

However, this increased share of the wind generation and together with the displacement of synchronous generators, will inevitably create new challenges that need to be tackled. In particular, contemporary power systems present less inertia and reduced short - circuit capacity and these features can potentially lead to less controllability and inevitably to stability issues [3].

1.2. Motivation

On the basis of the above, it can be concluded that in order to confront future stability problems, it is necessary to perform studies, using at first accurate and powerful software simulators. Utilizing them, one can test the controllers' efficiency of the different units that are comprised in the power system, which in the present report, as will be explained in Chapter 2, these units are Full Scale Converter Wind Generators (FSC WG). At the same time, the dynamic state of the power system after an applied contingency (e.g. fault, loss/ increment of load or generator) and the stability amount (or distance from instability) can be quantified by using appropriate Key Performance Indicators (KPI).

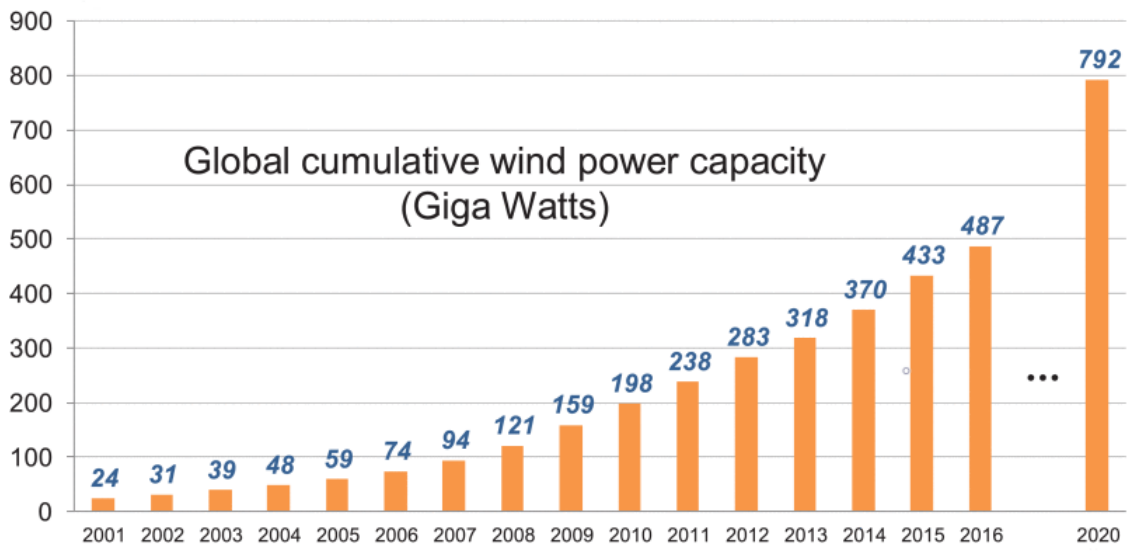

Figure 1.1: Cumulative Wind Power capacity during the last decade [2].

The indicators used in this report are defined in Chapter 2 and their implementation is done in Chapters 4 and 5.

Power System Stability, has been a major domain of interest for power system utilities researchers. The reason for that, is that the studies involved, are closely related to crucial power system properties. These principles are: continuity of supply achievement, avoidance of large-scale failures, restoration and black start capabilities [4].

According to [3], power system stability, is classified into three main categories: voltage, frequency and rotor angle stability.

- Voltage Stability: refers to the ability of a power system to maintain acceptable voltages at all system's terminals after being subjected to a disturbance. The main reason for voltage instability (or voltage collapse) is when active and reactive power flows through the inductive reactances increase beyond the capability of the network and the connected generation. Furthermore, after a disturbance, loads tend to be restored by distribution voltage regulators, tap- changing transformers and thermostats, which increase the reactive power consumption of the loads and increase further the voltage drop [5].

- Frequency Stability: refers to the ability of a power system to maintain acceptable frequency after an applied disturbance. The main driving factor is the active power imbalance between generation and load. In particular, if there is a load increment, then inherently the kinetic energy of the synchronous generators is retrieved to supply the load and the frequency drops. In contrast, when there is a load decrement, the speed of the synchronous machines and equivalently the frequency increases [5].

- Rotor Angle Stability: refers to the ability of the synchronous machines to remain in synchronism after being subjected to a disturbance. Under steady-state conditions, there is equilibrium between the mechanical torque and the output electromagnetic torque of each synchronous generator. This equilibrium will result in a steady speed of the machines. However, during a disturbance, the speeds of the machines will change and the rotors will be accelerated/ decelerated. For instance, the temporary accelerated machines will result in advanced relative angles of their rotors with respect to the slower rotor angle positions. This angle separation will lead the fast rotating machines to increase their active power dispatches, according to their power- angle relationship. However, taking into account the swing equation of the individual machines, it can be observed that the fast rotating machines, will eventually decrease their speeds and therefore the angle separation between the fast and slow machines will also be reduced. However, there is a threshold angle, in which an increase in angular separation will ensue in a decrease in active power injection

of the fast machine, so this will result in even a higher angle separation, and then rotor angle stability is lost [3].

Rotor angle stability studies are of high concern due to the fact that, the decommission of conventional power plants, will lead to a dramatic decrease of inertia and short-circuit capacity and also to the absence of conventional Power System Stabilizers (PSS). These units, are currently the basic units that lead to the damping of the critical swing modes. It is thus, interesting to investigate how the fast and decoupled active and reactive power injection of the Power Electronics driven Wind Generators (WGs) can compensate the less inertia and the unavailability of current stabilizing units in the future.

The purpose of this study is to analyze the dynamic behavior of the WGs during balanced faults, and to investigate ways in order rotor angle stability of systems with high share of Power Electronic Interfaced Wind Generation (PEIWG) can be further enhanced. From the aforementioned analysis it can be concluded a relationship of the synchronous generator rotor angle with it's speed. Therefore, apart from the machines' angles, the power system's frequency is also presented.

1.3. Literature Review

As indicated in Section 1.2, rotor angle stability can be considered as a crucial system property that needs to be maintained, otherwise power systems can be led to generator outages, load shedding, and even blackouts. In addition, the significant integration of WGs in the transmission systems, necessitates a careful investigation of their dynamic performance and their interactions with the rest power system components.

The dynamic behaviour of the motion of synchronous generators is directly coupled to the dynamics of electromagnetic power at the terminal bus, via the internal flux linkage [6]. This fact, as described in Section 1.2, enables the rotor of the machines to react in power fluctuations at the terminal bus, in the form of absorbing or releasing kinetic energy and helps to balance the post disturbance power flow and contributes to safeguard transient stability. However, the rotor response of wind generators is decoupled from power grid transients, because of Maximum Power Pointing Tracking (MPPT) control and power electronics interface [7], [8]. From this perspective, according to most studies of existing literature, the replacement of synchronous generators by wind generators is expected to worsen the transient stability performance of power systems [9]. On the other hand, regulating wind generator's power output may alleviate the torque imbalance of synchronous generator and in this way, the post-disturbance transient stability may be improved [10], [11].

Control methods for transient stability of a power system, having fully decoupled wind generators, can be based on: (i) addition of hardware components (e.g. crowbar, FACTS devices, fault current limiter); (ii) modification or addition of outer control systems on the power electronic converters that interface the wind generator with the electrical power system. Some research effort has been devoted to the addition of an energy storage system (ESS) on the point of common coupling of the fully decoupled wind generator to smooth the power output oscillations and enhance Low Voltage Ride Through (LVRT) capability for the wind generator [12]. In [13] a STATCOM based method has been proposed to enhance LVRT capability of four parallel-operated fully decoupled wind generators fed to a power system by a proportional–integral–derivative (PID) damping controller designed based on the modal control theory. Extra hardware-based methods may involve substantial capital investments, which may not necessarily entail effectiveness. Therefore, the modification of outer control systems of wind generator's converters is the preferred approach in this report.

Research efforts so far have been devoted to either modify the way current limitation occurs in the grid side converter, or to modify the way active and reactive power injection is performed, by considering signals taken from the connection point of the wind generator with the power system. In [14], active current reduction method is applied by adding a compensation torque signal depended on DC link current. An alternative vector current control is proposed in [15]. A decoupled and gain-scheduling controller is implemented in the outer loop of the grid side converter to tackle possible interactions between the active power and voltage control, when a fully decoupled wind generator should operate close to the nominal power and is connected to a weak transmission system. In [16], a sensitivity analysis of active and reactive power injection by fully decoupled power generation is presented. It is recommended that during the fault period, in order to enhance transient stability,

injection of additional reactive current dependent on the voltage deviation with a high gain, should be considered. Furthermore, a slight reduction of the active current dependent on the reactive current injection or on the voltage deviation is proposed.

A supplementary control scheme for the grid side converter is proposed in [17] to simultaneously adjust the active and reactive power injection by the wind generator to attempt to prevent first swing transient instability. Based on modal analysis, this study also suggest that use of remote signals related to rotor angle of synchronous generators could be an attractive option for development of future methods for transient stability enhancement. Nevertheless, there is lack of insight on how the selection of the remote signals should be performed, and what the implications on the dynamic response (frequency and rotor angle) of synchronous generators due to the use of remote signals are. Moreover, the effectiveness of such approach in power systems with high share of PEIWGs remains is an open research line.

In the last 20 years, significant research effort has been devoted to the tuning of wind generator controllers for transient stability enhancement, by using special techniques like sliding mode control [18], model predictive control [19] and artificial intelligence [20], [21], [22]. These methods show great potential to adjust the settings of wind generator controllers in near real-time context. Nevertheless, sensitivity to changes in operating conditions, network topology, and disturbances not considered in the training remains an open research gap.

1.4. Objectives & Research Questions

Different WG models, available in IEPG Section of TUD, as part of MIGRATE H2020 project [23], are used as starting point. In particular, RMS (e.g. DigSILENT PowerFactory) and EMT (e.g. RSCAD) simulators are used in this report, to evaluate the controllers. It is mentioned, that dealing with electromagnetic transient phenomena that stability studies demand, having a small time step simulation tool, increases the accuracy of the control. This feature as will be presented in Chapters 3 and 4 mainly differentiates the two tools.

In this report, the existing models of type IV wind generators will be expanded, using both the aformentioned software packages. In particular, the main objective is to modify the outer controllers of fully decoupled wind generators so as to ensure transient stability when increasing their share. To arrive to this goal, the following questions are formulated:

- What modifications should be done to the outer controllers of fully decoupled wind generators so as to integrate a proposed supplementary damping control feature?
- How does the supplementary damping control outperforms existing measures with wind generators to support transient stability?
- What are the signal inputs that can be used to ensure effectiveness of supplementary damping control?
- How to select the Wind Generators to be equipped with the supplementary damping control?
- In which extent the data latency deteriorates the proposed supplementary damping control's performance?
- In which way does optimization improve the performance of the proposed supplementary damping control?
- Does the observed performance of the proposed damping controller differ when simulations are implemented in RMS and EMT tools?
- Is the supplementary damping control more effective in wind generators with grid following or with grid forming control?

1.5. Thesis Contribution

It is worth pointing out that the methods presented in existing literature consider case studies confined to small size power system models, with exclusive focus on showing its feasibility from the point

of view of the operational boundaries of the wind generator, and with limited analysis on the impact on the synchronous generators connected close to the point of common coupling of the wind generator. Such small power system models confine conclusions on effectiveness of the proposed controllers to the possible improvement of the rotor angle stability of a single synchronous generation and cannot be extrapolated to the context of multi-machine power system nor systems with high share of PEIWGs.

In this thesis, a control method, applicable in FSCWGs, is proposed for enhancing the power system's transient stability. Furthermore, the key contributions of the thesis are:

- Development of a modified type IV wind generator model using RSCAD and DigSILENT PowerFactory. The modified models, can be used in different systems in future studies without major effort.
- Development of Benchmark power systems employing both these two aforementioned software packages so as to efficiently accommodate high wind share and to evaluate the wind damping performance. In particular, a simple single machine connected to an infinite bus system is used for fundamental analysis of main factors influencing damping controllers implemented at WGs. Next, modified IEEE 9 Bus system, is used to test the controllers in multi-machine context. Finally, the Great Britain transmission power system is used to further examine the controllers in larger multi-machine system, (which also has a different dynamic behavior). It is stated that, modifications are done to the Great Britain power system so as to achieve a realistic Critical Clearing Time (CCT), and test effectively the controllers.
- Evaluation of damping controllers with rotor angles as inputs, in wind generators with grid forming and grid following control.
- Script Developments for wind controllers' parameters tuning, based on minimizing a suitable KPI. Moreover, a co-simulation environment is developed for optimal tuning of damping controllers, by combining DigSILENT PowerFactory, Matlab, and Python.

1.6. Thesis Outline

The thesis covers the aforementioned topics based on the subsequent structure:

- Chapter 2: The different wind Energy Conversion systems are presented, emphasizing in the FSCWG configuration, which is the technology used in the report. Furthermore, the definition of the rotor angle and the way the conventional PSS works is briefly analyzed. Last, the proposed control scheme applied in the WGs, for rotor angle mitigation, is explained.
- Chapter 3: The mathematical modelling of the FSCWG and some basic components is presented. The implementation of the main proposed WG damping controller and a voltage dependent active power injection controller, using the EMT tool, is further elaborated. Comparative results between the aforementioned controllers and the default LVRT are also presented, for different wind share levels, and control parameters, using a modified IEEE 9 BUS system.
- Chapter 4: The implementation of the proposed damping controller is also compared with the default controller based on IEC 61400-27-1 standards. The superiority of the new controller is illustrated in the IEEE 9 BUS System. In this specific tool, the availability of multi-machine systems (e.g. reduced size test model of Great Britain transmission system), provides the opportunity to investigate the interactions between the controllers, while the integration with Python, arises the opportunity to come-up with a method to tune, in a universal manner, the controllers accordingly.
- Chapter 5: Mean- Variance Mapping Optimization is used MVMO, so as to optimally tune, in an individual manner, the controllers' parameters.
- Chapter 6: Details the main conclusions while the main research questions are thoroughly answered. Recommendations for future work are also included.

The research approach, is better illustrated with the following thesis work flow chart as presented in Figure 1.2. Finally, the scripts and annexes are attached in the ending part of the report.

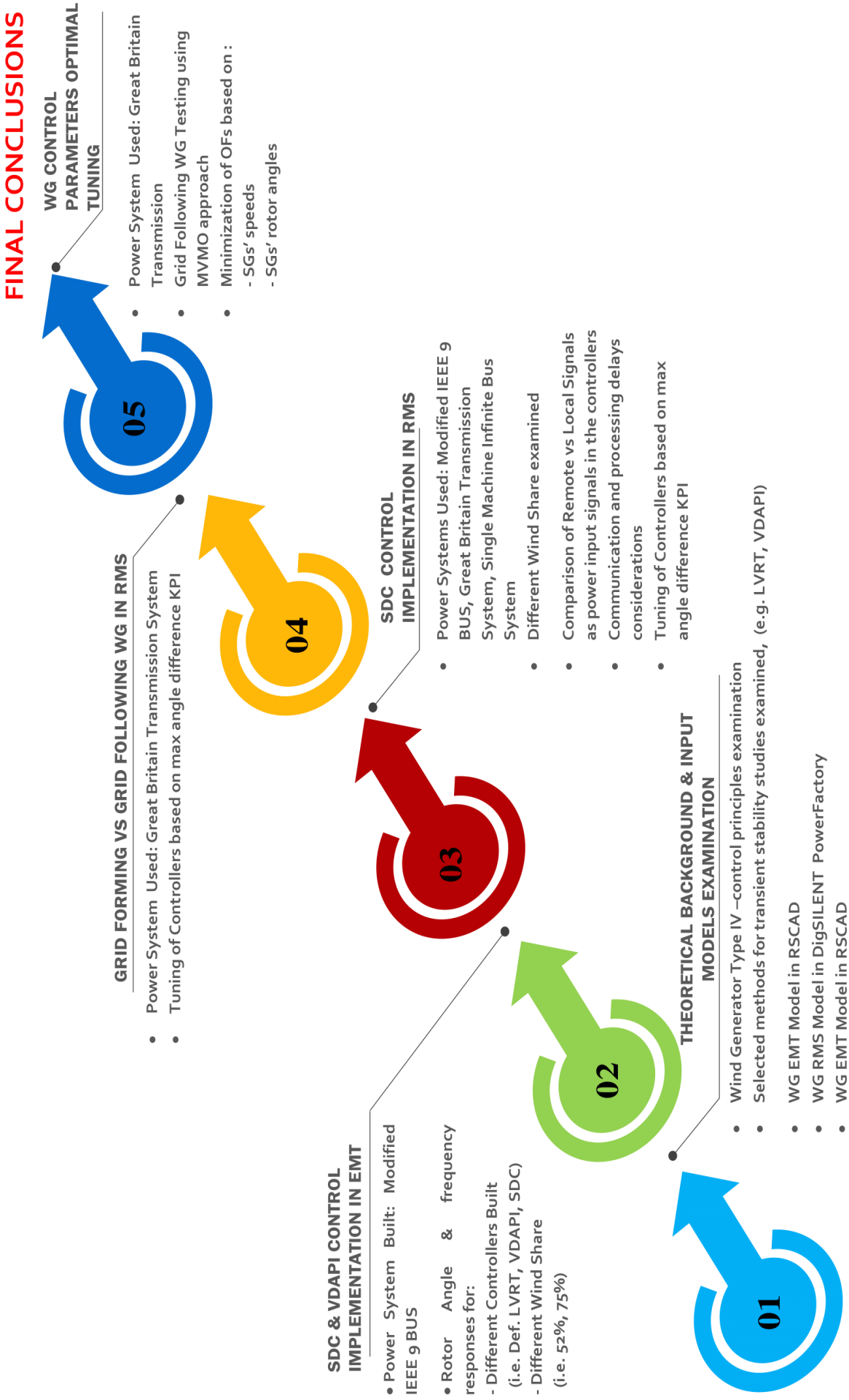

Figure 1.2: Thesis Work Flow.

2

Theoretical Background

In this chapter, a brief overview about the basic wind energy conversion systems, followed by fundamental concepts about wind turbine aerodynamics is included. Last, grid code requirements are also mentioned.

The second part of the current chapter, presents, synchronous generators' rotor angle definition, and the fundamental unit of PSS that Synchronous Generators (SGs) have, so as to mitigate their oscillations.

2.1. Fundamentals of Wind Energy Conversion Systems

2.1.1. Wind Generator Aerodynamics

It is well known, that wind energy, is the kinetic energy of a moving air mass. In particular, considering wind, as a rectangular cuboid packet, then the kinetic energy, U, of a parcel of air mass,m, moving with speed v_w, along direction x is [5]:

$$U = \frac{1}{2}mv^2 = \frac{1}{2}(\rho Ax)v_w^2 \tag{2.1}$$

where U is the kinetic energy [Jouls], A is the cross sectional area in $[m^2]$, ρ is the air density $[kg/m^3]$, x is the thickness of the parcel [m].

From the aforementioned, the power of the wind, P_w [W], is the time derivative of the kinetic energy, therefore:

$$P_w = \frac{dU}{dt} = \frac{1}{2}(\rho A v_w^2)\frac{dx}{dt} = \frac{1}{2}(\rho A v_w^3) \tag{2.2}$$

However, from this power only one fraction is extracted and converted into mechanical power P_M [W]. This fraction is described as follows:

$$P_M = C_p P_w = C_p(\lambda, \beta)\frac{\rho A}{2}v_w^3 \tag{2.3}$$

where C_p is the power coefficient of the blade and has theoretical maximum value of 0.59 according to the Betz limit. It is observed that, the power coefficient C_p is a function of the two parameters λ and β where:

- λ is the tip speed ratio defined as

$$\lambda = \frac{\omega_R \cdot R}{v_w} \tag{2.4}$$

ω_R is the mechanical angular velocity of the turbine rotor in rad/s, R is the blade radius of the wind turbine expressed in meters

- β is the blade pitch angle in degrees

In [24], the C_p-λ curves are derived for different pitch angles β, as seen in Figure 2.1. In Figure 2.1, the great advantage of variable speed wind turbine machines can be observed. In particular, for each wind speed and for a specific pitch angle, there is a specific rotational speed that corresponds to the maximum mechanical power retrieved.

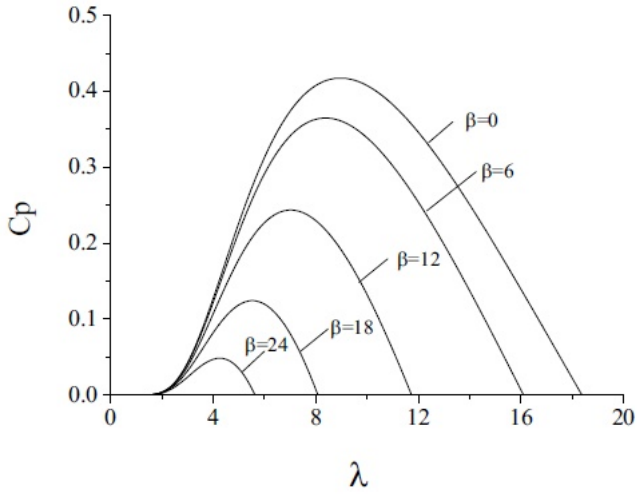

Figure 2.1: C_p-λ curve with β as a parameter [5].

Reforming equation 2.4 with respect to v_w, and replacing the wind speed at equation 2.3, it is observed that for a specific angle β (e.g assume β =0), the maximum mechanical power from the wind turbine, is proportional to the third power of the rotor speed. In particular:

$$P_{mech}^{max} = K_{opt} \cdot \omega_R^3 \tag{2.5}$$

with K_{opt} given by:

$$K_{opt} = \frac{Cp_{opt} \cdot A \cdot p_a \cdot R^3}{2 \cdot \lambda_{opt}^3} \tag{2.6}$$

In Equation 2.6, Cp_{opt} equals the maximum value of the power coefficient, for a given pitch angle.

Equation 2.5 can be expressed via the so called Maximum Power Point Tracking (MPPT) Curve and can be visualized as indicated in Figure 2.2. In Figure 2.2, it is also observed that there is one specific cut off wind speed in which the power becomes steady for protection purposes. This can be done by activating the pitch angle controllers.
More information, about MPPT control and the pitch mechanism can be found in Appendix A.

2.1.2. Wind Energy System Configurations

According to the wind generator's rotational speed, the wind generator systems can be classified into two categories; fixed speed and variable speed. This classification leads further to different types of technologies:

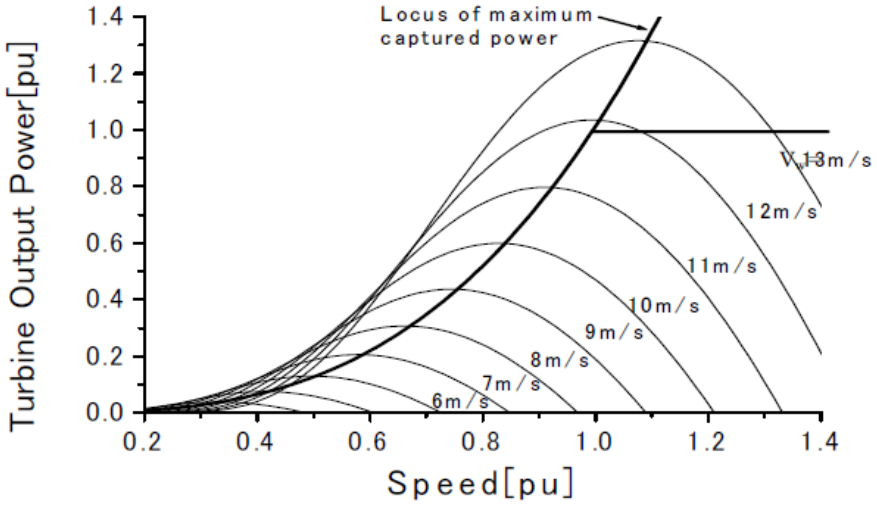

Figure 2.2: MPPT graph for variable speed Wind Turbine [24].

- Type I wind energy technology is a fixed-speed configuration. It is composed of the three-blade wind turbine, a Squirrel Cage Induction Generator (SCIG) and a gearbox that matches the low speed of the turbine, with the high speed of the generator. The speed of the generator is fixed and is determined by the grid frequency and the number of poles. Figure 2.3 demonstrates the fixed-speed wind energy conversion system. Compensating capacitors are used, since the squirrel-cage induction generator draws lagging reactive power from the grid for it's operation, so placing capacitors in the terminals, facilitates the operator to meet the grid-code requirements for reactive power compensation. Soft starters can also be used, so as to limit the AC inrush current during the start-up. They are basically AC voltage controllers that increase gradually the stator voltage, by decreasing the firing angle of the SCR thyristor devices.

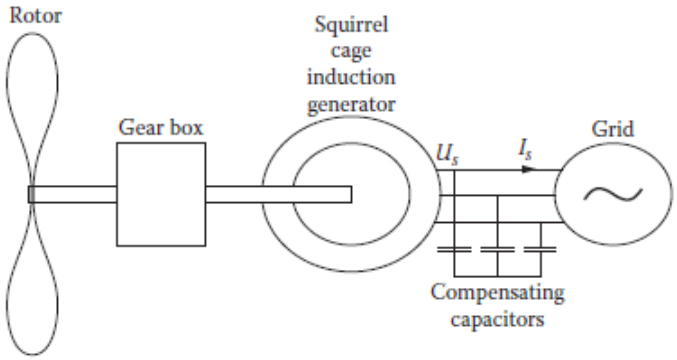

Figure 2.3: Type I wind energy system configuration [5].

Summarizing, fixed-speed wind generators, are simple configurations since the do not employ any power converter with sophisticated control loops. Furthermore, they are reliable since squirrel-cage rotor are used, without any windings or slip rings. However, they present low efficiency as MPPT can not be met. For instance, in Figure 2.4, MPPT can be achieved only for 1 pu wind speed, while for speeds below 0.6 pu, the mechanical power perceived is zero. Furthermore, due to the unavailability of Power Electronics, no LVRT capabilities are observed, while also high mechanical stresses occur caused by wind gusts.

- Type II wind energy technology is a (partially) variable speed configuration. The configuration is

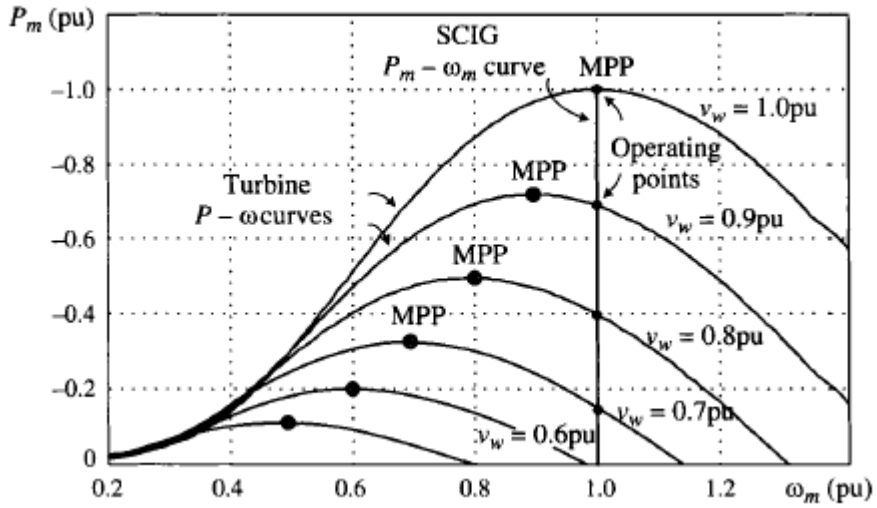

Figure 2.4: MPPT curve for Type I Energy system configuration [25].

the same comparing to the fixed speed energy system, as depicted in Figure 2.5, apart from the fact that the SCIG is now replaced by a Wound Rotor Induction Generator (WRIG). Moreover, adjustable resistance, controlled by a diode bridge and a chopper, is added to the rotor to give a speed range of 2-4%. Figure 2.6, illustrates the effect of the rotor resistance in the torque-speed characteristics. The main advantage of this technology is the simplicity , the cost-effectiveness and the reduction of the mechanical stresses in the turbine due to better torque control [26]. However, the controllability of the speed is limited, and also the efficiency is small due to the heat dissipation. Last, inability to control the reactive power is also observed. The aforementioned problems can be solved with the aid of Type III and Type IV Wind Generators.

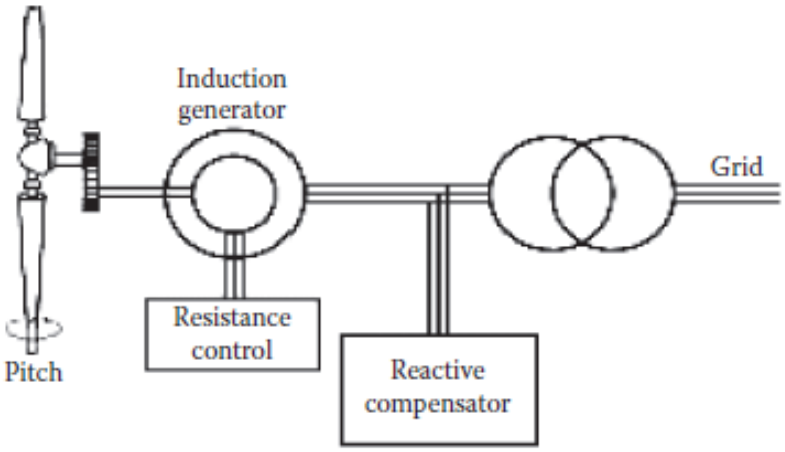

Figure 2.5: Type II wind energy system configuration [5].

- Type III wind energy technology is a variable speed configuration. As shown in Figure 2.7, the stator of the Doubly Fed Induction Generator (DFIG) is connected to the grid directly, whereas the rotor is connected to the grid via a reduced-capacity converter. A speed variation of 60% is obtained around synchronous speed (i.e. 30% above and 30% below synchronous speed). Operation outside of this speed range, is not feasible because higher than rated rotor voltages will be observed. If the generator is operating in the super-synchronous speed mode, then rotor delivers power to the grid, otherwise rotor is fed with power from the grid, thus bidirectional power converters are required. However, reduced- capacity converters are used, since the maximum slip

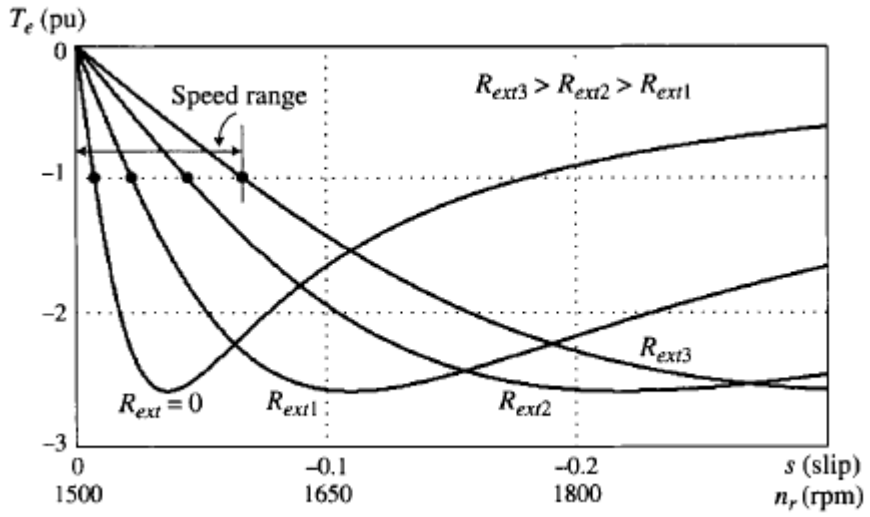

Figure 2.6: Torque-slip characteristic of type II wind energy system [25].

determines the maximum power to be handled by the converter. According to the aforementioned, the design of the converters is around 30% of the rated power of the machine. The use of reduced-capacity converters ensues them as cost- effective, whereas the size of the topology is also reduced. Moreover, it offers complete control of reactive and active power; the rotor side converter (RSC) controls the torque and the reactive power of the generator by controlling the rotor currents, whereas the grid side converter (GSC) controls the DC-link voltage and the AC- side reactive power. The drawback of the configuration is that slip-rings are needed which can ensue them as prone-to-failures topologies, while a second drawback is that they need gearbox to operate.

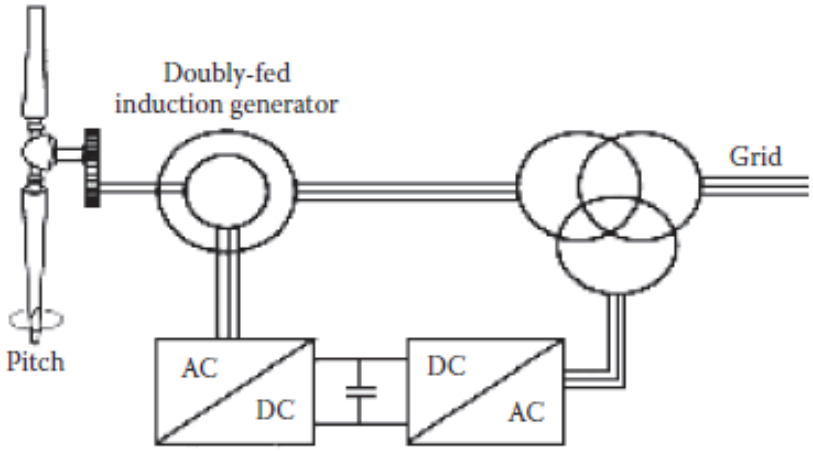

Figure 2.7: Type III wind energy system configuration [5].

- Type IV wind energy technology is a variable speed configuration. This configuration, is illustrated in Figure 2.8, and consists of a full-scale power converter between the Permanent Magnet Synchronous Generator (PMSG) and the grid. The converters are usually rated for AC- 690 V, and can handle up to 0.75 MW. If the wind turbines are larger than 0.75 MW, the power rating of the converter can be increased by having IGBT valves in parallel, while measures should be taken to minimize the circulating current between the parallel switches [27]. Typical converters include either two or three level voltage source converters. The advantages/disadvantages of each topology and their operational principle based on Pulse With Modulation (PWM) are presented

in Appendix B. The advantage of this topology is that it does not have any speed limitation, in contrast to type III configuration. Also, usually multi-pole PMSG are used, therefore gearboxes are not needed. However, employing PMSGs and full-scale converter renders this topology relatively costly. Wind Generators with Full-Scale Converters (FSC WG) will exclusively be analyzed for this report. The reason for that is that due to back-to-back controller, similar control analysis can easily be expanded for other RES like Photovoltaics and Electrolyzers. The controllers and the mathematical model of this configuration are analyzed in Chapter 3 and Appendix G.

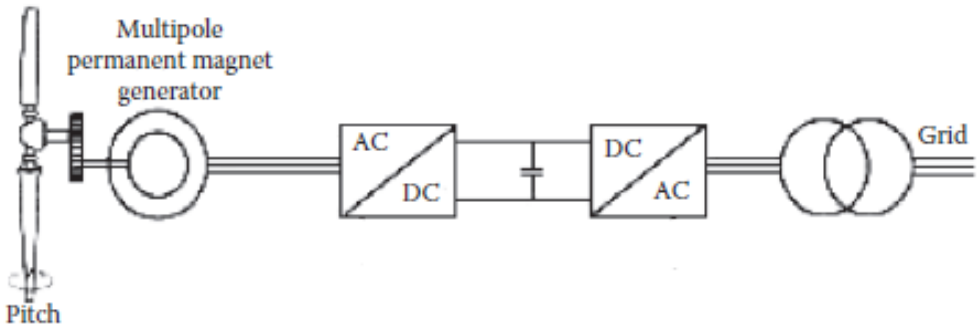

Figure 2.8: Type IV wind energy system configuration [5].

2.1.3. Grid Code Requirements

Network Codes on Requirements for Grid Connection of Generators (NC RfG) have been established and enforced in many countries by the European Commission, the Agency for the Cooperation of Energy Regulators (ACER), the European Network of Transmission System Operators (ENTSO-E) & market participants [28]. Their main goal is to ensure safe, reliable and economic operation of the power system. Due to the fast integration of RES into the grid, grid codes have been updated so as to incorporate their operation as well. For instance, nowadays, WGs should provide similar ancillary services, with conventional synchronous generation plants. According to these codes, WGs must comply with requirements including voltage ride through capabilities, frequency regulation, active and reactive power regulation. The following, provide a brief overview regarding the aforementioned services.

1. Fault Ride - Through Requirements: Each Transmission System Operator (TSO) should define a voltage-against-time-profile according to Figure 2.9 at the Connection Point for fault conditions. This profile describes the conditions in which the Power Generating Module shall be capable of staying connected to the Network. Above the limit line, the power module must stay connected, even if the grid voltage drops to really small values (i.e. U_{ret}). Uret is the retained voltage at the Connection Point During a fault, tclear is the instant when the fault has been cleared. Urec1, Urec2, trec1, trec2 and trec3 indicate certain points of the profile, which are defined by the corresponding TSO. Typical values are illustrated in Table 2.1

Table 2.1: Typical parameters for LVRT characteristics [28].

Symbol	Range	Symbol	Range
$U_{ret}[pu]$	0.05- 0.15	$t_{clear}[seconds]$	0.14-0.25
$U_{clear}[pu]$	U_{ret}- 0.15	$t_{rec1}[seconds]$	t_{clear}
$U_{rec1}[pu]$	U_{clear}	$t_{rec2}[seconds]$	t_{rec1}
$U_{rec2}[pu]$	0.85	$t_{rec3}[seconds]$	1.5 - 3.0

Grid codes also require the module to supply a certain amount of reactive power to support the grid voltage during the fault. Figure 2.10 illustrates a typical reactive current boosting curve. The magnitude of the reactive short circuit current should be provided to the grid as a function

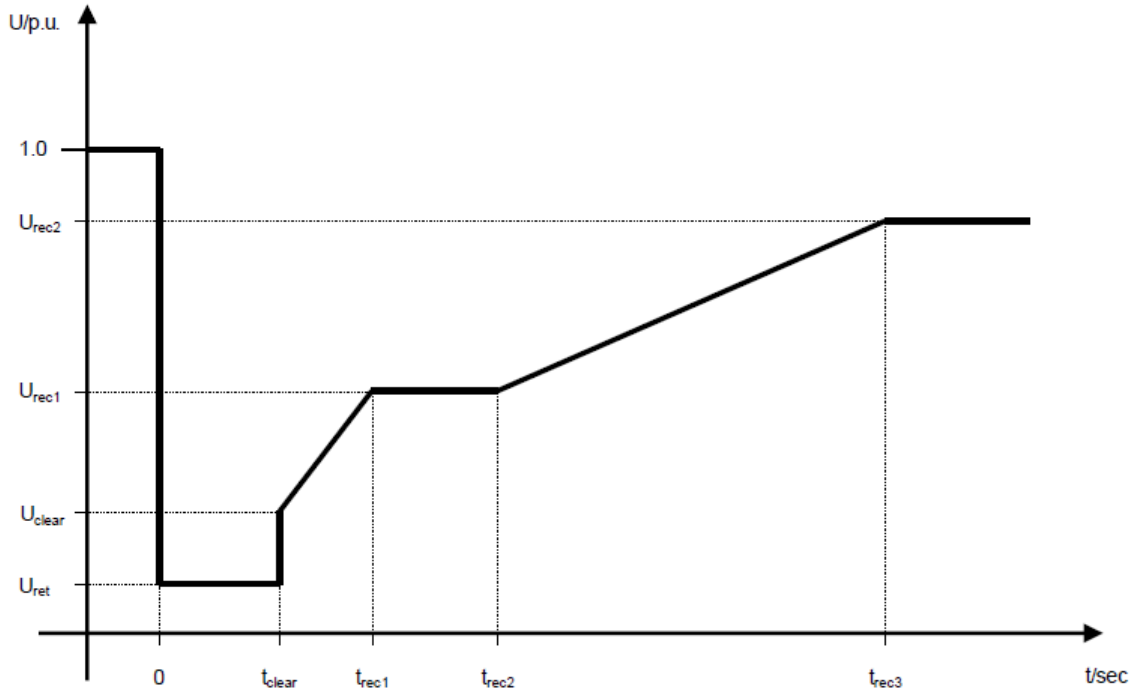

Figure 2.9: Grid Requirements for LVRT [28].

of the rms voltage deviation at the grid connection point. The slope of the curve is a variable which the relevant TSO need to specify and it is termed as 'k' gain or "k-factor". This is in fact a proportional gain applied at the outer control loops which relates the reactive current injection to the per unit voltage deviation. Moreover, if needed a dead band (i.e +/-5% or 10%) shall be selected in the range of nominal network voltage. This provision should be under 20ms after the fault identification (rise time). After returning the voltage magnitude inside the dead-band limits, the voltage support should be implemented further for 20-30ms. If the grid voltage is increased beyond 50% then the under-excited wind turbine is disconnected as the current that the machine draws activates the system protection [29].

It is mentioned that the reactive current injection improves the rotor angle stability of the generation units, as shown in Appendix E. In addition, as proved in [30], stability is enhanced when the dead-band is not considered, or when the proportional gain k, is increased.

2. Frequency and Active power control: The WG unit shall be capable of activating the provision of Active Power Frequency Response. Different frequency mode responses can be implemented. According to [28], one common approach is the so-called "Limited Frequency Sensitivity Mode for Over-frequencies" (LFSM-O) or for Under-frequencies (LFSM-U), respectively.The provision should be activated, as an emergency measure, when the frequency exceeds 50.2 Hz or drops below 49.8 Hz and should be given with a droop in the range of 2- 12%. Apart from the aforementioned method, there is also one other technique called Frequency Sensitivity Mode (FSM) in which, the wind generator assists the frequency regulation from the instant the frequency deviates from it's nominal value (if no dead-band is used). Figure 2.11, illustrates the case with zero dead-band. Typical values of the parameters for FSM are illustrated in Table 2.2 [1].[2] Synthetic inertia can be provided for this aforementioned frequency support.

[1]Insensitivity: inherent feature of the control system specified as the minimum magnitude of change in the frequency that results in a change of output power
[2]Dead-band: preset intentional value applied to the governor so as not to respond to frequency changes to reduce mechanical gear

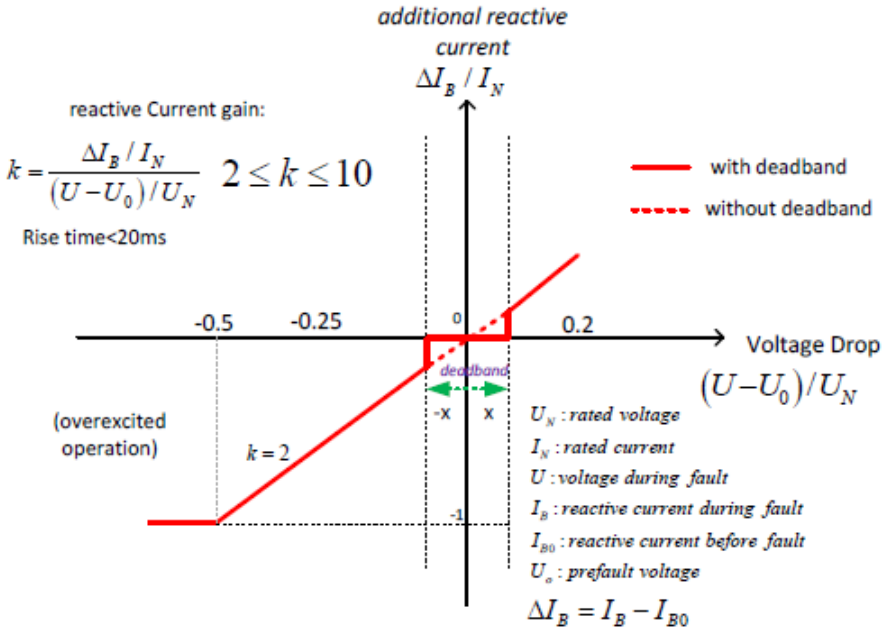

Figure 2.10: Reactive Power Provision-Absorption for voltage support [29].

Table 2.2: FSM- Typical Parameters [28].

Parameters	Range
Active Power range related to Maximum Capacity	1.5-10 %
Frequency Response Insensitivity	10-30 mHz
Frequency Response DeadBand	0-500 mHz
Droop	2-12%

3. Disconnection due to frequency extremes: a power generating module shall be capable of staying connected to the network and operating within the frequency ranges and time periods specified by each TSO. For all the European TSOs, disconnection is not permitted when the frequency range is between 49-51 Hz. However, for instance in the Great Britain system, that is examined in this project, even when the frequency drops at 47 Hz, the module should be remained connected for at least 20 ms [28].

More information about the reactive power requirements of the power unit during steady-state operation, or protection measures can be found in [28]. In the aforementioned reference it is clear that according to the current codes, rotor angle stability requirements are missing. However, in the future more wind contribution is expected, therefore their capability to damp out synchronous machines' oscillations will play an important role. In the following section a deeper insight about what is rotor angle, how rotor angle stability is defined and how is quantified, is provided.

2.2. Fundamentals of Synchronous Machine Rotor Angle & Stability Concepts

2.2.1. Definition of Rotor Angle

This section provides a brief theoretical overview about the synchronous machine modeling, the operational principle, and the way that rotor angle is measured.

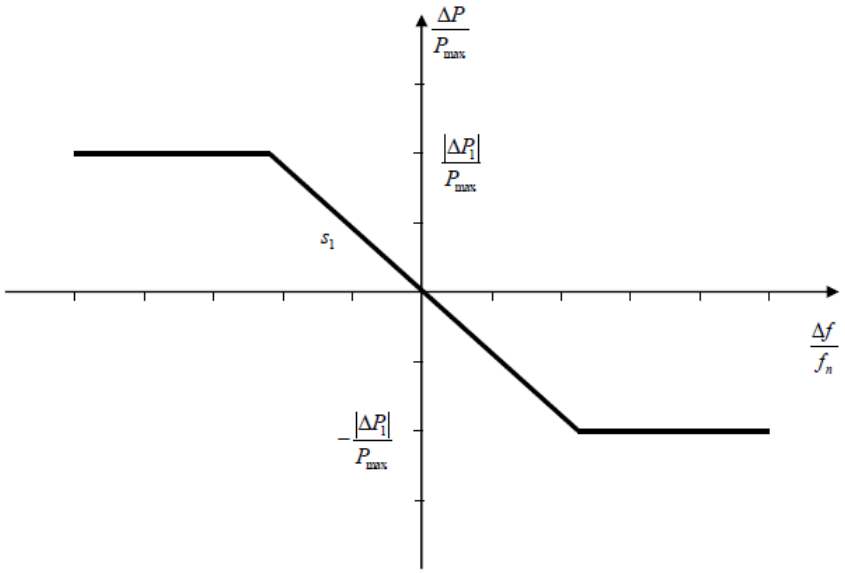

Figure 2.11: Active Power Frequency Response capability of Power Generating Modules in FSM illustrating the case of zero deadband and insensitivity. [28].

Synchronous machines are operating based on the principles of rotating magnetic field theory. The stator windings, are energized with alternating current which produces a synchronous rotating magnetic field in the air-gap. Rotor winding is the field winding and is fed with direct current. The magnetic field generated by the rotor, rotates with the rotor speed. In order to obtain constant power in steady state response, rotor magnetic field and stator one should be stationary to each other. Therefore, under normal conditions, rotor must rotate in synchronous speed.

A synchronous machine, consists of three stator windings which are spaced 120° electrical degrees apart. The machine's stator axis are depicted in Figure 2.12 [31]. Generator a, b and c-axis indicate the magneto-motive force (MMF) produced by the corresponding stator phases. In particular, stator axis is aligned with a-axis. Rotor axis is shown by the vector Generator d-axis and is representing the MMF produced by the field winding on the rotor. Q-axis is 90° electrical degrees behind the d-axis. Rotor angle is the angle between generator's d-axis and a-axis, shown by δ_{local}.

However, for multi-machine systems, machines' rotor angles can be specified not only with respect to their local voltage reference, but by using as their reference, either the voltage or the angle of one reference machine. This reference machine is usually the slack machine of the the system. For instance, in Figure 2.12, angles $\delta_{ref}, \delta_{ref_v}, \delta_{ref\_m}$ illustrate the reference machine rotor angle (as defined in the previous paragraph for one other non-reference machine), the rotor angle with respect to the reference machine voltage angle and the rotor angle with respect to the reference machine rotor angle, respectively. Angle a is the generator bus voltage angle (a-axis) with respect to the reference machine voltage angle (a-axis). In the followed stability analysis, the rotor angle of a specific machine is measured with respect to the angle of the reference machine, since it's a good indicator for transient analysis, according to the analysis done in Section 1.2. In general, for the rest part of this thesis, the considered δ_{ref_m} will be denoted as δ and for a stability aspect, this should be as small as possible.

2.2.2. Rotor Angle Stability- Classification

Section 1.2, familiarized the reader with the classification of the power stability. In this section, a brief further classification of rotor angle stability is presented.

According to [6], rotor angle stability can be classified into two categories: transient stability and small signal stability. Transient stability is defined as the ability of the system to maintain synchronism when is subjected to a severe disturbance, such as a fault in a line or terminal. On the other hand, small signal stability refers to the ability of the system to remain in synchronism when minor changes in the load or generation occur. In the current report, focus is given only to the transient stability

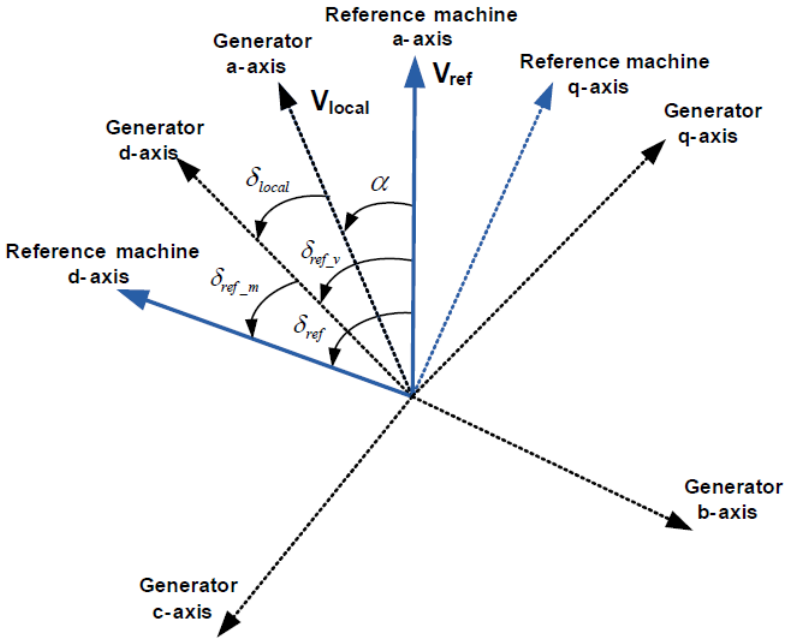

Figure 2.12: Different Synchronous Machine'S rotor angle measurements [31].

performance. The reason behind that is that RTDS does not provide an eigenvalue analysis capability that is mandatory to perform small signal stability studies. Furthermore, it is mentioned that an attempt was done to perform eigenvalue analysis using DIgSILENT PowerFactory, which offers this tool. However in the existing WG model, when a damping controller was employed, even if the time-domain rotor angle simulations were characterized by a damping trend, it was observed that the damping ratio of all the modes, in the frequency domain was remaining intact. The conclusion derived, is that the RMS WG model has to be reviewed again, in terms of the initialization of the differential equations that describe the different controllers. More information about small signal stability is provided in [3].

In [3] also it is stated that, the change in the electrical torque of a synchronous generator can be divided into two components: the synchronizing torque - which is proportional to the change in the rotor angle and the damping torque - which is proportional to the change in the speed. When both of them are sufficient, then the rotor angle after a fault undergoes decreasing magnitude oscillations (Case 1). If the damping torque is inadequate then oscillatory instability is observed (Case 2). Last, if the synchronizing torque is not adequate, then the rotor angle characteristic is increasing monotonically (Case 3). In this situation, the instability is termed as "first swing instability". The three cases are illustrated in Figure 2.13. The goal of the proposed wind generator controller is to increase the synchronizing and damping torques of the synchronous machines in the system.

According to [32] three types of oscillations have been observed in multi-machine systems:

- Inter-unit Oscillations: in which two or more machines swing against each other, with the frequency varying from 1.5-3 Hz.
- Local - Mode Oscillations: in which the machines are oscillating against a comparatively larger system. The oscillation frequency is at 0.7-2 Hz.
- Interarea Oscillations: in which machines of one system's part are oscillating against machines in one other part. These oscillations have frequency less than 0.5 Hz.

The proposed control schemes target to damp mainly the low frequency modes, since they are the most critical ones.

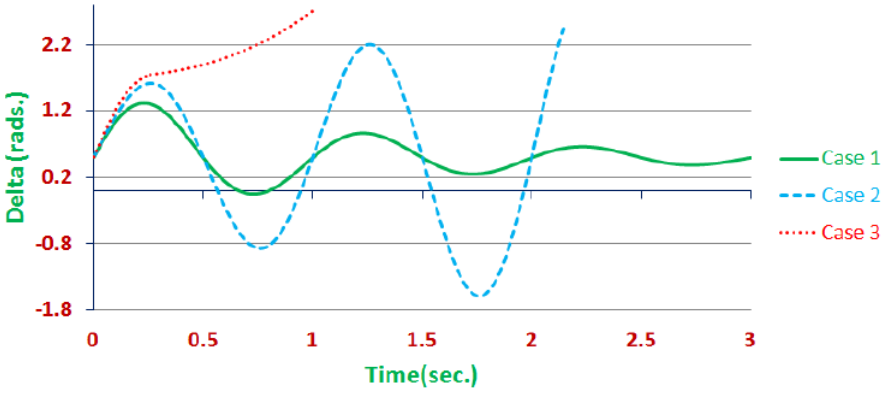

Figure 2.13: Different Synchronous Machine'S rotor angle measurements [3].

2.2.3. Basic Overview of Transient Stability Study

In order to have a better understanding related to transient stability concepts, the equation of motion, or equivalently, the so-called swing equation is first presented. In particular, the angle of the machine as already mentioned, is dependant on the mechanical and the electrical torques (or powers) of the machine.

$$J\frac{d\omega_m}{dt} = T_a = T_m - T_e[N \cdot m] \tag{2.7}$$

where J is the total inertia of the rotor mass $[kg \cdot m^2]$, ω_m is the angular velocity of the rotor $[mech \cdot rad/s]$, T_a, T_m, T_e are the net accelarating torque, the mechanical torque and the electromagnetic torque respectively $[N \cdot m]$.

Although the rest of this thesis analyses stability under transient conditions, such as faults, it is also mentioned that a power system can become unstable under steady-state conditions. From the theory of the synchronous machine, the synchronising power between the rotor and stator is nullified when the rotor angle reaches 90 degrees [33]. An explanation for that, from the power system perspective, can be given as follows: assuming that the operational point is in the maximum point of the power-angle curve and a slow increment in the mechanical input torque is implemented, then from the machine equation of motion, the angle increases. However, this means that active power of the machine decreases and the imbalance between the electrical and mechanical torques of the machine increases and the machine then, goes out of step. From the electrical machines perspective this instability can be explained as the inability of the rotor magnetic field to keep the rotor synchronized with the stator-rotating magnetic field, due to the applied mechanical torque in the machine. This phenomenon is more intense when the generator has a low field excitation, as this produces a weak magnetic field [34].

The previous discussion refers to gradual changes in the conditions affecting the torque angle, so approximately steady-state conditions always exist. However, under transient conditions this angle may temporarily exceed 90 degrees without loss of stability. As stated in [31], if after a disturbance the rotor angle exceeds 180 degrees then the Synchronous Generator (SG) will slip a pole and if conditions that caused the original disturbance are not corrected (e.g. activate circuit breakers), then the field rotor can not attain strength to lock the rotor back in synchronism with the stator, so the machine will continue to slip poles. Machines that have fallen out of step must quickly be brought back into step or disconnected from the system. When a generator loses synchronism, the resulting high peak currents and off-frequency operation can cause winding stresses, high rotor iron currents, pulsating torques and mechanical resonances that are potentially damaging the machine. To minimize damage the generator should be tripped without delay, preferably on the first slip cycle [35].

An example of a synchronous machine connected to an infinite grid is depicted in Appendix C, in which a rotor angle stability study is performed. Also it is elaborated how Automatic Voltage Regulator (AVR) can improve the transient stability. The aperiodic problem described, is tackled with voltage regulators, while oscillation modes are usually cancelled by means of power system stabilizers [35].

Appendix D illustrates the PSS structure and operational principle.

2.2.4. Key Performance Indicators (KPI) for transient stability studies

In order to assess the impact of high share wind generation on large-disturbance rotor angle stability, several indicators have been created. Critical Clearing Time and maximum angle difference are two widely indicators that are used in this thesis, since they do not require any demanded computing effort and moreover their operational principle is easy to grasp [39].

Critical Clearing Time, is the maximum duration that a fault can be applied, without any machine of the system transitioning in an out of step state. In the rest report, this time will be stated as Maximum Permitted Clearing Time and this is due to the fact, that frequency limits according to European standards have to be met also. For instance, if the frequency drops below 47.5 Hz instantly due to a fault, then the duration of the fault is defined as "maximum permitted" regardless of whether any machine is out of step or not.

Furthermore, in order to estimate the distance from the instability, a maximum angle difference indicator is defined as following:

$$Margin = 180^o - max\Delta\delta \tag{2.8}$$

where $\Delta\delta$ is the angle difference between any two generators in the system.

2.2.5. Methods for improving transient stability

The methods for improving transient stability can be identified by analyzing the swing equation of the synchronous machine. It is therefore comprehensible, that a high-speed fault clearing protection can improve the transient stability. Moreover, having fast AVRs with the ability to increase significantly the voltage level of the terminal voltage after the fault is also beneficial. The same also applies when the system reactance is smaller either by using series capacitors (static compensation) or FACTS (dynamic compensation). However, in the following sections, the aforementioned methods are neglected and the focus is given in finding controls to increase the damping forces applied in the machine.

In particular, utilizing wind generators, and modulating their active/reactive power injection one can damp the power system oscillations. It is mentioned, that, most commonly, the active power injection of the wind generator is the one that is modified, due to the fact that, SG instability is caused from the imbalance between mechanical and electrical power of each unit. This regulation can be used either with mechanical systems, or power electronics.

For instance, in [41] it is stated, that using the frequency error with a droop and PID pitch controller, one can affect the mechanical power of the turbine in such way that the oscillations of the synchronous machines can be decreased. The phenomenon described is called "active - stall control". The limitation of the system, is the relatively slow response of the controller, since it has a limit in the pitch range which is 15 degrees/second. It is mentioned, that this mechanical regulation is limited to fixed speed wind turbines. For fixed speed wind turbines, external equipment, can also facilitate the damping of the oscillations. Such devices can be dynamic Breaking Resistors (BR) which can only regulate active power, Static Synchronous Compensators (STATCOM) and Super Conducting Magnetic Energy Storage (SMES) devices which can change both active and reactive power simultaneously [5].

The aforementioned solutions, for transient instability mitigation, are out of the scope of the particular thesis, due to the fact that variable speed WGs have, by definition, their own power converters for modulating their active and reactive power. The advantage of this approach is the fast acting control, due to the small gating times in the converters, comparing to the mechanical approach described before. For instance, it is stated that the LVRT technology, described in Section 2.1.3, can influence the transient stability of the system. More information, about that is given in Appendix E.

In the following chapters, the implementation of such power-electronic based wind turbine controller is done, in order to mitigate the power system oscillations. The examined controller is based on the conventional PSS used for SGs logic, in which the input signal should be a signal that is affected by the interarea oscillations that are wanted to be mitigated, whereas the output signal should be one signal that can modulate the active power injection of the WG.

Adjustment of control parameters could be based by determining the bandwidth of the controller, [42], based on the determination of the cut- off frequency that the controller needs to have. However, the amount of damping (i.e. gain of the controller) can not be justified, and moreover, when many machines are involved, the time constants of the controllers used, need to be small, to avoid interactions with frequency control modes and not to excite excessive torsional oscillations of the synchronous machines [43], [44]. In particular, in the aforementioned sources, root locus analysis, by finding the damping ratio of the inter- area modes is used, for tuning the washout filter. In [45] the compensation that is done, is more complicated. It is based also in root locus technique and the main idea is to shift the closed-loop poles to the left plane by adding additional zeros and poles due to the controller. Last, it is mentioned in [46] and [47] that when the input is the speed of the machine and the output of the controller is modulating the active power, no lead-lag for compensation is needed. Further details, about the controller are analyzed in the following chapters.

3

Proposed SDC Controller- EMT Modelling

In this chapter, a brief introduction about the EMT environment's features is presented. The mathematical model of the WGs and the performance of the different control strategies tested, for rotor angle stability studies is additionally analyzed. Last, basic steps about how the benchmark and the controllers are built in the specific software are illustrated.

3.1. Real Time Digital Simulator tool

Real Time Digital Simulator (RTDS) is a powerful tool, designed for Electro-Magnetic Transient (EMT) studies. The Simulator, requires parallel processing, in order to compute the system's state during the time step that is chosen. Time steps are in the order of 25μs to 50μs. This time scale is called a large time step. But this time step is too big for power electronics simulation. Therefore, a small-time step is needed. As a solution, RTDS provides an additional small time step environment for simulating power electronics, in which a time step of 1400ns - 3750 ns is used. The user, can add the power electronics components in a specific small time step simulation block (e.g. the back-back Voltage Source Converters (VSC) of the WGs and can place the rest power system components outside this block. From the aforementioned, it can be understood, that one of the main advantages of this tool is the possibility to perform studies with very small time step, that enables monitoring and control for dynamic studies. RTDS can also be used for closed loop testing (HIL/SIL), which is essential for components' testing and control in the real world. However, the latter is out of the scope of this thesis

RTDS consists of two components: hardware and software. Hardware is not mentioned in the specific report. The different cards, processing and communication units for the interconnection of the power system simulator with the host computer workstation can be found in [48].

As stated, RTDS Technologies, provide a software called RSCAD, for interfacing to the simulator hardware. The different power components, can be designed, controlled and executed via different modules, that the software contains. More information about the modules can be found in [49]. Out of them, Draft and RunTime are essential in order to execute simulations.

The Draft module contains the drawing canvas in which the user can place the components that needs. The components are chosen from the libraries, on the right side of the user's screen. RSCAD provides also the flexibility to the user not to be restrained in the libraries' components but to create new ones also using the module Component Builder (CBuilder). In the Draft Module, the parameters of the components can be set. Last, the big time step can be defined, by right clicking in the white canvas background and selecting the option "Circuit Options". The draft layout can be seen in Figure 3.1.

The libraries that are used in the simulations are:

- Power System Component Library

- Control System Component Library
- Small Time Step Component Library

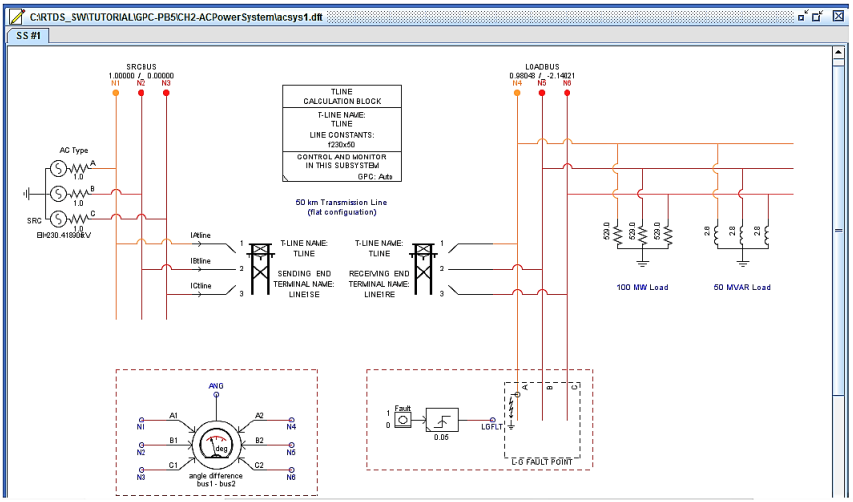

Figure 3.1: Power System Example built in Draft module .

The first two libraries are presented in Figure 3.2. In the left hand side of the red line the Control System Component Library is included, whereas in the right hand side the Power System one is presented. The small time step library is used to build the Power Electronic Interface of the Wind Turbine and to feed the valves based on the gating signals that they are computed in the corresponding controls of the big time step environment. More details about that specific library are presented in Appendix G. Among others, in Appendix G, the mathematical model of the FSC WG is analyzed, and the RSCAD blocks related to them are depicted. The way the different control strategies are built, is also presented in there. Before that, the Reference Frame transformation techniques are illustrated in Appendix F to facilitate the controllers understanding.

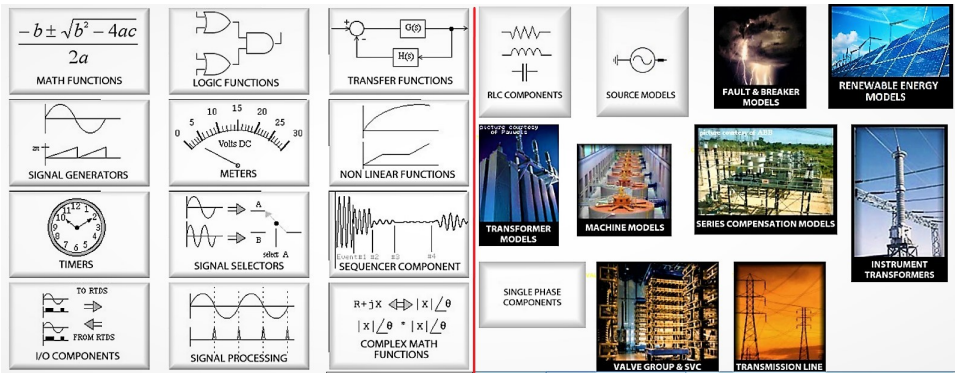

Figure 3.2: Control Power System Component Libraries

The user, in order to start the simulation, it has first to compile the draft file, by clicking in the corresponding button in the top of the draft canvas. The compiling procedure checks the components used and their parameters for potential errors. Apart from the data defined from the user, the compiler takes also as an input the configuration file, which includes the hardware information about the IP addresses of different rack ports and cards connected to each rack. RSCAD provides a tool to edit the hardware configuration known as the config. file editor, which can accessed under the Tool menu that is included in the main window of the RSCAD environment (i.e. in which the different modules can be seen). As output, the compiler produces all of the parallel processing code required by the digital signal processors to run the simulation.

The user with his host terminal can interact with the simulation in real time via a Graphical User Interface (GUI), called RunTime. This can be done by creating meters, plots, sliders, buttons, dials, switches, etc. in there. A typical example of this Interface follows in Figure 3.3.

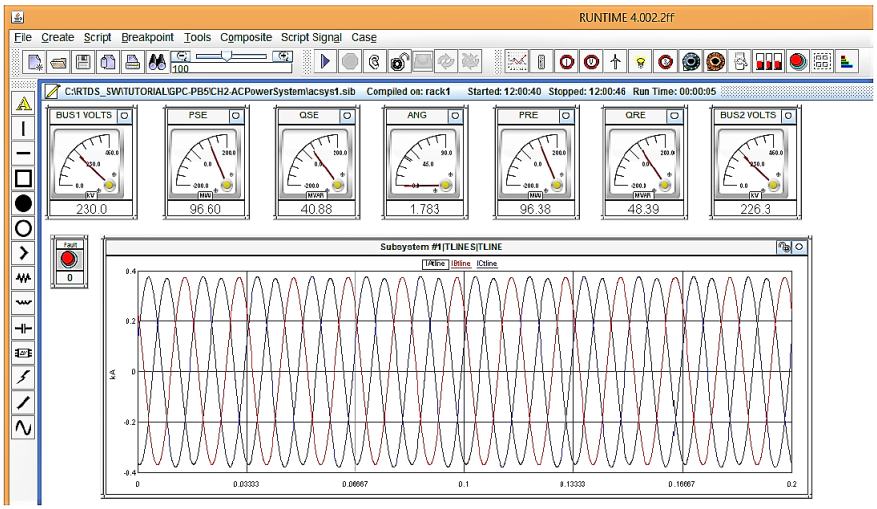

Figure 3.3: RunTime Module in RSCAD

3.2. Wind Generator Controllers - Description Logic

As shown in Appendix G, the main part of the FSC WG controller is related to the Rotor Side Converter (RSC) control and the Grid Side Converter (GSC) one. Each one of the two aforementioned converter controls, as presented in Appendix G, consists of an outer loop - that determines the set points AC currents, and an inner loop that receives the set points and computes the corresponding modulation signals in the valves of the converter that the controller belongs to. In this chapter, three different controllers are used, and their contribution to the rotor angle stability response of the SGs that are connected to the system, is analyzed. It is mentioned that the outer loop of the GSC, is the one that differentiates the three controllers. The RSC and the inner loop of the GSC remain the same as described in Appendix G. The three controllers are described in the following subsections.

3.2.1. Basic LVRT Controller

The first controller concerns the default case which is implemented by TenneT [50]. For this control, two flags are used. When the voltage in the Point of Common Coupling (PCC) drops below a threshold value - 0.8 pu, then Fault Ride Through (FRT) flag becomes zero. During normal conditions, this flag equals one. During the fault, WG is injecting reactive power for voltage support services. When the voltage level rises above a certain limit, the Ramp - Up flag becomes zero for a specific time period (e.g. 0.6 seconds). During this period (i.e. post-fault period), the active current increases linearly towards its pre-disturbance value. The slope is being determined by the gain G and the time delay of the transfer function as seen in Figure 3.4b. This current ramping is introduced for frequency stability enhancement of the system during the post-fault period.

In the simplified diagram in Figure 3.4a, it can be seen that the I_d^{ref} is zero, during the fault period. During the post-fault period, the I_d^{ref} reference will be computed by the first order transfer function as seen in Figure 3.4b.

The reactive current reference, during normal conditions, is computed exclusively with the cascaded controller of Figure 3.5a. During fault (FRT flag equals 0), it can be understood that the reference is determined by Figure 3.5b. Lastly, during post-fault period (FRT Flag=1, RAMP flag=0), the reactive current reference is returning to 0 pu.

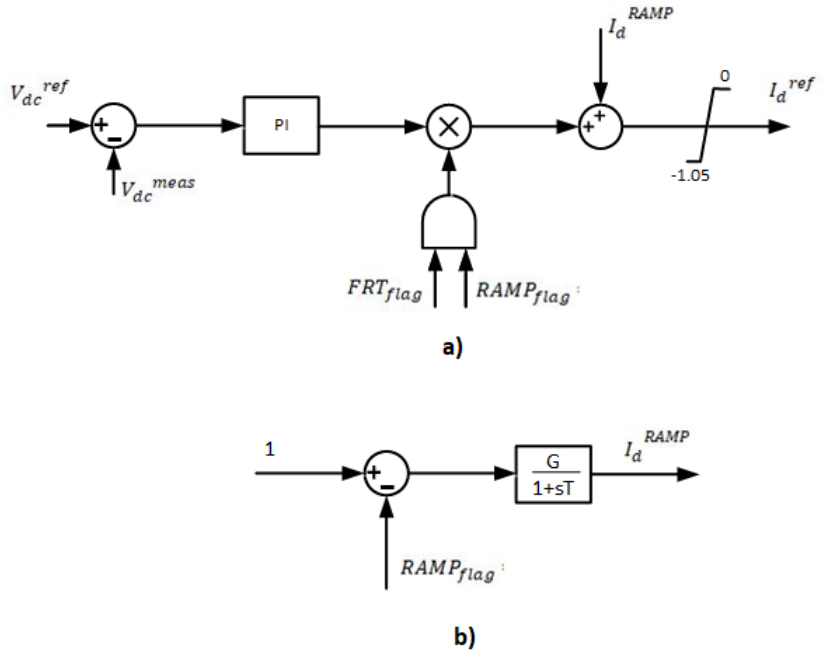

Figure 3.4: (a) I_d^{ref} computation, (b) Ramping - up of I_d^{ref} (post-fault)

3.2.2. Voltage Dependent Active Power Injection (VDAPI) LVRT Controller

The second controller concerns the ability of the WG to inject some active power during the fault. During the fault, the active power of the Synchronous Generators drops a lot. If the active power of the WGs also nullifies as in the first controller described previously, it can be easily understood that the imbalance between total generation and load will be also significant. This means, that the frequency deviates a lot from the nominal value. Since rotor angle of the machines and frequency are probably affected, this controller aimed not to nullify the I_d^{ref}, but to inject some reduced (comparing to the pre-fault case) active power. According to that approach, the active current reference (as computed from the conventional logic with the V_{dc} error as input) is multiplied with the squared value of a factor F. This factor F is dependent on the voltage measured value in the PCC of the WG. This approach is taken from [51], in which a reduction in the active reference current is needed, due to the increment of the installed wind capacity. This increased wind capacity adversely impacts the voltage at the PCC.

The controller is depicted in Figure 3.6. I_d^{ref} is computed from Figure 3.4, in which however, the AND gate in the multiplication point does not exist. During normal conditions, this F factor is one. I_q^{ref} during fault is computed using Figure 3.5a, but now the limits in Figure 3.5b (i.e. during fault) will be: $\pm\sqrt{1-(I_d^{'ref})^2}$).

3.2.3. Supplementary Damping Control (SDC) LVRT Controller

The third controller is related to Supplementary Damping Control (SDC) branch that is connected to the P-control loop of the Wind Generator.

In principle, the Supplementary Damping Control (SDC), implemented in the form of a power system stabilizer, can be added either into the active power (P)-loop controller of the wind generator (affecting the d- reference current) or in the reactive power (Q)-loop controller (affecting the q- reference current). Nevertheless, it was decided to add Supplementary Damping Control into the P-loop controller due to two reasons. The first one is associated with the electromechanical oscillations that lead to transient instability. These oscillations are caused by a mismatch (according to the dynamics described by the swing equation) between the electrical power and the mechanical power of the synchronous generators being in service in a power system with high share of power electronic interfaced generation.

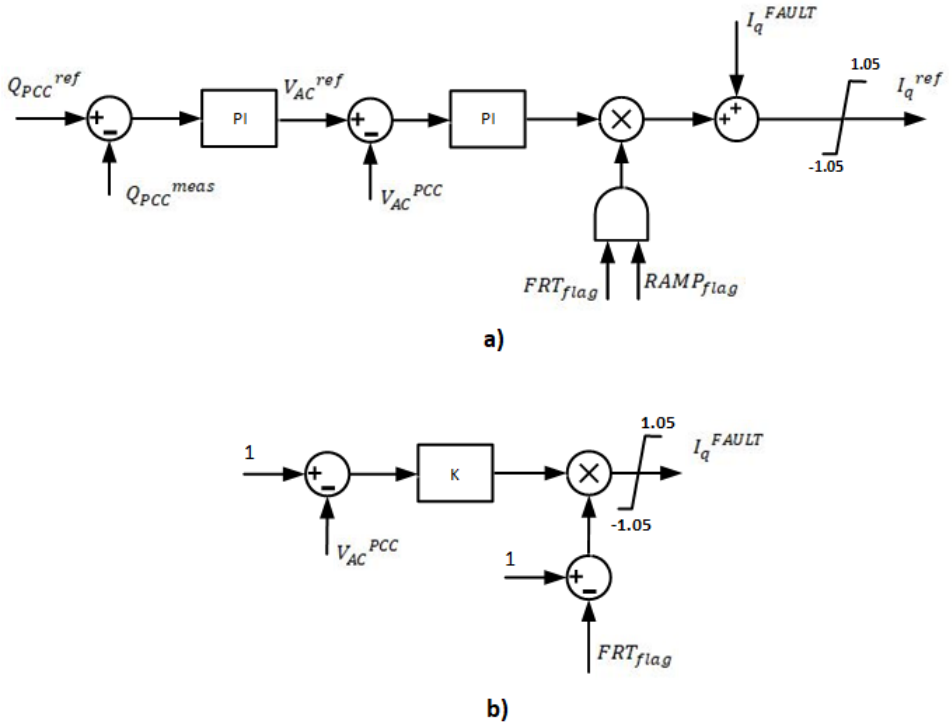

Figure 3.5: (a) I_q^{ref} computation, (b) LVRT I_q injection

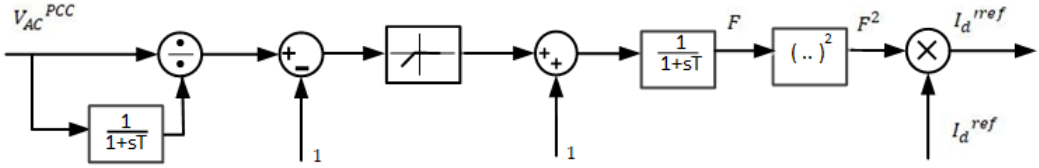

Figure 3.6: I_d^{ref} computation

Thus, controlling the active power of the wind generators, will affect directly the active power of the synchronous generators connected to the system. The second reason is related to the location of the wind generators with respect to the location of the synchronous generators. According to [53], the wind generators that are connected electrically close to synchronous generators will tend to have a stronger influence on the active power transfer from the synchronous generators if the wind generators have the supplementary damping control superimposed on the P-loop controller. In the systems that will be examined in this report, the Wind Generators are closely connected to the Synchronous Generators. It is worth mentioning that, according to existing literature, e.g. [54], a supplementary damping controller superimposed into the P-loop is less sensitive to the location of the wind generator than a supplementary damping controller superimposed into the Q-loop. As an example, [53] suggests that SDC attached to the Q-loop requires large reactive power reserve from the renewable generator. Such case should be evaluated carefully, considering possible adverse implications on the transient voltage support function provided by the renewable generator.

In addition, [54] shows that the above-mentioned findings hold when representing a wind power plant either with a detail model or by an aggregated model (e.g. wind power plant represented by a single wind generator). With existing computational resources and software packages, it is still not feasible to perform studies in which a whole interconnected power system and every wind power plant (or any other type of renewable energy based power plant) is modelled in full detail. In general, in both tools used (i.e. RTDS & PowerFactory, the model of a single unit is fully represented, and a scaling factor is introduced so as to represent a Wind Farm.

Figure 3.7, shows the structure of the supplementary damping controller, which is superimposed

on the output of the active power (P)-loop controller of the wind generator. As shown, the damping controller has the simple form of a washout filter. Unlike typical damping controllers attached to synchronous generators, the lead-lag compensation has not been considered, because a small phase lag between the modulated current reference in the d-axis and the active power output of the grid side converter is assumed. A similar approach for SDC added into WG control, without lead-lag consideration, has been extensively reported in [43], [55], [46] and [56]. Furthermore, in the case of the examined SDC, as shown in [47]: "The active power should be modulated in phase with the speed of the machine". Note that the rotor angle constitutes the integral of the rotor speed, and has a phase shift of -90 degrees with respect to the rotor speed. In addition, it is taken into account that the washout filter is a high pass filter, and introduces a phase shift of 90 degrees. Hence, no phase compensation is needed when rotor angle is given as input in the stabilizing control. The Bode diagram of the washout filter(G=10,T=0.1s) that is used in the simulations, explained in following sections in the current chapter, is illustrated in Figure 3.8. The phase shift of 90 degrees for the low frequencies of main interest is clear.

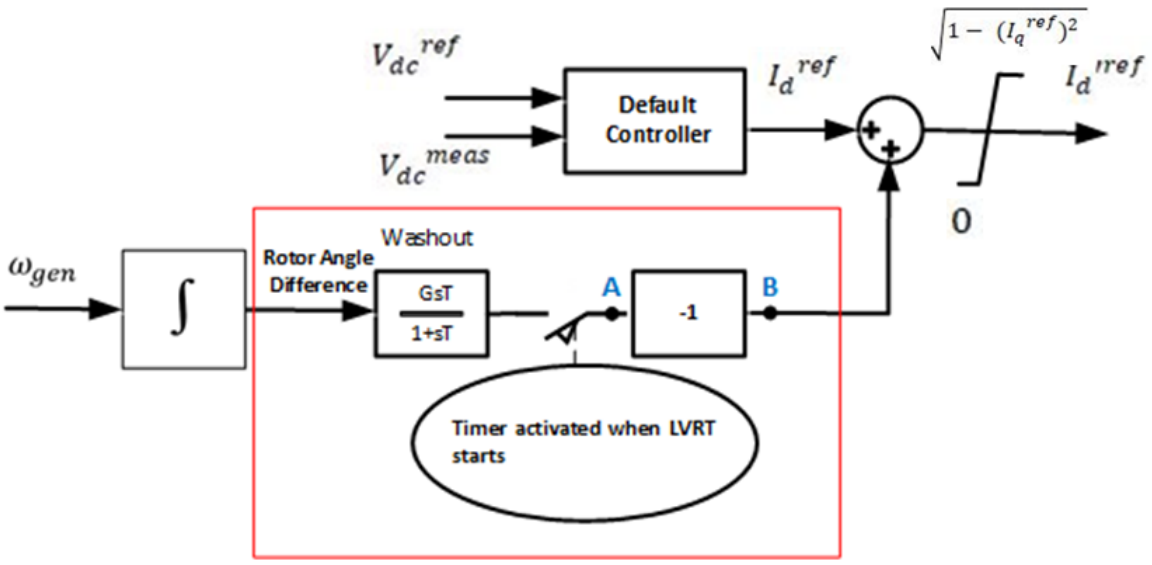

Figure 3.7: I_d^{ref} computation using the Supplementary Damping Controller

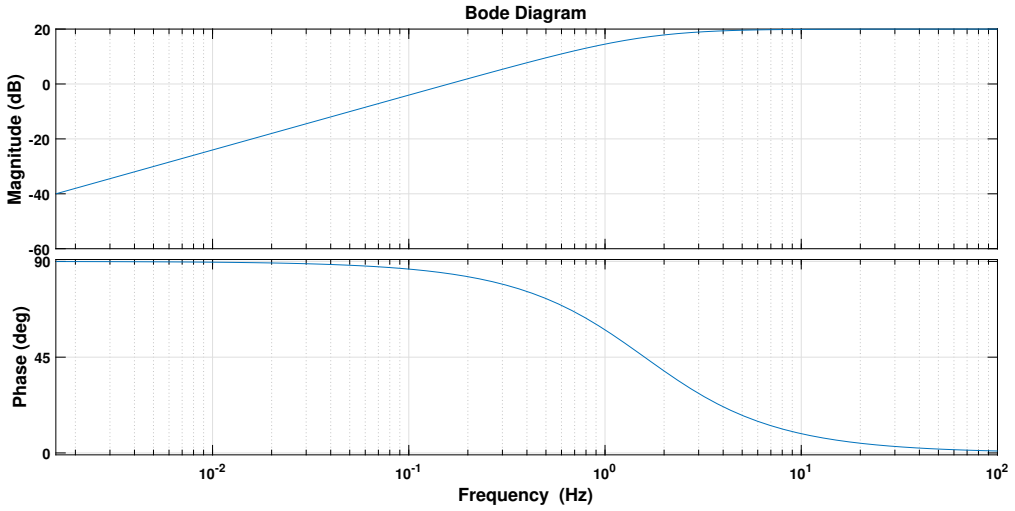

Figure 3.8: Bode Transfer Function for a (G=10, T=0.1) Wash - out Filter

In Figure 3.7, the implemented SDC controller is presented inside the red layout, while the input signal of the generator speed is added for operational demonstration. Modulating signal in point A, is in phase with the speed for the reasons discussed in the previous paragraph, whereas signal in point B, is in anti-phase with the speed, due to the existing configuration of the controller used.

Moreover, assuming that the synchronous generator and the wind generator are located in the same electrical area and that the synchronous generator oscillates against other area(s) of the power system, then, during the fault, due to the action of the proposed supplementary damping controller, the wind generator will decrease the active power production, so, this entails that the synchronous generator needs to increase the active power injection to feed the load, thus from its swing equation, the speed acceleration will decrease and a damping is introduced.

Note also in Figure 3.7, that a timer has been added at the output of the washout filter in order to activate and deactivate the damping controller. The activation is done when the LVRT function is triggered (i.e. when the point of common coupling voltage drops below 0.8 pu). The deactivation occurs within a certain time period from the activation time. As shown in [57], this time period may be between 10-15 s, which is usually the period in which relative rotor angle excursions should be significantly attenuated. However, as shown in sub-section 4.4.2, related to RMS studies in the test model of the GB system, and in particular in Figure 4.17, in order to prevent unwanted noise or high frequency oscillations, and to safely reach a steady-state post-disturbance condition in a multi-machine system, the deactivation time of the SDC loop, is set around 5 seconds after the fault was sensed and the LVRT mechanism was triggered.

As a general rule, based on the findings from [17], it can be considered that the rotor angle deviation between two synchronous generators in the power system is a suitable input of the damping controller. This assumption is taken here and additional reflections concerning this choice are given below:

- First, the rotor angle of a synchronous generator is directly related to the transient stability performance of a power system, because during faults, the rotor angular separation between the machines of a power system increases due to the electromagnetic torque imbalances. In order to maintain the fluxes, this angular separation should be kept as small as possible. When the maximum rotor angle difference between two generators exceeds 180° then the generators are out of step and stability is lost [39].

- Secondly, the rotor angle constitutes the integral of the rotor speed of the synchronous generator, which is directly reflected into the system frequency. This means that during a fault, if the frequency changes linearly, the rotor angle changes in a quadratic way (i.e. faster changes are better reflected in rotor angle variations). If rotor angle is to be controlled, the frequency response is expected to be implicitly improved.

- Third, the rotor angle is not directly available as measurement, and therefore it should be estimated from other measurements. Several methods for estimation of rotor angle have been proposed in existing literature. For instance, in [58], rotor angle is predicted by using PMUs that measure voltage and current signals in the system.

In addition, a polynomial function for injecting reactive current is used during fault as proposed in [59]. These characteristic figures were taken after studies in COBRAcable for MMC converters. This reactive power injection is dependent on the PCC voltage and a parameter alpha. This design was selected, because it overcomes voltage instabilities that may occur in low impedance faults, in RMS simulations (e.g. Power Factory) in which the time step is not negligible.

In the following sections, the power system that the aforementioned controllers were tested, as well as the system's response, in terms of SGs' rotor angles, the frequency and the voltages, are presented.

3.3. Benchmark Power Systems Developed for Controllers Testing

A modified IEEE 9-bus system is used to test the controllers; the topology is depicted in Figure 3.9. The Power System's and the Synchronous Generators' parameters, are included in Appendix G. Two wind share levels are examined; 52% and 75%. The transition from the low to the high wind share

configuration, was simulated in RSCAD, in such way so as the SGs that are connected in the 75% wind share, to have the same active power injection with the corresponding SGs connected in the 52% wind share. In that way the, pre-disturbance state of the synchronous machine is the same in the two topologies, for a fair comparison, so as more reliable results to be deduced. More information about how the systems are built in the software is found in Appendix G. Figure 3.10 illustrates the single line diagram of the two systems, while Table 3.1 depicts the load flow results for each case.

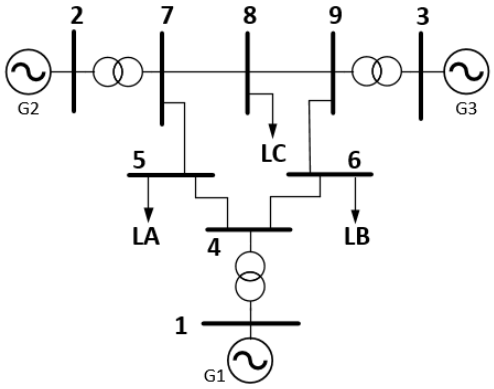

Figure 3.9: IEEE 9 BUS modified system with only SGs connected

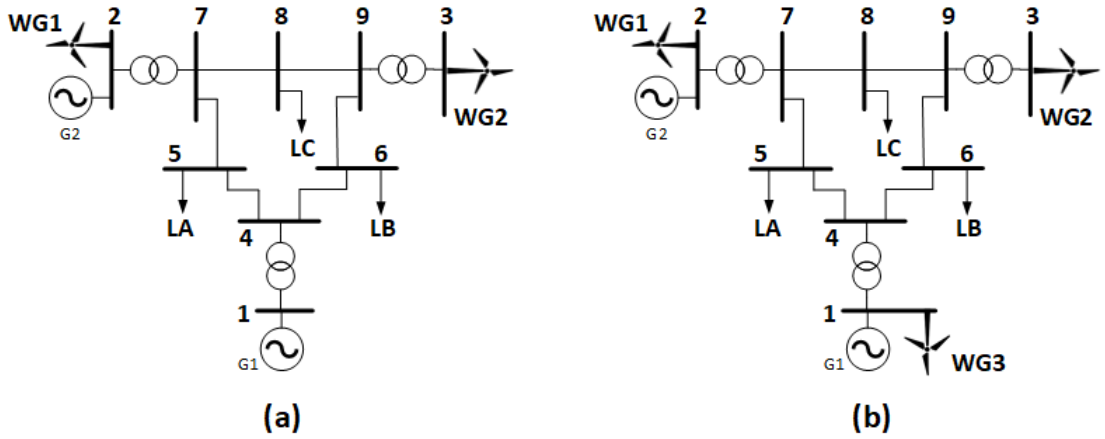

Figure 3.10: IEEE 9 BUS modified system a) 52% Wind Share, b)75% Wind Share

Table 3.1: Load Flow Results

Plant	only SGs		52% WG		75% WG	
	P[MW]	Q[MVar]	P[MW]	Q[MVar]	P[MW]	Q[MVar]
G1	73.06	36.11	73.02	36.02	35.3	20.4
G2	163.08	-9.1	81.5	-4.6	40.75	-2.6
G3	85.03	-4.943	-	-	-	-
WG1	-	-	81.5	0	124.9	0
WG2	-	-	85	0	83.6	0
WG3	-	-	-	-	38.7	0
LA	125	50	125	50	125	50
LB	90	30	90	30	90	30
LC	100	35	100	35	100	35

3.4. System Response under Transient Phenomena

All the results in the current and the following subsection are related to a three-phase fault performed at node 8, with fault clearing time of 120ms (6 cycles) and impedance of 0.2Ω. Results related to additional buses' faults, are illustrated in the next chapter using RMS simulations.

3.4.1. 52% WG Share- Responses

In Figure 3.11a, when the SGs are only connected, the frequency increases due to the high inertia of the system. (Load C due to the fault at bus 8 drops to zero, however, there is a delay in the generation drop, therefore, in that case, the frequency initially increases). In the default case, the total generation drops way more than the load and the frequency decreases significantly. With the Voltage-Dependent Power Injection, since the WGs continue injecting some active power during the fault, the frequency decreases less. Last, SDC equipped WGs are also improving the frequency.

In Figure 3.11b, the high inertia of the system when only SGs are connected is clear, from the lagging characteristic comparing to the WG connected cases. Moreover, SDC equipped WGs are the only measure that improves rotor angle responses.

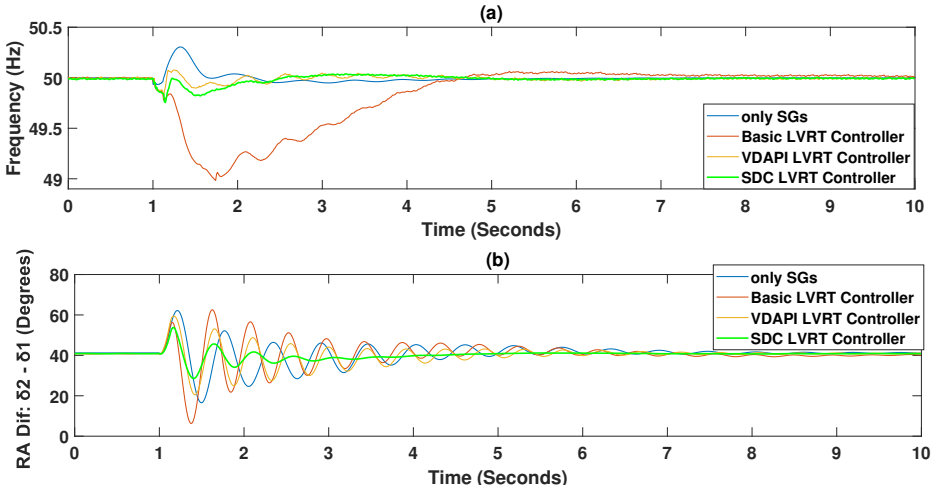

Figure 3.11: Fault at Bus 8- 6 cycles: a) frequency response, b) rotor angle deviation response

In Figure 3.12, it is shown that electromechanical oscillations are evident, when SGs are only connected, or when Voltage-Dependent Active Power Induction (VDAPI) or default-mode WGs is used. These oscillations are undesired because they can cause equipment damage or activation of protection equipment. With SDC employed (Figure 3.12d), the oscillations are damped out quickly.

Due to the fault, the voltage drops more in the WG2 PCC, due to the low line impedance. WG1 reactive control is more effective with the polynomial controller, which injects more reactive power. As seen in Figure 3.13, in low impedance faults, the three methods inject the same reactive power.

During the fault, the DC voltage in the interconnection point of the two VSCs lasts more due to the ramping-up of the d reference current during the post-fault period. With the SDC connected, the oscillations observed in the id current due to the washout filter will be reflected in the DC voltages as well.

In Figure 3.14 and Figure 3.15, it is clear that the active power and i_d currents and similarly the reactive power and i_q currents have the same waveform. For a matter of convention the i_d current is negative when it is injected from the WG to the grid. As stated previously, the reactive power injected from WG1 when the rotor damping controller is activated is bigger compared to the other two control methods. For WG2, the voltage drops significantly for all the 3 methods. This fact leads WG2 to inject the maximum reactive power possible.

Last, considerable spikes are observed in the currents for both the two d, q axis. This is due to the simple PI control logic used, for the inner controllers that will eventually create the modulating PWM

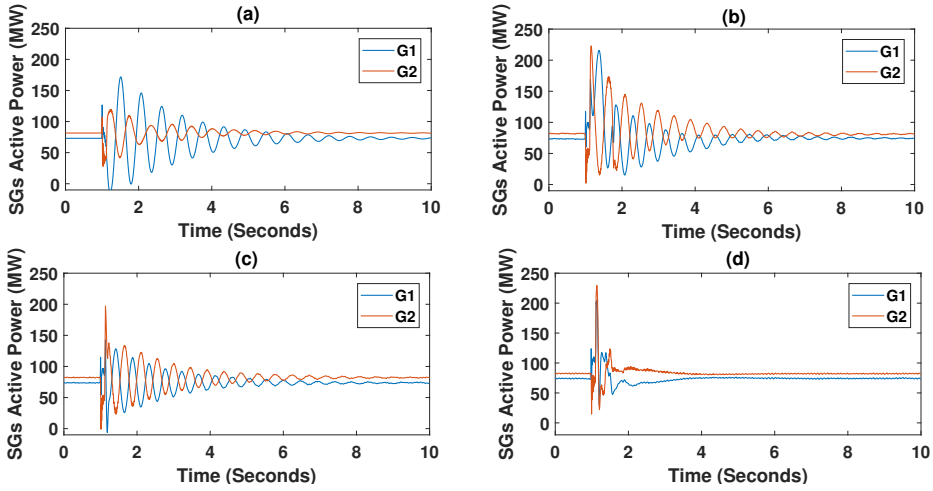

Figure 3.12: Active Power from SGs due to a Fault at Bus 8- 6 cycles: a) only SGs connected, b) Basic LVRT controller applied in WGs, c) VDAPI LVRT controller applied in WGs, d) SDC LVRT controller applied in WGs

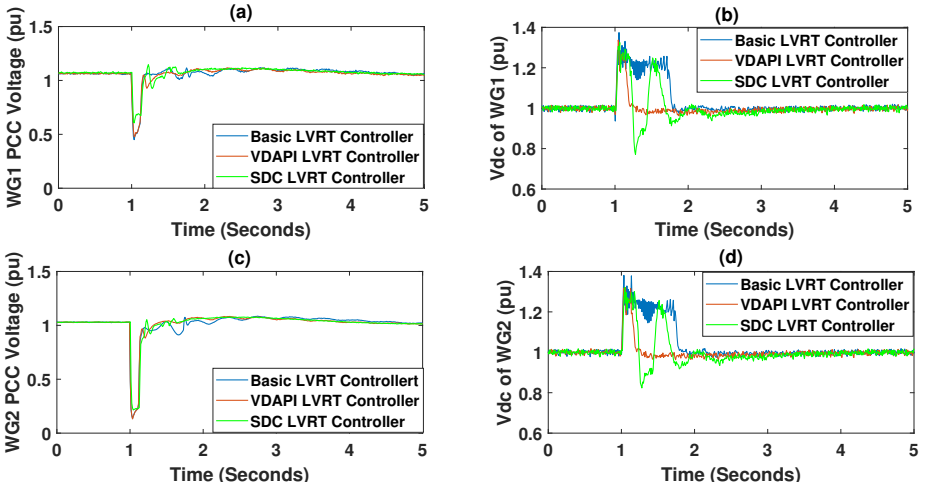

Figure 3.13: Voltages due to a Fault at Bus 8- 6 cycles: a) PCC voltages of $\mathrm{WG}_1, b)\mathrm{V}_{dc}$ voltage of WG_1, c) PCC voltages of WG_2, d) V_{dc} voltage of WG_2

signals for the valves. Better tuning or anti-windup logic to avoid saturation in the integral part can be used.

For the three-phase fault at Node 8, it was found that the Theoretical maximum Fault Clearing Time (FCT) when the two WGs are in the default mode is at 380ms, when they are in the VDAPI mode at 390ms, whereas when SDC is used, then the FCT is at 640ms.

3.4.2. 75% WG Share- Responses

For a higher share of wind power generation, the results are illustrated in Figure 3.16 . The system is stable for a three-phase fault at bus 8 with FCT at 120ms, only when SDC is used. It was found that the default case was not stable even for 1-cycle of fault duration at node 8 for 75% share of wind power generation. In comparison, the FCT for the same fault, when SDC is used, is at 400ms.

3.4.3. Key - Takeaways

The main conclusions derived from the analysis done in this section:

- Basic LVRT controller has the worst frequency behavior due to the big imbalance between gen-

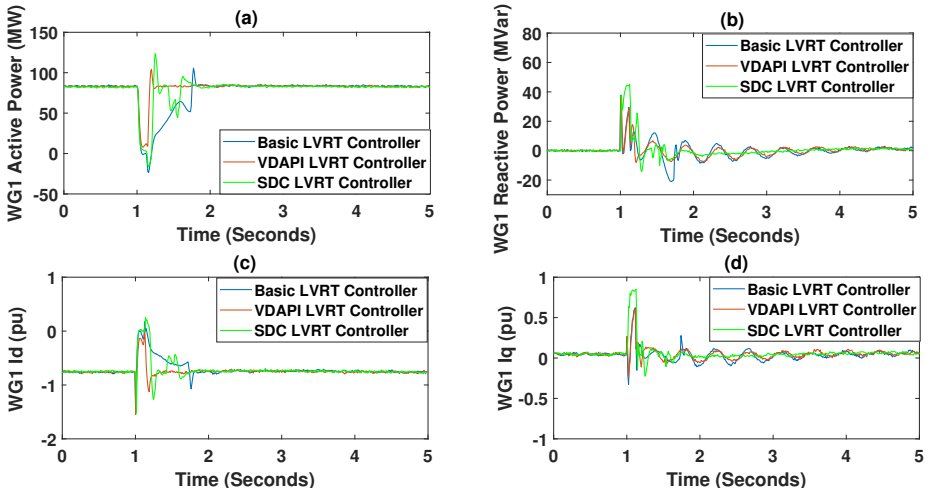

Figure 3.14: WG_1 waveforms due to a Fault at Bus 8- 6 cycles: a) WG_1 active power, b) WG_1 reactive power, c) WG_1 i_d measured, d) WG_1 i_q measured

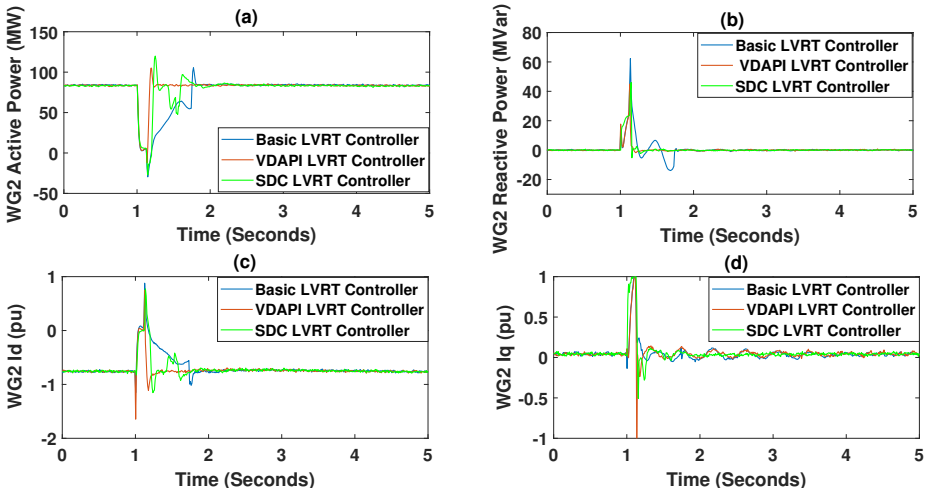

Figure 3.15: WG_2 waveforms due to a Fault at Bus 8- 6 cycles: a) WG_2 active power, b) WG_2 reactive power, c) WG_2 i_d measured, d) WG_2 i_q measured

eration and demand. Since no damping enhancement controller is applied and the inertia of the system is smaller, rotor angle response is deteriorated comparing to the only SGs situation.

- With the VDAPI controller, the frequency response is improved, since the imbalance between consumption and generation is decreased. The rotor angle first swing is worse comparing to the id nullification case, due to the fact that during the fault, the SGs are injecting less power comparing to the first case in which the WGs do not inject any active power. Therefore, the synchronizing torque is better but the damping torque is not affected that much.

- SDC controller can improve both frequency and rotor angle response comparing to the case in which only LVRT control strategy is used during the fault period. For higher wind share (75%) it was proven that only this control strategy is capable to avoid transient stability for a considerable FCT of 120ms.

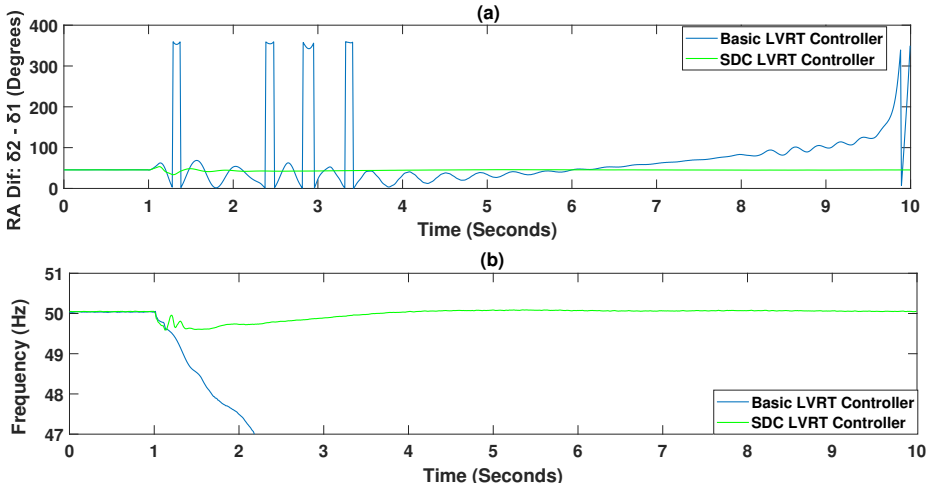

Figure 3.16: Fault at Bus 8- 6 cycles: a) frequency response, b) rotor angle deviation response

4

Proposed SDC Controller- RMS Modelling

The majority of the studies concerning damping controllers that can be attached to a wind generator, have been evaluated by using small size power system models [65], [66]. The conclusions drawn from these studies cannot be guaranteed in analysis of systems with different structure and dynamic characteristics (including interconnected larger size systems), nor systems with a high share of Power Electronic Interfaced Generation (PEIG).

This section shows several tests of the proposed controller, which were performed by using the modified version of the IEEE 9 Bus System, and also, by using a larger system, i.e. a synthetic model of the Great Britain (GB) system [39]. The goal is to show the effectiveness of the controller when increasing the share of power electronic interfaced generation. The theoretical maximum fault clearing time (FCT), is used as an indicator for monitoring the transient stability state of the system, whereas the tuning of the SDC controllers is based, as explained in Appendix I, on the maximum angular difference performance indicator. These two indicators are described in Section 2.2.4. RMS simulations are done by using DIgSILENT PowerFactory 2018. The effect of the communication delays for wide area monitoring, is included in this Chapter, whereas a comparison between local and remote signals as inputs in the proposed SDC controller is further illustrated. A guidance regarding which WGs should be equipped with SDC and which SGs should be involved for the input determination of the SDC conroller is also given. Moreover, a methodology is proposed in which one, can tune the SDC controller, based on time-domain simulations. Last, a comparison between the examined grid-following WG based power system and a new grid-forming WG approach is performed, in terms of the SGs' rotor angle damping that the two different wind configurations incur.

4.1. RMS WG Model Description

As stated in Section 3.1, the main difference between the RMS and EMT simulations, is the time step solver of the tools. In particular, 50μs time step is used for EMT simulations, whereas for the RMS ones, a step of 0.01 seconds is employed.

Figure 4.1 illustrates the structure of the wind generator control. As shown in [67], the control logics based on IEC 61400 standards are used to determine the current references in the d and q axis. Detailed description of the model can be found in [67],[68]. The main features of the controller are:

- Absence of PE components; this ensues that the complete layout of a fully decoupled wind generator, with consideration of the DC link, and the grid and rotor side voltage source converters (VSC) with their corresponding controllers, is not represented.
- Measurements blocks include frequency, voltage and power in the PCC; i.e. signals that are required in the controllers. Due to the proposed SDC integration, Synchronous Generators' rotor angle signals are additionally measured.

- The Aerodynamical and Mechanical model part includes a GE model for Maximum Point Power Tracking and a single mass shaft model. These blocks are computing the mechanical torque and power of the wind turbine, and also the actual rotational speed of the generator.
- The generator block contains a PowerFactory model, referred as static generator which operates as a Norton current source.
- The controllers include a P controller for the determination of the active component reference of the current that the WG should inject; a Q controller for the determination of the reactive component reference of the current that the WG should contribute; a Pitch angle control which receives the power reference from the "P choice and reduction block" and the actual measured PCC power. If the measured power exceeds the reference power calculated from the "P choice and reduction" block, then pitch angle is increased. It is stated that during over-frequencies, "P choice and reduction block" can potentially curtail the injection, but this feature is not enabled in the current study. Moreover, inertia emulation can also be utilized, but for the rotor angle stability studies, in order to have a fair comparison with the EMT model described before, also this property is not used.
- Current limitation is also used, with the saturation point being defined at 1.1 pu.

As an additional comment, the inputs of the P controller are uWT (i.e. measured voltage at the wind generator terminals), ipmax (i.e. maximum allowed active power), wgen (i.e. speed of the wind generator), pWTref and pWT (i.e. reference and measured active power at wind generator terminals respectively). The output signal is the ipcmd (i.e. reference value for the id current), which is modified by the proposed Supplementary Damping Controller (SDC). As shown in [67], the mechanical torque is computed based on the measured speed. Next, the mechanical power is calculated. Finally, assuming that the electrical and mechanical power are approximately equal, the value of ipcmd is computed by dividing the mechanical power by the magnitude of the voltage at the PCC.

The P- loop control model is modified, according to Figure 4.1. Similarities are observed with the SDC control modelled in the EMT environment, whereas the reactive current prioritization is also clear during the fault.

4.2. Justification of a Remote Signal Consideration as Input in the SDC

In this section a theoretical explanation, for the reason why a remote signal can be beneficial, is given, especially when a big power system is considered. A comparison with the aid of simulations, is reinforcing the following statements.

As shown in [69], when the delay associated to the data latency is relatively small (e.g. around 200ms), then, remote input signals of any type of supplementary damping controller, entail more effectiveness in increasing the overall damping performance of a power system, when compared to the case when local signals are given as inputs to the SDC. This is attributed to the fact that wide area measurements can offer higher observability of critical oscillations than local measurements [70]. In addition, for the case of electromechanical oscillations, the observability of states related to the dynamics of synchronous generators is higher than the observability associated to other power variables (e.g. measurements in intermediate buses of a transmission network) [71]. This statement has also a physical reasonable approach, since the inter-area low frequency modes are excited between machines in different areas, therefore, retrieving signals as inputs that are associated with machines located relatively far, will introduce better damping.

As shown in [72], communication and estimation (typically in the order of 20ms) time delays do not cause significant impact on the confidence of the estimated values of rotor angles.

The effect of delays is illustrated in Appendix H and Figures H.5, H.6, by representing the delays with two typical approximations in existing literature (e.g. first order, Padé).

Next, the SDC attached to a fully decoupled wind generator is used in two case studies. The first case study (modified IEEE 9 Bus System) aims to show the working principle of the proposed damping controller for fully decoupled wind generator, whereas the second one shows effectiveness of SDC in a larger size system (i.e. GB System).

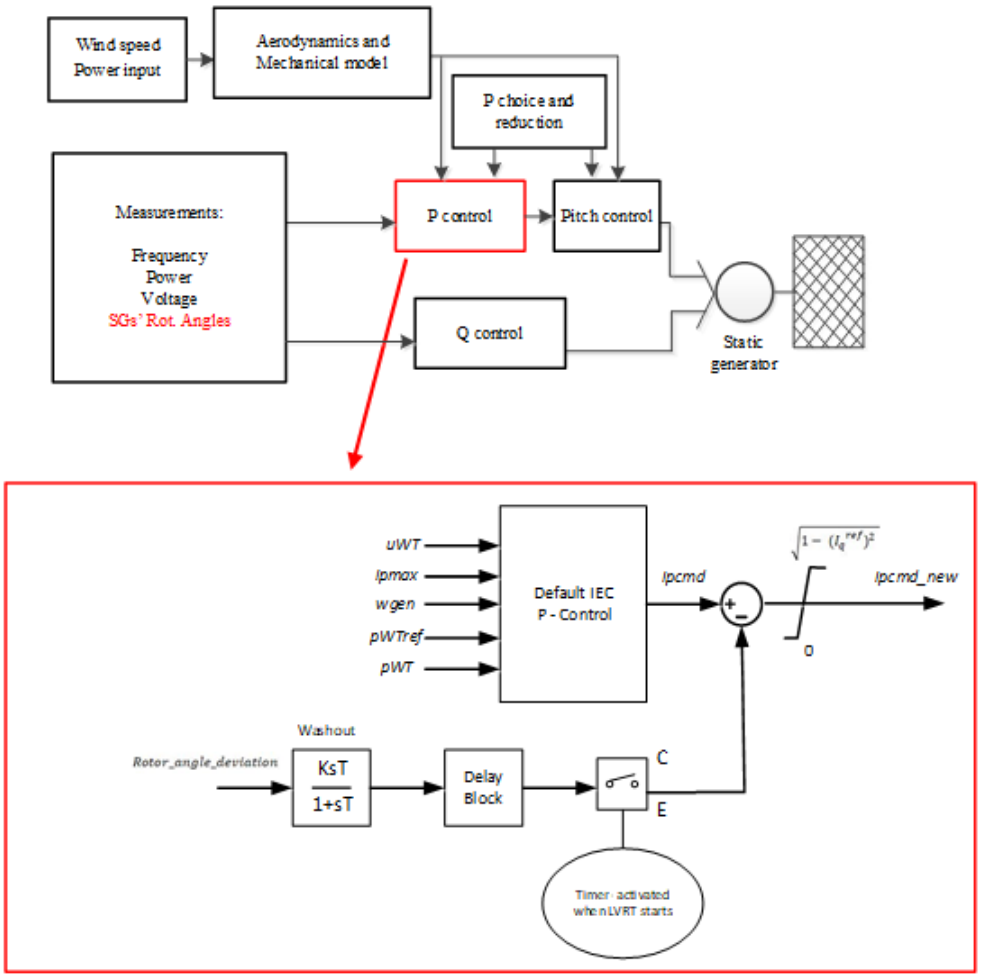

Figure 4.1: Control structure of the RMS full converter generator and SDC modification

4.3. Study case I: IEEE 9-BUS System

The system is described in Chapter 3 with the aid of Figure 3.10(a), so there is no need for any repetition in this section. It is mentioned that only the 52% wind share model is considered, for the RMS studies. Moreover, the line parameteres between RMS and EMT model slightly differ, therefore load flow results are not exactly the same, and also the SDC controllers' tuning differs as well. Based on sensitivity analysis, it is found that a gain of G=10 pu and time constant of T=0.01 s gives a good damping performance. The difference in the tuning of SDC, can also be explained by the different time-step solver of the two tools (0.01 seconds for RMS/ 50μs for EMT).

The tuning of the time constant T of the washout filter can be done by using conventional techniques like Bode analysis. By applying such techniques, for instance, ([57], page 246) suggests that the corner frequency (1/T) should be chosen around one decade below the frequency of the electromechanical oscillation to be mitigated. Other references, like for instance [44], have shown that a considerably smaller value of washout time constant, T may be chosen to prevent adverse impact on the damping of control modes (associate to governor systems) or torsional modes. The tuning of the gain of the SDC can be done by using root locus or eigenvalue calculation. Due to the boundaries of the wind generator model used in PowerFactory, it is not possible to perform the calculations to obtain the state-space representation needed for root locus or eigenvalue calculation. Hence, the gain of the SDC was chosen for the 9 Bus System, via parametric sensitivity. It is stated that for multi-machine systems, as the GB one described in Section 2.2.4, a method based on the maximum angle difference indicator, is employed so as to define universal parameters for all the washout filters utilized. Chapter 5, is based

on optimization techniques which enable individually tuning of the controllers.

Since in this case only two synchronous generators exist in the system, the problem of selecting the input signal (i.e. rotor angle deviation) for the supplementary damping controllers is relatively straight-forward. The synchronous generator G1 is the reference (slack) generator of the system, so the reference angle of the system is the angle of G1. Thus, the rotor angle deviation that will be fed into the supplementary damping controllers is the rotor angle variation of G2 with respect to the rotor angle of G1. To illustrate the influence of the supplementary damping controllers on the overall rotor angle stability of the system, three phase faults with duration of 120 ms, are applied at different buses of the system.

Figure 4.2 corresponds with the case when three phase faults occur in the vicinity of the wind generator locations (i.e. faults at buses 7, 8, 9). Note from these figures that the supplementary damping control ensures fast damping of the rotor angle deviation between G1 and G2 (i.e. Rotor Angle Deviation = δ_2- δ_1), thus, wind generators effectively support the synchronous machines of the system to manage instantaneous variations of the electrical output power, cf. Figure 4.2(d) vs Figure 4.2(e). The supplementary damping controllers also help in reducing the amplitude of the frequency deviation due to the variation of the active power balance during and after the fault, cf. Figure 4.2(a) vs Figure 4.2(b). Note also in Figure 4.3 that when SDC is applied, WGs support transient stability by modulating their sharing of the load (i.e. injecting active power that is in antiphase with the active power injected by SGs) so as to best decrease the rotor oscillations.

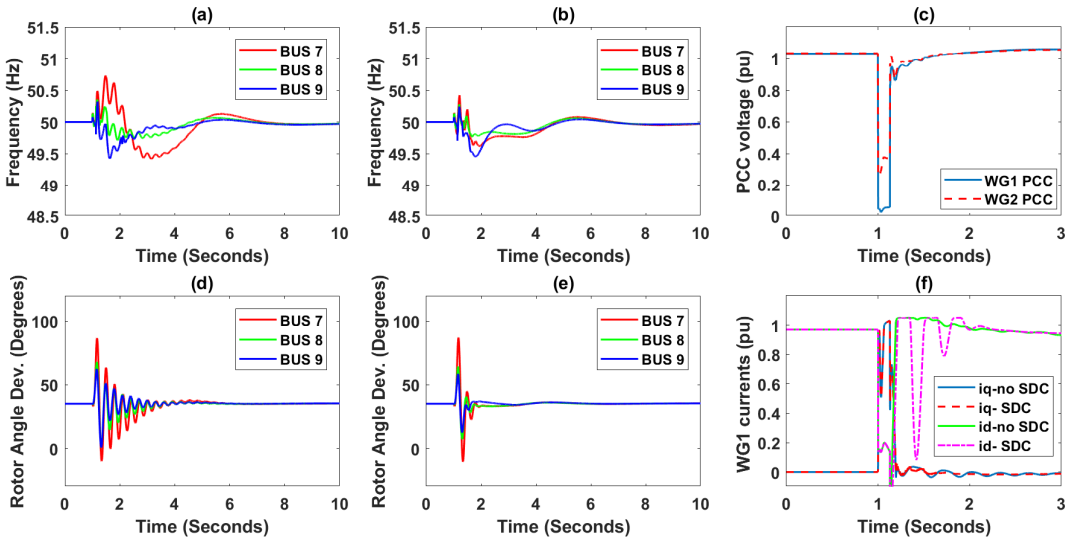

Figure 4.2: Faults implemented in the proximity of the wind turbines a) frequency response without SDC connected, b) frequency response with SDC connected, c) voltage drop in the WGs PCC voltages for BUS 8 fault, d) rotor angle deviations without SDC, e) rotor angle deviations with SDC, f) WG1 currents after BUS 8 fault

Figure 4.4 corresponds with the case when the three phase faults occur far from the wind generators (i.e. faults at buses 4, 5 and 6). Note in Figure 4.4(a) that the frequency deviation in this case is higher, which is attributed to the fact that the faults occur close to the main load centers, and, the biggest synchronous generator of the system (i.e. G1) has to suddenly cope with the active power imbalance, highly exciting its dynamic behavior. However, as shown in Figure 4.4(b), the SDC attached to the wind generators helps to significantly reduce the frequency excursions. The supplementary damping control ensures fast damping of the rotor angle deviation between G1 and G2, cf. Figure 4.4(d) vs. Figure 4.4(e).

Comparing Figure 4.2(e) and Figure 4.4(e), it can be seen that the decrease of the amplitude of the first swing of the rotor angle deviation is more significant when the fault is located far from the wind generators (i.e. fault at buses 4, 5, or 6). As shown in Figure 4.2(c) (in contrast to Figure 4.4(c)), when the fault is located close to the wind generators (i.e. fault at buses 7, 8, or 9), the voltage magnitude at the PCC decreases prominently, so the wind generators have to inject more reactive current, which affects the available margin for modulation of the active current injection, thus reducing the degree of

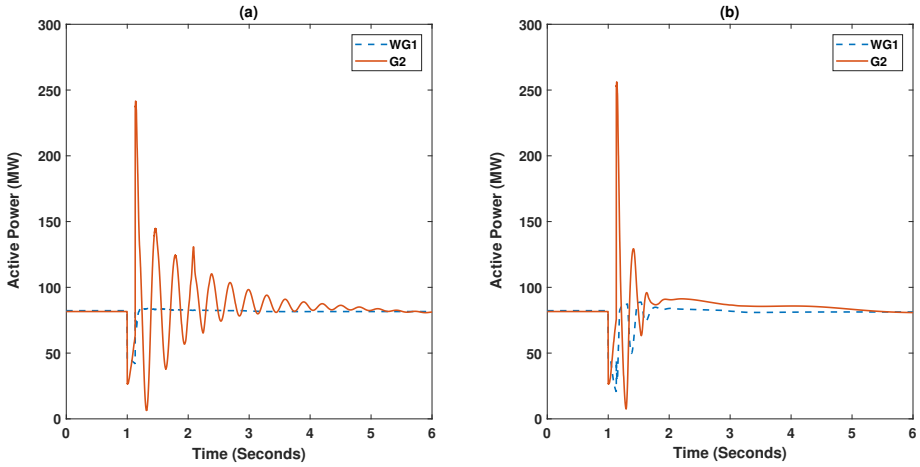

Figure 4.3: Active Power of SG2 and WG1: a) without SDC, and b) with SDC when a fault at bus 8 for 120ms is implemented. 3 phase fault at BUS 8 (cleared after 120 ms)

effectiveness of SDC, cf. Figure 4.2(f) vs Figure 4.4(f).

When the SDC controller is enabled, then it provides an antiphase oscillation, by injecting some extra energy. The main objective of the damping controller is to have a small injection of energy during the SDC acting time, so as the operator not to be affected in a negative manner in terms of it's revenues.

In Figure 4.5(a) and (b) the active power outputs of the wind generators are presented, comparing the dynamic response when the wind generators operate with and without SDC. A three-phase fault of 0.2 ohms is implemented at Bus 8 with a duration of 120 ms. By comparing the area of each of the two curves, the additional energy coming from the stored energy of each wind generator can be estimated. Thus, trapezoidal numerical integration was used to find the time integral (i.e. the wind generators' additional energy) within the window from the time of occurred of the fault (e.g. from 2 s in Figure 4.5). It was found that WG1 needs to additionally inject energy of approximately 10.26 MWs, whereas WG2 needs to additionally inject energy of approximately 10.89 MWs. Since there is no DC link nor battery in the RMS model of wind generator type 4 (used in PowerFactory), the additional energy is retrieved from the kinetic energy of the wind generators (represented in the model by a single mass model [67]). In the RMS model of the generic test case 2, WG1 is an aggregated model of 35 smaller wind generator units, while WG2 consists of 36 wind generator units. Each of the small wind generator units has an active power injection of 2.35 MW, and the combined mass moment of turbine and generator is H=1.5 s. This entails that the total plant WG1 has stored energy of (1.5 s $\cdot$ 2.35 MW) $\cdot$ 35 units = 123.39 MWs. In addition, WG2 has stored energy of (1.5 s $\cdot$ 2.35 MW) $\cdot$ 36 units = 126.90 MWs. Therefore, the wind generators provide almost 8% (e.g. 10.26 MWs out of 123.39 MWs for WG1, 10.89 MWs out of 126.90 MWs for WG2) of their stored energy to help in mitigating the oscillation of the synchronous generators. As shown in [73], this extra energy can be provided without tearing the mechanical parts of the wind generator nor oversizing the VSCs used of the wind generator type IV. In terms of the cost of the service, according to [86], in sites with medium wind speeds, the cost of wind energy is nearly 7 cents of euros/ KWh. This accounts nearly for 20 cents per wind plant (i.e 7cents $\cdot$ 10.26 $\cdot$ 10^3 KW $\cdot$ s /3600 KW $\cdot$ s). It can be understood that the cost of service, is negligible comparing to the annual revenues of the plant, even if the controllers need to be activated several times throughout the year. When the wind generators operate below rated power, the amount of extra energy needed to ensure effective modulation of the active current injection by SDC will be higher. To achieve this amount several options have been reported in existing literature, for instance, addition of batteries [74], or increasing the DC voltage level (done by either increasing the rate of the VSC converters or by increasing rating of the capacitor connected to the DC bus) of the back-to-back interface of the wind generator type IV [75]. The dimensioning of the battery or the oversize of the design parameters of the back-to-back converter requires a sophisticated approach (e.g. based on probabilistic methods [76]) to properly account for the level of variability of the generator active power output as affected by stochastic wind speed variations. This topic is suggested for future research.

However, in general, it is noted that repeated overloading of under sized inverter when delivering

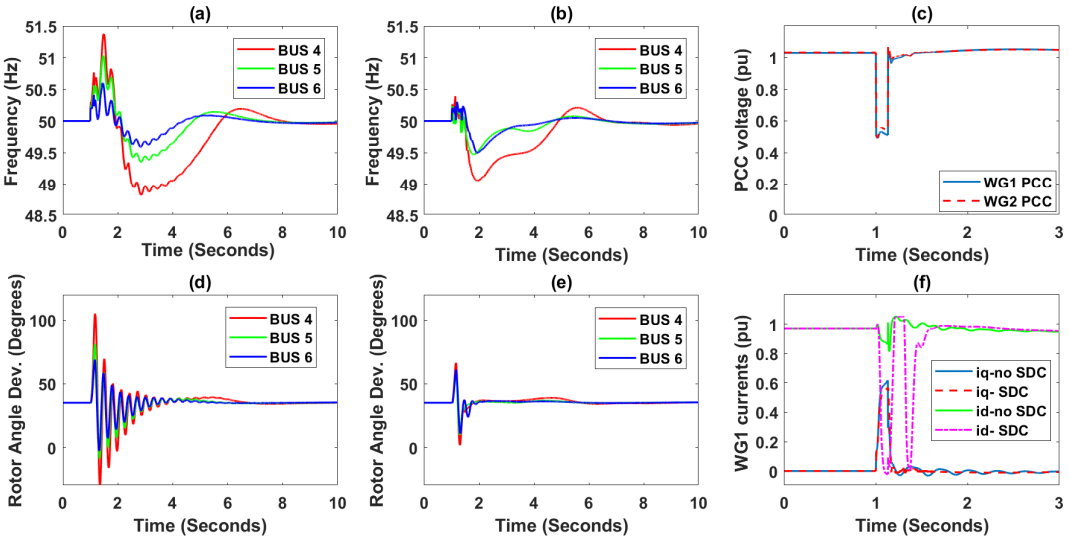

Figure 4.4: Faults implemented far from the wind turbines a) frequency response without SDC connected, b) frequency response with SDC connected, c) voltage drop in the WGs PCC voltages for BUS 5 fault, d) rotor angle deviations without SDC, e) rotor angle deviations with SDC, f) WG1 currents after BUS 5 fault

high starting surge power may result in premature failure of the inverter and the load. However, as mentioned in the controllers, a limit of 1.1 pu is applied for the outer current references. According also to manufacturers, surge capacity of converters may vary from as little as 20% to as much as 300%. In general, for wind generator applications, high frequency inverters are employed, (e.g. typical manufacturers: Statpower, Exeltech, Power to Go e.t.c), which are typically from 25% to 50% maximum overloaded. It is therefore understood, that the 10% extra reference current limit set, is lower than the maximum permitted, so no oversizing is needed. The fact that, smaller surge power limits are achieved for high frequency inverters, is mainly attributed to the fact that small transformers are utilized.

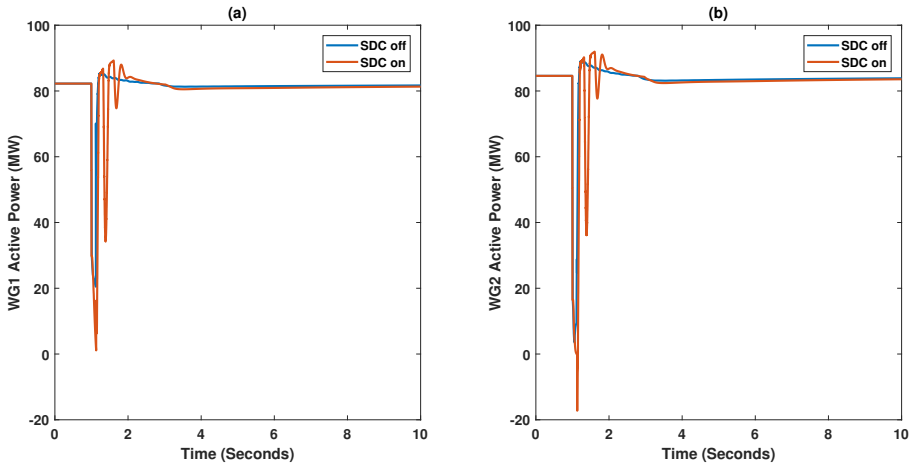

Figure 4.5: Active Power of a) WG1 and b) WG2 with and without SDC when a fault at BUS 8 for 120ms is implemented

The computed values of theoretical maximum FCT for each fault location are shown in Figure 4.6, in which the resulting theoretical maximum FCT results when the wind generators operate without and with SDC, are compared. Following common practice in stability studies, protection devices were not modelled in the system. Overall, SDC can lead to an appreciable increment of the FCT value, which depends on the fault location. Besides, as indicated in Figure 4.6 (text within some bars), the theoretical maximum FCT value may be bounded by the resulting magnitude of frequency deviation,

which should technically be confined within a pre-defined limit (e.g. 47.5 Hz in continental Europe [77]). For instance, note in Figure 4.6 that when SDC reacts following a three-phase short circuit fault at BUS 4, the theoretical maximum FCT is 250 ms, in which the extreme situation of being at the allowed frequency deviation limit can still be hold. The bars of Figure 4.6 without any text indicate that the theoretical maximum FCT is only bounded by the reaction of out-of-step protection. Additionally, if the fault is applied at BUS 7, then WG and SG are isolated electrically, and the WG cannot transmit the anti-phase active power that is needed. Also the contribution of the other WG is less important since it is far from synchronous generators. In summary, SDC can help to extend the large disturbance rotor angle stability margin, and the selection of a desired theoretical maximum FCT should also contemplate the fulfilment of the allowed frequency deviation limit.(It is mentioned that the out-of-step indication, when no frequency limits are violated, is observed when the rotor angles between two synchronous machines are apart 180 degrees. In that situation it can be understood that the maximum FCT is an equivalent of critical clearing time CCT.) From the aforementioned analysis, the SDC control contributes not only to the rotor angle damping enhancement, and it also can improve the synchronizing power (enhancing the CCT). An explanation for the synchronizing power enhancement can be given with the aid of Figure 4.2 (f). During the fault, when SDC is employed, due to the washout-filter, the id current will face a spike downwards immediately from the occurrence of the fault. This action counterbalances the active power imbalance of the system caused by the fault, thus, contributing to reduce the active power imbalance experienced by synchronous generators. In this way, the magnitudes of the rotor angle and speed excursions are considerably less, even in the first swing.

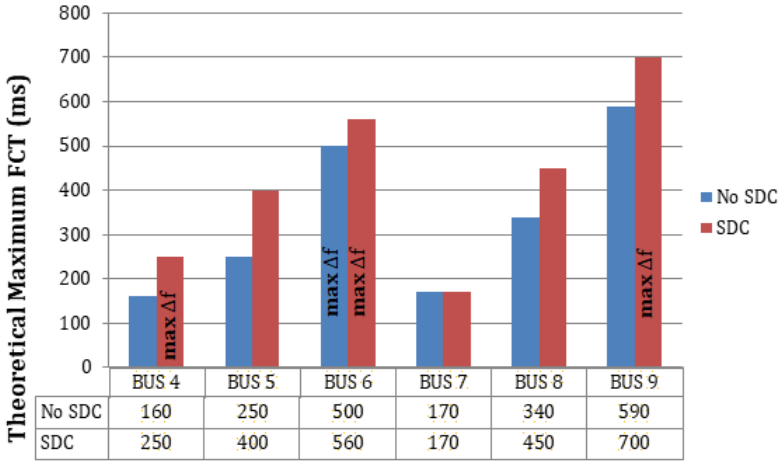

	BUS 4	BUS 5	BUS 6	BUS 7	BUS 8	BUS 9
No SDC	160	250	500	170	340	590
SDC	250	400	560	170	450	700

Figure 4.6: Theoretical maximum FCT for different faults locations in the IEEE 9 Bus System when WGs are considered with and without SDC

The synthetic model of the GB system in PowerFactory is used in the remainder of this section to elaborate on two important aspects concerning the addition of SDC on wind generators to support large disturbance rotor angle stability in a multi-machine system:

- Location of SDC in selected wind generator locations: According to literature, for instance [78]-[79], the problem of SDC location can be analytically tackled by computing metrics of controllability, which are derived from the state-space representation of the differential-algebraic equation system that describes the dynamic behaviour of an electrical power system. However, due to the boundaries of the wind generator model used in PowerFactory, it is not possible to perform the calculations to obtain the state-space representation.
  As an alternative, the problem of SDC location is tackled here based on analysis of time domain simulations performed in PowerFactory. As shown with a small-size test system in Appendix H, the wind generators placed close to the synchronous generators that are prone to loss of synchronism when large disturbances occur, should be equipped with SDC to contribute effectively to enhance the large disturbance rotor angle stability performance of a power system.
- Selection of the input signal of SDC: The problem of input selection for SDC can be analytically

tackled by computing metrics of observability [79]-[80], which are also derived from the state-space representation of the differential-algebraic equation system that describes the dynamic behaviour of an electrical power system. However, due to the boundaries of the wind generator model used in PowerFactory, it is not possible to perform the calculations to obtain the state-space representation.
As indicated, the rotor angle deviations of the machines are used as inputs of the SDC. That means that for each SDC to be added in a particular wind generator, the rotor angle measurement associated to a given nearby synchronous generator with respect to a reference rotor angle is used as input.
As shown in Appendix H with a small-size test system, the reference rotor angle is referred to the synchronous generator with largest inertia that is relatively distant from the wind generators to be equipped with SDC. Besides, Appendix H provides an illustration that better large disturbance rotor angle stability performance is achieved when using remote rotor angle signals as input (which allow capturing larger relative angle deviations) to the SDC, when compared to the case in which local signals in the vicinity of the wind generator are used. The findings provided in Appendix H are in line with the conclusions drawn in related studies [69], as mentioned before.

4.4. Study case II: GB System

Great Britain Transmission System, is also examined, for the SDC controller's effectiveness examination, when many Synchronous Machines and Wind Generators are involved. Two wind share levels are examined as shown in the following two subsections; a 66% wind share scenario is first examined, whereas after, a 75% wind share scenario is after tested.

4.4.1. 66% Wind Share Case Scenario

The synthetic model of the Great Britain system was examined to further study the effectiveness wind generators with SDC. In particular, the Gone Green Scenario of 2030 [39]. This scenario corresponds with 66% wind generation share. The values of nodal load and generation dispatches can be found in Appendix J All synchronous generators are equipped with power system stabilizers. The diagram of the Great Britain system, highlighting the locations of wind generators and nearby synchronous generators is shown in Figure 4.7 below.
The wind generators that are equipped with SDC are listed in Table 4.1. These generators are electrically close to the synchronous generators in different control zones (cf. Figure 4.7) of the synthetic model of the Great Britain system. The parameters of the SDC are T=0.01 s, G=50 pu. The parameters were selected based on a selectivity analysis implemented via Python. The objective is to find the parameters of the washout filters, tuned in an universal manner, so as to achieve the maximum value of the maximum rotor angle difference among all the pairs of the system. The drawback of this method, is that the controllers are not treated individually and furthermore, not the whole transient time span is taken into account, since the maximum angle is associated with the first 1-2 seconds after the fault implementation. More information of the tuning based on this stability related KPI is given in Appendix I. Based on this analysis gains of 50 pu for all the WGs lead to efficient damping for the SGs connected to the GB system. The values are according to guidelines and reference values provided in [44].

The input signal of the SDC of each wind generator is selected as the relative rotor angle of a nearby synchronous generator which is sensitive to large rotor angle excursions when a large disturbance occurs. The relative rotor angle is synthesized from the difference between the measured rotor angle of the synchronous generator and a reference angle. The reference angle used to measure the relative rotor angle deviations belongs to the synchronous generator SG11, which is located in zone 11.

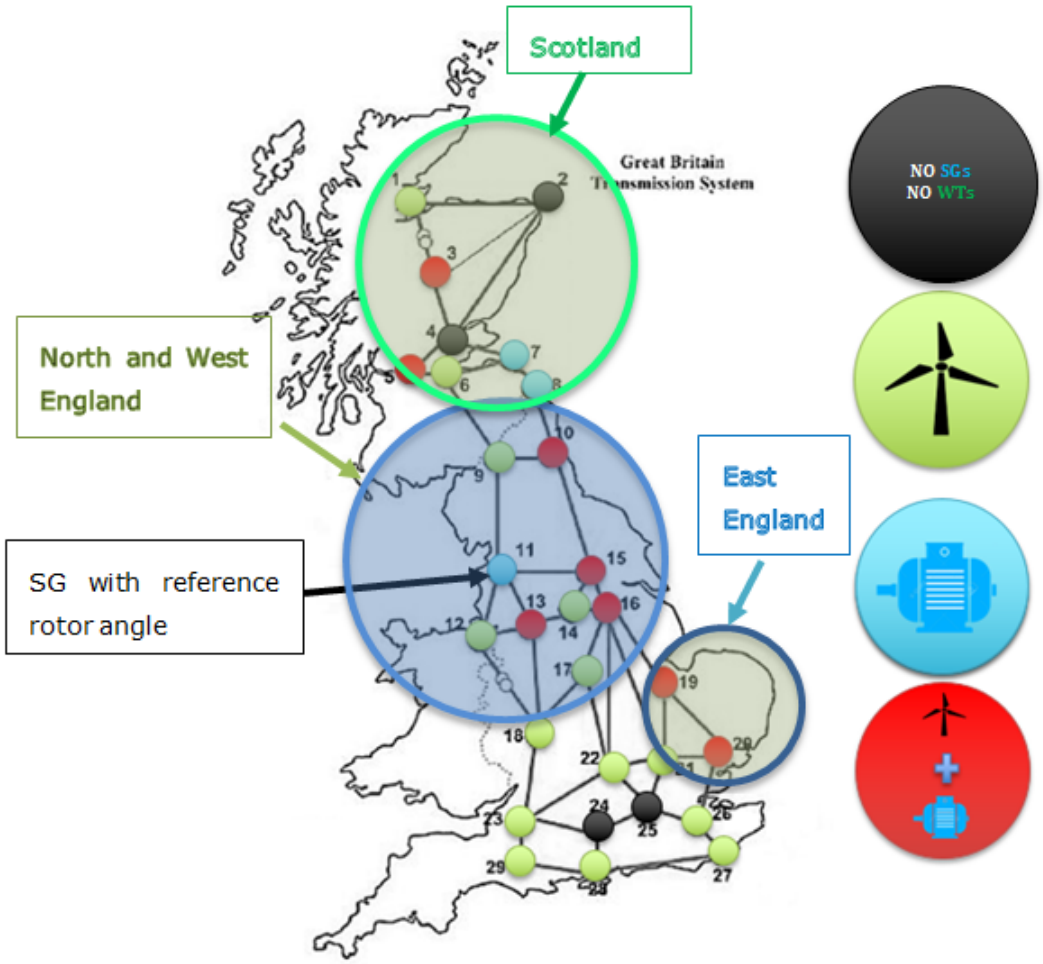

Figure 4.7: Geographical spread of conventional power plants with only synchronous generators (points with blue colour); only wind power plants (points with green colour) and zones with combined power production (points with red colour), in the synthetic model of the Great Britain system. The location of generator that serves as reference for relative rotor angle position is indicated with the black arrow.

Table 4.1: WGs equipped with SDC for the 66% wind share scenario

WG	Reference SG Angle	Measured SG Angle
WG3 (SCOTLAND)	SG11	SG3
WG5 (SCOTLAND)	SG11	SG5
WG10 (NORTH ENG)	SG11	SG10
WG16 (NORTH ENG.)	SG11	SG16
WG13 (WEST ENG.)	SG11	SG13
WG15 (WEST ENG.)	SG11	SG15
WG19 (EAST ENG.)	SG11	SG19
WG20 (EAST ENG.)	SG11	SG20

This selection is due to the fact that SG11 is the least sensitive synchronous generator to high rotor angle excursions caused by large disturbances. This is attributed to the fact that G11 belongs to a cluster of generators with high inertia, and is far from other control zones that are sensitive to oscillations caused by large disturbances. For the sake of illustration, it is worth to mention that the inertia constant of the synchronous generators 10, 11, 13, 15, and 16, is 7 seconds, whereas it is 2 seconds for synchronous generators 3, 5, 7, 8, 19, 20. In addition, control zone 11 is the only one that

exclusively comprises synchronous generation (no wind generation in this zone).

Before starting analyzing the time domain performance of the system under different fault scenarios, the modifications made in the GB system, itself are mentioned. When the GB system was tested for the first time, it was observed that it was designed to be very stable. For instance, the average Critical Clearing Time (CCT) for different faults performed was about 1 second. In order to reflect real values of CCT in a better way, some changes were implemented in the transmission system. First, the inertia constants of the machines were set as defined in the previous paragraph. The ones that are of 7 seconds, initially they had constants of 9 seconds, while the ones with 2 seconds inertia value, initially had 3 seconds inertia. Additionally, in order to make the system more unstable, Static Var Compensators were set out of service, in all over the power system's hubs. Furthermore, in order to make the system in Scottish area, a little more unstable, Line 6-9a was changed from having two parallel segments into one segment. The same also modification, was performed for lines Line7-8a and Line7-8b. Last, the nominal apparent power of synchronous machines G3, G5 and G7 was changed from 108 MVA, 100 MVA and 93 MVA, to 100, 94 and 90 MVA respectively, whereas the LVRT gain of WG in zone 1, was reduced from κ=2 to κ=1, because as explained in Appendix E, LVRT also influences positively transient stability when the gain κ is relatively big.

From time-domain simulations with faults applied in different locations, it was found that the Scottish area is the more prone to instability area of the system. A three-phase fault applied at BUS 5 at time t=3 seconds, with Fault Clearing Time (FCT) of 120 ms, is first tested, with and without the SDCs used in the WGs as described in Table 2.3. As seen in Figure 4.8, the contribution of the SDC in the machine that the fault occurs (i.e. SG5) is negligible. This is reasonable, since as described previously in the Section 4.3, when the fault is performed in the terminal of a specific SG, then, during the fault, the WG active power modulation is limited by the action of the FRT function, and, therefore, it cannot influence the power transfer from the SG (indirectly reflected in the phase of the voltage at the terminal in which the SG is connected to), so the damping is ineffective. As seen in Figure 4.8, we do not have either improvement or deterioration of machine's 5 dynamics. This observation will be reflected also in the theoretical maximum FCT graph in Figure 4.13 below.

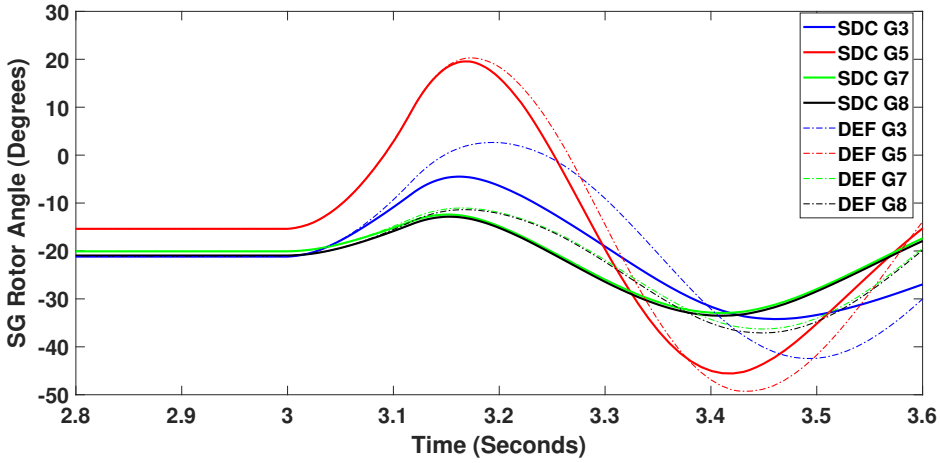

Figure 4.8: SDC performance when fault is performed in the Scottish area - Fault at Bus 5, FCT of 120 ms. Scottish Area Rotor Angles when SDC is applied (solid lines) and when SDC is not used (dashed lines)

It can be concluded that since SG located in the Scottish area are the most vulnerable machines, then the closer the fault implemented in Scottish Area, the higher the excursions of the angles of these machines, and the higher the instability risk. In that sense, since the critical faults are of interest, faults at BUS 9 and Line 6-9 were tested. The results are depicted in Figure 4.9 and Figure 4.10, respectively. It can be concluded, that the first swing oscillations are mitigated, and the transient stability of the system is improved for the aforementioned faults, comparing to the case in which only the typical LVRT was employed. It is also observed that the better damping is achieved in the Scottish and East England Areas of the GB system and this is in line with the observations from the simulations of the study case presented Appendix H, in which it was shown that the higher the impedance (i.e. the bigger the distance) of the WG equipped with SDC with respect to the reference machine, the better the damping

caused by the WG equipped with SDC. The reference machine is generator 11, located in the centre of the map (see Figure 4.7), whereas Scottish and East England Areas are located far from the reference machine.

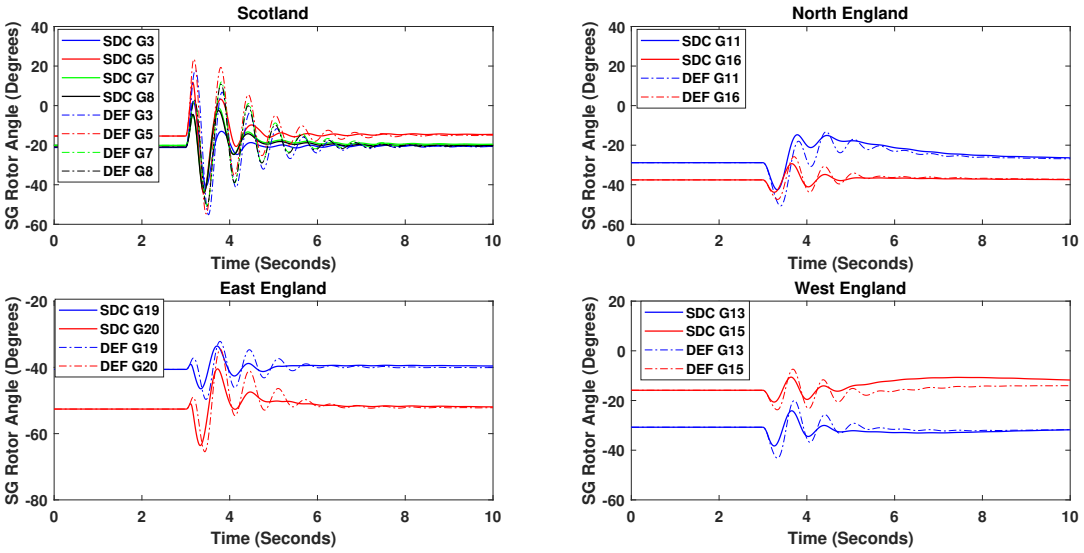

Figure 4.9: 66% share of wind generation in GB system, year 2030. SGs' Rotor Angles for a 120 ms three phase fault at Bus 9. Solid lines- WGs with SDC, dashed lines- WGs without SDC

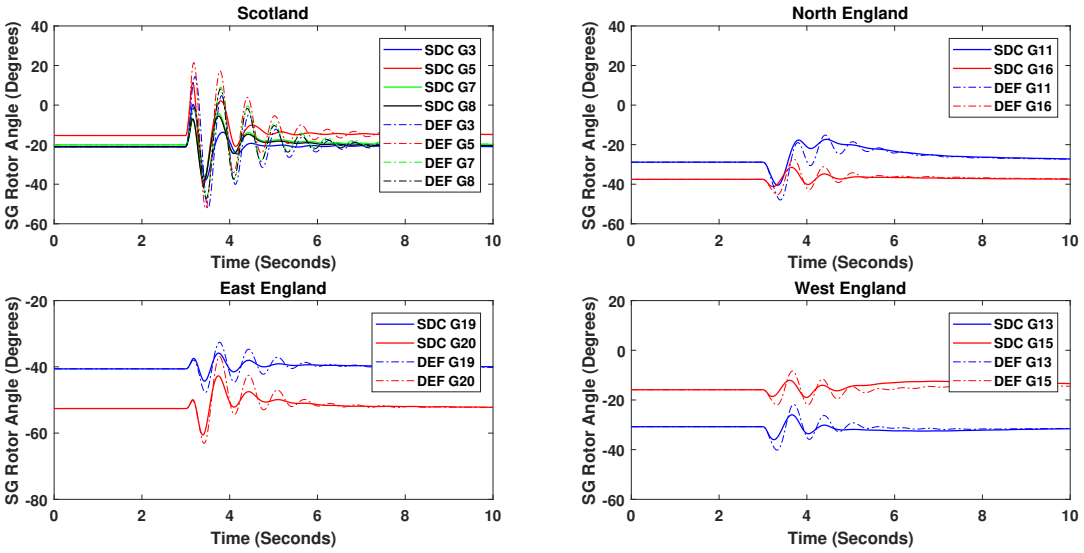

Figure 4.10: 66% share of wind generation in GB system, year 2030. SGs' Rotor Angles for a 120 ms three phase fault at Line 6-9. Solid lines- WGs with SDC, dashed lines- WGs without SDC

Figure 4.11 visualizes the active power injections of all the SGs when the same fault is applied at Line 6-9 with FCT of 120ms. Better stability is observed for all the machines in the system, when the damping control is used. Besides, improvement of the system frequency (as observed in the machines' speeds) is illustrated also in Figure 4.12.

Figure 4.13 shows, for 66% share of wind generation in the synthetic model of the GB system, the theoretical maximum FCT values, computed with and without SDC for different fault locations. (It is mentioned, that for the GB system, the FCT for all the faults tested is equivalent to CCT and this is the time when the rotor angles of two machines are set apart for 180 degrees.) It is observed, that the

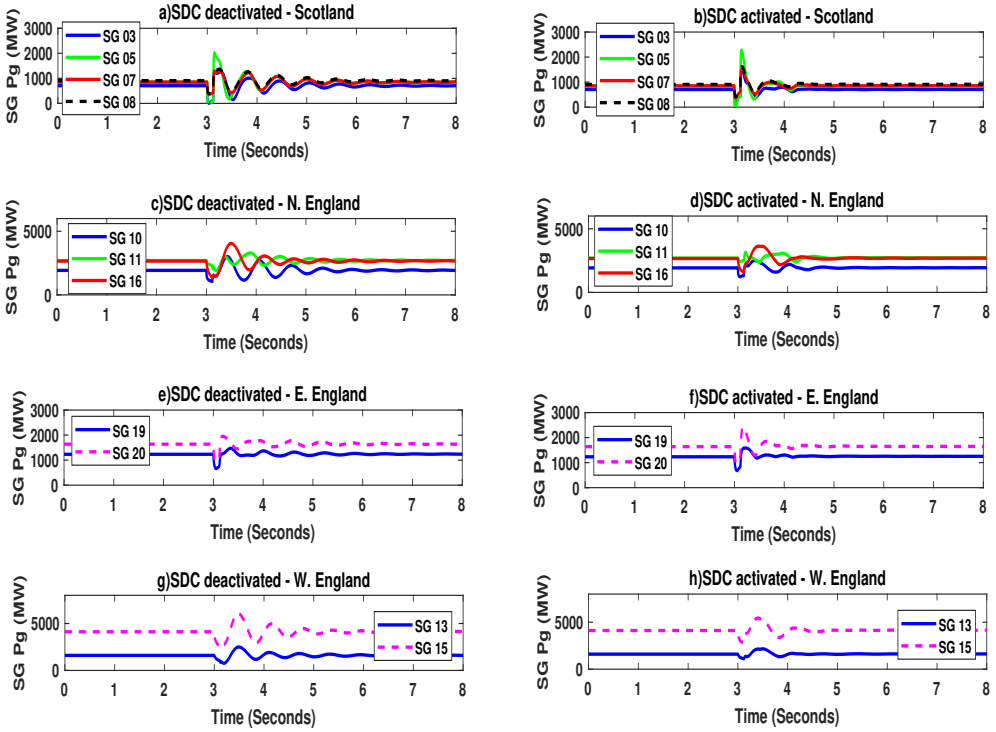

Figure 4.11: 66% share of wind generation in GB system, year 2030. Active Powers of synchronous generators (per control zone) for a 120 ms three phase fault at Line 6-9 (FCT: 120ms) with and without SDC.

theoretical maximum value of the FCT is low when SDC is not used, and it is slightly higher when the faults occur far from the Scottish area. In all the faults, SGs located in Scottish area were the first that were going out of step when the FCT was increased beyond the values indicated in Figure 4.13.

Note also in Figure 4.13 that, when all WGs of the GB system perform SDC, higher FCT values are obtained when increasing the distance of the fault from the Scottish Area. This is because the voltages in the vicinity (Scottish area) of the WGs do not drop significantly when the fault is distant, so the WGs in the Scottish area have enough margin to modulate the active power injection, thus supporting the SGs of the Scottish area more effectively.

4.4.2. 75% Wind Share Case Scenario

A modified GB system was tested with 75% share of wind generation. Appendix J, shows the decrement (w.r.t. 66% share of wind generation) of installed capacity of synchronous generation vs the increment of the installed capacity of the wind generation per region of the synthetic model of the GB system. The increase of installed capacity of wind generation was implemented by adding more WGs in parallel. Additionally, some units of SGs have been set to be off-line in the generation dispatch for 75% compared to the 66% case. Hence, the list of WGs equipped with SDC given in Table 4.1 is also used in 75% share of wind generation. To evaluate the transient stability performance of the system in relatively similar conditions of loading of synchronous generators, the dispatches of all generators were adjusted such that the loading of the remaining synchronous generators in 75% share of wind generation is similar to the loading of synchronous generators in 66% share of wind generation.

Figure 4.13, depicts the theoretical maximum FCT that can be achieved without losing transient stability. Observing Figure 4.13, the term “all“ is used to indicate that all the WGs mentioned in Table 4.1 for the 66% wind share are also equipped with SDC for the 75% wind share. A case scenario for the 75% share with less WGs equipped with SDC will also be examined in this subsection.

By comparing Figure 4.13 and Figure 4.14, it can be seen that in the case that no SDCs are used, the FCT values in 75% share of wind generation are relatively similar to the values in 66% share of wind generation. Note also in Figure 4.14, that when all WGs of the GB system perform SDC, higher

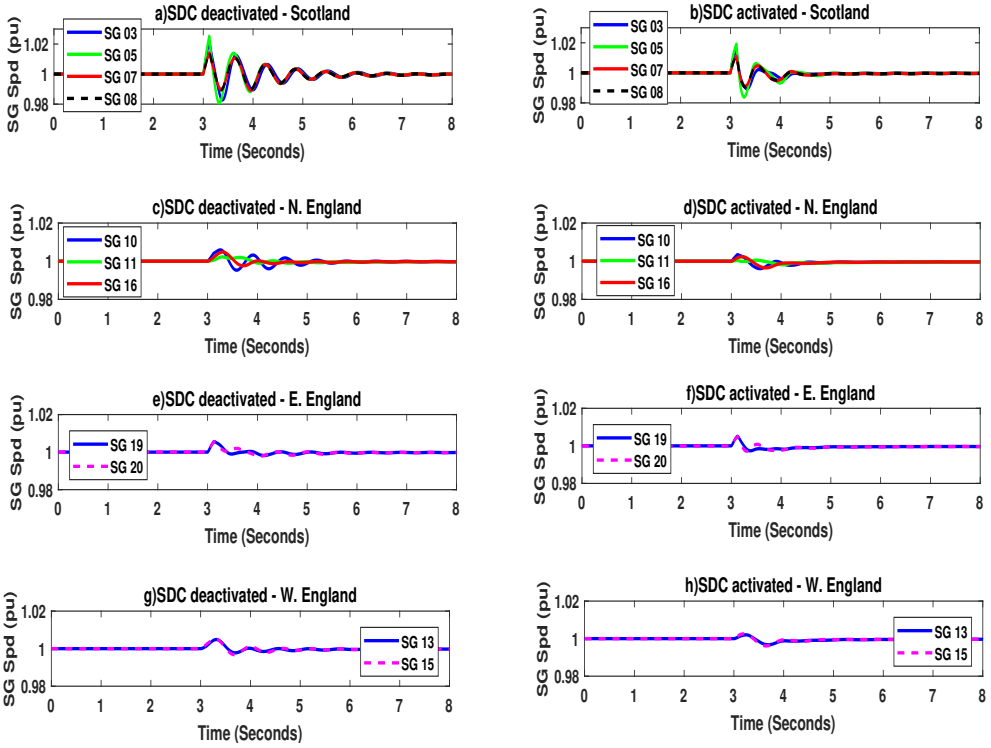

Figure 4.12: 66% share of wind generation in GB system, year 2030. Speeds of synchronous generators (per control zone) for a 120 ms three phase fault at Line 6-9 (FCT: 120ms) with and without SDC.

FCT values are obtained with larger distance of the fault from the Scottish Area (cf. similar findings in Figure 4.13). The FCT values obtained by using WGs with SDC in 75% is relatively higher than the FCT values obtained in 66%, due to the increase of installed capacity of wind generation, which entails more resources for fast active power support.

Furthermore, as shown in Appendix K, for the case of 75% share of wind generation in the synthetic model of the GB system, the degree of increase of the theoretical maximum FCT will depend if SDC is implemented in all wind generators of the system or only in wind generators within a transient stability vulnerable area. Concretely, Appendix K shows that the achievable reduction of amplitude of the first swing of rotor angle oscillations and the increase of damping is nearly the same (similar value of FCT) for faults occurring close or far from a transient stability vulnerable area (e.g. Scottish and East England area), when only WGs within the vulnerable area perform SDC vs the case when all WGs in the system perform SDC. This entails that increasing the number of WGs with SDC should be done only if significantly higher FCT values are of interest; approach however bounded by the need of communication infrastructure for acquiring the measurements for every WG with SDC. For the following analysis in this chapter SDC equipped WGs are located only to the Scottish and East England areas.

By considering one critical fault (120ms three phase fault at Line 6-9), Figure 4.17 illustrates the implications associated to the duration of the reaction of the SDC attached to wind generators of the Scottish control zone. As indicated in Section 3.2.3, a timer is added at the output of the washout filter of the SDC in order to activate and deactivate the SDC. The activation is done when the LVRT function is triggered. Exiting literature suggests that the deactivation time can be in between 3 -10 s [57], [81], [3]. Following the suggestion in ([81], page 462): “The time of interest for large perturbations stability ranges from 3 to 5 s and may extend to 10 s for very large power systems with weak interconnections between remote generator”, the deactivation time was initially set to 10 s to investigate if unwanted noise or high frequency oscillations are excited in the condition of 75% share of wind generation. Figure 4.15(a) and Figure 4.15(b) correspond with the case when 10 s is considered for deactivation of SDC. Note in these figures that sub-synchronous oscillations (with frequency around 5 Hz) are excited if the SDC lasts for 10 s. The reason is that the washout filter, if acting longer than necessary (i.e. active power modulation for extended period), may amplify the magnitude of local oscillations (e.g. frequencies

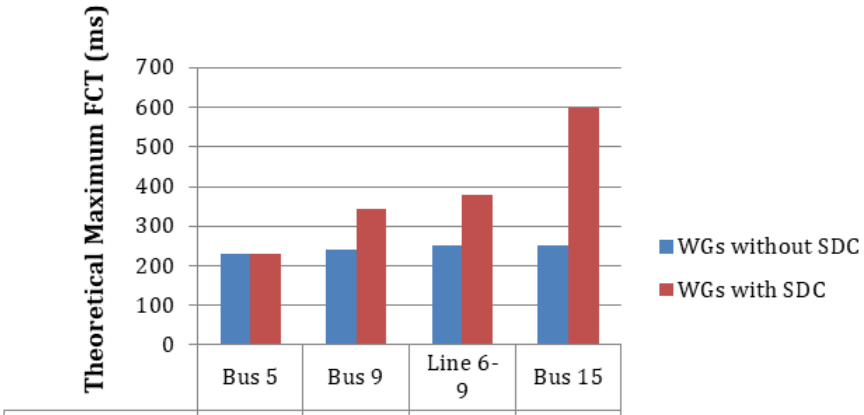

	Bus 5	Bus 9	Line 6-9	Bus 15
WGs without SDC	230	240	250	250
WGs with SDC	230	345	380	600

Figure 4.13: Theoretical maximum FCT for different faults locations in the synthetic Great Britain system with 66% share of wind generation.

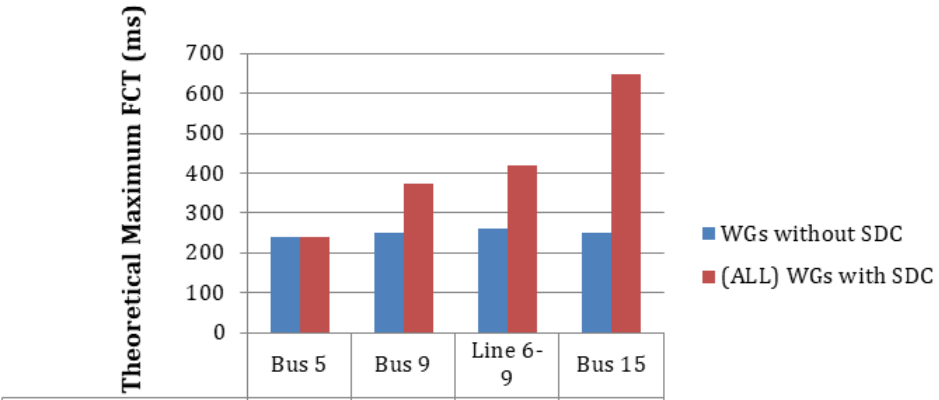

	Bus 5	Bus 9	Line 6-9	Bus 15
WGs without SDC	240	250	260	250
(ALL) WGs with SDC	240	375	420	650

Figure 4.14: Theoretical maximum FCT for different faults locations in the synthetic Great Britain system with 75% share of wind generation.

between 1-5 Hz) that are also excited by the occurrence of large disturbances. These harmonics, even of higher order than the inter-area that SDC focuses to reduce, can also be harmful for the power system; they can cause mechanical fatigue in the rotor shafts, load misoperation, increased copper losses, faulty operation of breakers and fuses, saturation on transformers e.t.c. Therefore, a re-tuning of PSSs of the remaining synchronous generators should be explored as one first possible mitigation measurement against this effect. Therefore, a reduction of the deactivation time of SDC should be considered in multi-machine systems with high share of renewable generation. The reduction of the deactivation time of SDC will depend on the dynamic properties of each system, the controllers' settings, as well as the type, location, and duration of a disturbance. Although being out of scope of this study, it is mentioned that a low pass filter may be integrated to pre-filter the input of the SDC to prevent the excitation of sub-synchronous oscillations as a consequence of the reaction of the SDC. Based on parametric sensitivity analysis, and as shown in Figure 4.15(c) and Figure 4.15(d), it was found out that a deactivation time around 1.5 – 4 seconds for all the WGs equipped with SDC will be necessary to prevent unwanted noise or high frequency oscillations in the synthetic model of the GB system.

An explanation of the medium frequency modes observed, can be also justified with the aid of Prony Analysis applied in the active power injection of the Synchronous Machines. In particular, a method based on the Yule–Walker algorithm is used as a signal processing mechanism so as to retrieve frequency data by offline time domain waveforms. To this aim, Power Spectral Density (PSD) is

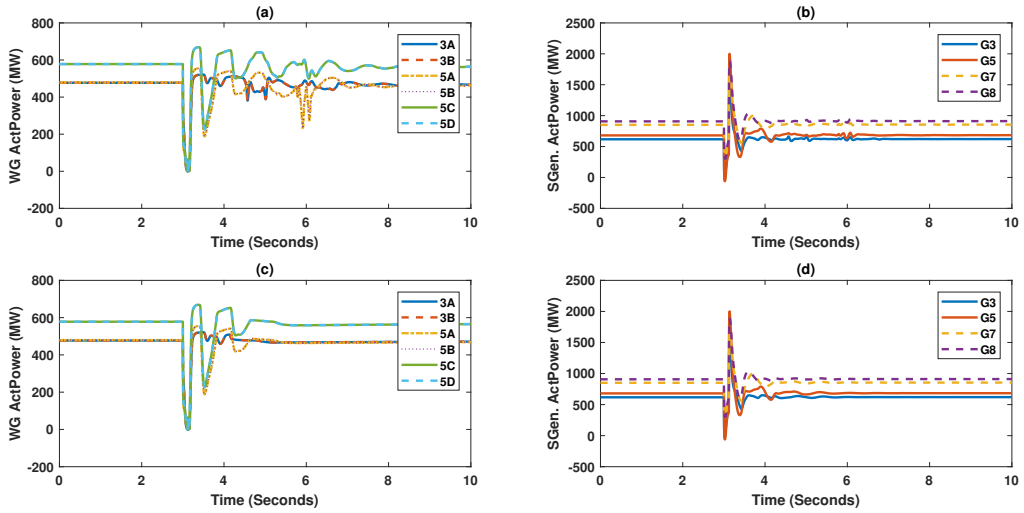

Figure 4.15: 75% share of wind generation in GB system, year 2030. Impact of the duration of SDC attached to wind generators in the Scottish control zone; 120 ms three phase fault at Line 6-9 applied: a) and b) SDC in the Scottish WGs, enabled for 10 seconds after LVRT triggers; c) and d) SDC in the Scottish WGs, enabled for 1.5 seconds after LVRT triggers

used which provides a visualization of the amplitudes of the modal frequencies present in the off line waveforms. Significant peaks in the PSD show dominant frequencies present in the measurements. For instance, in the PSDs of SG3 (see Figures 4.16), it is observed that the low frequency oscillations are mitigated when SDC is applied, something not observed with the medium frequency oscillations. In addition, when the acting duration of the SDC is also limited, it is observed that the controller does not introduce any medium frequency (around 5Hz) component enhancement. Moreover, in general, the medium frequency spectrum when the SDC acting time is small, is less comparing to the case in which the SDC acting time is high.

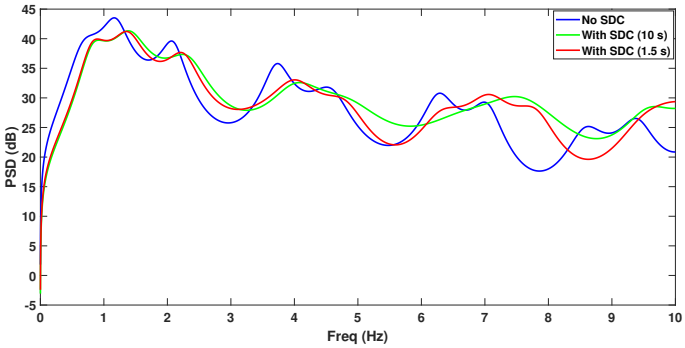

Figure 4.16: Yule–Walker PSD estimates for the G3 active power signal

Up to now, WGs with SDC were examined in the ideal case in which no time delay was considered. The impact of the communication and data processing delays was examined for the case of 75% share of wind generation of the GB system, when a three-phase fault of 120 ms occurs in Line 6-9. A first order transfer function was used to represent the delay (as also shown in Appendix H). Time delays up to 200ms are tested so as to have a good representation of a realistic Wide Area Monitoring System.

The rotor angles of the SGs, clustered by the areas they belong to, are visualized in Figure 4.17 – Figure 4.19. In these figures, it is observed that the achievable reduction of the magnitude of the first swing and the increase of oscillation damping becomes more limited with increasing time delay. Note also that, for the investigated maximum time delay, i.e. 200 ms, SDC still helps to ensure transient stability.

As is also shown in Appendix H, if the time delay is bounded around 100 ms or less, the impact of

the delay on SDC performance is less significant (e.g. closer to the case when time delay is neglected). From Figure 4.17 and Figure 4.18, it can be noticed that the effect of the time delay is more observable in the rotor angle responses of the synchronous generators of the Scotland and East England areas (which are prone to transient instability). In this example, the Scotland and East England areas are the only ones in which WGs perform SDC. From Figure 4.19 and Figure 4.20, the effect of the time delay on the synchronous generator belonging to the West and North England areas is considerably less noticeable, due to the fact that these areas have high inertia and the WGs of these areas do not perform SDC.

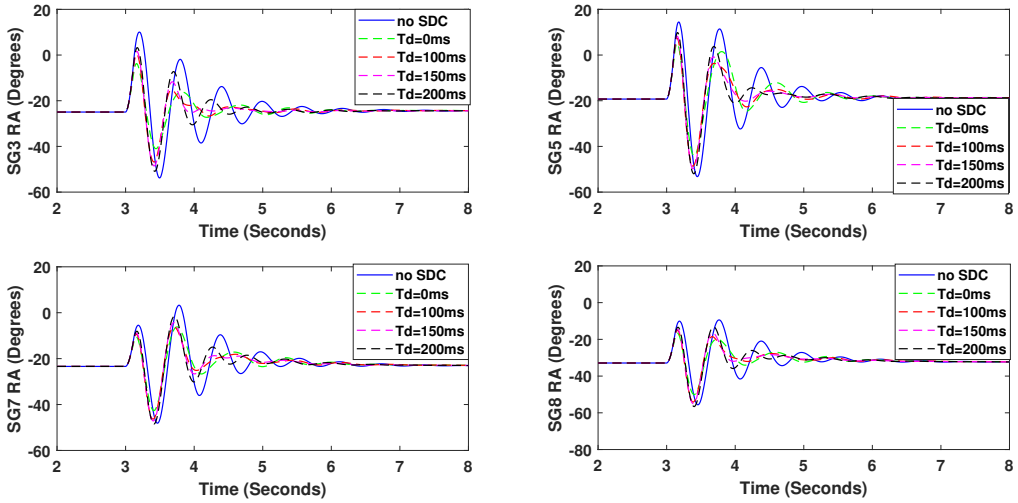

Figure 4.17: Dynamic response of rotor angles of Scotland area. Different time delays are considered when simulating a three-phase fault at Line 6-9 (75% share of wind generation in GB system). FCT=120 ms.

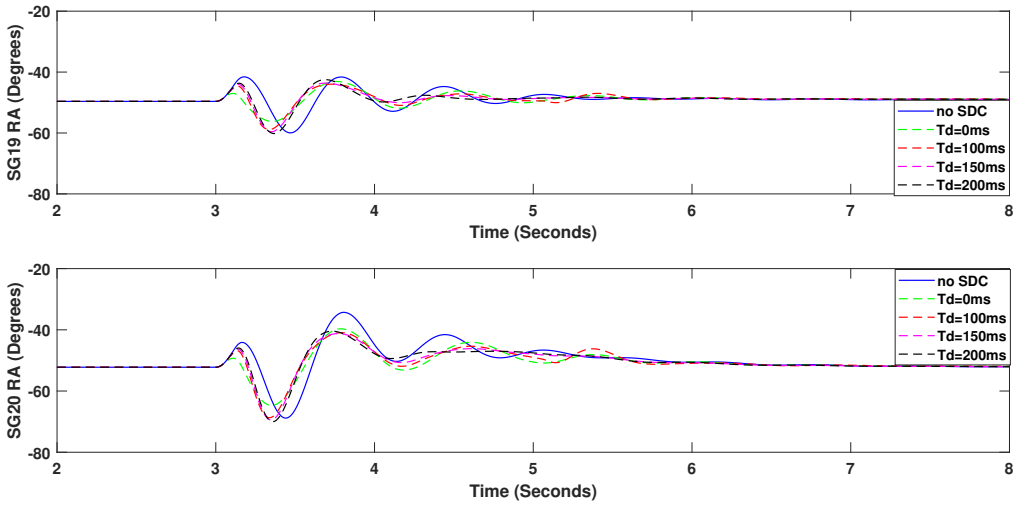

Figure 4.18: Dynamic response of rotor angles of East England area. Different time delays are considered when simulating a three-phase fault at Line 6-9 (75% share of wind generation in GB system). FCT=120 ms.

Last, in Figure 4.21, a comparison is performed between the remote signal described above, and other options with local signals given as inputs to the washout filters. For sake of comparison, no time delays nor phase compensation have been modelled in any of the simulations. Figure 4.21 shows that the use of rotor angle deviations as inputs of the SDC attached to WGs leads to effective reduction of the magnitude of first swing and a significant increase of oscillation damping. It is mentioned that δ_1 and δ_2 represent the rotor angles of two synchronous machines in the system, P_{SG} the active power

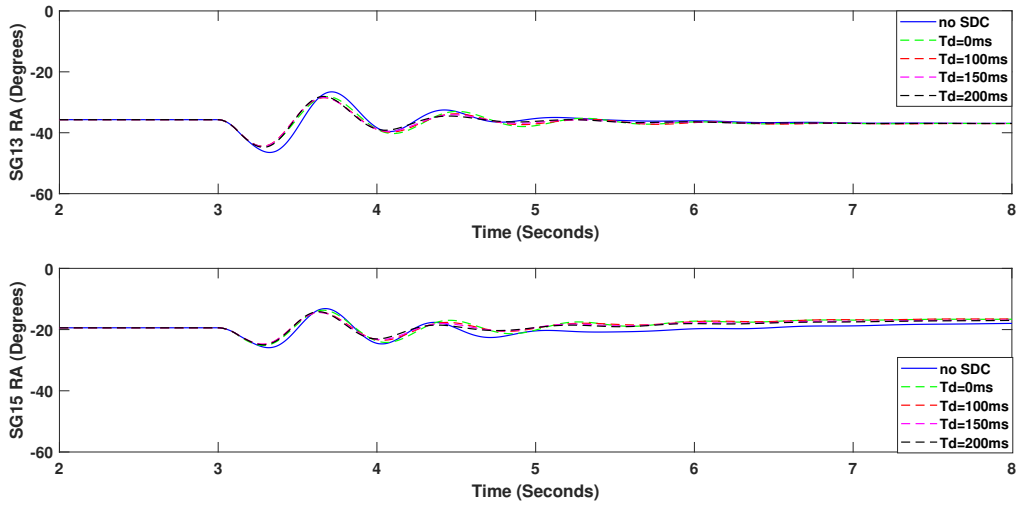

Figure 4.19: Dynamic response of rotor angles of West England area. Different time delays are considered when simulating a three-phase fault at Line 6-9 (75% share of wind generation in GB system). FCT=120 ms.

injection of the synchronous machine that is in the proximity of the wind generator, θ_1 and θ_2 are the electrical angles of the terminals that the synchronous machine and the wind plant are connected to respectively, and ω_{SG} is the speed of the synchronous machine that is nearby the wind power unit which is equipped with SDC.

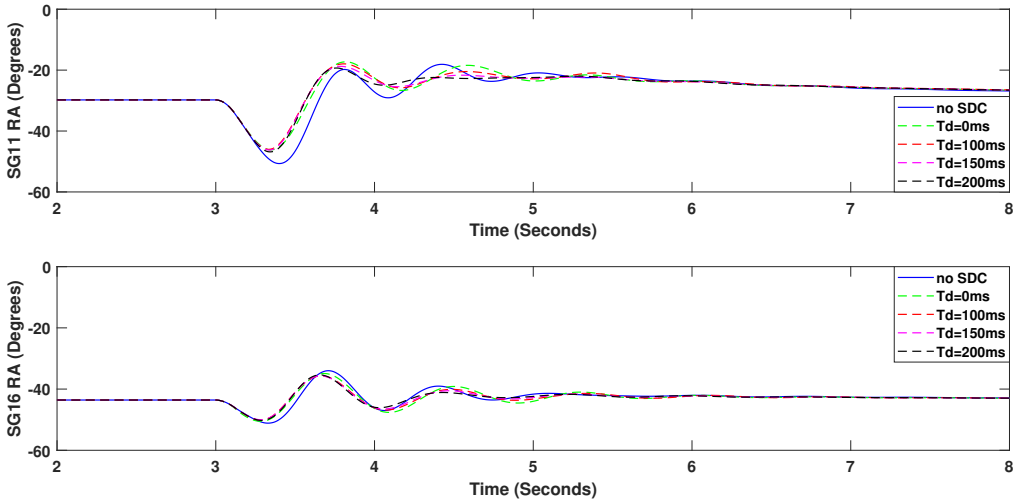

Figure 4.20: Dynamic response of rotor angles of North England area. Different time delays are considered when simulating a three-phase fault at Line 6-9 (75% share of wind generation in GB system). FCT=120 ms.

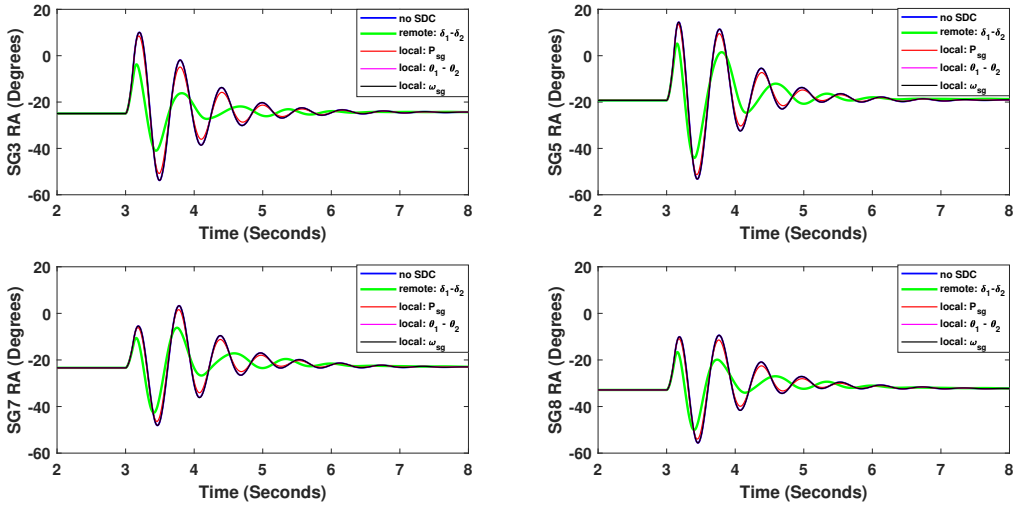

Figure 4.21: Dynamic response of rotor angles of Scottish area for a three-phase fault at Line 6-9 (75% share of wind generation in GB system). FCT=120 ms, remote vs local signals

4.5. Grid Forming Wind Generator Configuration

It is well known, that RESs are intended to be the dominant source of power in the power system networks of the future. This ensues, that RESs should have a grid forming behaviour, which ensues that they should be the ones that are associated to the voltage - var and frequency regulation.

In the power systems formed as nowadays, the already described grid-following wind turbine configurations are operating in a good manner. The reason for that is that the power network is strong (low impedance & high short - circuit power), which means that is capable to absorb the injected current and the synchronous machines can regulate the frequency and the voltage. However if low number of synchronous machines are existing and the PEIGs inject more current than the network can consume, it will result in problem , because wind generators or photo-voltaic plants can not consume power but only generate. In the future scenarios, new controllers are required, which will adapt to the grid conditions, and regulate the frequency and voltage in the grid.

A further limitation, of the existing grid following topology, has been observed in cases in which offshore wind power plants, connected via HVDC cables to the main grid, suddenly are operating in island mode due to converter blocking. In that case, the frequency in the islanded network can not be controlled, since the grid following wind generators are not equipped with such controllers, and also since no local loads are existing, reactive current injection for voltage support is not efficient. However, the grid- forming control proposed in [87], can solve the aforementioned problems

Details about the proposed controller can be found in [88]. For the transient stability studies, two are the main control loops that are to be considered; the var - voltage control loop and the active power control loop.

The var - voltage control loop is shown in Figure 4.22. The outer part is based on a slow droop controller which determines the voltage reference in the terminals of the machines, based on a measured voltage in a remote site of the grid. The controller is slow so as to avoid acting during short circuits, but quite fast so as to avoid unnecessary changes in the tap transformers [88]. During faults, the inner proportional controller acts, whereas the elimination of a dead-band, ensues continuous voltage control. It can be observed, that unlike the grid following configuration, the reactive current is not directly used in the controllers, as in the grid following configuration; instead the d- voltage reference of the inverter is formed. This ensues, that the converter voltage is the one, that changes according to the network conditions, and this change indirectly changes the current injected from the converter. Therefore, this control approach resembles more in the conventional synchronous machine voltage control.

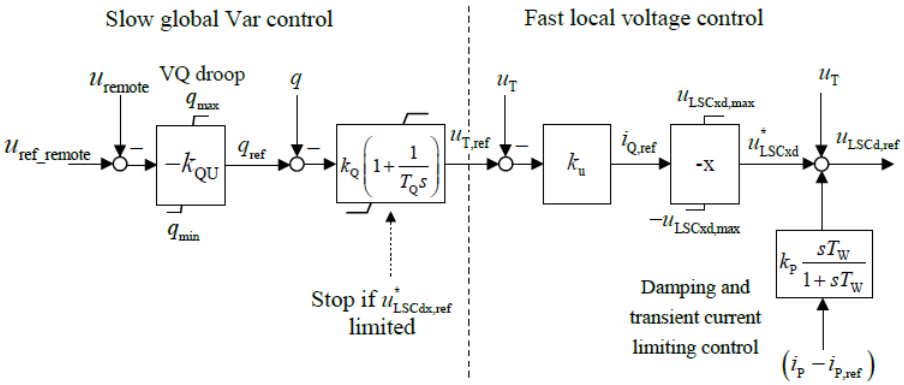

Figure 4.22: Grid Forming Reactive Power Control [88]

The active power control loop, is illustrated in Figure 4.23. As seen, it is based, similar to the grid following configuration, on the DC voltage PI controller. The active power is calculated from:

$$p = v_t \cdot i_p = -v_t \cdot \frac{v_{sq}}{x} \tag{4.1}$$

where v_t is the terminal voltage of the WG, i_p is the p-loop current in the AC side of the converter, and v_{sq} is the q- component voltage in the AC side of the grid side VSC.

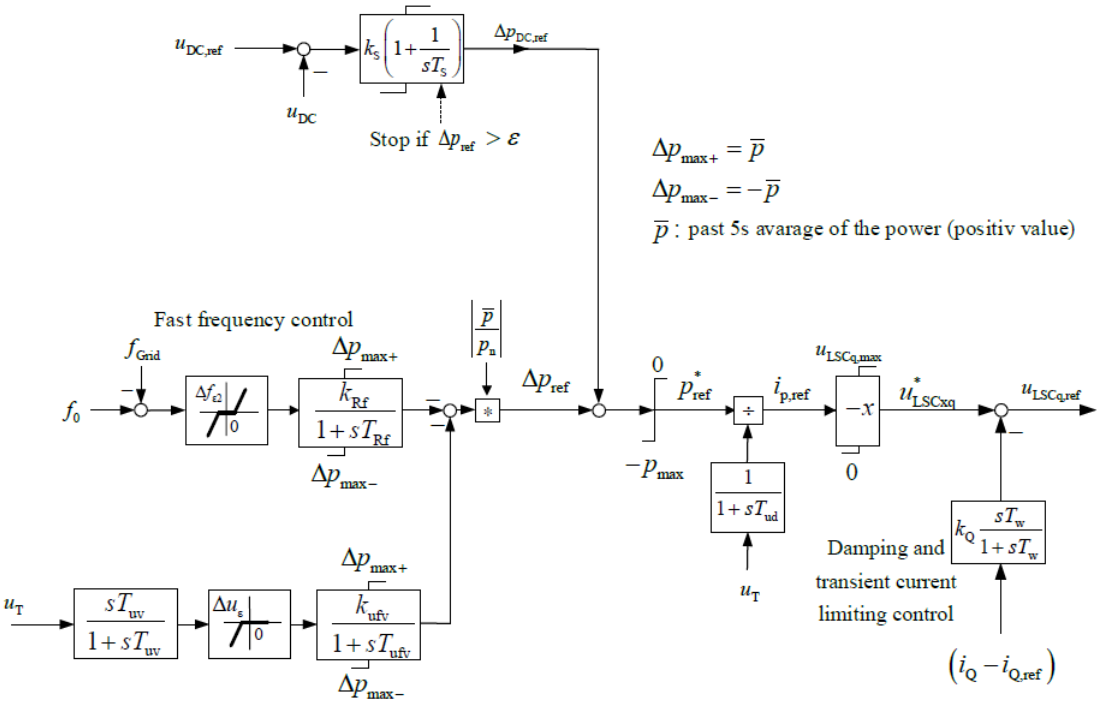

Figure 4.23: Grid Forming Active Power Control [88]

Therefore in order to regulate the active power injection, regulation of the q- component of the inverter voltage is needed. As mentioned before, no direct current control is performed, and the current reference is adjusted based on the power flow equations of the system.

The frequency control is activated when the frequency deviates from a permitted range, which is defined from 49.8 - 50.2 Hz. Also a voltage dependent active power injection is used so as to reduce the reference power set-point according to the WG terminal voltage drop. This technique can also improve the transient stability of the system.

As observed, the two loops described before, have additionally, two washout filters before the determination of the determination of the voltage references of the grid side inverter. The main objective of this block is to provide oscillation damping during the transient time window. The selection of this block is based on the following consideration.

The washout block in the output of the controllers, is used to emulate a series resistor in the output of the VSC. If physically this resistor was utilized in the power system, then voltage and current damping during the transient time would be introduced, however, power loss would also be observed, therefore the wind generator efficiency would be low. Therefore, a virtual resistor can be introduced with the aim of the wind generator controllers. The voltage drop in the resistor is calculated as:

$$\Delta v_r = R \cdot i \tag{4.2}$$

which can be analyzed in the d and q components as seen in Figure 4.24.

Comparing Figure 4.24, with Figures 4.22 and 4.23, it is concluded that the gain of the washout filter is the value of the pu virtual resistance in the Grid Side converter. It is observed, from the Table I.5 in Appendix I, that the gain in the washout filter can not be very high, because the system after the application of the fault deteriorates it's stability. An explanation to that phenomenon can be attributed to the fact, that when the resistance is high, then the voltage drop will also be very high, so the new voltage reference in the AC side of the grid side VSC will be negative. This ensues that a negative current flow will be injected in the wind generator, therefore, this means that the connected to the power system network, need to inject high active power, which may exceed their stability limits. It is also stated, that a washout filter - (high pass filter) is used so as to limit this damping effect only during the transient time period and not affect the injection of the wind generator during the steady state.

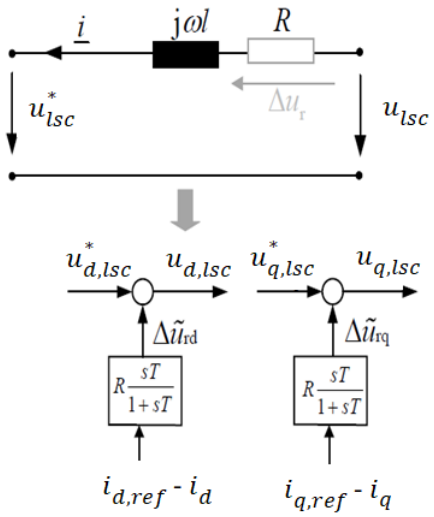

Figure 4.24: Physical meaning of damping control

The next section provides a comparison between the SDC controller applied in the grid following wind generator model, and the grid forming wind topology. The tuning of the washout - filters (common parameters used for the two P and Q loops) is based on the KPI of maximum rotor angle difference, exactly in the same manner as analyzed in the grid following configuration. The system used is the GB model designed for 75% wind share with SDCs/GridForming WGs applied in Zones 3,5,10,13,15,16,19 and 20. The tool for the simulations is DIgSILENT PowerFactory.

4.6. Grid Following WGs equipped with SDC vs Grid Forming WGs performance

Appendix I, presents a way based on a KPI, which can be used so as to tune the WGs' washout parameters. According to the analysis, regarding SDC controllers, a universal gain G=50 and a time constant of T=0.01s for all the washout filters, is selected. Additionally, regarding the grid forming configurations, a universal gain G=0.03 and a time constant of T=0.01s for all the washout filters, are selected. The rotor angles of the machines with respect to the slack machine are visualized in the following figures. It can be concluded, that Grid Forming WGs and Grid Following WGs when equipped with SDC, contribute in a very similar way in the transient stability performance of the power system. The SDC equipped WGs and Grid Forming configurations, are located in all the hybrid zones of the GB system for this comparison.

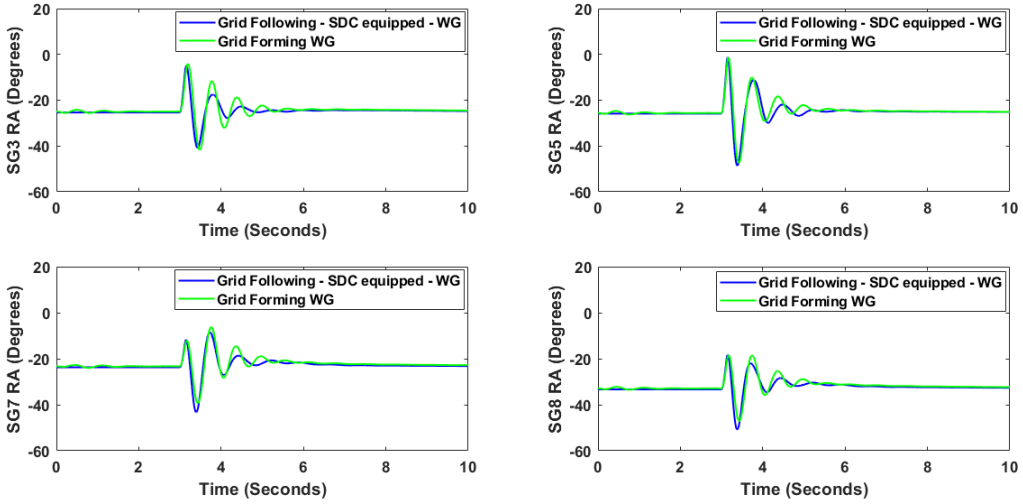

Figure 4.25: Dynamic response of rotor angles of Scottish area for a three-phase fault at Line 6-9 (75% share of wind generation in GB system). FCT=120 ms, Grid Following SDC vs Grid Forming WG contribution

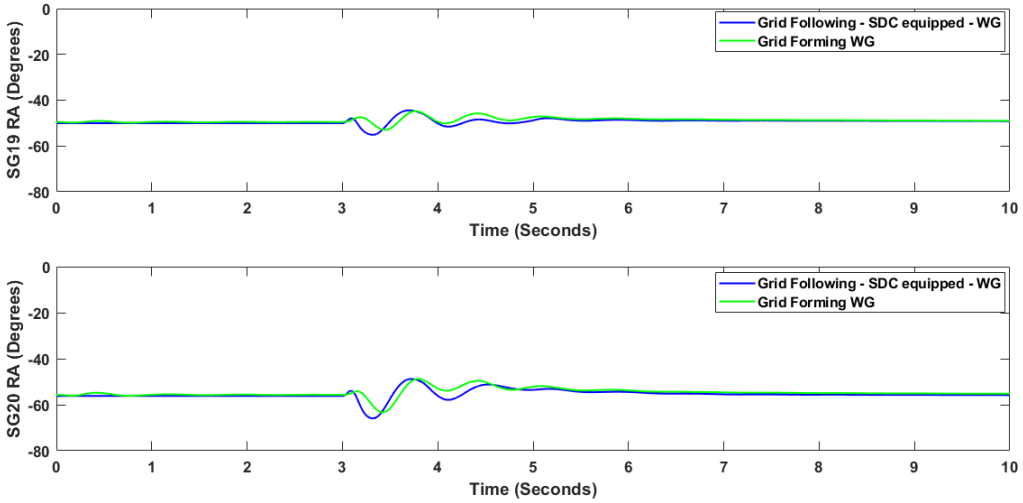

Figure 4.26: Dynamic response of rotor angles of Eastern area for a three-phase fault at Line 6-9 (75% share of wind generation in GB system). FCT=120 ms, Grid Following SDC vs Grid Forming WG contribution

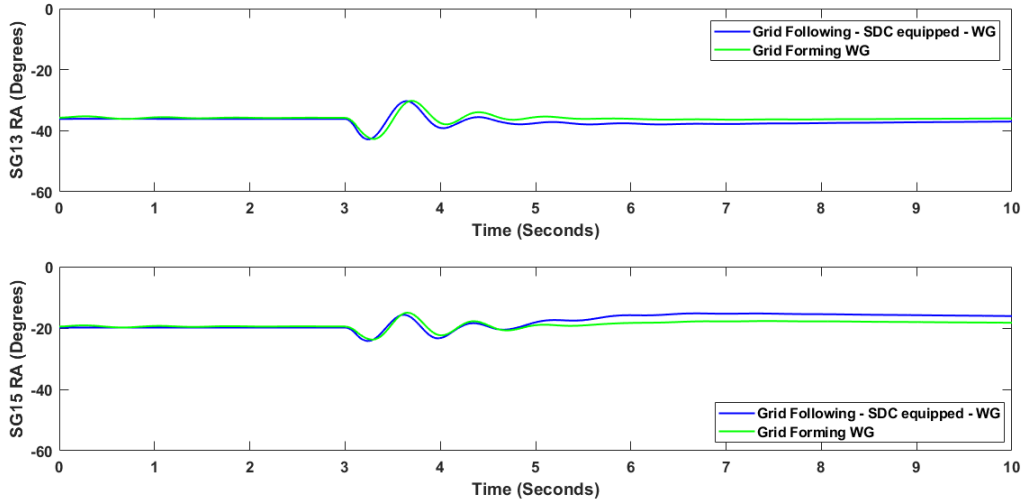

Figure 4.27: Dynamic response of rotor angles of West area for a three-phase fault at Line 6-9 (75% share of wind generation in GB system). FCT=120 ms, Grid Following SDC vs Grid Forming WG contribution

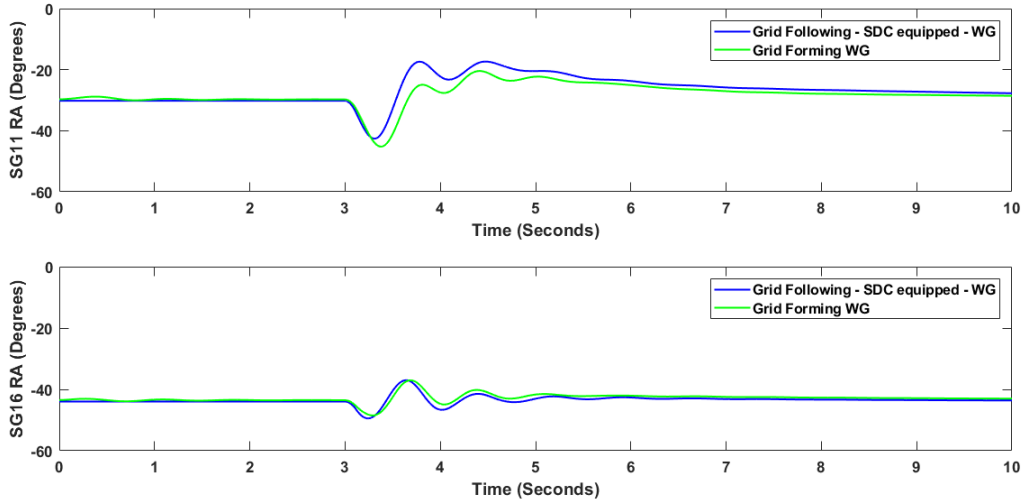

Figure 4.28: Dynamic response of rotor angles of North area for a three-phase fault at Line 6-9 (75% share of wind generation in GB system). FCT=120 ms, Grid Following SDC vs Grid Forming WG contribution

5

An Optimization Technique for WG Controllers' Tuning

In Chapter 4 a sensitivity methodology based on the maximum angle difference as transient stability KPI was formed. This strategy however, even easy to implement, is characterized by specific drawbacks. First, the implementation assumes the same controllers' tuning for all the wind generators' which is not necessarily correct, since the inter-area oscillations are not observed from all the sites of the existing power system in the same way. Secondly, the aforementioned technique, since based on the maximum angle difference formed, is focusing mostly on finding parameters that increase the synchronizing torque of the machines, which does not always ensues that the damping torque is also improved. The aforementioned, led to the investigation of one other manner to tune the controllers' parameters.

5.1. Optimization problem - formulation

In this Chapter, an optimization method is proposed, which can off-line tune the parameters of the wind generator controllers, using time - domain simulations. As proposed, the objective function is the minimization of the total (cumulative) area which is formed between each one of the 55 rotor angle after-fault waveforms with respect to their initial "virtual" lines that represent their pre-fault rotor angle values. This ensues, that both synchronizing and damping torque increment is taken into consideration, while an individual settings' tuning is applied. The mathematical description of the problem is given with the aid of Equation 5.1:

$$OF = \sum_{i=1}^{\#sc} \sum_{j=1}^{\#p} Area_{SGpair-RA}(\vec{x}) \tag{5.1}$$

Where $\#sc$ is the number of study-cases (i.e. study case in the current project means different location faults examined), $\#p$ the number of SGs pairs that can be formed in a given power system. Additionally, $Area_{SGpair-RA}$, is the area formed between the angle time-reponse of a given SG pair and it's pre-fault value , when a fault is applied. The previously described area, is illustrated in Figure 5.1. It can be understood, that the optimization problem for the current report, is a minimization problem. Furthermore, in Equation 5.1, $\vec{x}$ is the solution vector. It comprises the parameters of all the SDC controllers, in the grid following WG configurations. It is noted, that due to the very small range of parameters in grid forming controllers, optimization is not applied in this technology.

In particular, for the grid following configurations:

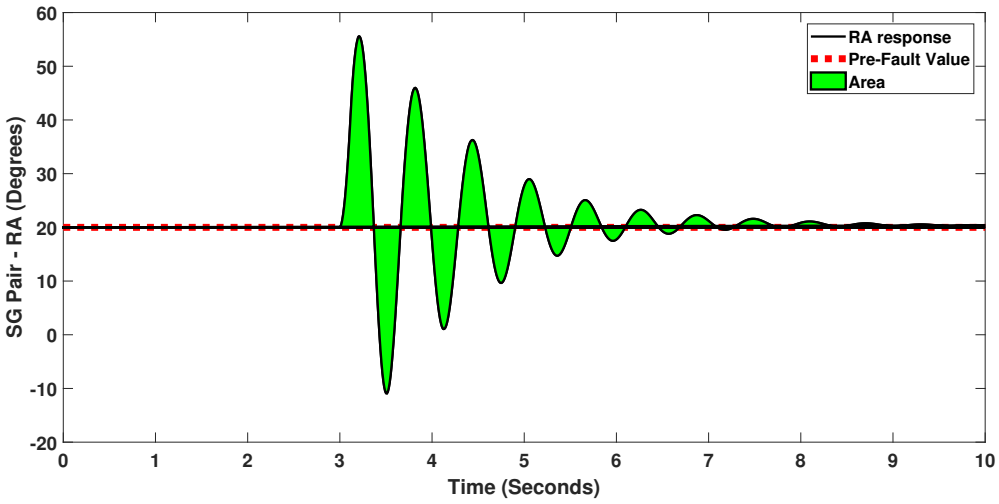

Figure 5.1: Area of a SG pair; formed by the time domain RA response after a fault application and it's pre-fault value

$$\vec{x_k} = [K_{wash_1}, T_{wash_1}, T_{num_1}, T_{denom_1}, ..., K_{wash_M}, T_{wash_M}, T_{num_M}, T_{denom_M},] \tag{5.2}$$

where M is the number of the SDC equipped WGs, K_{wash}, T_{wash} are the gain and the time constant of the washout filter used in the controller, while T_{num}, T_{denom} are the time constants used in the numerator and the denominator of the lead-lag compensators. As explained in the following sections the studies optimization problem is a bound constraint single objective computational expense problem. This ensues that the variables in Equation 5.2 are bounded between minimum and maximum values, whereas only one objective function values is to be optimized.

It is mentioned that the previous solution vector, is expanded according to the number of the equipped with SDC WGs in the power system. For instance, in this chapter, the 75% GB system is examined, with SDC equipped grid following WGs in Zones 3, 5, 10, 13, 15, 16, 19 and 20. This corresponds to a 4x8=32 dimensional optimization problem.

In the following sections, the optimization algorithm employed is presented. In addition, the main principal framework considering the implementation of the Objective Function using Python and its' communication with Matlab, in which the optimization algorithm is built, is presented. Last, the tuning results and time domain- simulations based on that results are further illustrated.

5.2. Mean Variance Mapping Optimization (MVMO)- Background

Due to the complex nature of power system dynamics, optimization techniques are arising, so as to efficiently tackle them. In particular, several optimization approaches have been proposed in the bibliography for tuning the controllers' parameters. Among others, particle swarm optimization and the evolutionary particle swarm optimization [89], [90] have been used. The aforementioned are heuristic optimization algorithms, which means that they, in an iterational manner, find new candidate optimal solutions, based on previous found solutions [91].

Mean - variance mapping optimization (MVMO), is a new heuristic optimization algorithm. As others heuristic algorithms, the solutions' selection procedure, that is analyzed in this section, is based on a random-sequence mechanism. This ensues that does not always guarantee global optimums, but provides near to optimum solutions [92]. MVMO is an evolutionary optimization algorithm with a single parent - offspring approach (i.e. a single solution vector is iteratively evolved). The searching mechanism for finding the best values of the variables to be optimized, is based on the following procedure described in sequential steps [93], [94]. The algorithm flow - chart is presented in Figure 5.2.

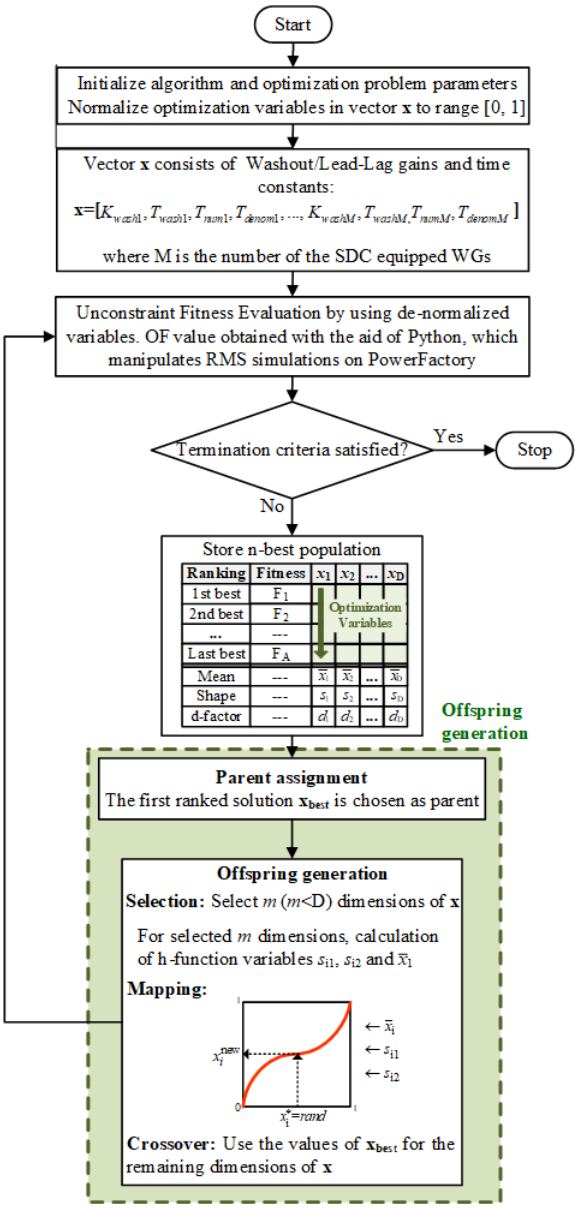

Figure 5.2: MVMO - Flow Chart [39]

5.2.1. Initialization

The first step, is the initialization of the solution variables, which compose vector $\vec{x}$. As mentioned, the solution vector, comprises the gains and the time constants of the WGs' washout based stabilizing controllers and the parameters of the lead-lag compensators. The initial solution is generated based on randomness, while the optimization variables (e.g. gains and time constants) should be within their maximum and minimum limits defined by the user. For instance, the Equation 5.3, is used for the initialization of the solution vector related to i^{th} variable.

$$x^i_{init} = x^i_{min} + rand(x^i_{min}, x^i_{max}) \tag{5.3}$$

where rand is a real number between the x^i_{min} and x^i_{max} values.

Further initialization parameters and their permitted minimum and maximum limits are also defined initially via scripting; these parameters are related to maximum number of iterations performed until MVMO is finished, the achieve size for the stored n-best population, number of mutated parameters,

scaling and asymmetry factors, parameters related to the initial shape factor e.t.c. These parameters are explained later. The variables of $\vec{x}$ vector are then normalized to range [0,1]. Equation 5.4, illustrates the manner the normalization is performed for the i^{th} variable of the solution vector.

$$x^i_{norm.} = \frac{x^i_{denorm.} - x^i_{min}}{x^i_{max} - x^i_{min}} \tag{5.4}$$

where $x^i_{norm.}$, $x^i_{denorm.}$ are the normalized and denormalized values of the i^{th} solution vector's variable.

This is done, so as the generated offspring/ new solution will never violate the search boundaries. If not normalization is implemented, there is a danger that the computed solutions violate the permitted limits, so the iteration should start again decreasing the efficiency of the algorithm.

5.2.2. Fitness Evaluation

In the next step, the iterative loop starts, in which a fitness evaluation of the denormalized (original min,max range of variables used) candidate solution $\vec{x}$, is performed. In particular, when unconstrained problems encountered, then fitness evaluation f* coincides with the objective function value f. If equality and inequality constraints are to be used then penalty coefficients are added to the objective function value, and thus increasing the fitness evaluation value.

Then a termination criterion is checked. Usually, the termination criterion is when the fitness evaluations performed reach a maximum number set by the user, or when there is no improvement on the fitness evaluation value over repetitive iterations.

5.2.3. New Solution - Potentially Stored

Depending on the fitness evaluation value with respect to the previous computed evaluations, and of course whether the optimization problem is minimum or maximum seeking one, then the fitness evaluation is stored in the n - best population achieve (along with the solution vector $\vec{x}$ that was used for the specific evaluation), or excluded from that. A size, referred as n, of achieve 2 - 5 is usually efficient, otherwise the computation effort increases. The achieve also is sorted in ascended or descended order, so the first ranked solution (i.e. defined as "parent") is the best solution found so far.

Once, the achieve is full, every new update will change, if eligible to enter the n-best population achieve, the mean (i.e. $\bar{x}_i$, i=1,2,..,D) and the shape variables (i.e. s_i, i=1,2,..,D) of each one of the D - dimension solution vector. The mean and shape variables are calculated by using the following equations:

$$\bar{x}_i = \frac{1}{n}\sum_{j=1}^{n} x_i(j) \tag{5.5}$$

$$s_i = -ln(vi) \cdot f_s \tag{5.6}$$

where the variance v_i is given by:

$$v_i = \frac{1}{n}\sum_{j=1}^{n}(x_i(j) - \bar{x}_i)^2 \tag{5.7}$$

The scaling factor f_s is a number defined by the user, ranging from 0-10, and used to control the form of the mapping function (defined later in this section) and therefore affects the new solution searching generation.

5.2.4. Offspring Generation

The first ranked solution in the achieve (i.e. "parent"), is modified to generate the new solution (i.e. offspring). The user has to define the number of dimensions m, out of the available number D, of the solution vector $\vec{x}$, which are to be mutated. The rest dimensions of the parent vector x (i.e. D-m), will be intact and remain the same in the new offspring. The selection of the variables that are to be mutated is usually done either randomly or moving consecutive variables with multiple/single steps, or moving only the first variable with single steps and the rest randomly [94].

The new value of each one of the selected variables to be mutated (i.e. x_i^{new} is determined with the aid of a mapping function h, which is described by the mean (i.e. $\bar{x}_i$) and shape variables (i.e. s_{i1} and s_{i2}) related to the specific variable. The determination of x_i^{new} is also dependant upon the random number x_i^* which is given as input to the mapping function. The i^{th} variable of the new offspring is computed by:

$$x_i = h_x + (1 - h_1 + h_0) \cdot x_i^* - h_0 \tag{5.8}$$

where h_x, h_1 and h_0 are the outputs of the mapping function h, when x=x_i^*, x=0 and x=1 respectively.

The mapping function is given by the following formula:

$$h(x) = \bar{x}_i \cdot (1 - e^{-x \cdot s_{i1}}) + (1 - \bar{x}_i) \cdot e^{-(1-x) \cdot s_{i2}} \tag{5.9}$$

As mentioned in [94], the variation of the $\bar{x}_i$, shifts the mapping function vertically, whereas the shaping parameters s_{i1} and s_{i2} affect the degree of bending. By default, it is assumed that the shaping parameters of each solution variable are equals and also equal to the shape variable of the solution variable (i.e. s_{i1}=s_{i2}=s_i). If the shaping parameters increase, then the curve is getting more flat, and this means that the search area is more probable to be around the already found mean value of the x_i parameter. It is also mentioned that s_{i1} and s_{i2} do not necessarily need to be equal. If $s_{i1} < s_{i2}$, then the mapping curve is more flat for high values of x, and vice versa. In order to differentiate the two shape parameters, the concept of Asymmetry Factor (AF) is introduced (i.e. AF>1). For instance, when $x_i^{parent} < \bar{x}_i$, then it is better to increase s_{i2} w.r.t. s_{i1}, because this means that the new variable, will be with higher probability closer not to the mean value, but to the parents' value parameter, which is a good parameter that contributes positively to a good fitness evaluation value.

In general, during the initial iterations, the search should be focusing in all the space. This initial stage is called exploration and the mapping curve should be highly bent. After some iterations, it is desired to focus mostly in the area around the mean value obtained so far. This stage is called exploitation and the curve should be more flat. One can also understand that if the number of the population, n, that is stored in the achieve is large, then more focus is given in the exploitation stage, as the mean values of each variable is easier to change. However, the computation effort of such scenario is bigger comparing to the case in which smaller population is considered.

Furthermore, as stated in [94], if the number of the mutated variables m, is small, then early stagnation can be observed. This means, that the variance of each one of the variables of the solution vectors in the achieve can be zero in the initial iterations and remain zero until the end of the algorithm. To put it differently, the variables do not change over iterations, and from Equation 5.6, since variation equals zero, the shape variable is very high which make the curve flat. Specific parameters are used, in order to change the scaling factor f_s dynamically (and therefore the geometric form of the mapping curve), when the variance decreases a lot in the initial iterations of the algorithm run. More information can be found in [94].

In the following section, the way in which MVMO is utilized for the tuning of the WG controllers, is described. In Appendix M, the Python code for the Objective Function Calculation and some basic points related to the MVMO algorithm implemented in Matlab are further illustrated.

5.3. MVMO Implementation for Wind Generator Control Tuning Purposes

Figure 5.3, illustrates the way in which Python and Matlab integration is set. For this integration, two flags are used; the first one is referred as "flag to matlab" (i.e. flag set by python) and the second one referred as "flag from matlab" (i,e. flag set by matlab). The two flags are located in the corresponding .txt files. Moreover, a .txt file in which python writes the OF value, and also one .csv file in which matlab writes the offsprings computed after MVMO iteration, are utilized. Other files are also created/processed by the two aforementioned software tools, however they are only needed for the user, so as to understand better the communication procedure. The reader, is highly advised to refer to Appendix M.1.4, for more information about the files and how they are used. In this section, a brief introduction about the steps illustrated in Figure 5.3 is given.

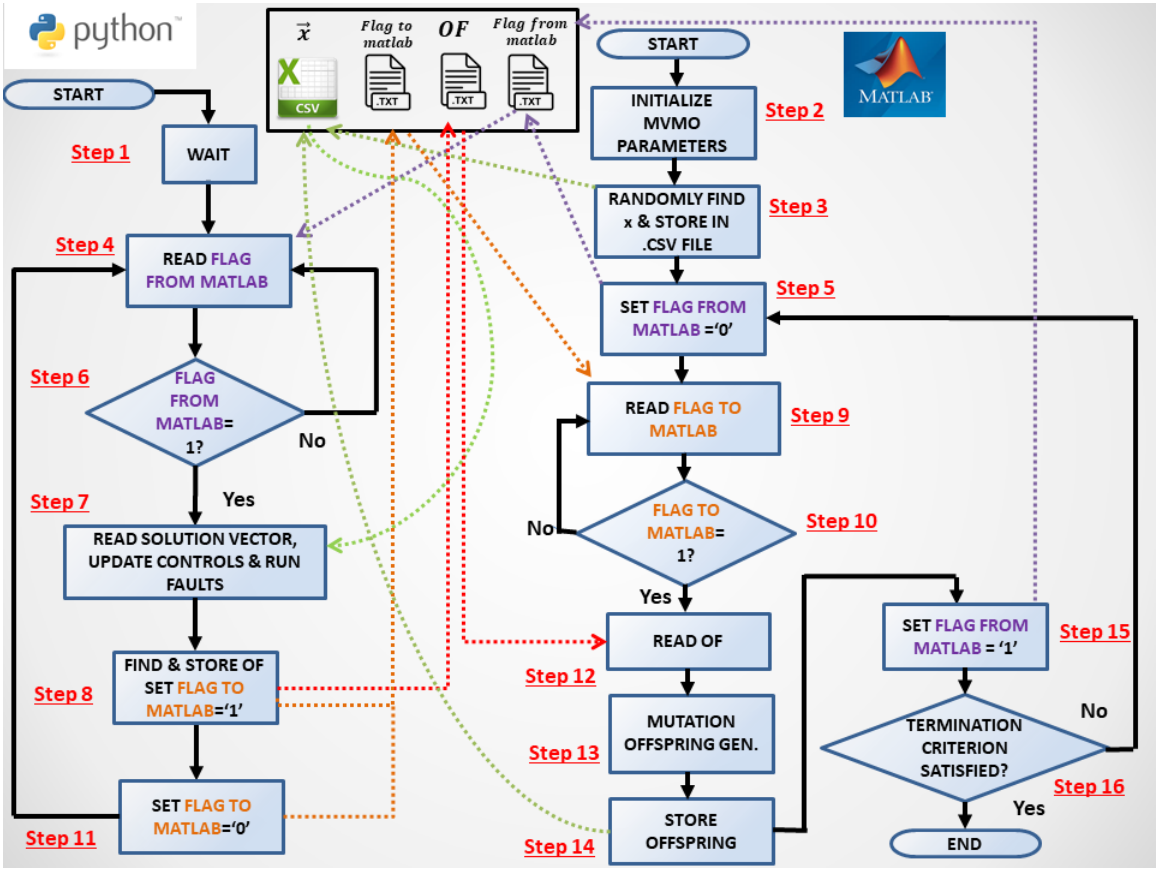

Figure 5.3: Communication between Matlab & Python - Flow Chart

It is mentioned, that before the MVMO algorithm starts, only the two flags are needed. The data files related to the Objective Function and the solution vector are created by the two tools. In particular, initially, the "Flag From Matlab" file should have value of one/ "1", whereas the "Flag To Matlab" file should have value zero/ "0". The importance of the aforementioned flags is highlighted in the description of the procedure:

- Step 1: In Python, when the MVMO starts to be executed, there is a timer introduced, so as to wait some time, before the Matlab MVMO, initializes it's MVMO parameters (i.e. step 2), find and store in a .csv file the denormalized values of the randomly chosen (only for the first iteration) solution vector. This delay is introduced, because accessing the same .txt file from different platforms at the same time is not permitted. Therefore, prioritization is given to Matlab

to store the solution vector, and then the rights to process the file (i.e. read the solution vector values), are given to python.

- Step 2: While Python, is in idle mode (i.e. Step 1), Matlab initializes the parameters related to the MVMO procedure. This initialization comprises the range of the solution vector parameters (e.g. gains and time constants of washout filters and lead- lags compensators used), the achieve size, the number of mutated variables when the algorithm starts and when the algorithm finishes (i.e. this number can be iteratively be decreased over MVMO evaluations), the scaling factor f_s when the algorithm starts and finishes, the maximum number of MVMO iterations e.t.c.

- Step 3: After initialization, Matlab chooses arbitrary a solution vector which should be complying with the lower and the upper limits, as set in Step 2. The denormalized vector is stored in a .csv file, referred as ”offspring.csv”.

- Step 4 & 5 & 6: Python script at this point exits the initial ”wait” mode. It reads the ”Flag From Matlab” which initially it was set from the user at ”1”. Therefore, for the first MVMO iteration, Python directly will proceed to Step 7. At the same time, since Python read the ”Flag From Matlab” and managed to proceed to step 7, Matlab is setting the Flag from Matlab to ”0” and the communication between Matlab and Python terminates for a while. In general, the ”Flag From Matlab” is set to ”1”, whenever Matlab has a solution vector to give to Python, and is ”0” when Python has already read the solution vector.

  After storing the offspring value, Matlab enters the idle mode, since it is waiting for an objective function value from Python, so as to execute the optimization task. This happens, because the ”Flag to Matlab” has value ”0” as initially set from the user.

- Steps 7 & 8: Python, reads the solution vector, that Matlab created in Step 3, updates the controllers’ parameters and runs the dynamic simulations. The dynamic simulations, can include many faults/ study cases, the number of which can be selected from the user as seen in Appendix M, and in particular, in Section M.1.4. The python script then stores this Objective Function value in a .txt file called ”OF.txt” and updates the ”Flag to Matlab” .txt file by setting it’s value to ”1”.

- Steps 9 & 10: In Step 8, the ”Flag to Matlab” became ”1” so Matlab MVMO, can read the Objective Function Value.

- Step 11: The flag ”Flag to Matlab”, is set at ”0”. This flag, i.e. ”Flag to Matlab” is set to ”1”, whenever Python has an Objective function value to give to Matlab, and is ”0” when Matlab has already read the Objective Function Value. Then Python enters again the idle mode, and waits for a new solution vector from Matlab. In particular, Python waits, until the flag ”From Matlab Flag” is ”1”, which is done in Step 15. MVMO.

- Steps 12,13, 14 & 15: Matlab, reads the OF value and executes the main core of the MVMO algorithm as described in Section 5.2. Then it stores the new solution vector in the ”offspring.csv” file (by erasing the previous one which was written in Step 3) and also sets the flag ”Flag From Matlab” to ”1”. Therefore, it can be understood that the two flags have, in Step 15, the same values as when they were initialized, before Step 1; i.e. ”Flag From Matlab” = 1 ”Flag to Matlab” = 0.

- Step 16: In the previous 15 steps one whole MVMO iteration was described. The same procedure is repeated for the rest MVMO iterations. However, then the number of the MVMO iteration reaches the maximum value already defined by the user in Step 2, then the algorithm terminates.

5.4. MVMO Tuning Results for Grid Following Wind Configurations

Several attempts, with sensitivity analysis for the MVMO parameters were performed, so as to find the optimal parameters. Fault at Line 6-9 was tested, as a critical study case. The fault was applied in

the GB configuration of 75% share, with all the WGs in the hybrid zones equipped with SDC. Initially, the MVMO algorithm is executed without any lead-lag consideration. The MVMO parameters' table is illustrated below.

Table 5.1: MVMO basic parameters

Parameters	Value
Archive Size - A	5
Number of Decision Variables - D	32
Initial Scaling Factor - f_s^{init}	1
Final Scaling Factor - f_s^f	30
Initial Number of Mutated Variables - m^{init}	D/2
Final Number of Mutated Variables - m^f	1
Minimum - Maximum values of washout filter Gains G	1 - 100
Minimum - Maximum values of washout filter time constants T	0.003 - 0.05

The rotor angle results, under three scenarios, i.e. when no SDC is used, when (universal) sensitivity based tuning is implemented as presented in the previous chapter, and when MVMO optimization is used, are illustrated in Figures 5.4 - 5.7, whereas Table 5.2 includes the solution vector that leads to optimal results. It can be concluded, that MVMO optimization with this objective function and these MVMO parameters used, introduces the same first swings mitigation, but some small angle oscillations occur after. These oscillations, since 55 SGs pairs are considered, contribute in a minor way in the total angle area formed, so it is difficult for the algorithm to focus on them and minimize their contribution. It is mentioned, that the same oscillations were observed with the sensitivity tuning, however manually they were tackled, by decreasing the acting time of the SDC controller. It can be expected, that by introducing the duration time of all the SDC controllers in the solution vector of the optimization algorithm, these oscillations can be mitigated too.

Table 5.2: MVMO solution results

Parameters	Washout Filter Gain - Value	Washout Filter Time constant - Value
WG3	65.14278	0.00713
WG5	15.72762	0.00726
WG10	28.13276	0.01712
WG13	73.37549	0.00785
WG15	30.43566	0.01265
WG16	42.46380	0.01624
WG19	45.50589	0.01097
WG20	12.97458	0.01650

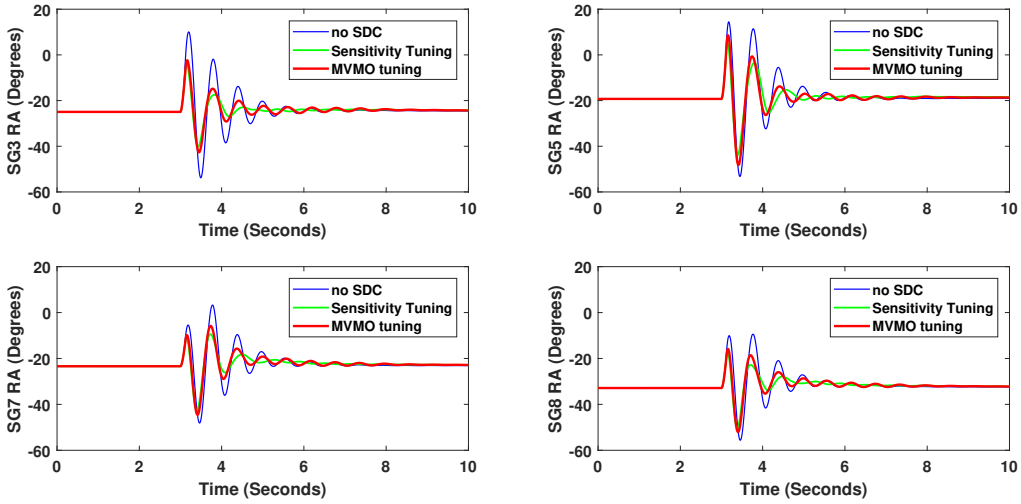

Figure 5.4: Dynamic response of rotor angles of Scotland area: without SDC, with sensitivity tuned SDC, with MVMO tuned SDC. Examined study case is a three-phase fault at Line 6-9 (75% share of wind generation in GB system). FCT=120 ms.

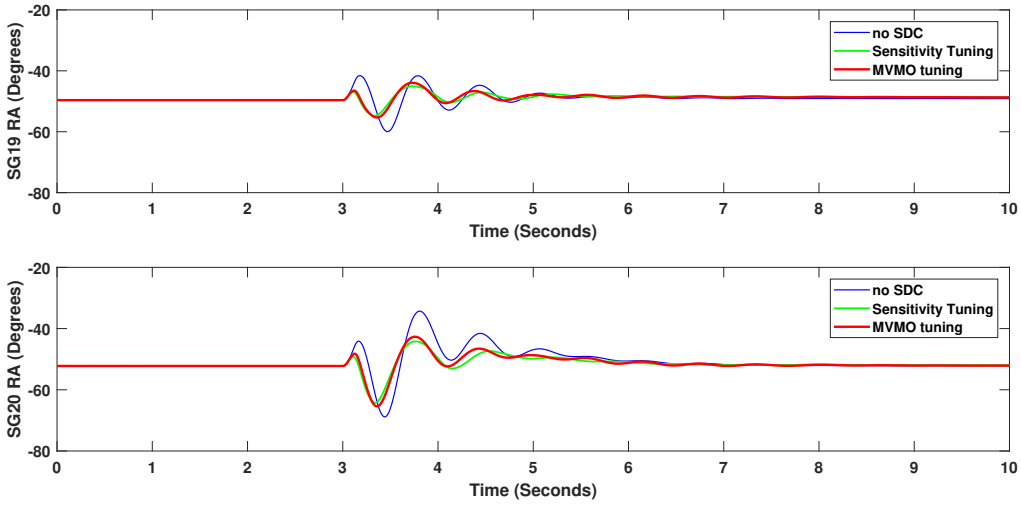

Figure 5.5: Dynamic response of rotor angles of East England area: without SDC, with sensitivity tuned SDC, with MVMO tuned SDC. Examined study case is a three-phase fault at Line 6-9 (75% share of wind generation in GB system). FCT=120 ms.

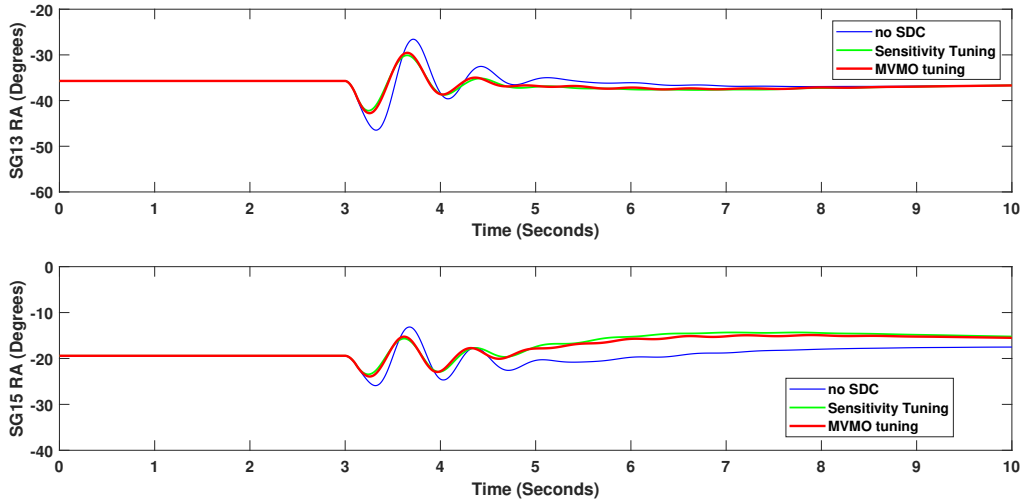

Figure 5.6: Dynamic response of rotor angles of West England area: without SDC, with sensitivity tuned SDC, with MVMO tuned SDC. Examined study case is a three-phase fault at Line 6-9 (75% share of wind generation in GB system). FCT=120 ms.

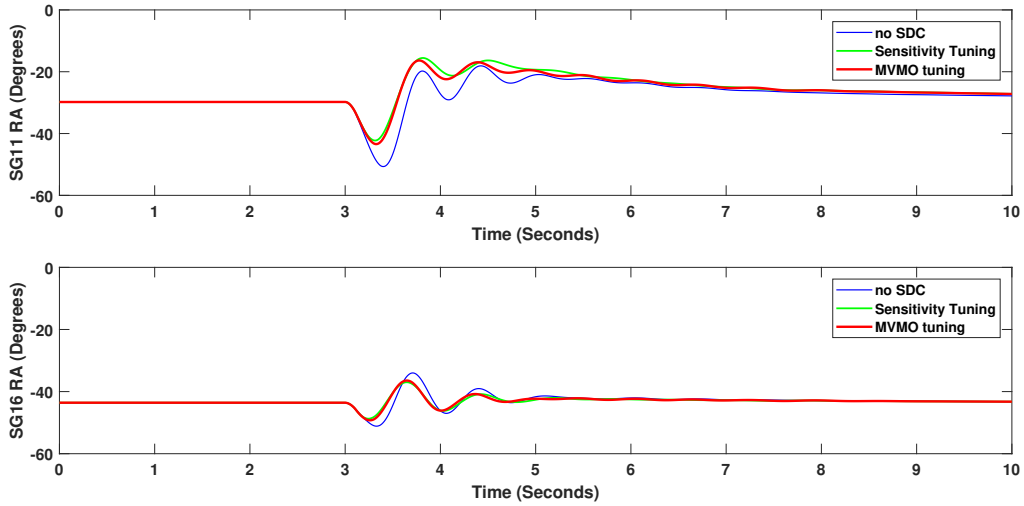

Figure 5.7: Dynamic response of rotor angles of North England area: without SDC, with sensitivity tuned SDC, with MVMO tuned SDC. Examined study case is a three-phase fault at Line 6-9 (75% share of wind generation in GB system). FCT=120 ms.

Results with higher time constants in the washout filters are presented in Figure 5.8. In this case, the maximum permitted time constant value for the MVMO parameter is set at 0.1 s. The insufficiency of the SDC controller for high time constant gains, as presented, in previous chapters, is obvious.

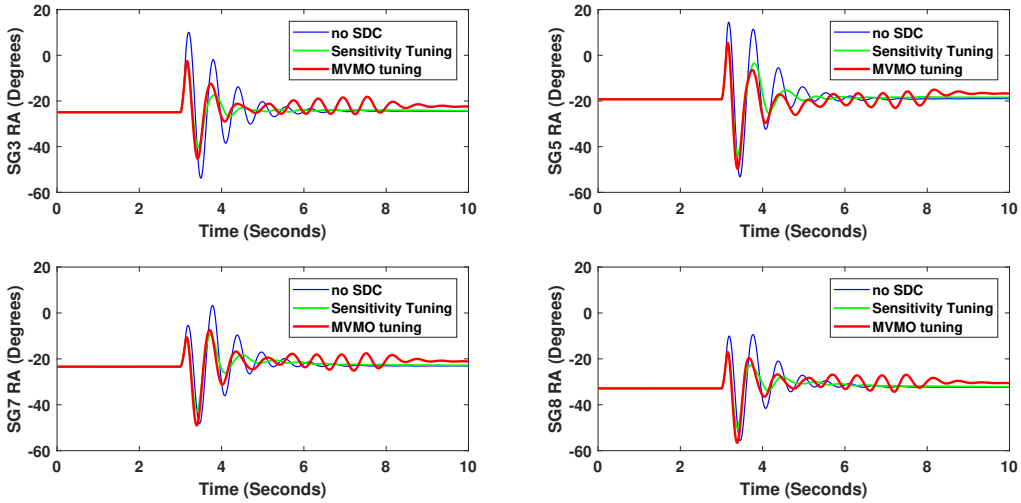

Figure 5.8: Dynamic response of rotor angles of Scotland area when higher time constants considered: without SDC, with sensitivity tuned SDC, with MVMO tuned SDC. Examined study case is a three-phase fault at Line 6-9 (75% share of wind generation in GB system). FCT=120 ms.

Last, phase compensation with lead- lag consideration is also attempted. The range of parameters is taken from [96], in which conventional Power System Stabilizers are examined. Figure 5.9 illustrates two lead - lag time constants considered:

- Case I: T_{num1}= 0.05-1 seconds, and T_{num1}/T_{den1}= 1-10
- Case II: T_{num2}= 0.05-2 seconds, and T_{num2}/T_{den2}= 1-20

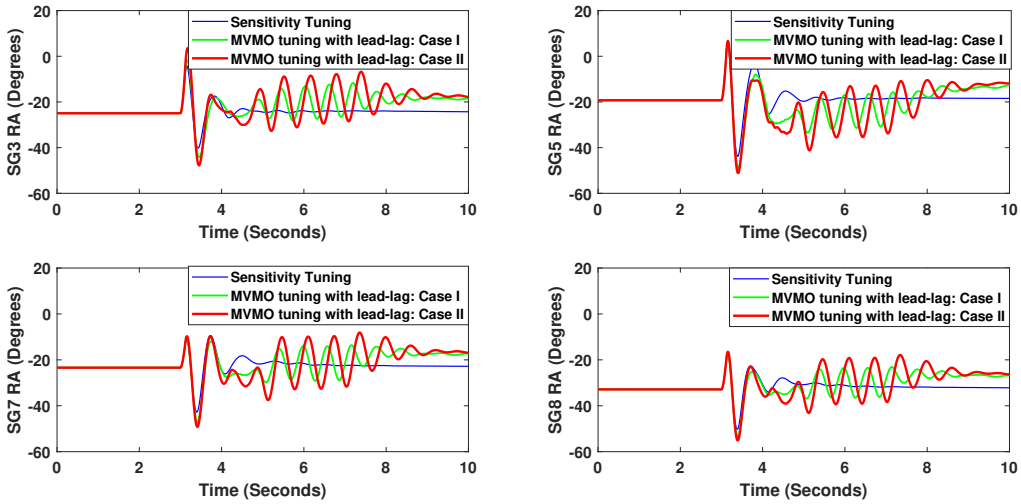

Figure 5.9: Dynamic response of rotor angles of Scotland area when higher time constants considered: without SDC, with sensitivity tuned SDC, with MVMO tuned SDC. Examined study case is a three-phase fault at Line 6-9 (75% share of wind generation in GB system). FCT=120 ms.

As mentioned in the previous chapters, and as can be deducted from [47], phase correction is unnecessary when rotor angles are used as inputs in the stabilizing controllers.

5.5. Additional Objective Functions Consideration

Three further objective functions, are also considered, for trying to achieve even better rotor angle damping from off-line time domain simulations.

1. The first additional objective function is based on the minimization of the cumulative area derived from the 11 SGs' speed oscillations with respect to their initial speeds of 1 pu. The ineffectiveness of the method can be explained due to the fact that the area formed by the p.u. speeds is already very small, so the algorithms stagnates very easily. Additionally, SDC focuses in the angle perturbations minimization, and not the speed ones. The speed oscillations are mitigated with SDC as seen in 4.12, indirectly due to the angle mitigation. However, the opposite can not be achieved.

2. The second additional objective function was based on the minimization of the maximum rotor angle deviation value, of all the 55 SGs. However, also this approach was ineffective, and this can be explained, that the minimizing only the maximum angle, does not guarantee that the other angles are mitigated as well.

3. The third additional objective function, was based on the objective function based on Section 5.1. However, instead of computing the area of all the 55 angle SGs pairs, only the areas of the SGs angles with respect to the slack machine (e.g. SG10) are computed. For the reader to have better insight, the cumulative area comprises the smaller areas formed by SG3-SG10, SG5-SG10, SG7-SG10, SG8-SG10, SG11-SG10, SG13-SG10, SG15-SG10, SG16-SG10, SG19-SG10 and SG20-SG10. This, approach has the same first swings synchronous machines' responses as the MVMO algorithm with the 55 angle areas considered, however the oscillations are better damped. This can be explained, that this medium frequency oscillations if were existing they would consist of a significant ratio of the final total area or equivalently objective function value. Therefore, the algorithm manages to eliminate them. The solution vector, that is computed from Matlab MVMO, in this case, is depicted in Table 5.3.

The effects of the objective functions in the SGs angles, are visualized in Figure 5.10

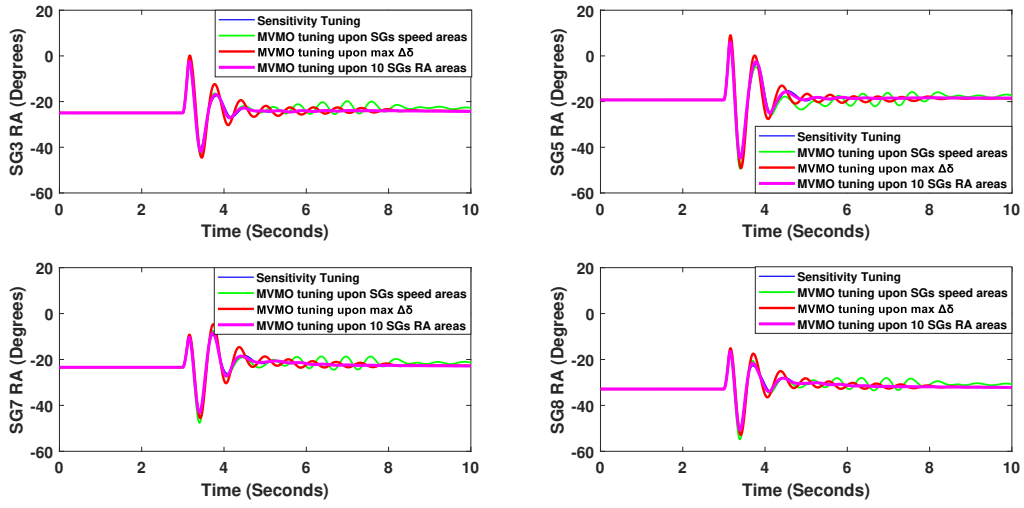

Figure 5.10: Dynamic response of rotor angles of Scotland area when different objective functions are used. Examined study case is a three-phase fault at Line 6-9 (75% share of wind generation in GB system). FCT=120 ms.

As a final key take - away, sensitivity analysis as presented in Chapter 4, has already some satisfactory damping results. MVMO with the efforts achieved so far, have similar responses. In order to achieve even better swing stability, MVMO optimization in the MVMO parameters could be used, or simpler use Objective Functions based on small signal stability concepts, so as not to be restrained in time-

domain simulations. The optimization algorithm itself, apart from just changing some settings, can be tuned/modified to perform better.

Table 5.3: MVMO solution results with the 10 SGs rotor angle pairs

Parameters	Washout Filter Gain - Value	Washout Filter Time constant - Value
WG3	19.67341	0.01911
WG5	29.47981	0.01426
WG10	49.28106	0.01001
WG13	36.92419	0.01790
WG15	52.57345	0.01397
WG16	26.81379	0.00884
WG19	69.33790	0.00874
WG20	13.28935	0.00936

6

Conclusions

This chapter provides key takeaways about the thesis project elaborated in the previous chapters, answers to research questions that were set in Chapter 1 and last, some proposals for future research are referred.

6.1. Summary of Study Cases Examined

In the current report a Supplementary Damping Control (SDC) was proposed as a method for modification of outer controls of grid following wind generators to safeguard large-disturbance rotor angle stability, when increasing the share of PEIG.

As shown in Chapter 3, the adopted structure of SDC is similar to the typical power system stabilizers implemented by utilities. A practical implementation is in principle not a major drawback. Future research should be conducted to determine if more sophisticated stabilizer models (e.g. multi-band stabilizer [95]) should be used, which depend on the dynamic properties of a particular power electronic converted dominated power system. The basic structure of SDC shown in this study, proves already that wind generators can effectively contribute to mitigate large excursions of rotor angle by exploiting the available margin for active current modulation. The grid following technology, equipped with SDC was tested in EMT simulations for a modified IEEE 9 bus system, and the superiority damping capability of the controller was obvious, comparing to default controllers. In the 75% wind share, moreover, SDC manages to maintain transient stability in contrast to the other methods. As expected, similar results are observed for the RMS simulations.

The SDC control was furthermore tested, in multi- machine systems, using RMS simulations. The SMIB system is used, as a prototype model, so as to facilitate the effect of the distance between the SG and WG in the SDC performance, and also to demonstrate the effectiveness of the controller especially when implemented with the aim of mitigating the oscillations of a synchronous machine located far from the system's Center of Inertia.

The SDC control is last tested in the GB transmission system simulation model, for two different wind shares 66% and 75%. Based on RMS simulations it was found that the use of rotor angle deviations as inputs of the SDC attached to WGs leads to effective reduction of the magnitude of first swing and a significant increase of oscillation damping. Comparing CCTs, for the two different share levels, it is found that they are similar; this can be interpreted as following: the lower inertia of the higher wind share power system, is counterbalanced by the higher effectiveness of the SDC controller, as more SDC equipped units are employed. One additional observation is that this rotor angle input, leads to better performance when compared to the choice of using local signals for mitigation of large-disturbance rotor angle instability. Moreover, the contribution of wind generators with SDC was found to be higher if the wind generators with SDC are dominant (a better mitigation of first swing magnitude and better oscillation damping is achieved with higher the share of wind in this area) in a synchronous area that is prone to large-disturbance rotor angle instability. Last, as shown in Section 4.4.2, communication time delays can reduce the effectiveness achieved by SDC. With the studied systems, and even considering a maximum delay of 200 ms, it was found out that SDC still helps in safeguarding large-disturbance

rotor angle stability. Simulations with the synthetic model of the GB system also showed that time delay around 100 ms or less seems to lead to minor impact on the performance of SDC.

Grid Forming wind generation technology, was also tested. The benchmark system used, is the 75% wind share GB system, with the grid forming configurations located in zones 3, 5, 10, 13, 15, 16, 19 and 20. The transient stability of the system in the previously mentioned topology is compared with the case that SDC equipped grid following WGs, are located in the same mentioned sites. The results, show that grid following technologies equipped with SDC contribute in a similar way as the grid forming technologies.

The tuning of the controllers is based on two approaches both for the grid following and grid forming wind topologies. The first approach is based on a (universal) sensitivity-based tuning of all the controllers. This manner focuses on maximizing the maximum angle difference observed in the system, from all the pairs in the system. The advantage is the easy tuning, but the drawback is that synchronizing torque is targeted to be enhanced, while damping torque is neglected. MVMO is used so as the tuning to be based on the damping torque.

6.2. Thesis Main Conclusions

The main take - aways from the studies performed are summarized as following:

- SDC performance superiority when based on an active power modulation technique, when rotor angle is used as input, and when not lead- lag compensator is used. The absence of needed phase-compensation, when rotor angle input is used is highlighted, as mentioned in Section 3.2.3 and can be deducted from [47]. The absence of needed leag-lag filters, which can also be verified by the MVMO results, shown in Figure 5.9, is an important advantage of the proposed controller, since no additional tuning of lead-lag parameters is needed.
- SDC depends on the rotor angle signals which are not directly available as measurement. However, synthetized rotor angle signals computed by PMUs, might be utilized.
- If the time delay associated to the rotor angle signals computation, is higher than 170ms, the SDC performance can be degraded. Nevertheless, a phase compensation block might be added to the SDC scheme to reduce the impact of time delays on the SDC performance.
- Small time constants need to be used in the SDC controllers, and this is due to adverse interactions incurred in the governors of the synchronous machines as shown in [44].
- Deactivation time of SDC can be set smaller than 10 s (e.g. between 1.5 s - 4 s for the study case with the synthetic model of the GB system) to prevent excitation of high frequency oscillations (if higher deactivation time is desired, a low pass filter should be integrated to pre-filter the input of the SDC).
- Not all WGs are required to perform SDC, i.e. WGs located close to synchronous generators vulnerable to lose of synchronism are of preferable for SDC.
- The Grid Forming Technology studied and the Grid Following one with SDC as proposed, result in a similar transient stability of the power system.
- MVMO tuning results in a similar damping as the one derived from the selectivity method with universal washout parameters, proposed also in this report. The MVMO Objective Function that seems to give the best results is the minimization of the rotor angle areas of all the synchronous machines in the system with respect to the slack-reference machine, as can be seen in Figure 5.10.
- MVMO approach for tuning can be considered that has two advantages over the selectivity tuning.

    1. It is mentioned, that the results in Chapter 4 are derived after a proper tuning of the time that individual SDC controllers act. In other words, the selectivity analysis was performed, then the washout filters' constants were updated in a (universal) sensitivity- based manner, and then the acting duration of some SDCs was decreased manually by the user, in the wind

plants that were close to the synchronous machines that encountered the medium frequency oscillations. In MVMO, as seen in Figure 5.10, the algorithm itself, finds new washout parameters, but at the same time the medium frequency oscillations are mitigated, without the user to be needed to manually re-tune the acting time of individual SDCs.

2. Table 5.3, reveals that some low gains in the washout filters, can be used. This ensues, that the corresponding wind generators do not need to give much kinetic energy, to perform damping. This fact as explained in Section 4.3, results in higher enumeration for the operator comparing to the universal tuning, in which all the wind generators are equipped with relatively high gain. In Table 5.3, the high gain of the SDC in WG19, is not a major issue, since the capacity of this plant is already big as seen in Tables J.1 & J.2 in Appendix J.

After conducting the simulations mentioned above, and mentioning the main observations, it is now possible to provide answers to the Research Questions, which were stated in Chapter 1.

- `What modifications should be done to the outer controllers of FDWG so as to integrate a proposed supplementary damping control feature?`

  The P- outer channel is only proposed to be modified, because rotor angle stability is mainly associated, with the balance between mechanical and electrical power of the SGs, therefore modifying the electrical power injection of the WGs, directly the transient stability of the system is affected. Modifying the Q- outer channel, is proposed for future research.

  A basic stabilizing controller is used, i.e. a washout filter, to introduce the desired stability. The input signal is the rotor angle difference between synchronous machines, whereas the output signal is added with an opposite sign in the point where the d- reference current is computed with the default controllers. In order to reduce the inter-area oscillations, the active power modulated signal, should be in anti-phase with the speed of the SG that is nearby. Therefore, lead lag filter, as explained, is not needed.

- `How does the supplementary damping control outperforms existing measures with wind generators to support transient stability?`

  Using EMT simulations, it is observed that SDC outperforms significantly other options (e.g. voltage-dependent active power reduction) suggested in existing literature, which are conceived to react based on exclusive observations from local measurements (e.g. voltage measurements in the PCC). In Section 3.4.3, it is mentioned SDC leads to good rotor angle (first & second swings) and frequency response, whereas VDAPI improves frequency performance, but the rotor angle performance is not improved that much.

- `What are the signal inputs that can be used to ensure effectiveness of SDC?`

  In the current report, remote and local inputs are tested. In general, input signals can be considered, all the measured signals that can be affected, by the oscillations occurring after a fault. These can be remote: e.g. rotor angle differences between synchronous machines, or local ones: e.g. speed of SGs that is close to the WG, active power injection of the SG, electrical angle difference of the terminals that the WG and the SG are connected to. It was found, that when no lead-lag is used (which is beneficial, since this would introduce more tuning complexity for big power systems), then rotor angle as input is a better approach comparing to other local inputs. The rotor angle input is the difference between the rotor angle of the SG, that is located close to the WG, whereas the reference angle is the one, that belongs to a SG in a high inertia area.

- `How to select the Wind Generators to be equipped with the SDC?`

  Not all wind generators are required to perform SDC, i.e. wind generators located close to synchronous generators vulnerable to lose of synchronism are of preferable for SDC. This statement can be elaborated in Appendix K, in which it is proven that even if SDC is not used in the middle of the high inertia part of GB test system, but only in the prone to instability areas, then the damping is similar with the case that all the GB areas are equipped with stability units.

  As a general observation, addition of SDC in renewable energy based power plants should be considered when the traditional measures (including addition and/or re-tuning of PSSs) are not

sufficient to ensure desired CCT values when a certain amount of synchronous generators in conventional power plants has been decommissioned.

- `In which extent the data latency deteriorates the proposed SDC performance?`

  RMS simulations using the SMIB and the GB system, showed, that there is indeed a small deterioration of the SDC response when time delays are introduced. However, even for 200 ms latencies, which are typical maximum latencies for Wide Area Monitoring Systems, damping is achieved comparing to the scenario where no SDCs are used.

- `In which way does optimization improve the performance of the proposed supplementary damping control ?`

  The performance of the controller can achieve a satisfactory damping. However, a more thorough examination of additional parameters (e.g. duration activation of SDC after LVRT is triggered), MVMO parameters and new objective functions can be tested. For the simple objective functions that were tested in the report, without any constraints, it is observed, that similar response to the sensitivity based universal tuning can be achieved.

- `Does the observed performance of the proposed damping controller differ when simulations are implemented in RMS and EMT tools?`

  The responses of the SGs angles, are similar no matter of the tool used. Deviations in the system parameters and also the wind generator models, differentiates slightly the damping.

- `Is the supplementary damping control more effective in wind generators with grid following or grid forming control?`

  Grid following WGs equipped with SDC and grid forming technologies are similar in terms of the damping that contribute. However, as seen in the grid forming technologies, the damping blocks with the washout filters is almost inactive, due to the low permitted gains in their transfer functions. Moreover, the comparison can be tested for even higher penetration levels, to see if the same findings hold. A mixture of grid forming and grid following with the proposed damping controllers could be also examined.

6.3. Future Research Proposals

This section provides future work related to the SDC performance. The future research on this domain comprises:

1. Future research should be conducted to determine if more sophisticated stabilizer models (e.g. multi-band stabilizer [95]) should be used, which depend on the dynamic properties of a particular power electronic converted dominated power system.

2. A broader performance comparison (e.g. to consider uncertainty of operating conditions, time delays, failure in the communication infrastructure) of wide-area signals (e.g. rotor angle signal) against different local signals as input options in SDCs, is suggested as future work.

3. The selection of the different operational scenarios for each configuration zone could be also done in a probabilistic way. Criteria for example could consider the probability of a fault to occur, costs of load curtailment or generation re dispatch, high or low risk of circuit breaker failures etc. Different also scenarios could be done for N state and N-1 state. However, all the aforementioned scenarios require knowledge of probabilistic distribution functions of wind speed fluctuations, fault locations, load demand variations, and component reliability. In the future, the provided analysis can be extended by having such validated distribution functions.

4. Analytical assessment of rotor angle stability based on state space model. The WG models used in PowerFactory require revision to ensure that there is correspondence between state matrix based modal analysis and modal analysis of signals generated via time-domain simulations.

5. Multi-scenario (e.g. different fault locations considered with different fault impedance or fault clearing time) and multi-objective based optimization (e.g. minimize angle areas and the maximum angle difference observed) for simultaneous determination of the minimum set of SDCs needed, their best inputs and outputs, and their best settings.

6. Application of SDC to other controllable components such as Storage Energy Systems, FACTS, responsive demand (e.g. large size electrolyzers) should be investigated to define the best strategy for location and tuning of SDC when considering multiple resources.

7. Integration of SDC to reactive control loop, in order to evaluate the damping contribution. Literature states, that this configuration is not thus efficient as when integrated to active control loop. Interesting to investigate, how it intervenes together with LVRT control, also implemented in the reactive control loop.

8. The Objective Function Python script illustrated in Appendix M, is designed so as to determine the Objective Function value, based on the number of the faults that the user desires so as to cover several critical faults and tune the parameters accordingly. Initially, during this project three faults were considered per MVMO iteration, in order to find the solution vector based on a variety of study cases. However, it was found that after some iterations, the simulations collapse because of the big number of the calculations. Therefore the algorithm was terminating. As a solution, in the future, three instances of Power Factory can be used (i.e three different computer terminals running the same code), and each one can be activated with a flag to run it's own fault simulation, so as to decrease the computation effort of the machine and the probability of the out of memory problem can be also less prone to appear. One other PowerFactory version (e.g. version 2019) can also be used to facilitate this problem tackling.

9. Sensitivity analysis, can be also applied for the MVMO parameters used (e.g. achieve size, starting and ending value of scaling factor during the MVMO time duration e.t.c), so as to find the minimum objective function value out of all the minimums.

10. In the MVMO optimization problem, apart from the washout and lead-lag washout gains and time constants, more parameters can be examined, which can affect the transient stability of the system, increasing however the complexity and the computation effort. For instance, the LVRT parameters as mentioned in Appendix E, could also be integrated in the solution vector for testing. In addition, the deactivation time of SDC, for the medium frequencies mitigation that are excited, could also be further tested.

11. Other Optimization Functions, could also be tested for the MVMO algorithms. For instance, if the small signal model of the RMS wind generator model is fixed, then the solution of the optimization problem could be based on the difference minimization of the smallest damping ratio (of all the system's modes) from a minimum acceptable damping threshold (e.g. $\zeta_{th} = 15\%$).

12. Constraints can moreover be used, for the computation of the fitness evaluation. For instance, the minimization of the rotor angles areas, as implemented in this project, does not necessarily mean that the first swing is safeguarded. For instance there could be a threshold value in the angles, in which, after the fault, if the maximum angle of any synchronous machine pair exceeds this value, then a penalty will be introduced in the fitness evaluation of the specific iteration.

Appendices

A

MPPT Control & Pitch Mechanism

A.1. MPPT Control

This section provides information about the ways in which MPPT can be implemented. The significance of this control is elaborated in Figure 2.2, provided in section 2.1.2.

The first way to find the optimal power is based on measuring the speed of the WG shaft. Then according to Figure 2.2, if the aerodynamic model of the WG is known, the maximum mechanical power that can be derived can be found. This maximum power is compared with the actual power retrieved from the machine and the error is used to control the power electronic converters.

One second way is based not on the measurement of the generator shaft speed, but on the measurement of the wind speed. For a given wind speed, and assuming the ratio λ_{opt} /R is known then their product will result in the reference mechanical speed. This speed is compared with the measured speed and the error is used to compute the reference reactive stator current component .

The disadvantage of the methods is that they are requiring the WG optimal power curve, which demands accuracy of the parameters and constants involved. It is mentioned, moreover, that the parameters change as the rotor ages, which adds further complexity. Accurate anemometer, with extra processing specifications, so as to get rid of the wind gusts is also needed which increases the system cost [5].

A.2. Typical Wind Turbine Design Speeds

As illustrated in Figure 2.2, WGs are designed based on three basic wind speed thresholds [5]:

- Cut- in Speed: which is the minimum wind speed in which the turbine can generate mechanical power. Typical range is between 3 - 4.5 m/s.
- Rated Speed: is the minimum wind speed in which the turbine generates the rated power. From the cut- in until the rated wind speed, the output power of the wind generator increases, with the increment in the wind speed. Typical range includes 11- 16 m/s wind speeds.
- Cut- out Speed: This is the speed in which the wind turbine shuts down for safety reasons. Typically is above 21 m/s.

A.3. Pitch Mechanism

The main purpose of employing pitch controller is to restrain the mechanical output of the WG, to a constant value, when the wind speed increases beyond the nominal power. This mechanism targets on turning the blades out of the wind, by using a control system. The control diagram is depicted in the following Figure G.10.

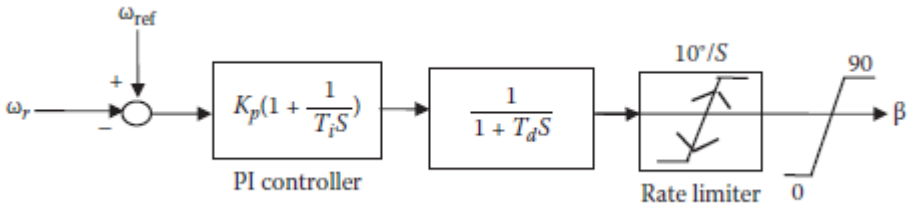

Figure A.1: Pitch Controller Configuration [5].

B

Two - Level & Three - Level Voltage Source Converters (VSC)

B.1. Two - Level VSC

This converter is widely used in industry for many applications, among others, for WG interface with the main grid. The circuit diagram is shown in Figure B.1. It consists of six valves (e.g. IGBTs, IGCTs e.t.c) and an anti-parallel diode for each valve. The converter is bidirectional. This ensues that it can operate as an inverter that can transform a fixed DC voltage into a variable magnitude and frequency three phase AC voltage, or vice versa, it operates as a rectifier in which a fixed AC voltage can be transformed to a variable DC voltage.

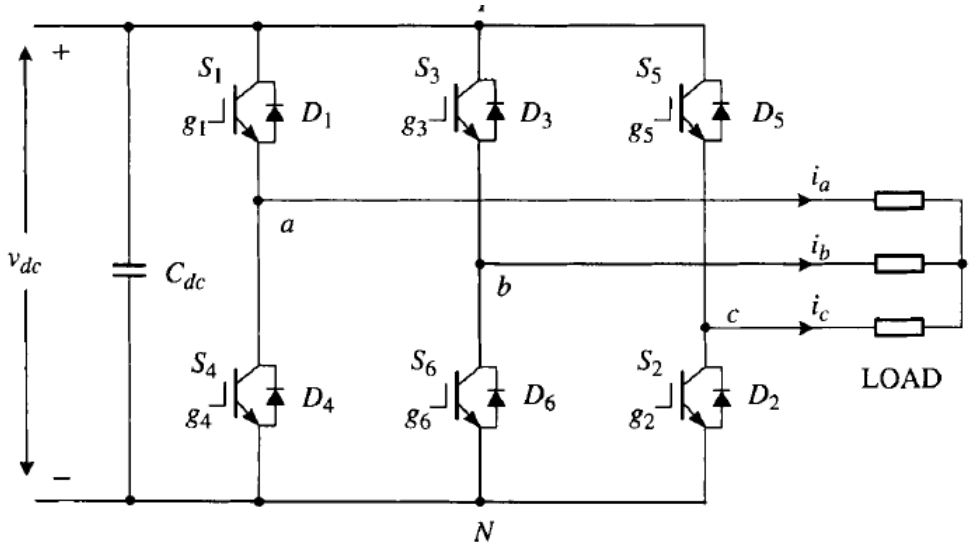

Figure B.1: Two - Level Converter Topology [25].

The inverter topology is examined for the Pulse - Width Modulation (PWM) schemes, but the analysis can be likewise extended to the rectifier configuration. The principle of the sinusoidal PWM technique (SPWM) is depicted in Figure B.2 As observed, v_{ma}, v_{mb} and v_{mc}, are the three- phase sinusoidal modulation waveforms, and they are 120 ° apart. The frequency of the modulation waveforms, is the frequency of the fundamental voltage in the AC side of the converter.

As observed in Figure B.2 valves' conducting relies on the comparison between the modulating waveform with the triangle carrier waveform. When $v_{ma} > v_{cr}$, then S_1 conducts and v_{aN} voltage equals V_{dc}. The lower switch of the same leg, operates in a complementary mode, and during this time

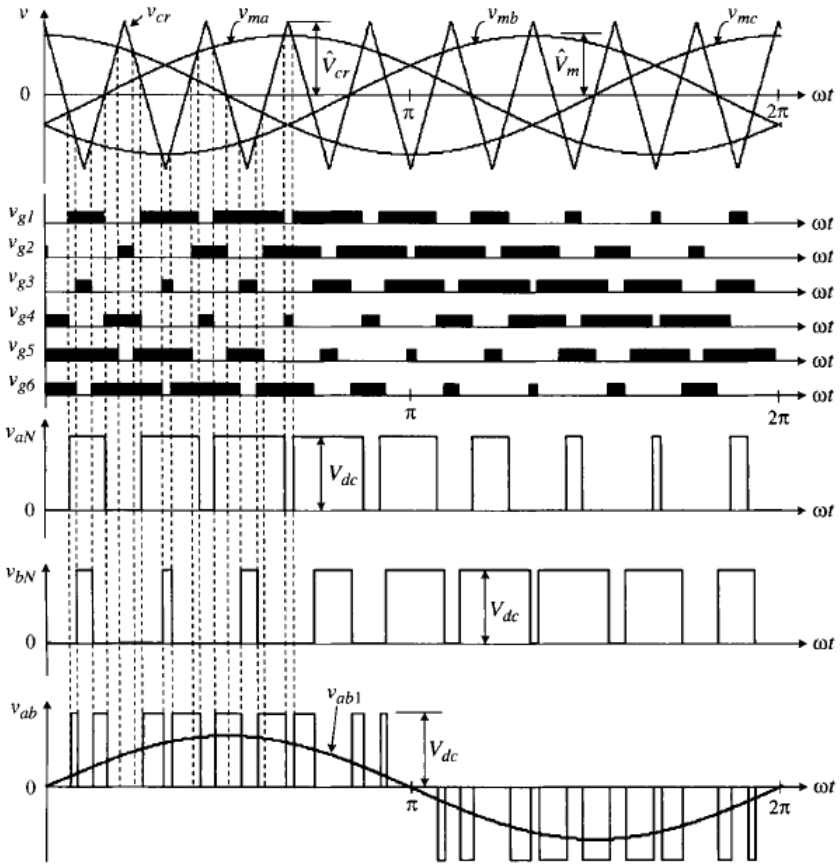

Figure B.2: PWM Basic Waveforms [25].

v_{aN} equals zero. In Figure B.2, the two levels of the phase AC voltage are depicted; this is the reason why this converter is referred as two level configuration. It is also mentioned that in order to avoid short-circuiting, a blanking time between the switching of the upper and lower valve of each leg, should be implemented.

Two modulation indices are used for the description of the SPWM technique. These are, the amplitude modulation index m_a and the frequency modulation index m_f, which are defined as following:

$$\begin{cases} m_a = \frac{\widehat{V_m}}{\widehat{V_{cr}}} \\ m_f = \frac{f_{cr}}{f_m} \end{cases} \tag{B.1}$$

where , $\widehat{V_m}$ and $\widehat{V_{cr}}$ are the peak values of the modulating and carrier waveforms, whereas $\widehat{f_m}$ and $\widehat{f_{cr}}$ are the frequencies of the two aforementioned waveforms. It is mentioned that the amplitude-modulation index is adjusted usually based on the adjustment in $\widehat{V_m}$, whereas $\widehat{V_{cr}}$ is kept fixed.

The fundamental frequency component in the inverter output voltage of each leg can be expressed as a function of the modulation index, as shown in the following Equation:

$$\begin{cases} V_{aN}^1 = m_a \frac{V_{DC}}{2} \\ V_{bN}^1 = m_b \frac{V_{DC}}{2} \\ V_{cN}^1 = m_c \frac{V_{DC}}{2} \end{cases} \tag{B.2}$$

where V_{dc} is the capacitor voltage in the DC side of the converter.

This topology is the one that is used in the current thesis. Generating the pulses with this configuration is relatively easy and is done with the aid of digital signal generators, and micro-controllers. However, the disadvantage is that it can generate high content of harmonics, which they can be also of low order which is difficult to filter out.

B.2. Three - Level VSC

In literature, this converter is also referred as Neutral Point Clamped (NPC) inverter. The main advantage of this converter is the reduced dv/dt and THD in the AC output voltages, compared to the two - level converter mentioned before. The schematic of the three - level inverter is presented in Figure B.3

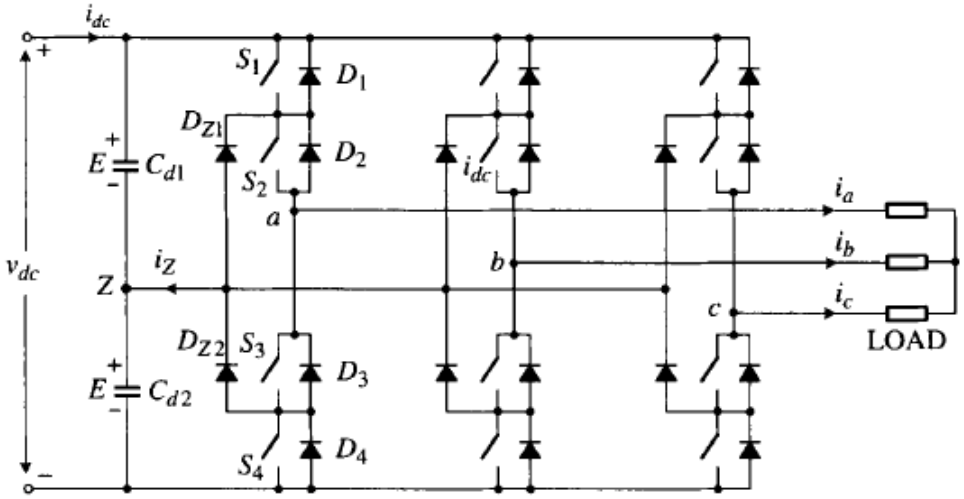

Figure B.3: Three - Level Converter [25].

Each leg, comprises four valves with their antiparallel diodes, whereas the DC capacitor is split into two smaller connected with a neutral point Z. Diodes D_{Z1} and D_{Z2}, are called clamping diodes.

Three operating states are utilized according to the valves that are conducting each moment. These are presented in Table B.1. As illustrated when the upper valves of the leg are conducting, then the phase terminal voltage is equal to the voltage of the capacitor, E, whereas if the lower valves are conducting the phase voltage is the negative value of the capacitor's voltage. During switching state O, the phase voltage becomes zero, due to the short circuit with the inner valves and one of the clamping diodes. If the AC current is positive, during that state D_{Z1} is the one that conducts for example and vice versa.

Table B.1: NPC - Switching States [25].

Switching State	S1	S2	S3	S4	V_{AZ}
P	ON	ON	OFF	OFF	E
O	OFF	ON	ON	OFF	0
N	OFF	OFF	ON	ON	-E

Figure B.4 illustrates the gate signals and the three- level phase voltage of leg a, according to Table B.1.

Last, the line to line voltages can be found by subtracting the phase voltages. In Figure B.5 it is clear that the harmonic distortion is less comparing to the two - level converter.

More information about the power electronic converters, and also about other gating schemes that can be utilized (e.g. vector control e.t.c) can be found in [25], [52].

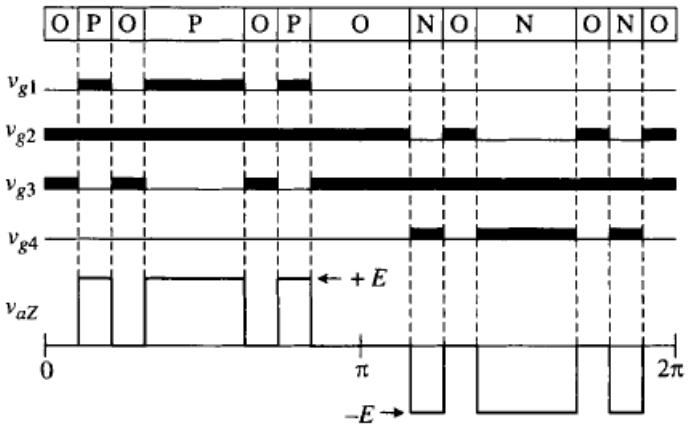

Figure B.4: Gate Signals and Phase Voltage [25].

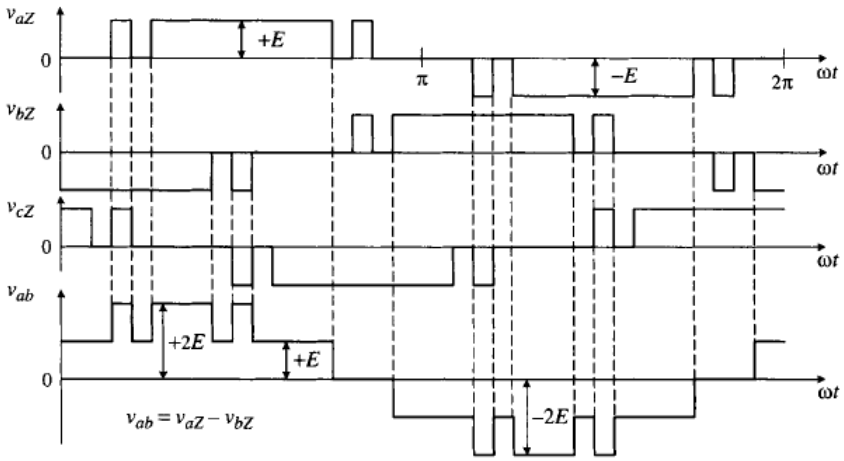

Figure B.5: Line - Line Voltage [25].

C

Rotor Angle Stability for a Single Machine Infinite Bus (SMIB) system

C.1. SMIB example

In the current Appendix, a simple system with a synchronous generator connected to an infinite bus through two tie-lines is examined as seen in Figure C.1.

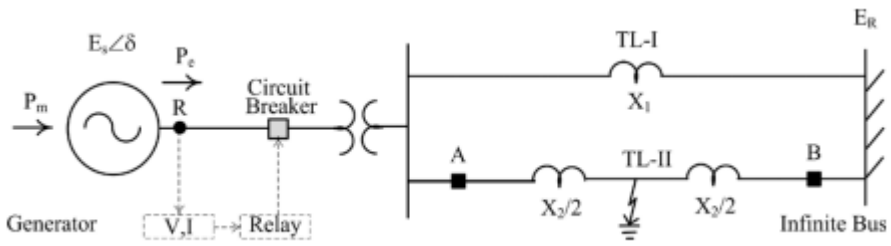

Figure C.1: Single Machine Infinite Bus System Configuration [36].

It is assumed that a a three phase bolted fault is being implemented in the middle of one of the two lines. In that case, even during the fault, a small amount of power is still transmitted. The power-angle characteristic during the fault, can be analyzed, by changing the impedances from star to delta and finding an equivalent impedance between the terminal voltage of the machine and the infinite grid. The power-angle graphs for the cases before, during and after the fault are illustrated in Figure C.2.

Assuming that the mechanical torque applied in the shaft remains constant, then during the fault the electrical power is less, comparing to the mechanical one and therefore, from the swing equation of the machine, the rotor accelerates and the angle increases. After the fault is cleared, the system operates with one line. It is observed that the electrical power in the post- fault period is greater than the mechanical one, so the machine will start to decelerate. However, due to the previous acceleration during the fault, the machine will continue to increase it's angle until it will return back all the extra kinetic energy it took during the fault period. Then the machine, after some oscillations around the new operation point (which is the intersection point of the post-fault power curve and the and mechanical power), will stabilize in that. It is mentioned that if the impedance of the still connected after the fault line is high, and the maximum point of the post - fault power-angle curve is lower than the mechanical power applied in the shaft of the machine, then the machine will not manage to return the increased kinetic energy, so instability is achieved. In a similar manner, if the clearing time is high enough after the fault is applied, then the machine during the post-fault period may will not manage to return back all the extra energy, and if the new electrical power will become smaller than the mechanical power,

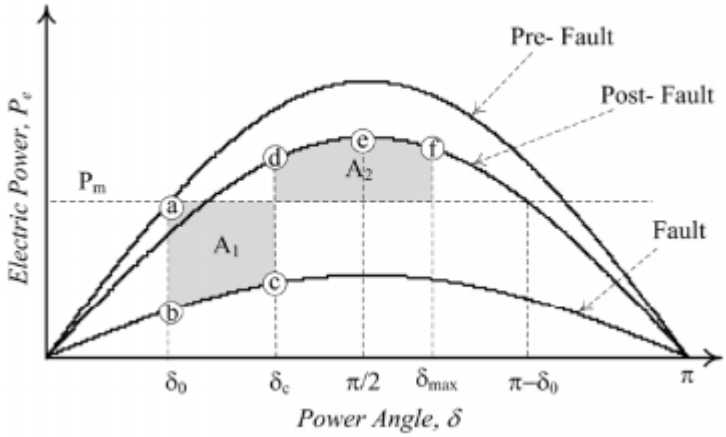

Figure C.2: Power-Angle Characteristic Curve [36].

then the machine will again start to increase it's speed (and equivalently it's rotor angle) and instability is observed.

C.2. AVR contribution in transient stability

In Section 2.2.3 it is stated that underexcited machines are more prone to instability. In fact, the excitation system of the machine provides the energy for the magnetic field that keeps the generator in synchronism with the power system. Supposing that a fault is applied in the terminal of the machine, then the voltage drops to zero, the injected power is also zero and the machine accelerates. However, after the fault is cleared, the voltage returns rapidly to the pre- disturbance value. The voltage level and the new rotor angle in the time of fault clearing will determine the new power to be delivered. However, if this power is smaller than the mechanical power of the machine, then instability is achieved. In that case AVRs with high voltage ceiling and fast response can increase fast the voltage level and the acceleration of the machine is decreased, increasing the probability that the kinetic energy gained during the fault will be removed. In that sense, AVR helps the machine to increase it's synchronizing torque and remain in synchronism with the system.

D

Conventional Power System Stabilizers on Synchronous Machines

D.1. Operational Principle & Structure

Fast AVRs, even if they are presenting a beneficial contribution during the fault, they can deteriorate the power oscillations in the post-fault period. PSSs can modulate the exciter response in that period. However, PSS is generally not effective in first swing instability tackling [35].

SG's active power can be changed by changing not only the turbine's mechanical torque, but also changing transiently the field voltage (see Figure D.1.a). In Figure D.1.b, the PSS operating principle is presented. With the blue line, the machine's output power without PSS is visualized, while the PSS presence is obvious in the green line. It has to be mentioned that ideally the excitation voltage is in anti-phase with the machines' power oscillations, so as the damping torque provided by the PSS to be effective.

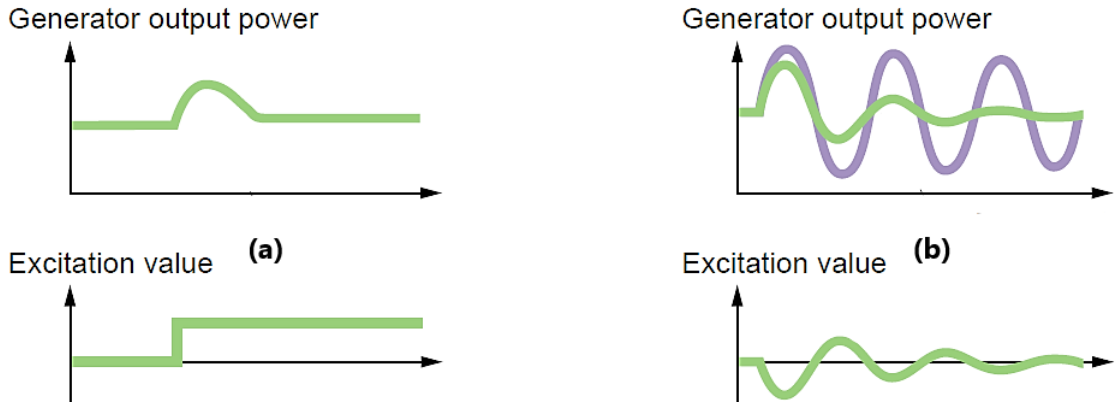

Figure D.1: Different Synchronous Machine'S rotor angle measurements [37].

The conventional PSS is illustrated at Figure D.2. The input signals are usually the shaft speed, terminal frequency and power and the output signal is fed to the machine's AVR system. The structure comprises: a washout filter which acts as a high pass filter and is designed to respond only to changes in the input signal (Typical values for the time constants are of 1s to 20s [3]). The lead-lag transfer function is used to compensate for the phase lag between the PSS input signal and the electrical torque generated. Finally, the gain determines the degree of damping introduced. In [3] it is stated that this gain should be as high as possible but after one critical value the system damping starts decreasing.

Last, a limiter is used in order to protect the machine from important under/over-excitation operating states.

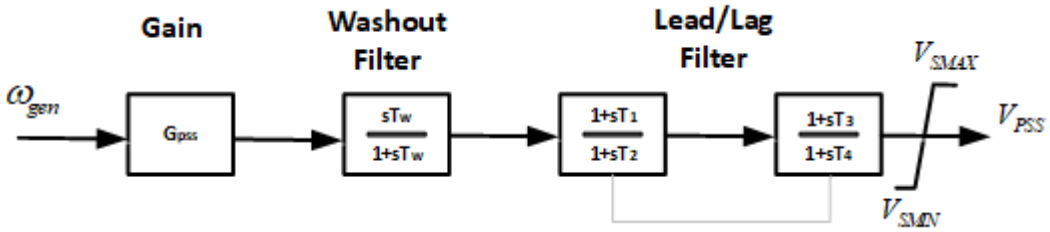

Figure D.2: Different Synchronous Machine'S rotor angle measurements.

E

The effect of WG's LVRT control in the Transient Stability State of a Synchronous Machine

E.1. Mathematical Approach using a simplified model

Wind generators usually are operated in one of the two states during normal operation:

- Constant Power Factor operation: in which the wind turbine usually operates under zero power factor, so as to nullify the reactive power exchange with the grid. This is the control approach of the examined wind generators in this thesis. It is mentioned that if the wind generators are connected with the grid via a long cable (e.g. offshore systems), then usually a non zero reactive power absorption is required, due to the excess reactive power from the cables. In that case, in order to maintain the voltage levels in the Point of Common Coupling, the machines need to operate using lagging reactive power set points.
- Voltage Control mode operation: in which the wind turbine will inject a certain amount of reactive power in order to maintain the voltage levels accordingly. In other words the wind generator behaves like a STATCOM technology.

During fault operation, an LVRT technology as described in Section 2.1.3 is used. Injecting reactive power,the system operator can not only control the voltage levels, but also improve the transient stability of the generators that are nearby. The physical explanation for the latter attribute, is as follows.

A WG, in a simplified manner (i.e. neglecting any mechanical, aerodynamical and Power Electronic Converter controllers), can be modelled as a negative load with a negative conductance G_{WT} and positive susceptance B_{WT}. The modelling of the WG, can be seen in Figure E.1 and is comprised inside the indicated frame. In this Figure, the WG is placed electrically connected to a SG, where a fault is applied in the common bus of the two plants. The values of the WG conductance and the susceptance are given as [40]:

$$Y_{WT} = -G_{WT} + jB_{WT} = \frac{P_{WT} + jQ_{WT}}{V_{WT}^2} \tag{E.1}$$

where P_{WT} and Q_{WT} are the wind farm's active and reactive power production, respectively; V_{WT} is the wind farm connection point voltage

Assumming that R_{GF} and X_{GF} is the fault impedance, then by Thevenin equivalent, the impedance seen by the SG, as illustrated in Figure E.1, is:

$$Z_{eq} = R_{eq} + jX_{eq} = \frac{G_{CF} - G_{WT}}{(G_{CF} - G_{WT})^2 + (B_{GF} - B_{WT})^2} + j\frac{B_{CF} - B_{WT}}{(G_{CF} - G_{WT})^2 + (B_{GF} - B_{WT})^2} \tag{E.2}$$

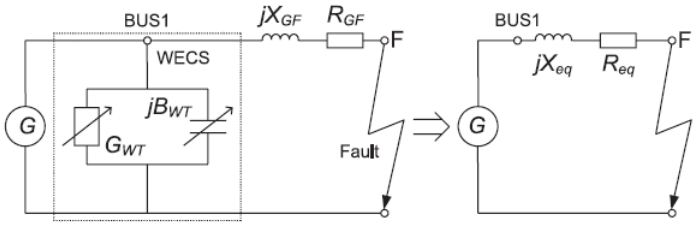

Figure E.1: Simplified WG model in parallel with a SG, when a fault occurs [40].

where $G_{CF} = R_{CF}/(R_{CF}^2 + X_{CF}^2)$ and $B_{CF} = X_{CF}/(R_{CF}^2 + X_{CF}^2)$.

As seen in Figure E.2, when the WG is operating with unity power factor during the fault, then the resistance that the SG perceives, is smaller comparing to the resistance that the SG perceives when the WG is not existing. This ensues, that the machine decreases more it's active power injection when WG is nearby, so from the swing equation, the machine accelerates more and the transient stability is endangered. However, if LVRT is applied, then the reactive power injected by the WG, will reduce the imaginary part of the total impedance that the SG perceives. Therefore, assuming that the total MVA of the fault is the same, then the active power of the machine can be increased during the fault, due to the increment of R_{eq} and this will improve the transient stability. As a conclusion, a decreased X_{eq}/R_{eq} seen from the synchronous machine, is beneficial for it's rotor angle stability. The affection of the LVRT parameters (e.g. "K" gain, dead band), in the transient state determination of the considered power systems, is beyond the scope of this thesis.

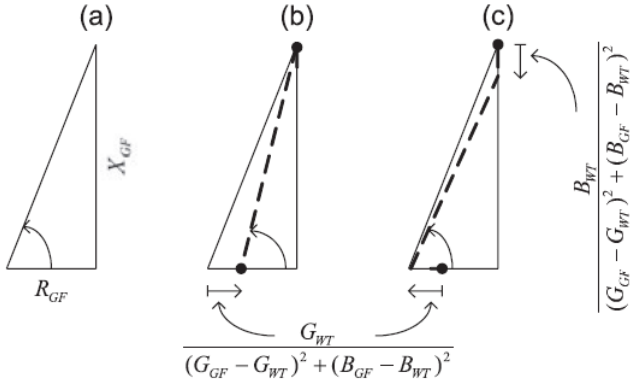

Figure E.2: The impedance seen by the SG during the fault, when (a) WG is not existing, (b) WG exists and operates at a unity power factor and (c) WG exists and operates with LVRT [40].

F

Reference Frame Transformation Schemes

F.1. Introduction

The reference frame transformation is an important tool that can be used to facilitate the analysis of the machines and in general to effectively design controllers for them, or for their PE interface. The three-phase stationary frame (or equivalently abc frame), the synchronous rotating frame (or equivalently dq frame) and the two- phase stationary one (or equivalently $\alpha\beta$) are the ones that are most commonly used. The mathematical transition between the frames is following below.

F.2. Three - phase Stationary to Synchronous Rotating Frame Transformation

The three-phase variables of any AC signal x, (i.e. $x_a(t)$, $x_b(t)$ and $x_c(t)$) can be represented by a space vector $\vec{x}$, which rotates at a speed ω, which equals to the angular frequency of the three AC signals. The instant values of the three variables can be retrieved by projecting, the space phase vector into a, b, c stationary axis respectively. Figure F.1 illustrates the instantaneous values of the three-phase variables at the time instant t=t1.

The transformation of the variables from the abc stationary frame, to the dq rotating frame can be done with the aid of the matrix described as following. It is stated, that the 2/3 coefficient in front is placed such that the magnitude of the d-q components is the same to the magnitude of the a-b-c components.

$$\begin{bmatrix} x_d \\ x_q \end{bmatrix} = \frac{2}{3} \begin{bmatrix} cos(\theta) & cos(\frac{\theta-2\pi}{3}) & cos(\frac{\theta-4\pi}{3}) \\ -sin(\theta) & -sin(\frac{\theta-2\pi}{3}) & -sin(\frac{\theta-4\pi}{3}) \end{bmatrix} \begin{bmatrix} x_a \\ x_b \\ x_c \end{bmatrix} \tag{F.1}$$

As observed in Figure F.2, the dq- axis frame is rotating with the speed of the synchronous speed of the PMSG for the case of the wind generator systems. The transformation matrix elements are derived from the projections of the three- phase variables into the d and q axis respectively. One further important feature is that, since angle ϕ remains constant due to the synchronous rotating speed of the frame, the d and q components are DC variables which facilitate the control structure.

The inverse transformation from dq to abc is given by the transformation matrix as follows:

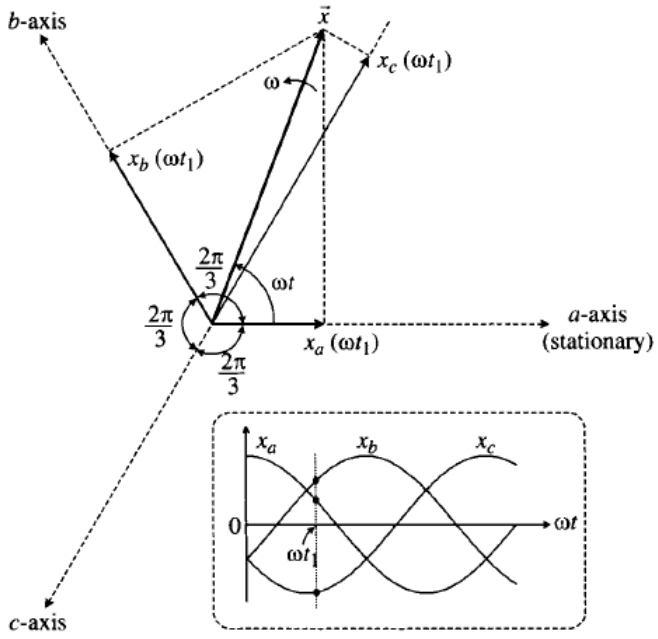

Figure F.1: abc Reference Frame [25].

$$\begin{bmatrix} x_a \\ x_b \\ x_c \end{bmatrix} = \begin{bmatrix} cos(\theta) & -sin(\theta) \\ cos(\frac{\theta-2\pi}{3}) & -sin(\frac{\theta-2\pi}{3}) \\ cos(\frac{\theta-4\pi}{3}) & -sin(\frac{\theta-4\pi}{3}) \end{bmatrix} \begin{bmatrix} x_d \\ x_q \end{bmatrix} \tag{F.2}$$

F.3. Three - phase Stationary to Two - Phase Stationary Frame Transformation

The $\alpha\beta$ frame is not rotating in space and assuming angle θ zero, (a axis coincides with the α one), then the transformation matrix can be derived from the abc/dq one as:

$$\begin{bmatrix} x_\alpha \\ x_\beta \end{bmatrix} = \frac{2}{3} \begin{bmatrix} 1 & -\frac{1}{2} & -\frac{1}{2} \\ 0 & \frac{\sqrt{3}}{2} & -\frac{\sqrt{3}}{2} \end{bmatrix} \begin{bmatrix} x_a \\ x_b \\ x_c \end{bmatrix} \tag{F.3}$$

The inversed transformation is performed from:

$$\begin{bmatrix} x_a \\ x_b \\ x_c \end{bmatrix} = \begin{bmatrix} 1 & 0 \\ -\frac{1}{2} & \frac{\sqrt{3}}{2} \\ -\frac{1}{2} & -\frac{\sqrt{3}}{2} \end{bmatrix} \begin{bmatrix} x_\alpha \\ x_\beta \end{bmatrix} \tag{F.4}$$

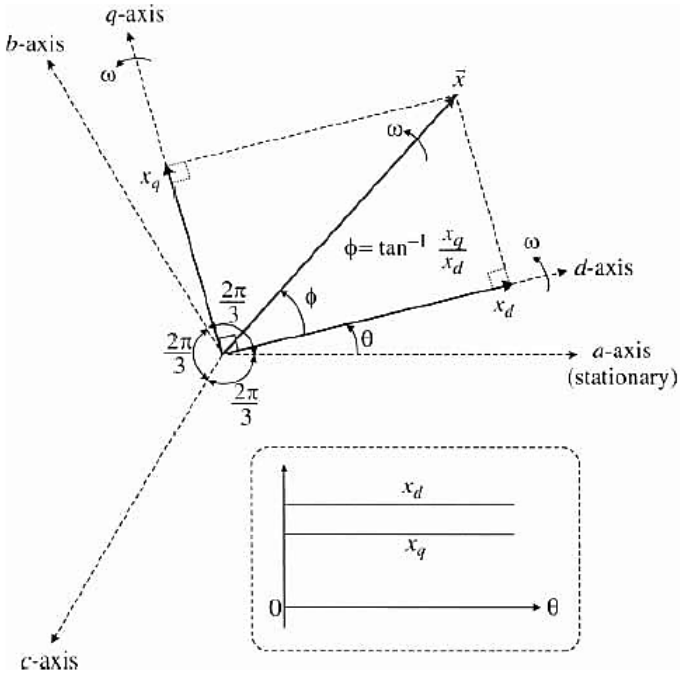

Figure F.2: abc/dq Reference Frame Transformation [25].

G

Detailed Description of the WG model used in RSCAD software

G.1. Description of the given WG model - Basic Blocks illustration

In the current section, the basic block diagrams of the WG detailed model already developed by TU Delft in the context of the MIGRATE project will briefly be analyzed. Understudying the control logic of these models, is the first step so as to integrate WGs in Power Systems, and examine their transient behavior. Additionally, after observing the operational principle of the current wind generator controllers, one can define new controller structures so as to improve the performance of the system.

Before analyzing the main framework of the controllers, it is mentioned that the WG unit is of type IV, the rate capacity of the unit is 6 MVA, whereas the PCC line to line voltage is 33 kV. A high pass filter is further placed in the PCC to mitigate the harmonics introduced by the grid side converter.

G.1.1. Small Time Step and Wind Turbine System

Generally, RTDS uses a time step of 50 μs, which is called a large time step. This time-step can be changed manually, by right - clicking in any point in the canvas .dft file and then selecting "Circuit Options". However, this time step is too big for power electronics simulation. Therefore, we need a small-time step. As a solution, RTDS provides a small box (Figure G.1) for power electronics, which uses a time step of 1.4 μs - 2.5 μs. The small- time step can be determined by right clicking in the blue small time step block » Edit » Parameters. The value the user enters to the 'dt_size' parameter in the VSC bridge box is just a guess for the small dt and the compiler will determine the actual value of the small time step. This value, will be printed in the MAP file upon successful compilation of draft circuit. The user can view the MAP file by right clicking on some white space in the .dft file and then » View » MAP file. It has also to be mentioned that when there is an interface between the main dt and small dt, the ratio between the main dt and small dt must be an integer greater than 17 for PB5 based rack and the ratio must be greater than 12 for NovaCor.

The user puts power electronics interfaced components in this block, due to the high operational frequency (i.e. 19*50Hz used) and puts other components outside this block. In this way, RTDS represents enough exactly power electronics behaviours, and at the same time, requires less computation resources. For further reading, right click on this block and continue by clicking "help" on the pop-up menu as shown in Figure G.1.

Inside the small time step box the wind generation system is modelled. The system includes one PMSG, two VSC converters, DC capacitors and interface transformers, as observed in Figure G.2.

The PMSG is modelled as an interior magnet machine, with sinusoidally distributed windings. Damper windings are ignored. The rated power is 6 MW and the rated phase to phase voltage is 0.9 kV. The block is illustrated in Figure G.3. Moreover, as can be seen, in RTDS there is a switch (in the

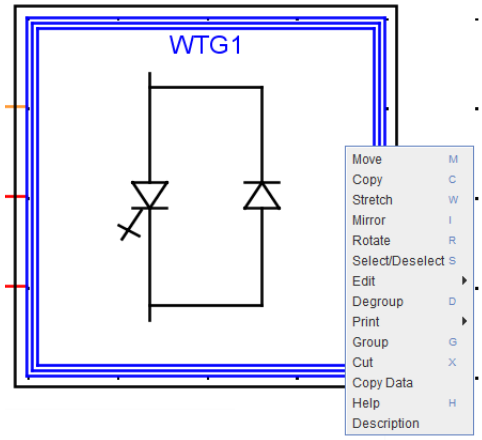

Figure G.1: Small time step box

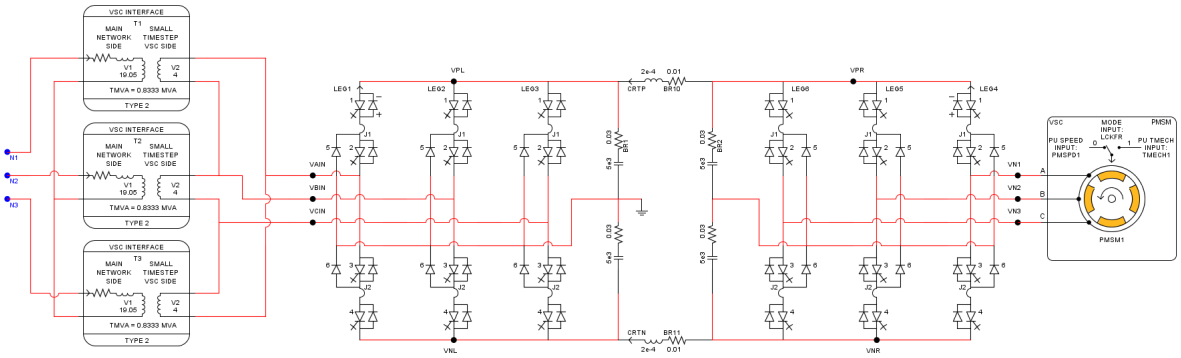

Figure G.2: Wind Generator System

draft file named as LCKFR), and the value of this parameter determines whether the machine operates in the lock/speed mode (when LCKFR=0) or in the free/torque mode (when LCKFR=1). In the lock mode, the mechanical equations are ignored, and the speed of the machine is decided by a control input (i.e. determined with the aid of a slider, which affects a variable named PMSPD1). In the free mode, the mechanical torque in the shaft is an input from a control signal (named as TMECH1) and the speed of the machine is computed after solving the swing equation; this ensues that the speed of the machine (SPDPU as named in RSCAD environment), is determined by the sum of the torques that act in the total inertia of the machine. It is therefore, understood that for transient stability studies, LCKFR should have the value of one. Apart from the previously described mode of operation, the user can select the electrical parameters of the machine, as well as the name of the variables that are to be plotted in the .sib file.

It is mentioned, that the small-time step layout includes some further blocks apart from the power system components described before. These blocks are related to the gating of the IGBTs. To this end, a triangular wave form block is needed. This block as seen in Figure G.4 requires some data coming from the GSC and RSC controllers that exist in the big time step environment. The data needed are the slope of the desired carrier waveform and some discreet points of it. In addition, for the creation of the gating signals, a comparator block is needed as indicated in Figure G.5. For an illustration about the comparator's operational principle, the block related to Leg 4 gating, which belongs to the RSC, is examined. It is mentioned that each leg of the VSC, has it's own comparator block so as to control the valves independently. As observed in Figure G.5, this block receives the triangular waveform (i.e. TWAVE2) from the previous described block and the sinusoidal modulation waveform (i.e. MODWAV6) from the big time step controllers. The output of the comparator block (i.e. FPOUT4), is based on two comparisons. If the sinusoidal modulation waveform is higher that the triangle waveform then the output word will be 1_{dec} (i.e.00000001_b) and 2_{dec} (i.e.00000010_b). This ensues that the upper leg

valves, one and two, will conduct. In contrast, when the sinusoidal modulation waveform is lower that the triangle waveform then the output word will be 4_{dec} (i.e.00000100_b) and 8_{dec} (i.e.00001000_b). This ensues that the lower valves, three and four will conduct. In other words, the configuration of the converter is a three level one, but the valves are being gated as being comprised in a two level topology.

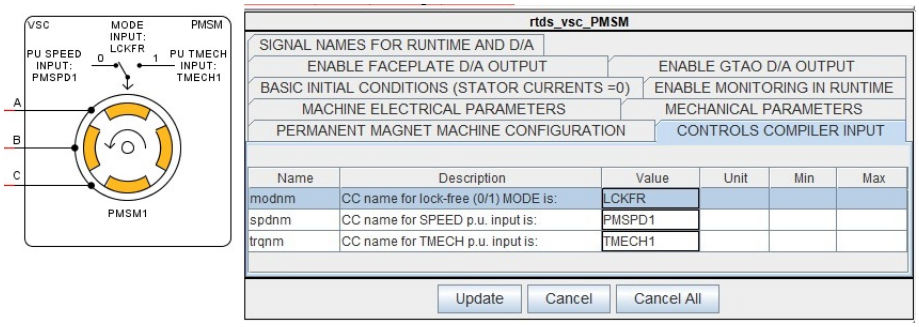

Figure G.3: PMSG block parameters

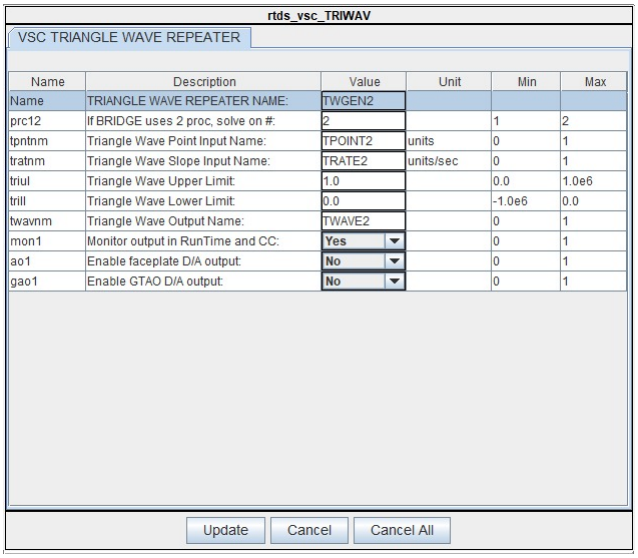

Figure G.4: VSC triangular wave forming

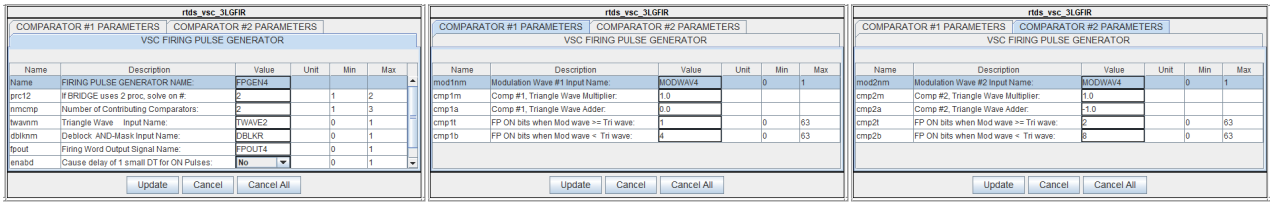

Figure G.5: Leg 4 VSC firing pulse generator

Three hierarchy boxes are shown in Figure G.6 labelled Grid VSC controls, PMSG VSC controls and Wind Turbine and Meters. They are developed to control wind turbine operation. For further reading, please follow Tutorial » Samples » Renewable energy » WindEnergy » Permanent Magnet Wind Turbine » PMTST550.pdf in the RSCAD environment platform.

The three control parts are analyzed in the following three subsections, by illustrating some basic blocks utilized, but a brief introduction considering the objectives is presented here. To this end:

- The ”GRID VSC CONTROLS” box, regulates the d- axis current to maintain DC voltage and also regulates q-axis current to regulate the reactive power output.

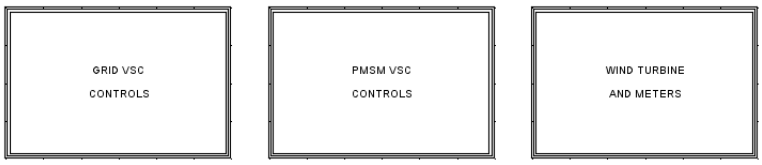

Figure G.6: Hierarchy control boxes

- The "PMSG VSC CONTROLS" box, regulates the d axis current to minimize the reactive power and improve the generator efficiency. Also it regulates q axis current to maximize the captured wind power.
- The "WIND TURBINE AND METERS", includes the aerodynamic model that computes the mechanical power of the turbine for a given wind speed, the pitch angle controller which is responsible to regulate the pitch angle of wind turbine following the change of wind speed and the two - area model to represent the torsional oscillations of the shaft. Inside this block there are also calculations for the PCC voltage, active power, reactive power transmitted.

G.1.2. Aerodynamic Model

Type IV model uses the RSCAD library model for the representation of the aerodynamic power. Figure G.7, presents the aerodynamic part of the wind turbine. One can observe the important delay of the anemometer to "measure" the wind speed, whereas PTRBMW is the real mechanical power of the turbine shaft. The gain of the transfer function is 6, as 6 MVA is the base apparent power of the machine.

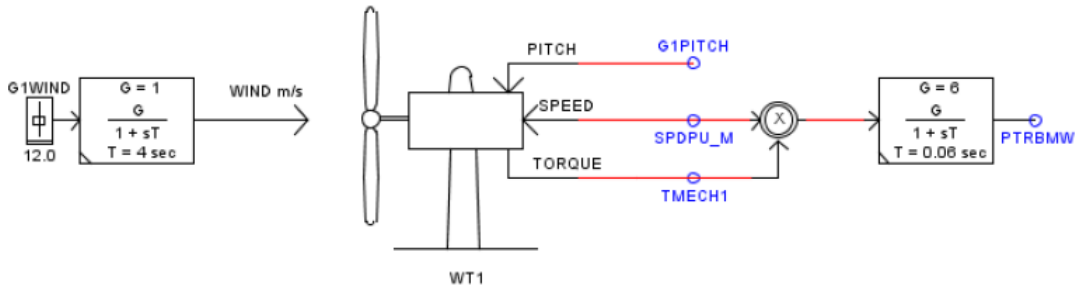

Figure G.7: Aerodynamic Model of type IV Wind Generator

In Figure G.8, the wind turbine data used and the C_p-λ parameters are defined. More details about how the coefficients are used in order to define the power coefficient, can be found in Tutorial » Samples » Renewable energy » WindEnergy » DFIG » WTG50R3.pdf, provided in the RSCAD environment platform. After compiling the draft file, as seen in Figure G.8, the user can plot the C_p-λ waveforms for default pitch angles, and the power output from the wind turbine with respect to the rotor speed for different (default) wind speeds. In order to do that, the user has to process the files CPdata.out and Pdata.out with matlab.

Figure G.9 illustrates that the existing model adheres to a two mass model [3], so as to represent the dynamic behavior of the mechanical part of the wind turbine. This model is capable to produce torsional modes of shaft oscillations, so as to model the wind turbine in a more realistic way. The damping of the torsional oscillating mode can be regulated by selection of the damping factor D_{shaft}. In steady state, the generator speed $SPDPU$ is equal to the turbine speed $SPDPU\_M$. However, in the case of a disturbance, such as three phase fault in the wind turbine terminal, the torsional mode will be excited, differentiating transiently the two speeds.

For protection purposes, in order to eliminate the mechanical stresses, the mechanical speed of the generator can not be infinitely large. In order to restrain the rotor speed, the so-called pitch angle controller is employed, which is presented in Figure G.10. In fact, for big wind speeds, the rotor speed should be restrained by a maximum permitted limit. This limit in the controllers is referred with the

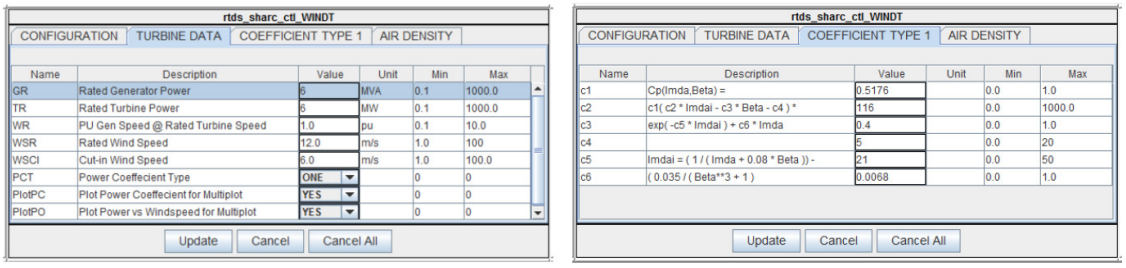

Figure G.8: Wind Turbine Data

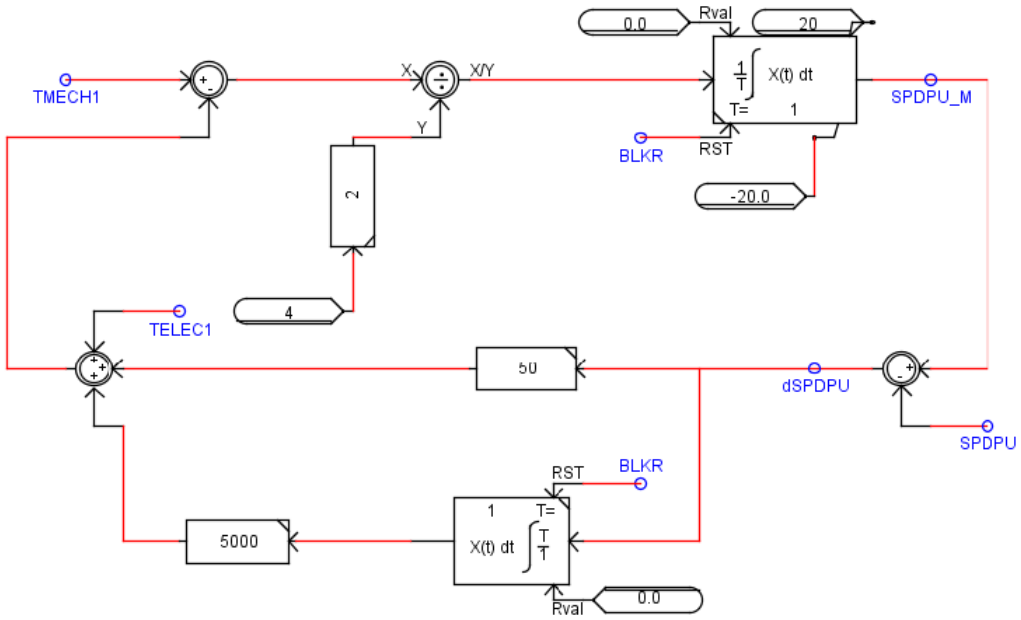

Figure G.9: Two mass mechanical model

parameter G1MXSPD. Thus, when the MPPT controller gives speed output, higher that the permitted limit, the error goes through a PI controller, in order to compute the pitch angle. As seen in Figure G.7, this angle is given as an input to the wind turbine model, and a new speed is computed, that dynamically minimizes the error between the actual speed (i.e. SPDPU) and the upper limit speed (i.e. G1MXSPD).

In Figure G.10, blocking signals BLKL (related to the left GSC) and BLKR (related to the right RSC), are used, so as to open-circuit the valves of the corresponding converter, when is needed during a fault for instance. It is also observed , that if the BLKL (or BLKR) logic is activated, obtaining the value of one, then the maximum permitted speed is limited to one pu. This is reasonable, because if BLKL is activated, then the capacitors in the DC link will suffer from over-voltages. An explanation to the DC voltage increment can be given from the power balance equation, as follows:

$$P_{input}^{inverter} = P_{output}^{rectifier} + P_{capacitor} = P_{output}^{rectifier} + \frac{C \cdot \frac{dV(t)^2}{dt}}{2} \tag{G.1}$$

where rectifier is the Rotor Side VSC and inverter is the Grid Side Converter.

During the pre-fault state, the voltage in the DC link is steady. This entails that the input active power in the inverter equals the output active power from the rectifier. However, during the fault, the output active power from the inverter is being reduced, while the output active power from the rectifier remains the same, as the controller reference did not change. In order to meet the power balance in equation the capacitors in the DC link will be charged and the voltage will be increased. To this end, during the fault and post fault period, a modelled chopper is responsible for controlling the direct

voltage.

Therefore, in order to mitigate this phenomenon, the mechanical power coming from the turbine has to be further minimized and a mechanical approach for doing that is by increasing the pitch angle.

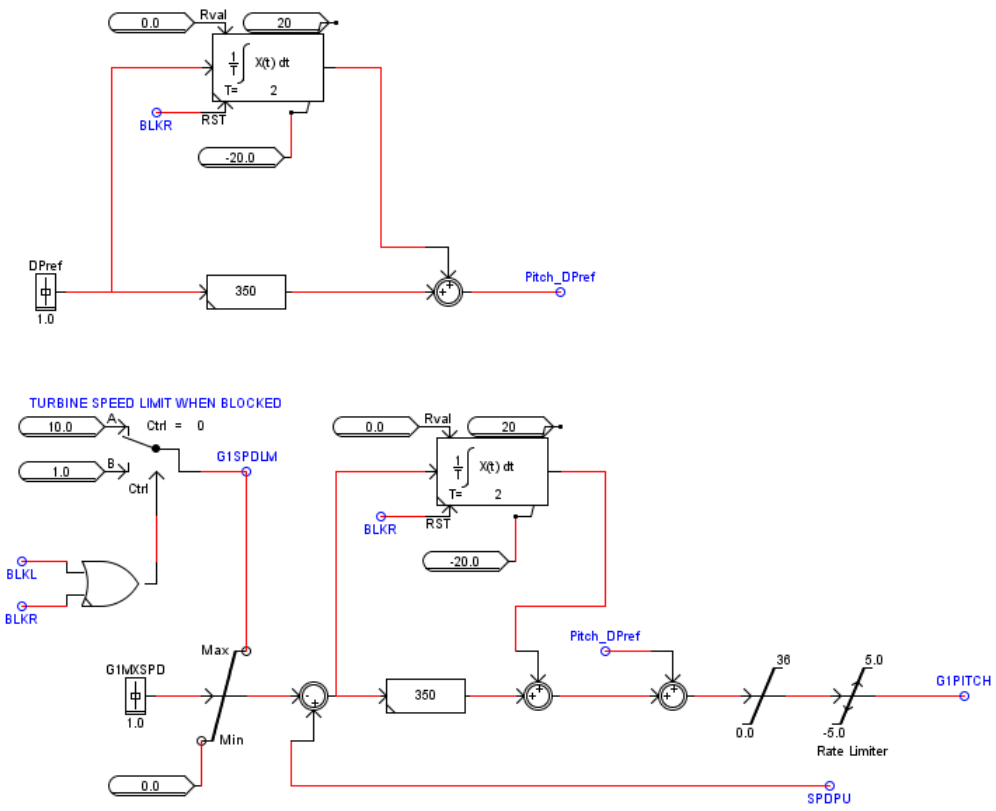

Figure G.10: Pitch Angle Controller

The user has also the ability to manually adjust the pitch angle G1PITCH. This can be done, with the aid of Pitch_DPref variable. The slider DPref, can take values in between the range of ±0.2 This, therfore, can be translated that the Pitch_DPref variable takes values from -90 until +90 degrees.

G.1.3. Rotor Side Converter (RSC) Model

Among all the control methods, Direct Torque Control (DTC) [60],[61] and flux oriented vector control (FOC) are the most common used in order to design the Rotor Side Converter controller. In this project, the FOC is used. In [62], it is explained that the machine's torque has two components; one due to the field flux and a second due to the reluctance torque. In particular, is given by the equation:

$$T_e = \frac{P_s}{\Omega} = \frac{3 \cdot p}{4} \cdot [|\psi_m| \cdot i_q + (L_d - L_q) \cdot i_d \cdot i_q] \tag{G.2}$$

where P_s is the stator active power (MW), Ω is the rotor speed (mech rad/s), p are the pole pairs, $|\psi_m|$ is the magnet flux or magnetic strength (V· m), L_d & L_q are the stator inductances in d and q axis respectively and last, i_d & i_q are the stator currents in the corresponding axis.

In non-salient pole generators (i.e cylindrical rotors), because $L_q = L_d$, machine is not able to produce reluctance torque, so based on Equation G.2, current component i_d has no role in torque production and for achievement to MTPA (Maximum Torque per Ampere), it is necessary that current equals zero. In other words, i_q is the only component responsible to match the power requirements, and contribute to the torque computation.

However, one of the primary functions of the PMSG side VSC, is to control stator current so that it is 180 degrees out of phase with the stator voltage. This maximizes PMSM effeciency as the reactive power in the stator is zero. Thus, in reality, the d-current component controls the armature reaction flux and is varied to keep the reactive power at a minimum as long as the power output of the machine is 1 per unit or less. If wind speed exceeds 1 p.u, then the d-axis current saturates and although the machine delivers the requested power, the power factor and efficiency reduce. The machine voltage decreases and absorbs reactive power. To summarize, the RSCAD controller is designed such that the I_d has to take a non zero value, so as the reactive power is approximately zero in order to minimize the losses in the stator [63].

According to [64], the machine is modeled in the synchronously rotating rotor aligned d-q reference frame as by the following two equations. It has to be mentioned that damper windings are ignored, by placing to the corresponding resistances and reactances in the RSCAD model, large values.

$$V_{sd} = R_s \cdot i_d + \frac{d\Psi_d}{dt} + E_d \Rightarrow \frac{m_d \cdot Vdc}{2} = R_s \cdot i_d + (L_d + L_L) \cdot \frac{di_d}{dt} - \omega_r \cdot (L_q + L_L) \cdot i_q \tag{G.3}$$

$$V_{sq} = R_s \cdot i_q + \frac{d\Psi_q}{dt} + E_q + \omega_r \cdot \psi_m \Rightarrow \frac{m_q \cdot Vdc}{2} = R_s \cdot i_q + (L_q + L_L) \cdot \frac{di_q}{dt} - \omega_r \cdot (L_d + L_L) \cdot i_d + \omega_r \cdot \psi_m \tag{G.4}$$

Where V_{sd}, V_{sq} are the voltages in the AC side of the VSC, E_d and E_q are the EMF voltages induced in the stator of the machine, m is the modulation control signal, V_{dc} is the dc bus voltage, R_s is the stator resistance L_d, L_q is mutual inductance, L_L is the stator leakage inductance, i is the stator current, w_r is the rotor electrical speed, and ψ_m is the permanent magnet flux.

The converter control is illustrated in Figure G.11. As observed. there is an MPPT controller, that adjust the speed reference "WMOPTPU" of the machine in order to harvest the maximum power from the wind. This speed defines the torque of the machine and as analyzed in the aforementioned paragraph adjusts the reference of the stator current in the q-xis. On the other hand, I_d reference is stored at a table, where the output is a function of machine speed. The current reference in the d- axis, is such so as the reactive power is approximately zero.

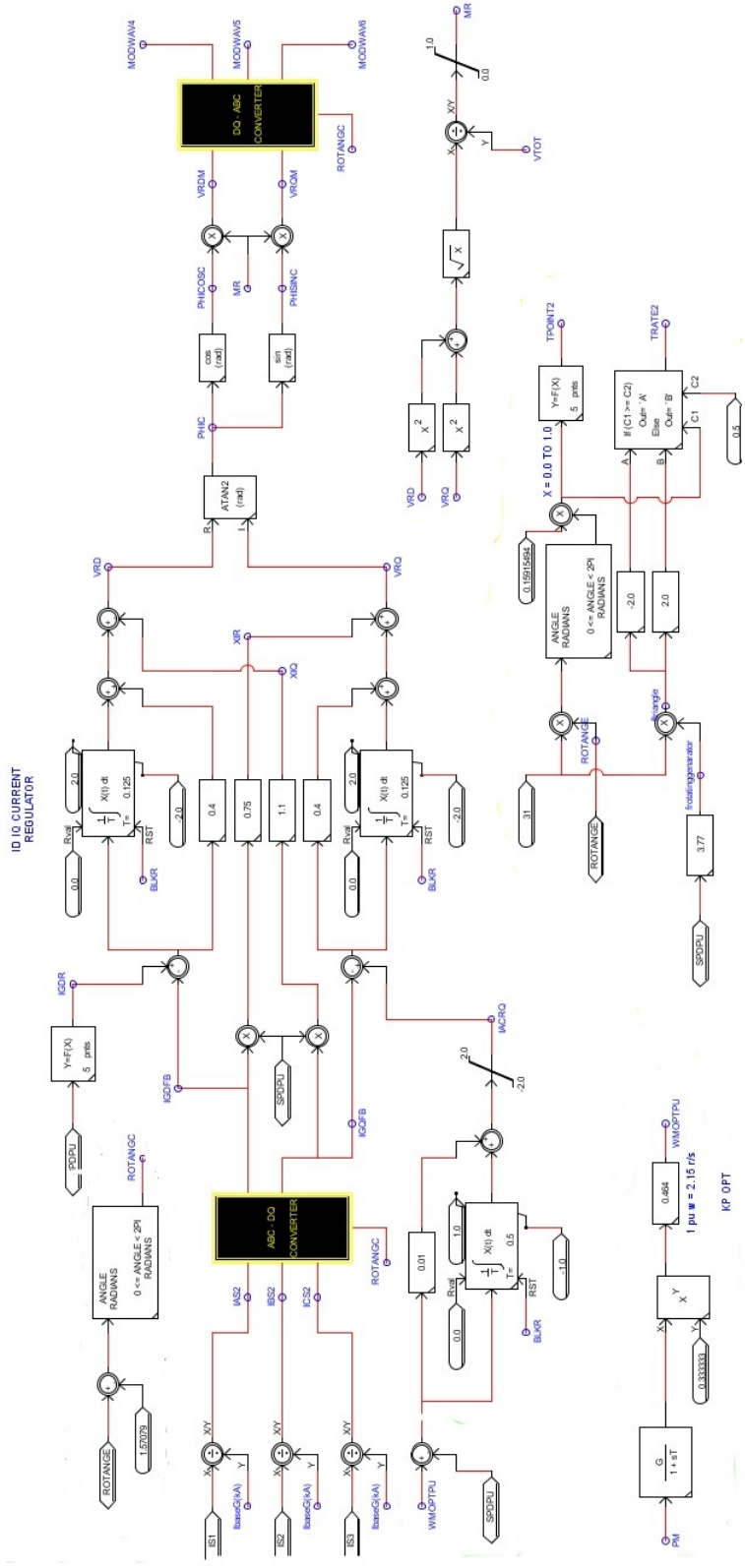

Figure G.11: RSC layout

Moreover, in Figure G.10, it can be seen that the triangle- carrier frequency is 31 times the frequency of the machine. The base frequency of the machine's rotor is 3.77 Hz, thus the actual rotor frequency can be computed from the multiplication of this base value with the pu measured speed. The slope that

will be sent in the small- time step block will be twice the value of the carrier frequency, as expected. Last, the rotor angle signal (i.e ROTANGE) is derived automatically from the PMSG block in RSCAD.

The last point of this sections is the MPPT logic and how this part is implemented. By examining Equations 2.5 and 2.6, it is observed that the optimal rotor speed can be computed as the third root of the active power of the machine divided by K_{opt}. This means that the gain of the transfer function G, in the MPPT loop is equal to the reciprocal of K_{opt}. Then the computed optimal rotor angle has to be expressed in pu so as to be applied in the controllers. To do so, it is assumed that the machine has 11 pole pairs and base frequency at 3.77 Hz. In particular, the conversion from real to pu rotor speed, relies in the following formula:

$$\omega_{pu} = \frac{\omega_r}{\omega_{base}} = \frac{\omega_r}{(\frac{2}{p}) \cdot 2\pi \cdot f_{base}} = 0.464 \cdot \omega_r \tag{G.5}$$

G.1.4. Grid Side Converter (GSC) Model

Before starting analyzing the basic controllers of the GSC, one essential block for the overall correct operation, the phase-locked loop (PLL) block is presented first. The synchronous dq-reference frame is used in combination to conventional current controllers, in order to control the active and reactive power injected (or withdrawn) to (or from) the grid. The synchronization with the grid is done using a synchronous reference frame phase-locked loop PLL, as shown in Figure G.12. The PLL block, gets as inputs the voltages in the PCC, and computes the frequency and the phase angle of the space time voltage vector. The angle of the PLL is defined so that the q-axis voltage is zero. This orientation is important, because decoupling, in terms of the injected active and reactive power, is achieved . In particular, the active power is proportional to the d-axis PCC current, whereas the reactive power is proportional to the q-axis PCC current [25].

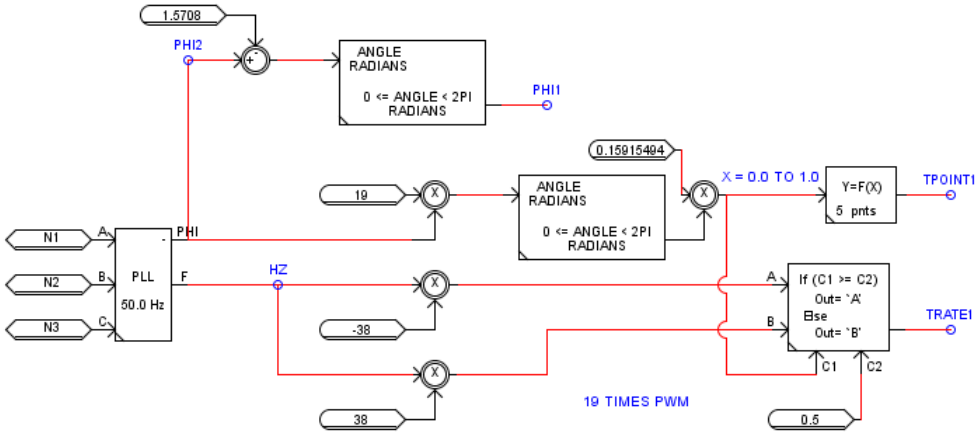

Figure G.12: PLL block & Signals Transmitted to small-time dt layout for PWM gating

In Figure G.12, the carrier signal for the PWM modulation is also computed. The slope and discreet points are computed and are sent in the triangle wave repeater in the small - dt block. This block will construct the final triangle waveform so as to compare it with the sinusoidal waveforms, as described in section G.1.1. The carrier signal will have $19 \cdot 50$ Hz frequency, thus the reciprocal of the slope will be either $+19 \cdot 2 \cdot 50$ (if x=1), or $-19 \cdot 2 \cdot 50$ (if x=0). Moreover, the angle takes values from 0 until 2π, thus in order to form the triangle wave from 0 to 1, the user has to divide by 2π.

The angle of the PLL is then used for the calculation of the d-q components of the grid voltages and currents in the PCC, as seen in Figure G.13. The transition from the abc domain to d-q one is performed via the Park transformation. The transfer functions in front, introduce a time delay and represent the sensors needed to take these signals in real world.

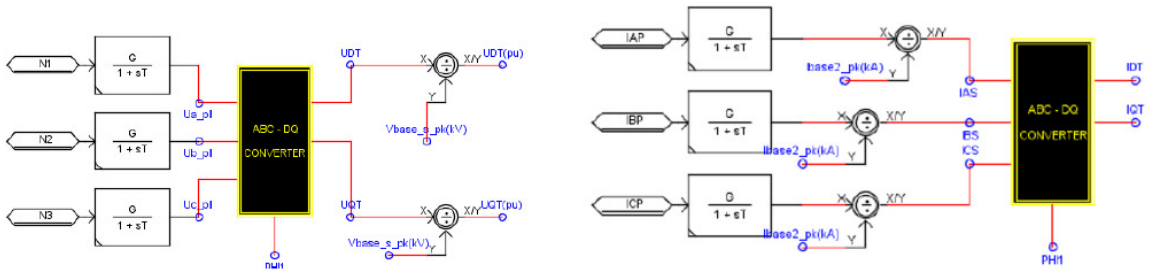

Figure G.13: Per Unit d-q voltages & currents

The inner current controllers of the Grid Side Converter are shown in Figure G.14. The parameters are defined based on the Internal Mode Control technique. The current controllers are derived from the differential equations of the VSC converter in the d-q frame. Having these equations, then taking the Laplace transform, the open loop model is derived. However, in order to enhance stability and robustness, the closed loop is used as seen in Figure G.14. In other words, the measured d and q currents in the PCC, try to reach the reference currents (i.e. IDR and IQORD), which are computed by the outer control loop, so as the desired internal voltages VTD and VTQ to be achieved. In other words,VTD and VTQ are the d, q components of the first harmonic phase to ground voltages at the AC side of the converter. As known:

$$\hat{V}_{an}^{1} = \sqrt{VTD^2 + VTQ^2} = m_a \cdot \frac{V_{dc}}{2} \tag{G.6}$$

where m_a is the modulation index, or equivalently the amplitude of sinusoidal waveform that will be given as input in the PWM comparator. Equation G.6 is represented in Figure G.15.

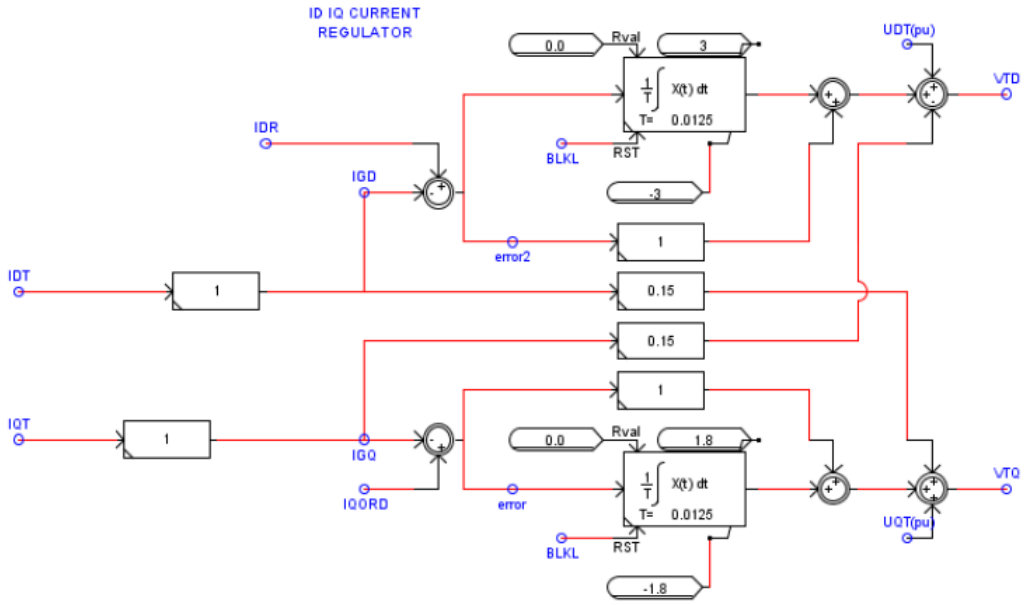

Figure G.14: Inner current control loop of the grid side converter

The current references of the inner current controller, as mentioned, are provided from the outer loop. Typically, the d-axis component is related to the control of the active power, and is implemented by the DC voltage regulator as seen in Figure G.16. As it will be analyzed, during normal grid conditions *"FRT_FLAG"* and *"RAMP_FLAG"* are one, whereas *"RAMP_signal"* is zero. This entails that the reference d current is computed only by the DC regulator. V1 and V2 are the voltages in the upper and lower resistive - capacitive branches in the DC side of the Grid Side VSC, and they have values at

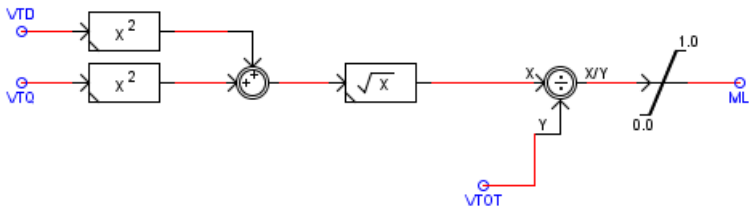

Figure G.15: Modulation Index Creation

V1=V2=$\frac{V_{dc}}{2}$. Therefore, V1PU=V2PU=VDCR= $\frac{V_{dc}}{4}$. It is mentioned that the rated - base voltage in the dc link is 4 kV, and VTOT= $\frac{V_{dc}}{2}$.

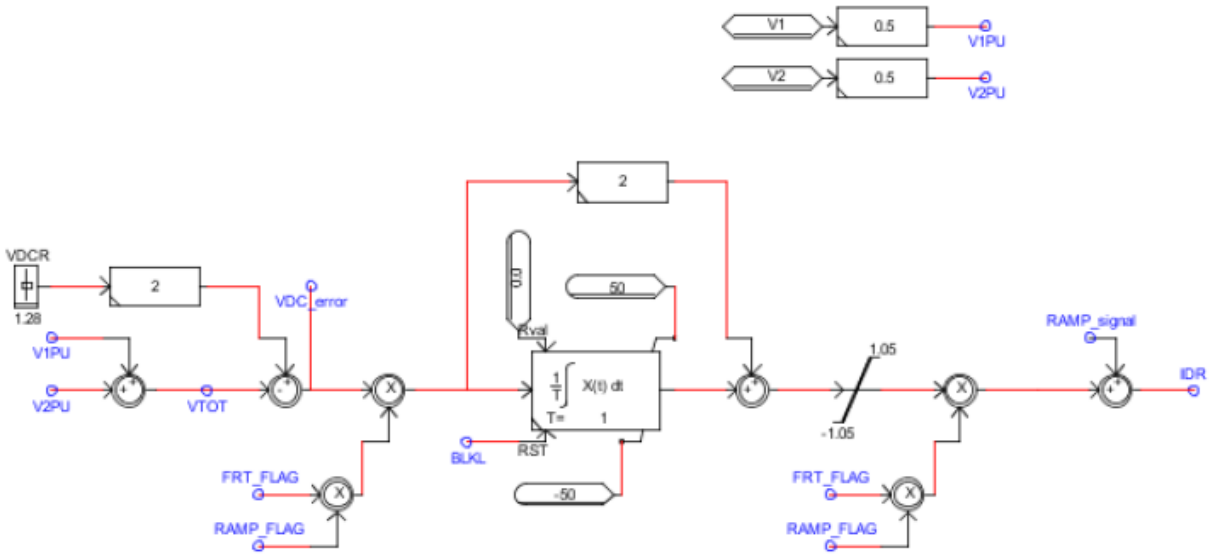

Figure G.16: Outer Loop- DC Voltage Regulator

Before examining the second outer loop in order to determine the reference current in the q axis, one additional control loop which determines the voltages V1 and V2 and most importantly, the PWM gating of the valves in the Grid Side VSC, is analyzed. As seen in Figure G.17, during normal conditions V1PU=V2PU and VBAL equals zero, thus the ALPHA parameter has zero value. However, the user can change the value of the slider "VBAL", so as the ALPHA parameter has a non-zero value. This will have as an impact that the sine waveform will have a positive (or negative) offset and it will not be any longer a sinusoidal signal around zero. If the offset is positive, the valves in the lower part of the legs will conduct longer and as a result the lower capacitor will be charged more. This voltage imbalance is an undesired phenomenon, since the capacitor with the high voltage wears down, and the current in the branch that has higher voltage, is also greater so losses are increased. Moreover, due to the offset the harmonic distortion in the AC side of the VSC is higher. Thus, this loop is actually a manner to see how the grid behaves when the harmonic content is important.

In Figure G.18, VACPCC is the pu, peak, phase to ground voltage in the PCC, and this is a variable used in the following section.

Regarding the outer loop in order to determine the reactive current, three ways can be implemented. These ways are presented as seen in Figures G.19, G.20 and G.21 respectively. In Figure G.22, the block used in order to select one of the three outer aforementioned controllers, is depicted. In particular, Figure G.19 presents a reactive power control loop based on the IEC61400 wind turbine generic model. This is a cascade controller that offers the advantage that regulates the reference AC voltage in the

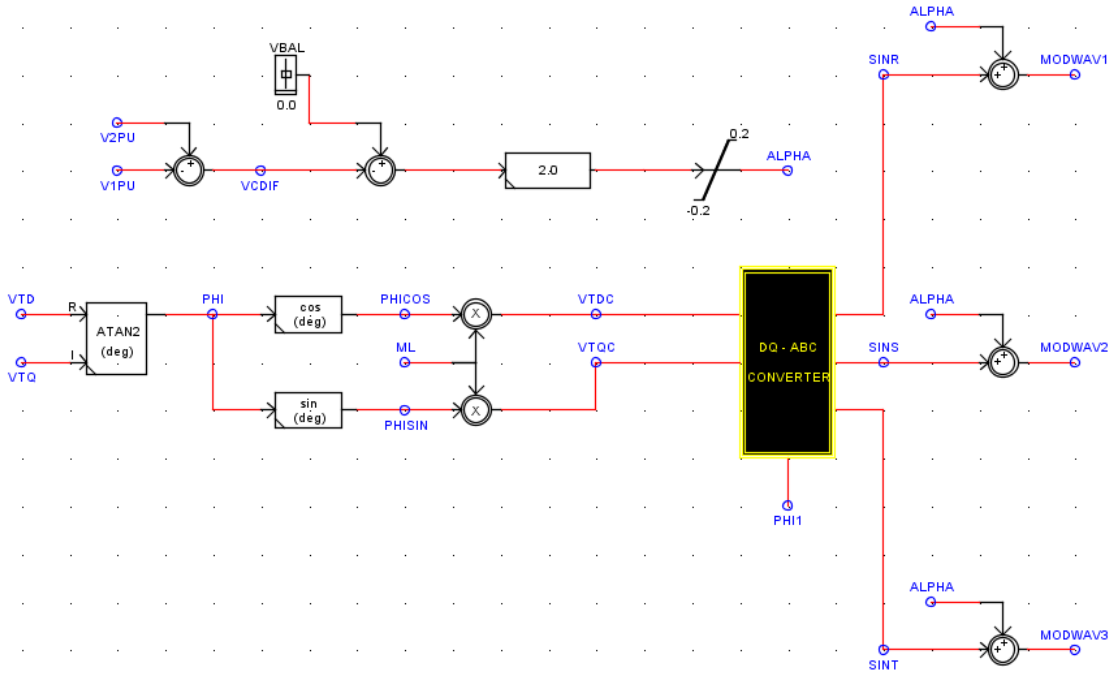

Figure G.17: VBAL slider and influence in the sinusoidal waveforms created

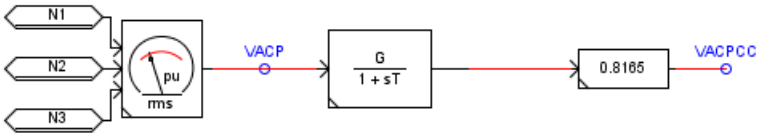

Figure G.18: Per Unit Phase Voltage Computation at PCC

PCC between the permitted limits. Besides the IEC controller loop, the GSC can also apply a voltage regulator as seen in Figure G.20 or a reactive power regulator as in Figure G.21.

During normal grid operations, FRT_FLAG and $RAMP\_FLAG$ have value 1. Moreover, in Figure G.22, the signal Diq_FRT has value 0. These signals are examined later in this section, as the logic of the controllers will be slightly modified to comply to the LVRT capabilities that the WG should provide during faults.

Based on ENTSO-E regulations [28], the converter station connected to the wind turbine should provide Fault Ride Through FRT / Low Voltage Ride Through LVRT capabilities. The LVRT logic is implemented in RSCAD as follows. As seen in Figure G.23, during a fault in the system, if the peak phase voltage in the PCC is reduced below 0.8 pu (indirectly the concept of dead-band is integrated by that manner), then the FRT_FLAG becomes 0. This ensues, that the signal Diq_FRT will no longer be zero. Observing, Figure G.16 and Figure G.22, the reader realizes that during the fault the reference of the PCC current in d axis is zero, while in q axis is given by the value of Diq_FRT. In other words, the wind generator does not inject active power but only reactive power so as to support the voltage drop.

The control logic in Figure G.23, suffers from one disadvantage. When over-voltages occur in the power system, the FRT_Flag doesn't get zero, so the Diq_FRT remains zero. In practice, it would be desired that during over-voltages, the Diq_FRT current is negative, so as the wind turbine has a inductive behavior and absorbs reactive power.

After the fault is cleared, we can expect that the d-axis and q-axis reference currents, return to their pre- disturbance values. However, this transition is not done abruptly. In order to protect the power electronics components from the fast transients during the post-fault period, the converter's active current is ramped-up with the so called ramp-up rate given in pu/s. In Figure G.24, the logic is presented. During the post- fault period, due to the injection of reactive power, the voltage in the PCC

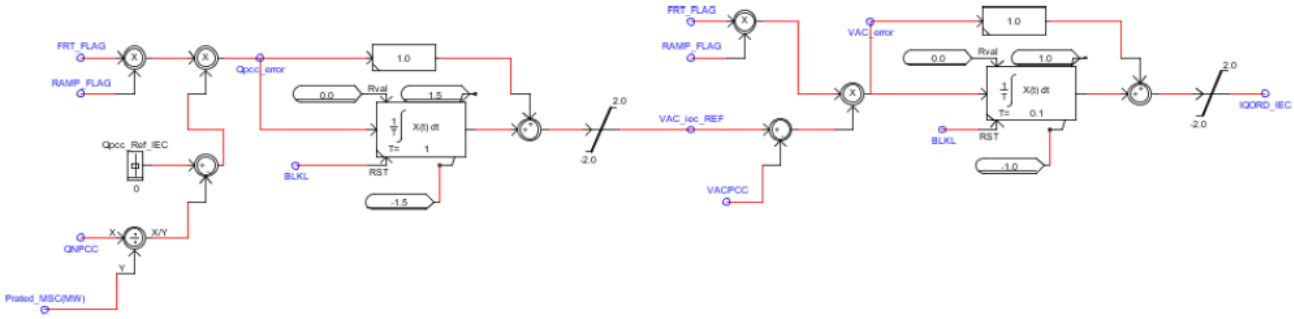

Figure G.19: 1st Outer Control Loop- Cascade based on IEC61400

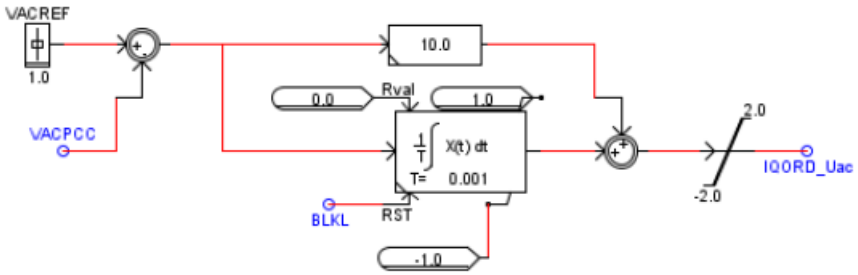

Figure G.20: 2nd Outer Control Loop- AC voltage regulator

is being increased. When the voltage is becoming bigger than 0.8 pu then the $RAMP\_FLAG$ is being activated, by having a value of 0, for 0.6 seconds. As easily understood, when the $RAMP\_FLAG$ is zero (during post-fault period), the FRT_FLAG is one. The slope of the current ramping up is defined, by the time constant T. The smaller the T, the higher the slope. In [29], it is proven that the slower is the ramping up of the onshore converter station active power, the slower will be the direct voltage recovery to the normal pre-fault value. Moreover, the slower is the ramping rate, the bigger is the burden placed to the chopper mechanism.

To wrap up, during the post-fault period, the active current reference is derived from Figures G.16 & G.23, while the reactive current reference from Figures G.19/G.20/G.21 & G.22.

During the fault and post fault period, the chopper is responsible for controlling the direct voltage while the DC voltage control loop is blocked. The chopper is actually a switch that is gated with the PWM technique. When V1 or V2 become higher than 2.2 kV, the switch is activated, as seen in G.25. The PWM comparison is between a carrier signal of frequency at 50Hz and the voltage difference between the upper permitted DC voltage limit and the measured DC voltage.

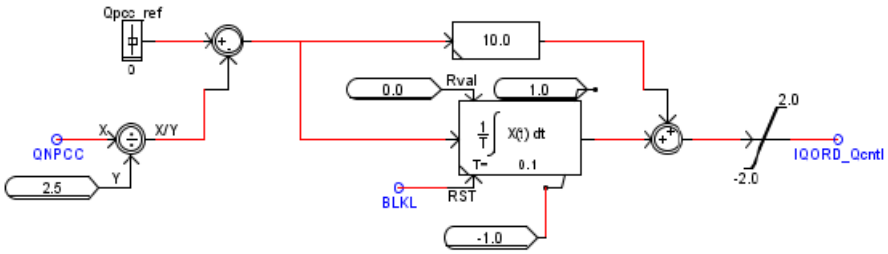

Figure G.21: 3rd Outer Control Loop- Reactive power regulator

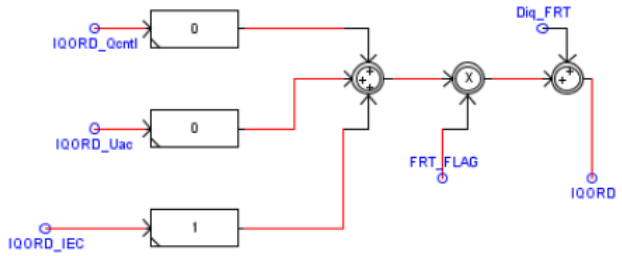

Figure G.22: Block for selection of the outer-reactive power control loop

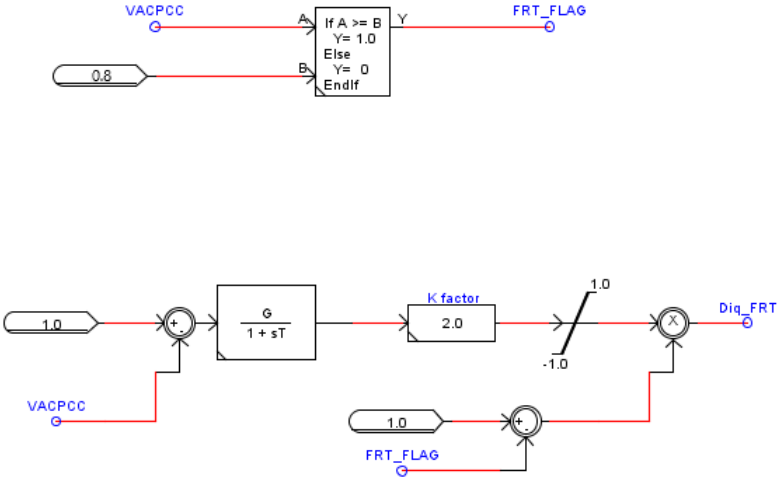

Figure G.23: LVRT logic in RSCAD

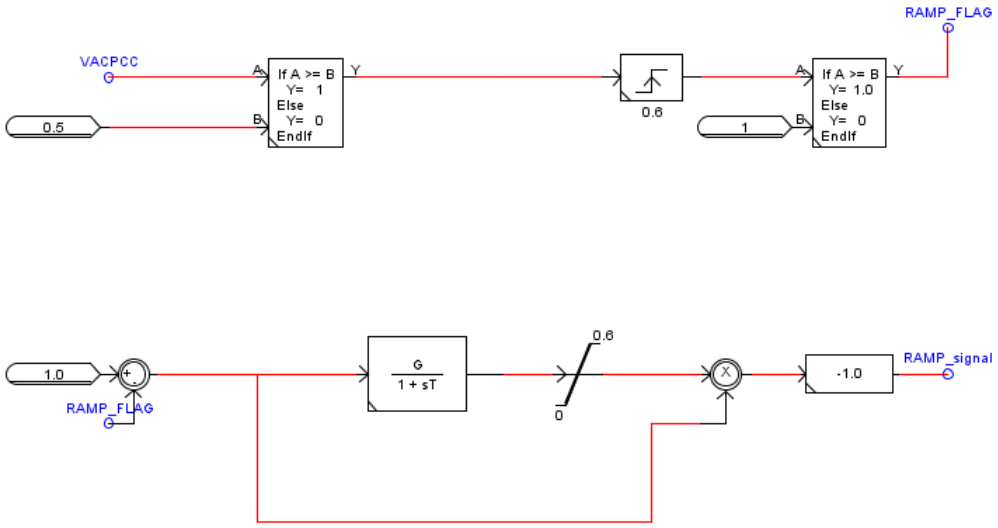

Figure G.24: Ramping of the active current in the post-fault period

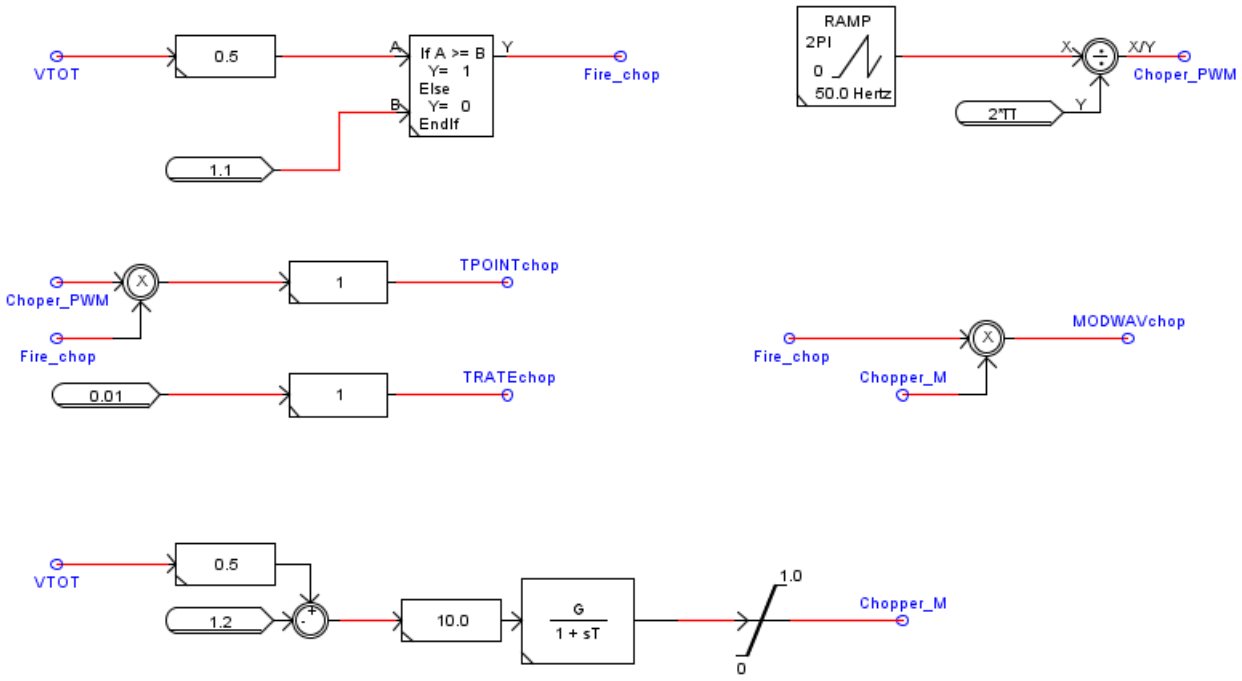

Figure G.25: Chopper Controllers

G.2. Modifications of WG model to enhance transient stability

G.2.1. PLL Low-Pass Filter Modification

In Figure G.12, by right- clicking in the PLL block, the user can see that there is a phase shift of 30 degrees lagging with respect to axis A. Then this angle is reduced by $\pi/2$ and then the angle goes to the Park Transformation Block. It is mentioned that the 30 degrees lagging that is used, is to compensate the phase shift introduced by the low pass filter (time constant = 0.002), which is exactly before the abc/dq transformation block. Subtracting $\pi/2$ is done so as to align the rotating reference frame with the d voltage component. However, using the filter transfer function as defined in Figure G.26, the lagging phase is not exactly 30 degrees, and thus the desired amplitude of the UDT component which should be equal with the phase-peak voltage in the PCC (i.e. $\sqrt{2/3} \cdot 33kV$), is not achieved, which ensues to incorrect current reference determinations. For this reason, the filter transfer function is changed according to Figure G.27. It is mentioned that for achieving the correct alignment, not only better compensation was chosen, but also one time-step delay in the PLL circuit was added, as observed in Figure G.28, since in RSCAD there is one time step difference between power system components and control components.

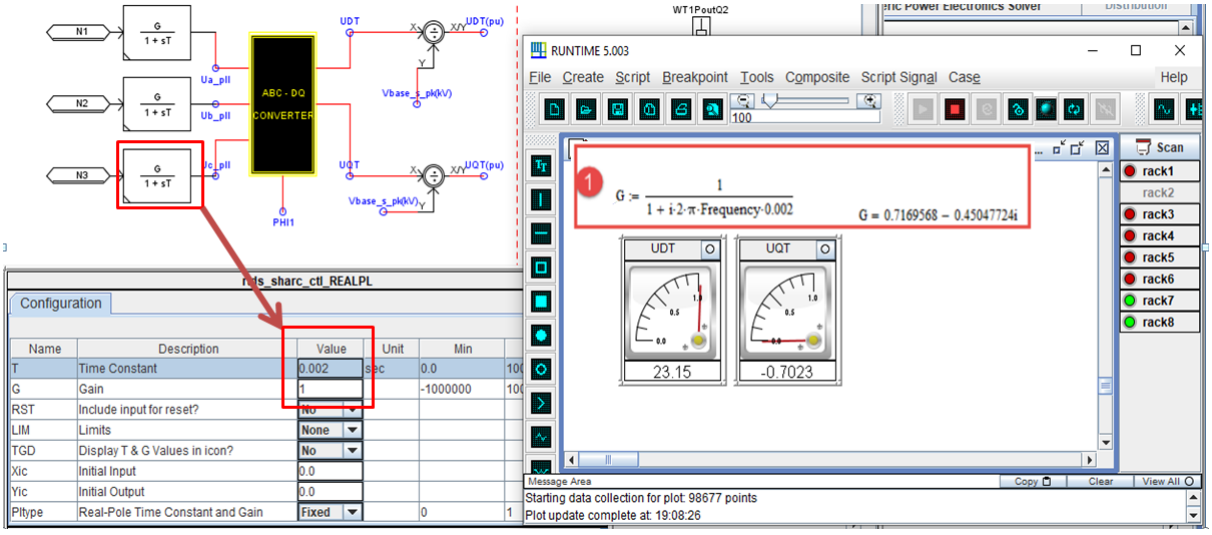

Figure G.26: Initial-Incorrect Filter

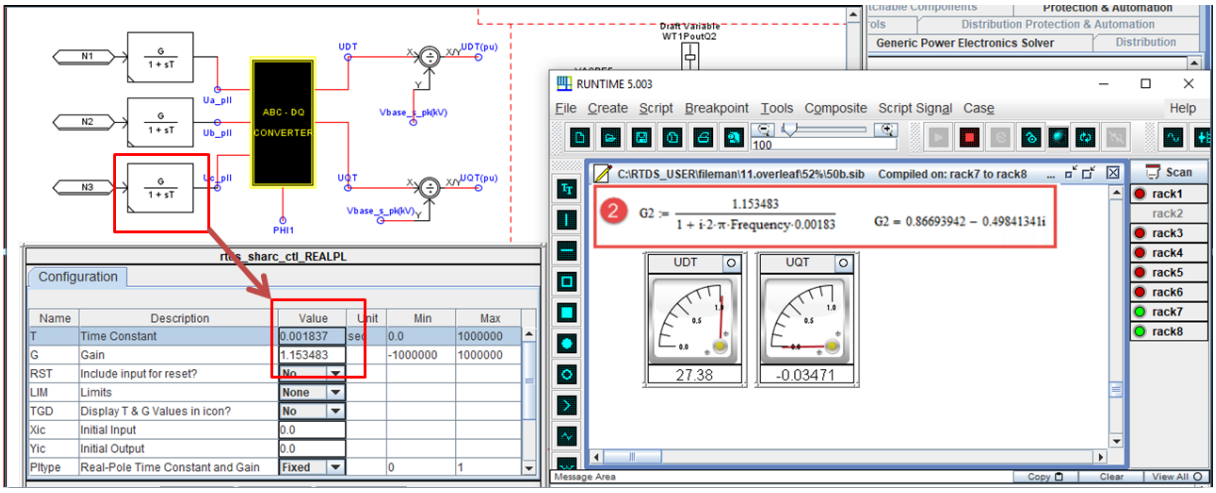

Figure G.27: Modified-Correct Filter

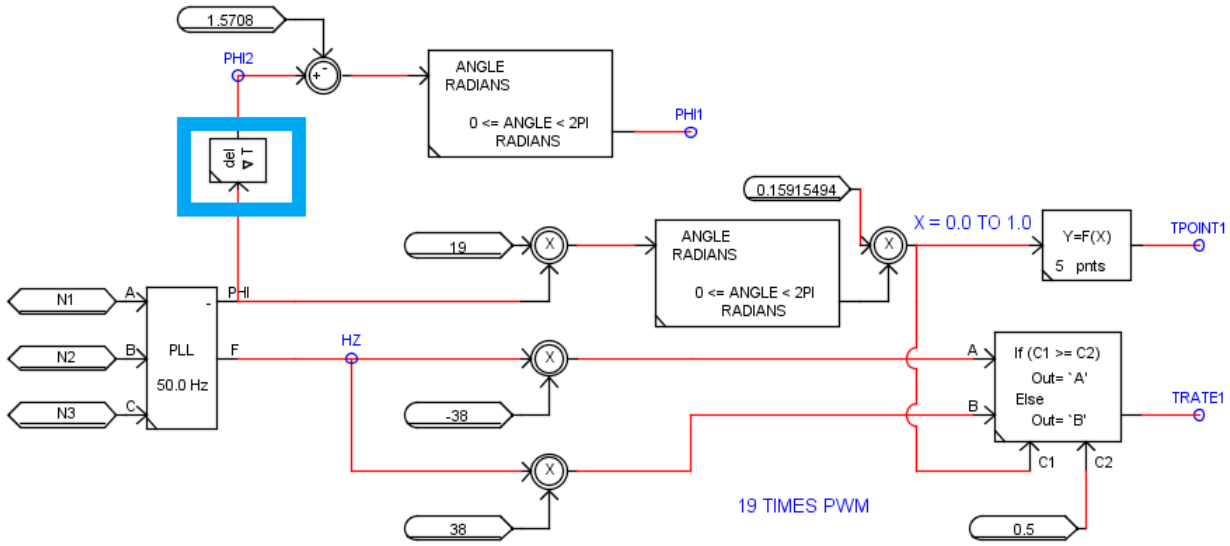

Figure G.28: Addition of one time step delay in PLL

G.2.2. RMS VS Peak Voltage values

Apart from the modifications implemented as described in the previous paragraph, some additional changes were made to the received model, described in section G.1. In Figure G.23, the LVRT strategy should be activated when the RMS Line to Line voltage is to be reduced below 0.8 pu. This ensues that, since the phase peak parameter UACPCC is used, 0.8 is multiplied with $\sqrt{2/3}$. One other correction done, is related to Figure G.20. There, the RMS line line to line voltage UACP, should be used for the determination of the q current reference injection.

G.2.3. Scaling- Up the Wind Power

In order to scale-up the power from one 6 MVA single WG unit, and to represent a bigger wind farm, the interface transformer inside the small - time step environment is to be used. A slider, so as the user to select the number of parallel units has to be also utilized, as seen in Figure G.29. Last, the measured active & reactive power in the PCC, has to be devided with the scaling factor selected by the user, since this signal, is used in the controllers of one single unit. Figure G.30 illustrates the aforementioned approach.

Name	Description	Value	Unit
namsc	Primary Scale factor, Input Name:	Scale	
tcnsc	Prim Scale factor, Smoothing time constant:	0.1	Sec.
scupr	Prim Scale factor, Limit at maximum expected:	10	pu
sclwr	Prim Scale factor, Lower limit:	1.0	pu
scini	Prim Scale factor, Initial value:	5.0	pu

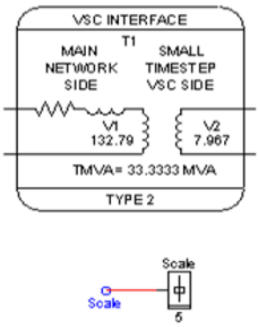

Figure G.29: Scaling-up the power of a single WG plant

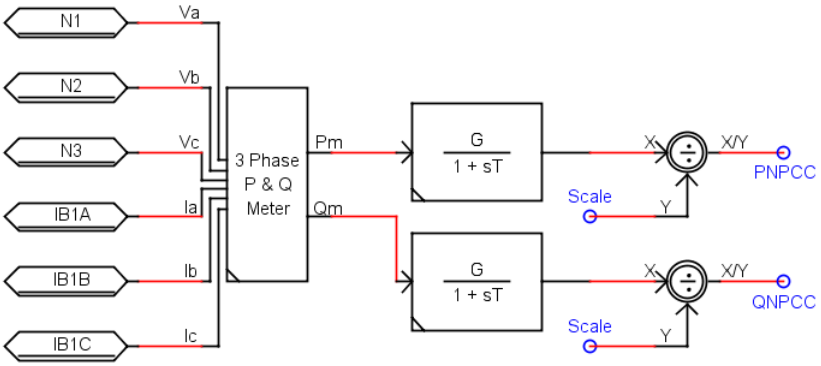

Figure G.30: Modification in measured PCC active and reactive power

G.2.4. VDAPI & SDC Controls Integration

Voltage Dependent Active Power Injection (VDAPI) and Supplementary Damping Controllers are tested, so as to evaluate the transient state of the system, whether it is improved or not under a fault condition.

In order to integrate the aforementioned controllers, the outer d and q reference loops, have to be modified. For the VDAPI integration the id reference loop is changed as indicated in Figure G.31. The VDAPI control description is done in Figure G.32.

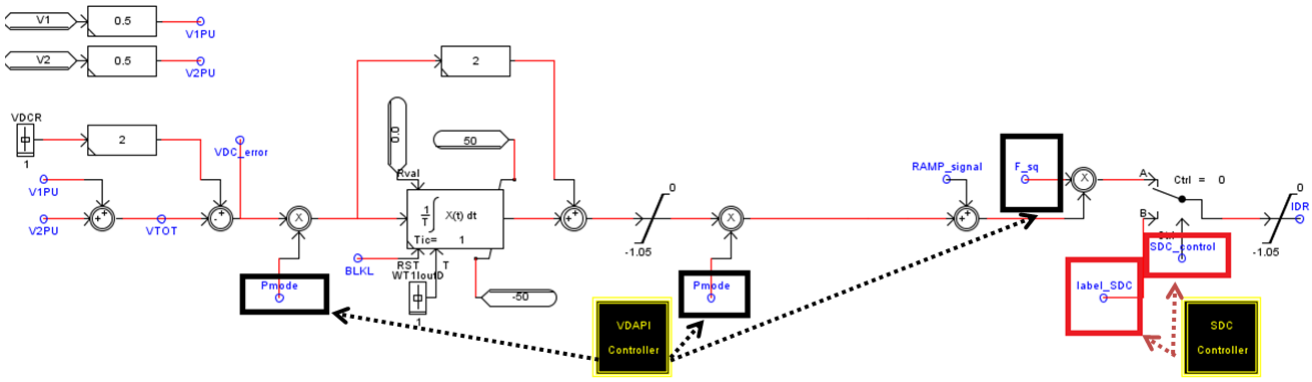

Figure G.31: Outer Active Loop Modification

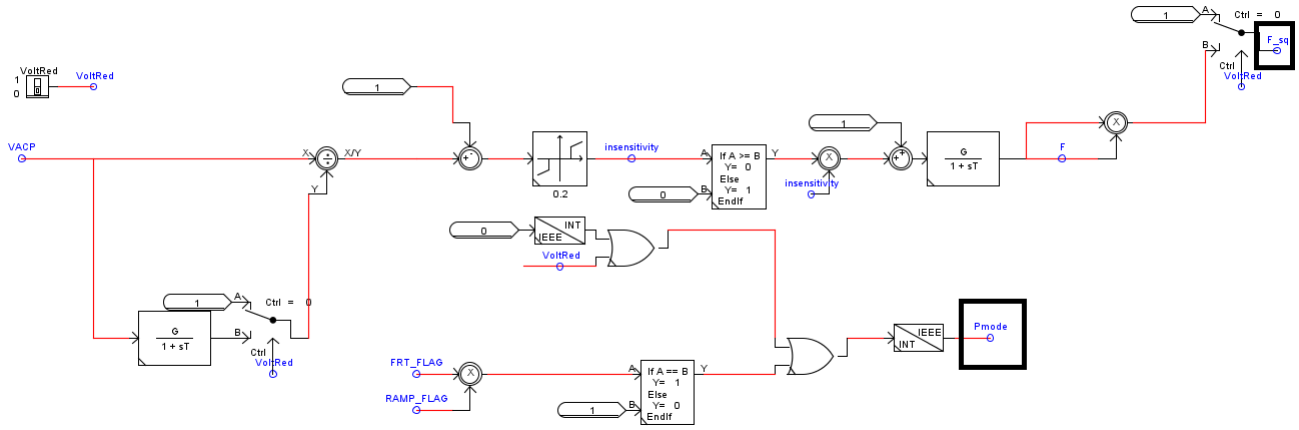

Figure G.32: VDAPI controller

SDC controller is described with the aid of the Figures G.33, G.34 and G.35. The reason why the deactivation is needed, after a specific time- period from the time LVRT condition ignited, is explained in multi-machine systems examined using RMS software. Last, Figure G.36, shows how the reactive power loop needs to be changed to accommodate the three controllers (i.e basic LVRT, VDAPI and SDC). The transition between the three controllers is done with the aid of specific switches in the .sib file as will be described in Section G.5.

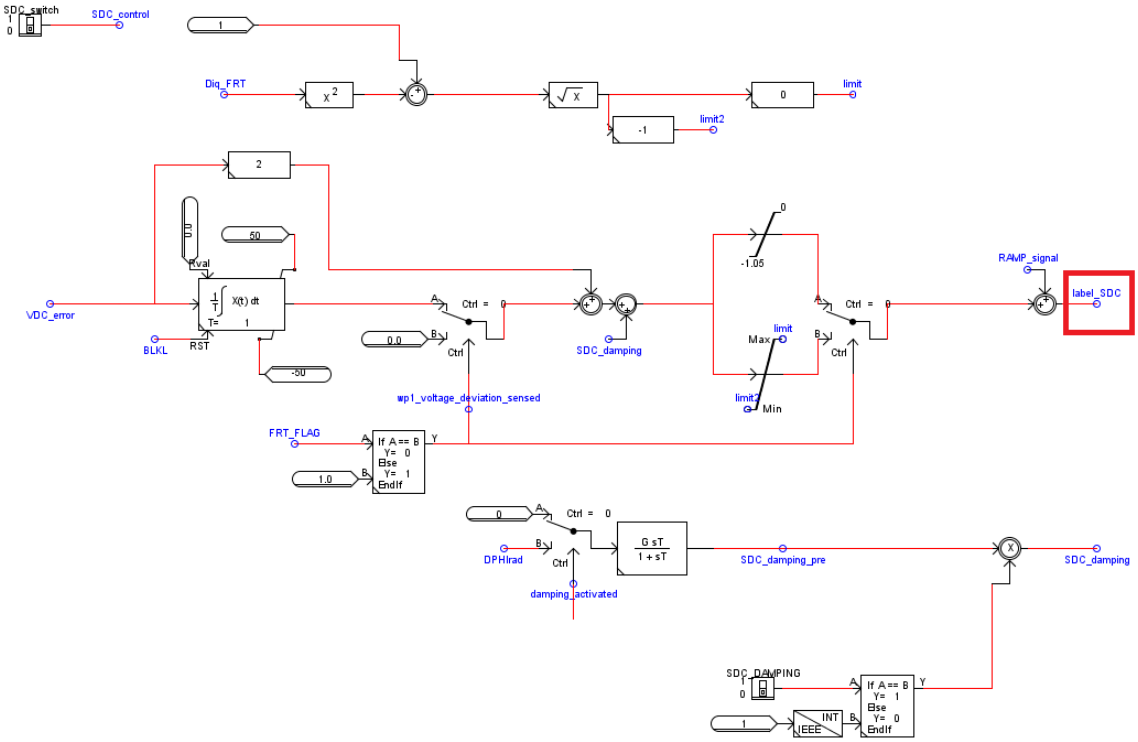

Figure G.33: SDC controller

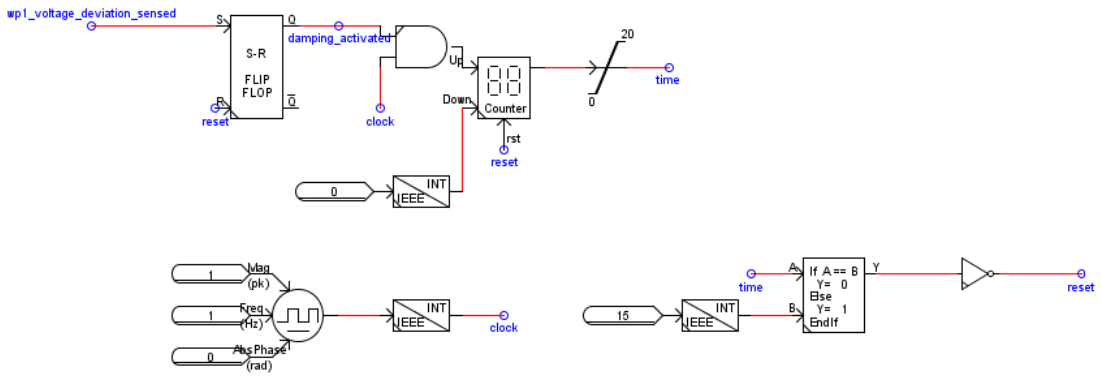

Figure G.34: SDC controller - acting time determination

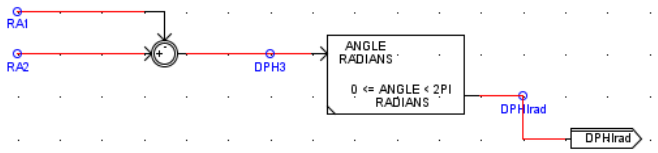

Figure G.35: SDC controller - input signal

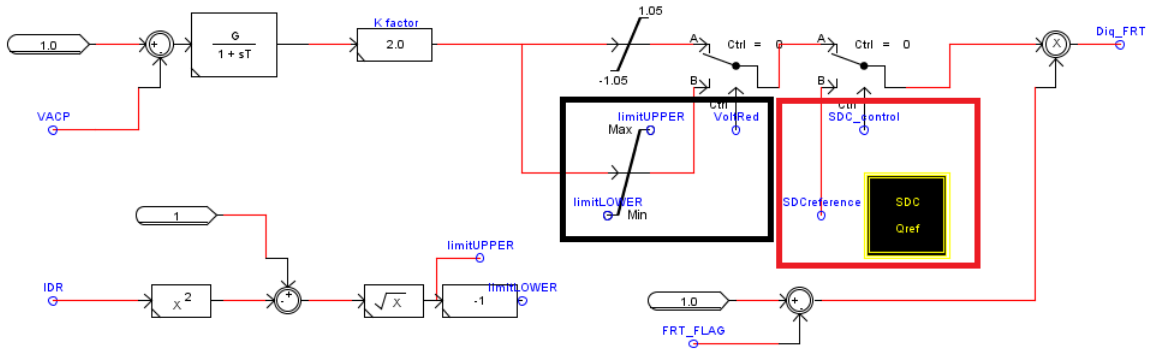

Figure G.36: Outer Reactive Loop Modification

G.3. Modifications of Benchmark System, to integrate the WGs

G.3.1. 60 Hz to 50 Hz Frequency Compliance

In this section, the IEEE 9 Bus Power System is examined. The Single Line Diagram is depicted in Figure 3.9, in Section 3.3

The system is taken from the samples systems that RSCAD offers. To do so, the user, should access Tutorial » Samples » Benchmark Power System Cases » IEEE 9 Bus Power System. The user should take all the related files and transfer them to the corresponding "fileman" folder that has already created. This folder is located, in the installation directory of RSCAD software, as depicted in Figure G.37.

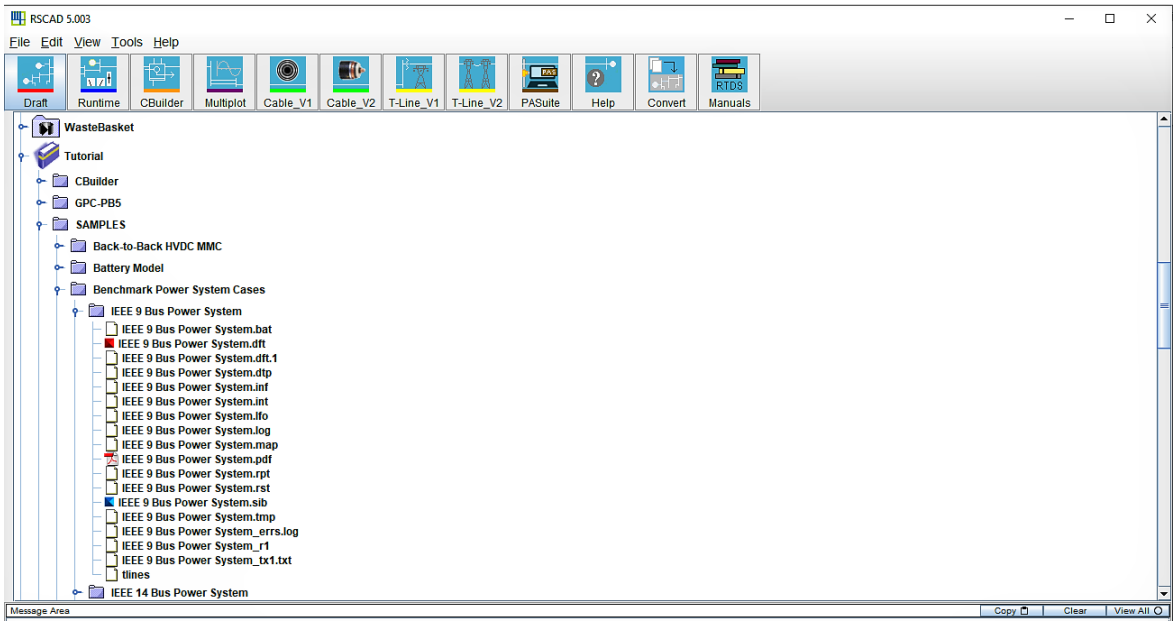

Figure G.37: System Location Folder in RSCAD

The benchmark system is designed for 60Hz, while the wind generator model is for 50Hz. In order be compatible, the user has to turn the benchmark power system to 50Hz. For that, the user has to change the base of all the parameters in the SGs (i.e. machine block, AVR block, Governor block) at 50Hz. It is mentioned that, conventional stabilizers are not employed in the synchronous machines. The user, should also change the base frequency in the loads and transformers at 50Hz. Last, the "tlines" file existing there, has to be edited. This file, contains all the information related to the transmission lines (i.e. positive, negative, zero impedance, line length, travelling time, characteristic impedance, base frequency etc.). The user needs to change the base frequency for each one of the lines to 50Hz. Figure G.38, contains the description of information for the data seen in the "tlines" folder.

After doing these modifications in the initial system provided by RSCAD, the user should run a load flow in order to initialize the system for the 50Hz frequency by clicking in the right-directional arrow in the following figure. As a note, the load flow analysis cannot be executed, when the WGs are connected in the system, due to the Power Electronics interphase that they employ; therefore it is done only with SGs connected in the system. It is observed that the voltages in the nodes are now changed with respect to the initial model that RSCAD provides for 60 Hz. The user can compile the system, by clicking the bented arrow button in the following figure. The two buttons are located in the draft module. Once the load flow, is executed, then ".lfo" folder is also updated. There, the load flow results for each line, the active and reactive power injections of the machines, the bus' voltages and the pu parameters of the lines, are stored. The machines' components and the +/-/0 sequence impedance of the lines in Ohms can be visualized in the ".map" file associated with the project. It is stated, further, that for a correct initialization, the governor and the exciter should activate their mode in which they

For a typical section of data in "tlines" as shown below:

T1,3

3 0 %3d %3d 60.00 50.00 1.000000 *0.0 0.0* /

%3d %3d 0.122746 1000.287788 19.837500 19.837500 5.773503e-01 8.164967e-01 0.000000e+00 / ----------(1)

%3d %3d 0.087676 400.115115 1.322500 1.322500 5.773503e-01 -4.082483e-01 7.071068e-01 / ----------(2)

%3d %3d 0.087676 400.115115 1.322500 1.322500 5.773503e-01 -4.082483e-01 -7.071068e-01 / ----------(3)

Color Zone	description
Color	T-Line Name
Color	Number of Conductors
Color	Base Frequency
Color	Base Frequency
Color	Line Length in Metres (Note – this is not the actual line length but set to 1.0 to scale the Resistance from ohms/m to ohms)
"0.0 0.0"	(Not Used information)
Color	Travel time $\tau\ (msec) = \sqrt{LC}$; L *in Henry*, C *in Farads*
Color	Characteristic Impedance $Z_c(\Omega) = \sqrt{\frac{L}{C}}$
Color	Series Resistance $R\ (\Omega/m)$; corresponding to the base frequency
Color	Series Resistance $R\ (\Omega/m)$; corresponding to the base frequency
Color	Transformation Matrix (modal domain → phase domain)

Row (1) --- For Zero Sequence; Row (2) --- For Positive Sequence; Row (3) --- For Negative Sequence; %3d --- Data Format

Figure G.38: Line Specifications included in tlines folder

are initialized based on the load flow results.

Figure G.39: Compile and Load Flow options in RSCAD

G.3.2. Subsystem extension

The considered benchmark system is split into two subsystems/ network solutions. A subsystem is defined as a part of a power system model which is mathematically decoupled from other parts of the system. The parts are then linked with each other, by travelling wave transmission lines to other subsystems. This is done, because the time required to solve a network grows exponentially with the number of nodes. Each network solution can solve up to 21 nodes, where node is defined as the interconnection point between two components in the draft model. Series connected components can be seen as an aggregated component thus, there is no need to place a node between them. From the aforementioned, in order to avoid compiling errors when the WGs are to be connected in the model, the model is divided into two smaller subsystems. If too many wind turbines are employed, then the computational effort increases so more than two subsystems need to be used. The user, in order to add a subsystem, he has to right-click in one existing subsystem in the draft file and then select the option "Add Subsystem". Just, as an additional comment, it is convenient to break the initial system into smaller segments, by using the line blocks (i.e the primary of the line will be present in one subsystem and the secondary will be contained in the other subsystem). In order to avoid compiling errors they should not use PI representation in their models as well.

G.3.3. WG model integration

Once the Power System with the SGs machines only has been constructed and initialized, then the WT inclusion has to be considered. For this report, two wind penetrations have been examined 52% and 75%.

- The 52% WT system has been described in Section 3.3 with Figure 3.10a. In the 52% WT penetration case, replacing SG3, with one WT of the same capacity can easily be done with the aid of one breaker. Initially, SG3 was connected and WT2 was disconnected. In the RunTime environment, the user with the aid of a switch, referred as $WINDTUR\_start$, can determine which one of the plants will be connected each time (i.e. if $WINDTUR\_start = 1$ then WT2 is connected and vice versa). It has to be mentioned, that the two plants have to be of the same capacity. The way to achieve wind penetration increment from the specific plant, has already been mentioned, in Section G.2.3.

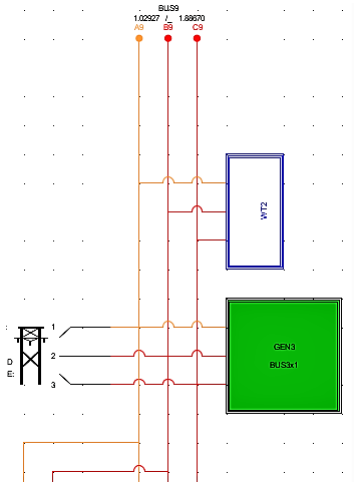

Figure G.40: Complementary usage of WT and SG

However, the replacement of the SG2 is not that much straightforward, because it has to be replaced partially, as initially this plant was injecting 163 MW, but with the 52% WG share it has to inject 84 MW. It was found, that if we were just connecting the WG plant with the desired capacity, by increasing the scaling factor, in parallel with SG2, then the system was not correctly initialized, and a complete division of active power injection between SG2 and WG1, without affecting the rest plants in the system. This was happening because the load flow results were already executed as mentioned before. Thus, when the WG is now connected and the simulation is run, the initial state of the SGs that was stored by the compiler without the WGs connected, (load flow as noted can't be executed with WGs connected in the system) will be different from its new actual state that the WT introduces.

A very important note that has to be mentioned, is that, even if the problem of the initialization was not occurring in the software, and RTDS could compute the initial state of the system, this approach of having the same initial model of synchronous machine when wind is included with comparison to the case that the wind is not included, would not be really correct for rotor angle stability studies. For instance, one can assume that SG1 is kept intact and a wind power plant is connected in parallel, which is modelled so as to inject half of the synchronous generator pre-fault active power dispatch. With this case scenario, having the same rated power in the SG machine, but having reduced the real operation point lower, in the power - angle curve (see Figure C.2), the machine inherently becomes more transiently steady.

The solution for that problem is that the SG2 can be split into two smaller machines. Each one of the two smaller machines, SG2a and SG2b, will have the half rated power and inertia of the initial "bigger" machine. Then the load flow only with the SGs connected (i.e. in that 50% case, the machines are: the two small machines that represent the initial SG2 machine, SG1 and SG3),

has to be again executed so as to initialize the two new small machines (their inner bus voltages and active reactive power injection). Then, WT1 will replace only one of the two synchronous machines (that together comprise the initial SG2 plant), with a breaker as seen in Figure G.41.

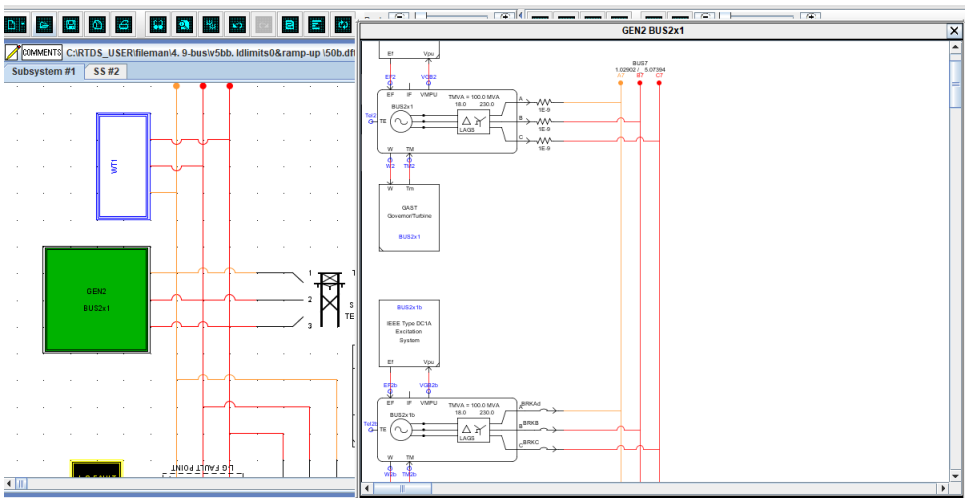

Figure G.41: Partial replacement of SG2 with the parallel connected WT1

- The 75% WG system has been described in Section 3.3 with Figure 3.10b. The same partial replacement logic of SGs was followed here. SG2 was divided into four smaller machines and WT1 replaces the three of them when connected. In addition, G1 is divided into two smaller synchronous generators and when WT3 is connected, it replaces one out the two. Last WT2, as in the 50% penetration case, replaces totally SG3.

To summarize, the steps done to create the benchmark system are:

- Split the System into two subsystems, to integrate the power and control components of the WGs needed.
- Change system parameters to 50 Hz.
- For rotor angle stability studies only (for frequency this step is not needed), as explained the SGs have to be split into smaller units for a fair comparison when wind share is increased.
- Change the governors maximum opening position to 1.2 pu in all the synchronous machines; initially in the model provided by RSCAD, this value was 5 pu, so the system was very stable and could not represent realistic CCT calculations
- Define SG2 as the slack machine since it has the biggest rated capacity.
- Run the load flow only with the SGs connected, and initialize the system. At the same time, notice the reactive power that the synchronous machines inject.
- Integrate the Wind Turbines in the draft file, see the PCC voltage phase and magnitude of buses that the wind generators are connected to and change accordingly the label of the wind generator node, so as to have the same amplitude and phase with the terminal in the system.
- Add a reactive load in the PCC of the wind generator, which will inject the reactive power needed so as the summation of the injected reactive power of the combined WG / SG in a particular area, will be the same as the reactive power injected from the initial SG in the same area, in the case of only SGs are connected in the grid. It is stated that zero reactive power is injected during normal conditions from the WG. With this step, the same load flows are assured as in the only SGs connected case scenario.

G.4. IEEE 9 BUS System Data

Some Basic Parameters of the SGs and WGs models used, are presented in Tables G.1-G.4. Additionally, G.5 includes basic information about the interface componnets between any WG and the grid (e.g. VSCs, DC Chopper and PCC Transformer).

Table G.1: SGs' parameters

Parameter	Symbol - Unit	Value (G1)	Value (G2)
Rated Power	$S_n - MVA$	100	93
Inertia Constant	H - s	9.55	2.132
Stator Resistance	$R_a - pu$	0	0
Stator Reactance	$X_a - pu$	0.0146	0.08958
Transient Time Constant-d	$T'_{d0} - s$	8.96	6
Transient Time Constant-q	$T'_{q0} - s$	-	0.535
Sub Transient Time Constant-d	$T''_{d0} - s$	0.01	0.01
Sub Transient Time Constant-q	$T''_{q0} - s$	0.01	0.01
Synchronous Reactance - d	$x_d - pu$	0.146	0.8958
Synchronous Reactance - q	$x_q - pu$	0.1	0.8645
Transient Reactance - d	$x'_d - pu$	0.0608	0.1198
Transient Reactance - q	$x'_q - pu$	-	0.1969
Subtransient Reactance - d	$x''_d - pu$	0.06	0.11
Subtransient Reactance - q	$x''_q - pu$	0.06	0.11

Table G.2: SGs' GOV parameters- govGAST

Parameter	Value (G1)	Value (G2)
R [pu]	0.05	0.047
T1 [s]	0.05	0.4
T2 [s]	2.1	0.1
T3 [s]	7	3
AT [pu]	1	1
Kf [pu]	2	2
Dturb [pu]	0	0.01
Pturb [pu]	0	0
Vmin [pu]	0	0
Vmax [pu]	0.85	1

Table G.3: SGs' AVR parameters- IEEE DC1

Parameter	Value (G1=G2)
Tr [s]	0
Ka [pu]	20
Ta [s]	0.2
Tb [s]	0
Tc [s]	0
Te [s]	0.314
Kf [pu]	0.063
Tf1 [pu]	0.35
E1 [pu]	3.3
Se1 [pu]	0.6602
E2 [pu]	4.5
Se2 [pu]	4.266
Ke [pu]	1
Vrmin [pu]	-5
Vrmax [pu]	5

Table G.4: WG PMSG parameters

Parameter	Unit	Value
Inertia Constant	MWs/MVA	1
Rated Stator Voltage (L-L RMS)	kV	0.9
Rated MVA of the Machine	MVA	6
Stator Leakage Reactance	pu	0.04
D-axis Unsaturated Magnet. Reactance	pu	0.28
D-axis Damper Leakage Reactance	pu	0.65
Q-axis Magnetizing Reactance	pu	1
Q-axis Damper Leakage Reactance	pu	1.175
Stator Resistance	pu	0.01
D-axis Damper Resistance	pu	0.055
Q-axis Damper Resistance	pu	0.183

Table G.5: Basic Interfacing Components Parameters

Parameter	Unit	Value
Valve Switching Voltage Magnitude	kV	2
Valve Switching Current Magnitude	kA	3
Capacitance in Type III VSC topology	μ F	25
Chopper Rated Voltage	kV	2
Chopper Rated Current	kA	1
Rated Transformer Power	MVA	6
Rated Primary RMS Voltage	kV	3.5
Rated Secondary RMS Voltage	kV	33

G.5. User Manual

In order to successfully initialize the 52% and 75% Wind Share models, the SGs connected in the system should operate in the ”Lock” speed mode as described in Section G.1.1. If ”Free” speed mode is being considered from the beginning of the simulation, so as to model the propel modelling of the mechanical dynamics, then instability is achieved. The cause of this phenomenon is prop ably the big measuring time of the wind generator's anemometer, thus the mechanical power of the WG remains zero, and therefore, synchronous machines have to increase more power to serve the loads from the initial point of the simulation. This is similar to a huge increment in the load perceived by the synchronous machines, which will lead to an increment in their rotor angles. This increment in load, is compensated by a decrement in synchronizing power from the side of the machine, so as to keep the rotor speed at the stator speed. Due to the high wind share, this instability is occurred. On the other hand, in the ”Lock” speed mode, because the rotor speed is remaining constant and equal to the synchronous speed, the synchronizing power is not affected and the stability of the system remains.

More specifically, for the 52% WG model layout, the user can also operate the system only with SGs connected to it. To do that, the leftmost switch in each one of the two WGs control panels should be down, as seen for instance in Figure G.42. This switch, called *WINDTUR_start*, deactivates the corresponding wind plant and activates the parallel connected synchronous machine, as they are connected in a complementary mode. It is mentioned that all the SGs can be initialized with their Free speed mode as expected. If the wind generators are to be considered, then the leftmost switch should be in the upper position. At the same time LockFree switch of the SGs should be zero as stated before, during the initialization period. After the initialization, the LockFree switches should be one, and then the faults can be applied. Figures G.42, G.43 and G.44 are given as a guidance to the user to choose the controllers according to it's needs. Similar steps for a successful operation of the model, should be followed for the %75 WGtopology.

It is last mentioned, that the user can simulate the 75% wind share case only using the Novacor chassis. If PB5 based rack is used, then a sub-step overflow is appearing in the .sib file of the model. This message, indicates that the minimum requirement between the small time step and big time step sizes used is violated. In Novacor this minimum requirement is less, therefore the simulation can be ran there.

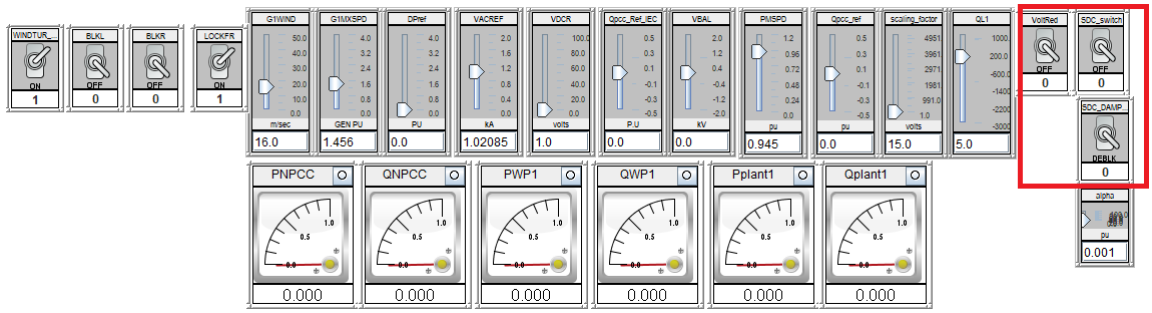

Figure G.42: Basic LVRT control scheme selection

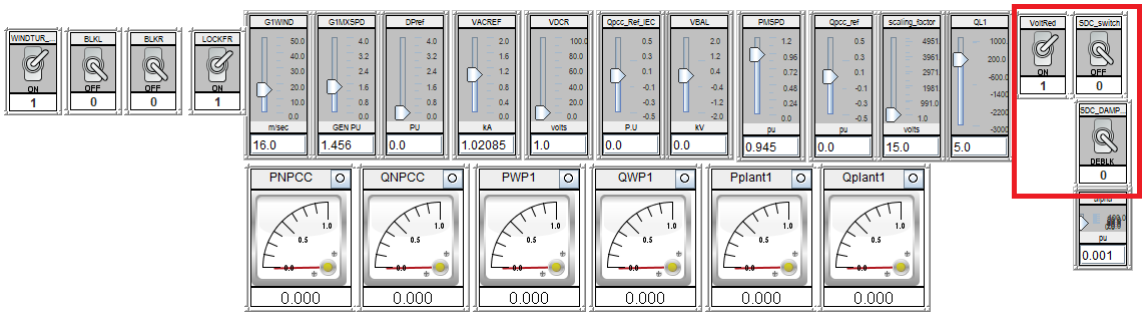

Figure G.43: VDAPI control scheme selection

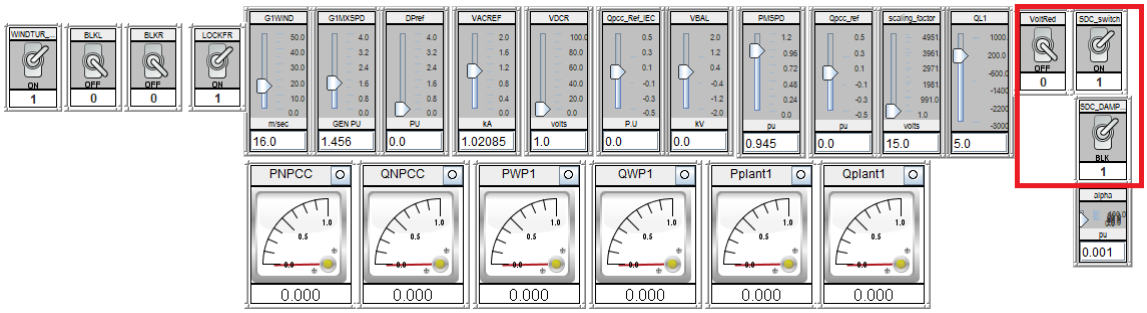

Figure G.44: SDC control scheme selection

H

Analytical foundations of the WG Supplementary Damping Control (SDC)

H.1. Mathematical Description

The rationale behind the need and role of SDC to be attached to a wind generators starts by considering the power transfer equations H.1-H.3, which for sake of facilitating the explanations and understating of fundamental notions, are derived by considering a reduced size AC network as shown in Figure H.1

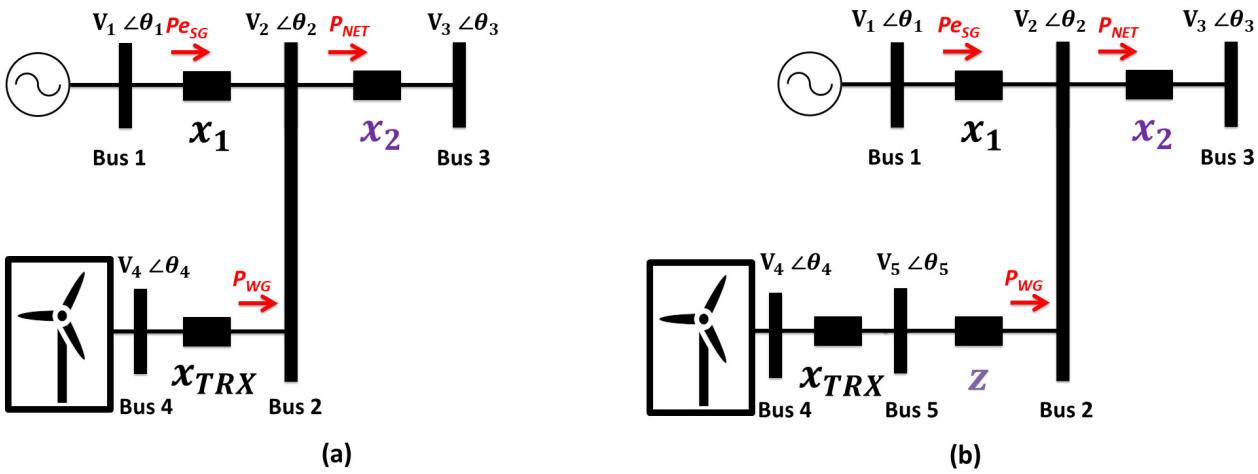

Figure H.1: Reduced size test system with hybrid generation connected to an infinite bus with wind generator located: (a) close to the synchronous generator; (b) far from the synchronous generator

$$P_{eSG} = P_{NET} - P_{WG} \tag{H.1}$$

$$P_{eSG} = \frac{V_1 \cdot V_2}{x_1} \cdot sin(\theta_1 - \theta_2) \tag{H.2}$$

$$P_{NET} = \frac{V_2 \cdot V_3}{x_2} \cdot sin(\theta_2 - \theta_3) \tag{H.3}$$

The active power P_{WG} injected into the network, is regulated by the control systems associated with the WG. Taking into consideration equations H.1-H.3 , it can be deduced that the injected power P_{WG} will influence the response of the θ_2 angle. This influence can potentially be used to enhance the large disturbance rotor angle stability performance of a power system with high share of renewable power generation, similar to the Flexible Alternating Current Transmission Systems (FACTs) action. That is, usually, the FACT devices employ passive elements (capacitors and inductances controlled by thyristors or IGBTs) to modulate the impedance value in a transmission line in order to regulate the active power flow through the line. In that manner, such devices manage to mitigate large rotor angle excursions in a power system. The SDC approach follows a similar direction, but instead of using passive elements, the SDC modulates the angular difference value presented in equation H.2 by regulating the active power P_{WG} after a large disturbance in the AC network is detected. The modulation of the value of the angular difference in H.2, by means of the P_{WG} regulation, is reflected in the values of θ_2 variable, which is a function of the value of P_{WG} and the value of x_2 variable. Consequently, the modification of θ_2 will affect the amount the P_{eSG} provided by the synchronous generator. Ergo, the $\delta(t)$ function in the following equation can be affected by modifying the P_{eSG} value (i.e. modulating the angular difference).

$$\frac{\partial^2 \delta(t)}{\partial t^2} = \frac{P_{mSG} - P_{eSG}}{2 \cdot H} \tag{H.4}$$

The estimation of the $\delta(t)$ values can be done based on measured values from PMU devices [58]. However, it is relevant to highlight that the $\delta(t)$ value needs to be computed with respect to the system angular reference. In other words, the location of the system angular reference will define the relative variation of the measurement value of the rotor angle $\delta(t)$ in the network. Usually, the system angular reference in a network is assigned to the SG with the highest inertia constant (i.e. reference machine). For the test system shown in Figure H.1, the angle of the Bus 3 is taken as reference. In Figure H.1, x_2 represents the impedance between the high voltage side bus of the step-up transformer of the synchronous generator and the system angular reference.

Note also in Figure H.1(a), that the wind generator equipped with SDC is connected in parallel with the synchronous generator, whereas in Figure H.1(b) the wind generator with SDC is located far from the synchronous generator. The voltage level of the transmission system is 230 kV. The amplitude V_3 and the angle $theta_3$ of the infinite bus are set to 1 pu and 0 degrees, respectively. A three phase fault with fault clearing time of 200 ms is applied at Bus 2 in all simulation shown in the current Appendix. The active power dispatches of the SG and the WG are 200 MW, respectively. The impedance x_1 equals 0.16 pu. The impedance x_{TRX} equals 0.06 pu for the case when the WG is located close to the SG. In order to consider the case when the WG is located far from the SG a transmission line is connected in series with x_{TRX}. The length of the line used is at 150km with positive sequence impedance of 115 Ohms.

In all simulations, the parameters of the SDC were set to T=10s, and G=0.8pu, which were taken from [57]. The following aspects are analysed:

- Influence of the distance of WG with SDC with respect to the system angular reference

  Three different values of x_2 were considered. The first case considers 1 km line, which corresponds to x_2 around 0.5 Ω. The second case is tested with a 60 km line, which corresponds to x_2 around 30 Ω. Last, the third case examines a 150 km line with positive impedance of 75 ohms. Figure H.2 shows the obtained responses of rotor angle and rotor speed as influenced by the x_2 parameter. Note than the larger distance from the system angular reference (i.e. increasing x_2 value) entails more effective reduction of the amplitude of the first swing and higher oscillation damping. This influence is related to the fact that P_{WG} regulation (affected by SDC addition in the active current control loop) has more impact on the value of θ_2, when there is a large impedance between the bus of common coupling (i.e. location of (θ_2) and bus of the system angular reference (i.e. $theta_3$). Having higher influence on (θ_2), entails that variations of P_{eSG} (e.g. during and after faults), can be mitigated promptly, thus helping to minimize the perturbation of the equilibrium between mechanical and electrical power of the synchronous generator. For the specific study case it is observed, that with a 1 km line considered, damping cannot be achieved, with a 60km line damping is effective but the first swing oscillation still remains as in the case in which no SDC is implemented, whereas with a 150km line considered, the damping is further enhanced and the first swing oscillation is also mitigated.

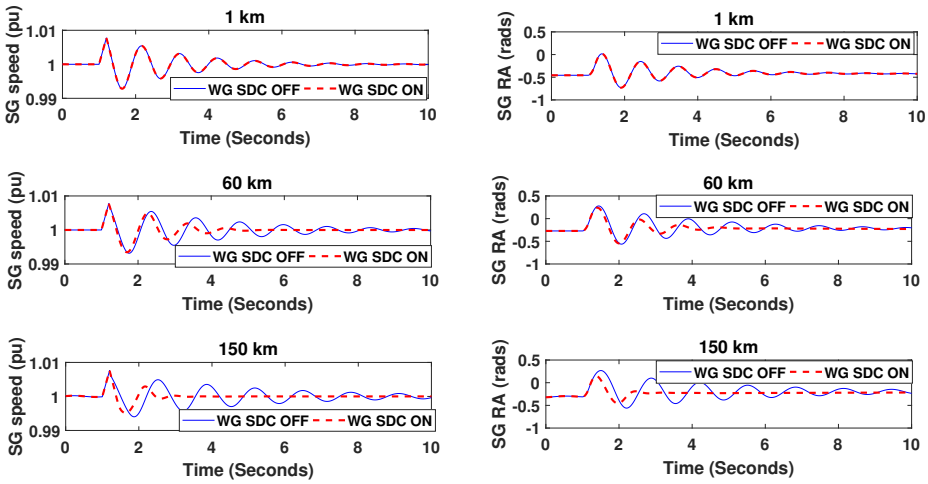

Figure H.2: Fault at Bus 2, FCT = 200 ms. Dynamic responses of SG rotor for different transmission line lengths (different values of increasing x_2)

- Impact of the location of WG with SDC

  Based on the above analysis, x_2 is set to 30 ohms (60 km line length). Next, simulations were conducted by varying the location of the WG with SDC. For this purpose, in Figure H.1 (b), it was considered that a 150km line (i.e. Z) with a total impedance of 115 Ohms was selected, to emulate the case when the wind generator is far from the synchronous generator. It is mentioned that the impedance of line Z is slightly high so as to comprise in a simplified manner, potential small local loads connected to the proximity of the wind generation and also to take into consideration the losses of the power converters used, that in the simulation software are neglected. Moreover, as mentioned before, the results obtained when the wind generator is located in the proximity of the synchronous machine are illustrated in Figure H.2 Figure H.3 shows the obtained performance when the WG with SDC is located far from the SG. Comparing Figure H.2 with Figure H.3, note that the support from the WG with SDC is significantly less when it is located far from the SG without having the SDC scheme activated. This effect is associated with a reduction of the maximum active power transfer from the WG due to the larger impedance between this generator and the SG that is experiencing an imbalance between mechanical and electrical power when a fault is performed at Bus 2.

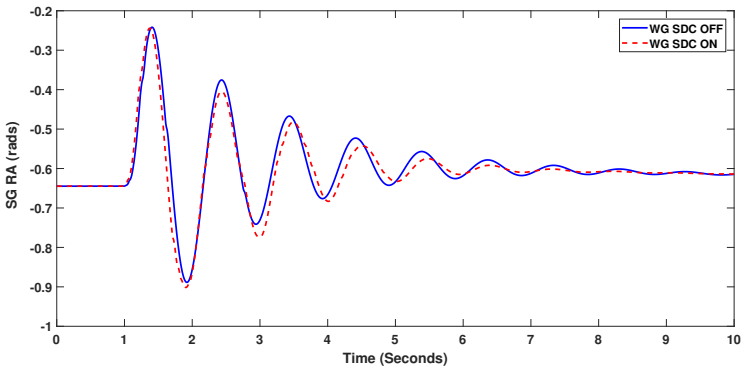

Figure H.3: Fault at terminal Bus 2, FCT = 200ms. Dynamic responses of SG rotor when WG is located far from the SG (length of line Z is 150 km).

- Influence of the use of local vs remote signal as input for SDC

  Like in the previous analysis, x_2 is set to 30 ohms (60 km line length) to consider effective influence of SDC on large disturbance rotor angle stability, and to focus the analysis exclusively

on the impact of the selected input signal for SDC. Moreover, WG is electrically close to the SG. Four options for input signal were compared:

1. Option 1 (remote): angular difference between rotor angle of the SG (i.e. δ) and the system reference angle (θ_3).
2. Option 2 (local): angular difference between rotor angle of the SG (i.e. δ) and the system Point of Common Coupling of the SG (θ_2).
3. Option 3 (local): active power output of the SG (P_{SG})
4. Option 4 (local): angular difference between phase angle of the terminal bus voltage of the SG (θ_1) and the angle at the point of common coupling of the SG (θ_2).

It is mentioned that phase compensation with a lead-lag transfer function is also used in for all the studied options used. The time constant in the numerator is set to chosen at 1 second, and in the denominator it is set to 0.1 seconds.

As shown in Figure H.4, the use of the relative rotor angle of the SG w.r.t. to the system reference angle leads to higher improvement of mitigation of rotor angle excursions. This is due to the fact that the options 2 and 3 listed above are sensitive to active power injection by wind generators, whereas option 1 with relative rotor angle has constant system reference angle (which is not affected by variable active power injection by wind generators). This finding is in line with observations given in [69], which points out that local signals can lead to less damping comparing to remote signals.

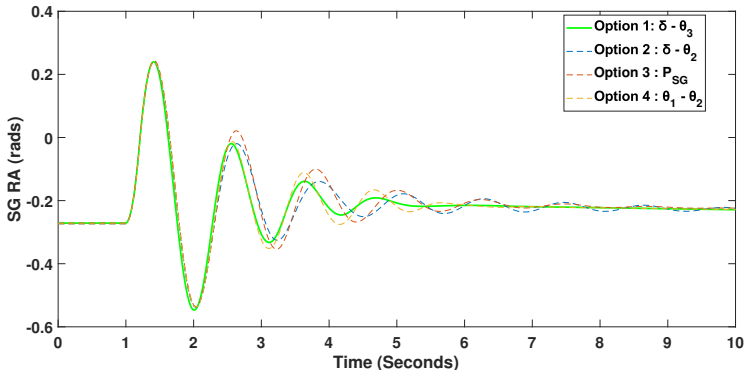

Figure H.4: Fault at Bus A- 200ms, SG rotor angle when local and remote input signals are used in the SDC.

- Impact of time delay on the performance of SDC

Lastly, two different types of transfer function were added separately to the SDC to represent the delays when remote signals are used. In the first method, a first order transfer function was used and set with different time delays T_d according to [82]. In the second method, a Pade approximation was used and set with different time delays T_d according to [83], [84] to represent the communication and signal processing delays. The transfer function is given by:

$$G_{approx} = \frac{12 - 6 \cdot T_d \cdot s + (T_d \cdot s)^2}{12 + 6 \cdot T_d \cdot s + (T_d \cdot s)^2} \tag{H.5}$$

Where T_d represents the time-delay considered.

The maximum delays considered in our analyses are 200ms, because typical Wide Area Monitoring Protection and Control Systems require 150-200ms total time delay for closed loop applications [85].

Regarding the system topology used, it is noted that the line between Bus 2 and 3 is considered at 60kms (i.e. 30 Ohms), whereas WG is directly connected to Bus 2, without any transmission line.

By comparing Figure H.5 and Figure H.6, it is observed that, a delay around or smaller than 100ms causes similarity in mitigation of rotor angle excursion when the time delay is neglected when modelling and simulating remote signals.

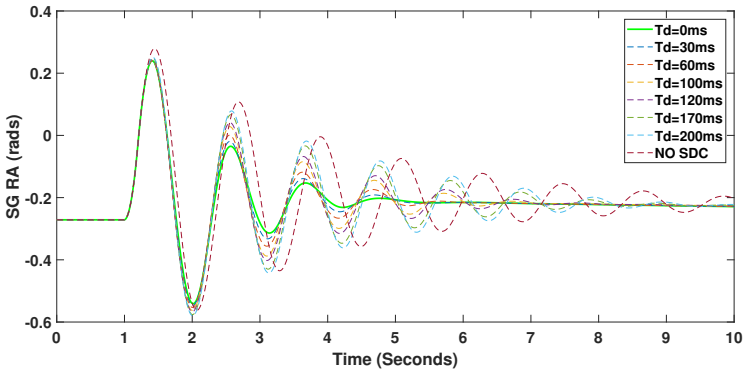

Figure H.5: Option 1 (i.e. remote inputs) with different delay effects first order transfer function used for delay representation

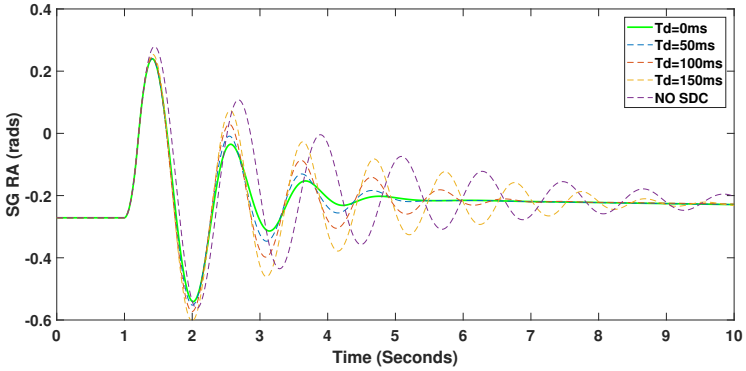

Figure H.6: Option 1 (i.e. remote inputs) with different delay effects Pade transfer function used for delay representation

I

Tuning of WG controllers - Approach based on a transient stability KPI

I.1. Introduction

In this section, the way in which one can tune the washout parameters based on time- domain simulations is illustrated. Figure I.3 is depicting the flow - chart that is followed. The user can define beforehand the parameters, needed to be changed. For the studies made, the following washout gains together with the following washout time constants were traversed. For each time constant and gain as aforementioned before, selected faults are implemented (i.e. Fault at Line 6-9 and Fault at Node 15) using RMS simulations with the aid of PowerFactory tool. The KPI chosen is the maximum angle difference between any couple of the ones that can be formed. In the system, 11 SGs are existing, therefore the possible pairs is retrieved from the following equation. This is the so called nC_r formula, used to find the unique permutations, or combinations, of n objects taking r items at a time.

$$SG_{pairs} = \binom{n}{r} = \frac{n!}{r!(n-r)!} \tag{I.1}$$

where n=11, is the number of the synchronous units, r=2. Using the aforementioned values a total number of 55 synchronous generator pairs is formed.

After the end of each simulation, the KPI is simulated, and the next parameters are to be tested under the same fault conditions, from which a new KPI is computed. When all the washout parameters are tested, then the user can select the ones that give, the highest of all the KPIs, because this ensues in higher stability in the system. It is mentioned that the python script also returns the pair of machines, that oscillate the most, as well as the time in which the maximum oscillation is happening. The python script, controls the PowerFactory environment and generates a ”test2.csv” file which has the time-domain rotor angle responses of the 11 SGs with respect to the slack machine. Then this .csv file is used so as to generate one other .csv file, called ”sensitivity_ultimate.csv”. This file is updated dynamically for each gain and time constant parameter examined. Typical screenshots of the aforementioned .csv files are illustrated in Figures I.1 & I.2.

As seen from Tables I.1 - I.4, small time constants in the washout filter lead to better transient stability. This fact, complies to references from literature [43].

	A	B	C	D	E	F	G	H	I	J	K	L	M
1	All calculations 1	z\G03	z\G05	z\G07	z\G08	z\G10	z\G11	z\G13	z\G15	z\G16	z\G19	z\G20	
2	Time in s	Rotor angle with referen	Rotor angle with	Rotor angle with re	Rotor angle w	Rotor angle	Rotor angle wit	Rotor angle wit	Rotor angle wit	Rotor angl	Rotor angle with r	Rotor angle with reference to	
3	0	-24.958726	-19.272342	-23.394319	-32.878157	0	-29.796988	-35.703562	-19.416181	-43.5752	-49.62684	-52.216747	
4	0.005	-24.958726	-19.272342	-23.394319	-32.878157	0	-29.796988	-35.703562	-19.416181	-43.5752	-49.62684	-52.216747	
5	0.01	-24.958726	-19.272342	-23.394319	-32.878157	0	-29.796988	-35.703562	-19.416181	-43.5752	-49.62684	-52.216747	
6	0.016667	-24.958726	-19.272342	-23.394319	-32.878157	0	-29.796988	-35.703562	-19.416181	-43.5752	-49.62684	-52.216747	
7	0.026667	-24.958726	-19.272342	-23.394319	-32.878157	0	-29.796988	-35.703562	-19.416181	-43.5752	-49.62684	-52.216747	
8	0.036667	-24.958726	-19.272342	-23.394319	-32.878157	0	-29.796988	-35.703562	-19.416181	-43.5752	-49.62684	-52.216747	
9	0.046667	-24.958726	-19.272342	-23.394319	-32.878158	0	-29.796988	-35.703562	-19.416181	-43.5752	-49.626841	-52.216748	
10	0.056667	-24.958728	-19.272343	-23.39432	-32.878159	0	-29.796988	-35.703562	-19.416181	-43.5752	-49.626842	-52.216749	
11	0.066667	-24.95873	-19.272346	-23.394321	-32.878161	0	-29.796988	-35.703562	-19.416181	-43.5752	-49.626846	-52.216753	
12	0.076667	-24.958735	-19.27235	-23.394324	-32.878164	0	-29.796988	-35.703563	-19.416181	-43.5752	-49.626852	-52.21676	
13	0.086667	-24.958743	-19.272356	-23.394328	-32.87817	0	-29.796988	-35.703563	-19.416181	-43.5752	-49.626861	-52.216771	
14	0.096667	-24.958754	-19.272366	-23.394335	-32.878179	0	-29.796987	-35.703563	-19.416181	-43.5753	-49.626875	-52.216786	
15	0.106667	-24.958771	-19.27238	-23.394344	-32.878191	0	-29.796986	-35.703562	-19.416181	-43.5753	-49.626893	-52.216807	
16	0.116667	-24.958793	-19.272398	-23.394356	-32.878207	0	-29.796985	-35.703562	-19.416181	-43.5753	-49.626916	-52.216834	
17	0.126667	-24.958821	-19.27242	-23.394371	-32.878228	0	-29.796983	-35.703561	-19.41618	-43.5753	-49.626945	-52.216867	
18	0.136667	-24.958856	-19.272447	-23.39439	-32.878254	0	-29.79698	-35.703559	-19.41618	-43.5753	-49.62698	-52.216907	
19	0.146667	-24.958898	-19.272479	-23.394413	-32.878285	0	-29.796976	-35.703557	-19.416178	-43.5753	-49.62702	-52.216954	
20	0.156667	-24.958947	-19.272515	-23.394439	-32.878322	0	-29.79697	-35.703555	-19.416177	-43.5752	-49.627066	-52.217006	
21	0.166667	-24.959003	-19.272556	-23.39447	-32.878364	0	-29.796963	-35.703551	-19.416175	-43.5752	-49.627117	-52.217065	
22	0.176667	-24.959068	-19.272602	-23.394503	-32.878411	0	-29.796954	-35.703547	-19.416172	-43.5752	-49.627172	-52.217129	
23	0.186667	-24.959139	-19.272651	-23.394541	-32.878464	0	-29.796942	-35.703542	-19.41617	-43.5752	-49.627232	-52.217198	
24	0.196667	-24.959217	-19.272703	-23.394582	-32.878521	0	-29.796928	-35.703536	-19.416166	-43.5752	-49.627296	-52.217271	
25	0.206667	-24.959302	-19.272758	-23.394625	-32.878583	0	-29.796911	-35.703529	-19.416162	-43.5752	-49.627363	-52.217347	

test2

Figure I.1: ”test2.csv” example after a fault implementation and a specific washout gain and time constant

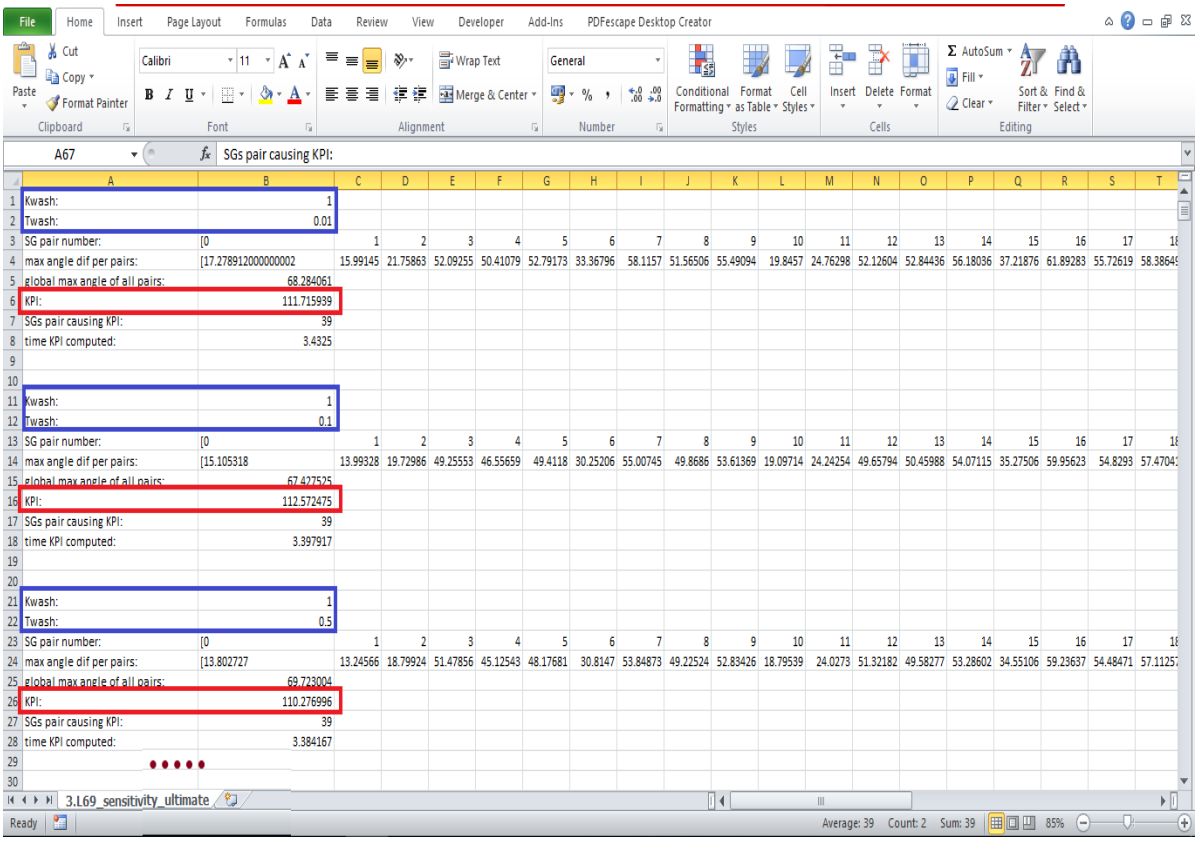

	A	B	C	D	E	F	G	H	I	J	K	L	M	N	O	P	Q	R	S	T
1	Kwash:	1																		
2	Twash:	0.01																		
3	SG pair number:	[0	1	2	3	4	5	6	7	8	9	10	11	12	13	14	15	16	17	18
4	max angle dif per pairs:	[17.278912000000002	15.99145	21.75863	52.09255	50.41079	52.79173	33.36796	58.1157	51.56506	55.49094	19.8457	24.76298	52.12604	52.84436	56.18036	37.21876	61.89283	55.72619	58.38649
5	global max angle of all pairs:	68.284061																		
6	KPI:	111.715939																		
7	SGs pair causing KPI:	39																		
8	time KPI computed:	3.4325																		
9																				
10																				
11	Kwash:	1																		
12	Twash:	0.1																		
13	SG pair number:	[0	1	2	3	4	5	6	7	8	9	10	11	12	13	14	15	16	17	18
14	max angle dif per pairs:	[15.105318	13.99328	19.72986	49.25553	46.55659	49.4118	30.25206	55.00745	49.8686	53.61369	19.09714	24.24254	49.65794	50.45988	54.07115	35.27506	59.95623	54.8293	57.4704
15	global max angle of all pairs:	67.427525																		
16	KPI:	112.572475																		
17	SGs pair causing KPI:	39																		
18	time KPI computed:	3.397917																		
19																				
20																				
21	Kwash:	1																		
22	Twash:	0.5																		
23	SG pair number:	[0	1	2	3	4	5	6	7	8	9	10	11	12	13	14	15	16	17	18
24	max angle dif per pairs:	[13.802727	13.24566	18.79924	51.47856	45.12543	48.17681	30.8147	53.84873	49.22524	52.83426	18.79539	24.0273	51.32182	49.58277	53.28602	34.55106	59.23637	54.48471	57.1125
25	global max angle of all pairs:	69.723004																		
26	KPI:	110.276996																		
27	SGs pair causing KPI:	39																		
28	time KPI computed:	3.384167																		
29																				
30																				

Figure I.2: ”sensitivity_ultimate.csv” example; computed outcome after different washout parameter examined, when the same fault is considered

I.2. Work Flow

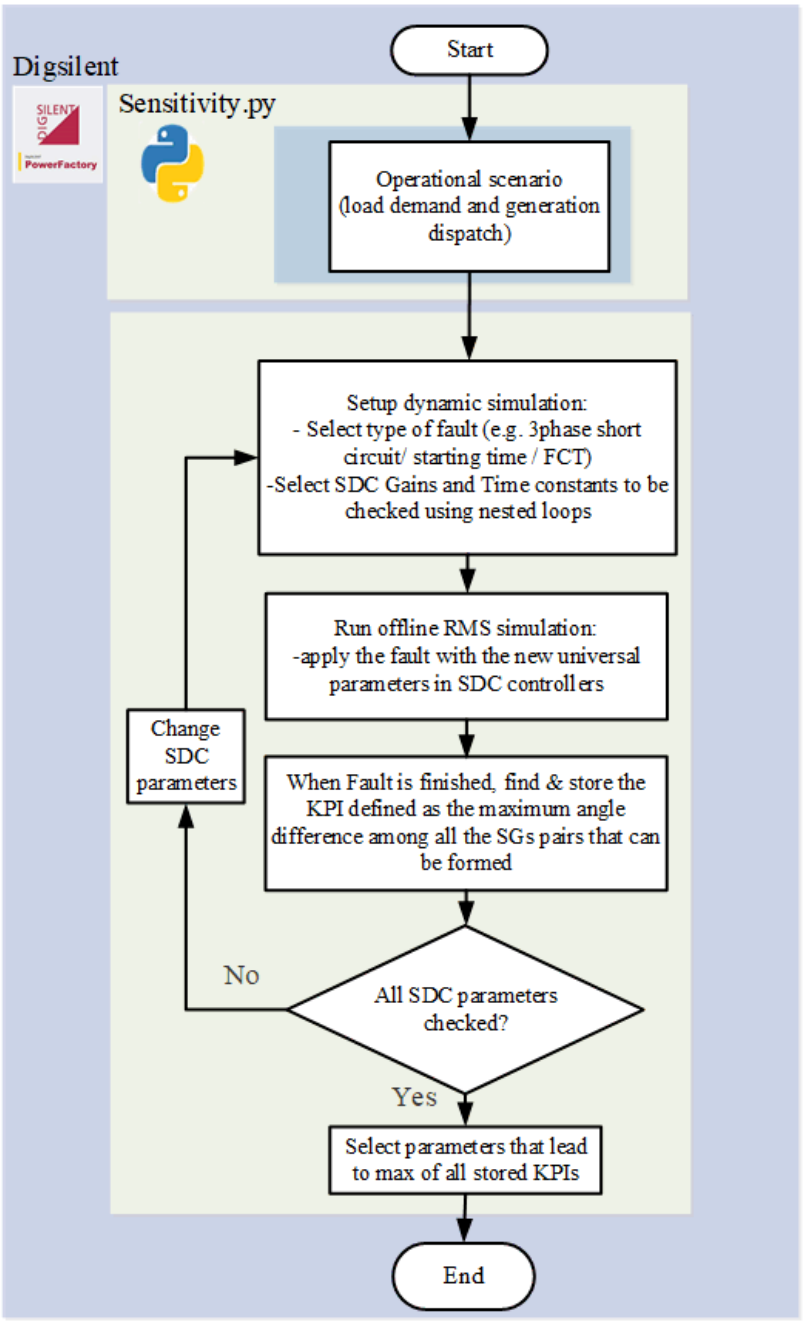

Figure I.3: Reduced size test system with hybrid generation connected to an infinite bus with wind generator located: (a) close to the synchronous generator; (b) far from the synchronous generator

I.3. Python Script

```
# -*- coding: utf-8 -*-
"""
Created on Wed Jul 10 21:01:25 2019

@author: stelios
"""

#############################################################
'''
import of modules
'''
import csv
import numpy as np
# import sys module in order to call sys.path.append()
import sys
 # adding path to the PowerFactory - module
sys.path.append (r"C:\Program Files\DIgSILENT\PowerFactory 2018 SP1
                 \Python\3.6")
 # importing the pf-module
import powerfactory
# calling app Application object
app = powerfactory.GetApplication()


#############################################################

'''
kpi computation function
'''

def computation():
    a = open("test2.csv",errors='ignore')
    print("Opened file, now processing it...")
    csv_f=csv.reader(a)
    columns = zip(*csv_f)
 #my_list is a list of lists. The inner lists are the columns
 #(rotor angle of each machine (w.r.t slack machine) VS time)
    my_list=[]
    for column in columns:
            c=list(column)
 #if you see the csv file from powerfactory has the two first row
 #without any data. In the lists above we want only numbers
            c=c[2:]
            my_list.append(c)

    '''
  for the GB, a_list should be my_list[1] because the first column
  is the time
    '''
    time_list=[float(i) for i in my_list[0]]
#convert the previous inner lists from type string to type float
#RA for 1st machine
```

```
    a_list= [float(i) for i in my_list[1]]
    b_list= [float(i) for i in my_list[2]]
    c_list= [float(i) for i in my_list[3]]
    d_list= [float(i) for i in my_list[4]]
    e_list= [float(i) for i in my_list[5]]
    f_list= [float(i) for i in my_list[6]]
    g_list= [float(i) for i in my_list[7]]
    h_list= [float(i) for i in my_list[8]]
    i_list= [float(i) for i in my_list[9]]
    j_list= [float(i) for i in my_list[10]]
#convert the previous inner lists from type string to type float RA
#for 11th machine
    k_list= [float(i) for i in my_list[11]]


#this is a list of 55 elements, that has the maximum angle differences
# between 2 pairs of the machines. We have 55 pairs, therefore 55 values
# contained. KPI will be basedn on the maximum value contained in that list
    max_angle_dev_for_KPI=[]

#this is a list of 55 elements, that will help us identify the
# time instant that each maximum value of the specific SG pair occurs.
    index_local_maxRA_happens=[]

    #1-2
    ra12=[]
    #the list that represents the angular difference between G1 and G2
    ra12=list(np.subtract(a_list,b_list))
    #take the absolute value
    ra12=[abs(number) for number in ra12]
   #the first element of this list will be the maximum RA dev.betwwen
   #G1 and G2
    max_angle_dev_for_KPI.append(max(ra12))
   #the first element of this list will be the index of the maximum RA dev.
   #betwwen  G1 and G2
    index_local_maxRA_happens.append(ra12.index(max(ra12)))


    #same steps as in lines 75-85 for all the 55 pairs formed are
    #illustrated in lines 92 - lines 217.

    #1-3
    ra13=[]
    ra13=list(np.subtract(a_list,c_list))
    ra13=[abs(number) for number in ra13]
    max_angle_dev_for_KPI.append(max(ra13))
    index_local_maxRA_happens.append(ra13.index(max(ra13)))

    #1-4
    ra14=[]
    ra14=list(np.subtract(a_list,d_list))
    ra14=[abs(number) for number in ra14]
    max_angle_dev_for_KPI.append(max(ra14))
    index_local_maxRA_happens.append(ra14.index(max(ra14)))
```

```
    ......
    ......

    #1-10
    ra110=[]
    ra110=list(np.subtract(a_list,j_list))
    ra110=[abs(number) for number in ra110]
    max_angle_dev_for_KPI.append(max(ra110))
    index_local_maxRA_happens.append(ra110.index(max(ra110)))

    #1-11
    ra111=[]
    ra111=list(np.subtract(a_list,k_list))
    ra111=[abs(number) for number in ra111]
    max_angle_dev_for_KPI.append(max(ra111))
    index_local_maxRA_happens.append(ra111.index(max(ra111)))


##################################################################

    #2-3
    ra23=[]
    ra23=list(np.subtract(b_list,c_list))
    ra23=[abs(number) for number in ra23]
    max_angle_dev_for_KPI.append(max(ra23))
    index_local_maxRA_happens.append(ra23.index(max(ra23)))


    #2-4
    ra24=[]
    ra24=list(np.subtract(b_list,d_list))
    ra24=[abs(number) for number in ra24]
    max_angle_dev_for_KPI.append(max(ra24))
    index_local_maxRA_happens.append(ra24.index(max(ra24)))


    #2-5
    ra25=[]
    ra25=list(np.subtract(b_list,e_list))
    ra25=[abs(number) for number in ra25]
    max_angle_dev_for_KPI.append(max(ra25))
    index_local_maxRA_happens.append(ra25.index(max(ra25)))

    ......
    ......

    #2-11
    ra211=[]
    ra211=list(np.subtract(b_list,k_list))
    ra211=[abs(number) for number in ra211]
    max_angle_dev_for_KPI.append(max(ra211))
    index_local_maxRA_happens.append(ra211.index(max(ra211)))



    #end of second
```

```
#############################################################

    #3-4
    ra34=[]
    ra34=list(np.subtract(c_list,d_list))
    ra34=[abs(number) for number in ra34]
    max_angle_dev_for_KPI.append(max(ra34))
    index_local_maxRA_happens.append(ra34.index(max(ra34)))


    ......
    ......

    #3-11
    ra311=[]
    ra311=list(np.subtract(c_list,k_list))
    ra311=[abs(number) for number in ra311]
    max_angle_dev_for_KPI.append(max(ra311))
    index_local_maxRA_happens.append(ra311.index(max(ra311)))



   #end of third
#############################################################
    ......
    ......

#############################################################

    #9-10
    ra910=[]
    ra910=list(np.subtract(i_list,j_list))
    ra910=[abs(number) for number in ra910]
    max_angle_dev_for_KPI.append(max(ra910))
    index_local_maxRA_happens.append(ra910.index(max(ra910)))

    #9-11
    ra911=[]
    ra911=list(np.subtract(i_list,k_list))
    ra911=[abs(number) for number in ra911]
    max_angle_dev_for_KPI.append(max(ra911))
    index_local_maxRA_happens.append(ra911.index(max(ra911)))

   #end of eninth
#############################################################

    #10-11
    ra1011=[]
    ra1011=list(np.subtract(j_list,k_list))
    ra1011=[abs(number) for number in ra1011]
    max_angle_dev_for_KPI.append(max(ra1011))
    index_local_maxRA_happens.append(ra1011.index(max(ra1011)))

   #end of tenth
#############################################################
```

```
#If one KPI is high (e.g. higher than 177 degrees system is unstable)
#I had to write this otherwise, I saw that in the max_angle_dev_ ,
#during instability, the deviation of 2 machines will go higher than 180
#degrees due to the absolute value of the angle difference used.

    for element in max_angle_dev_for_KPI:
        if (element>177):
            KPI=0
            return ('KPI= '+str(KPI) + ' : SYSTEM IS UNSTABLE')


#from all the local maximums of the pairs of the SGs we take the
# global maximum and we store it in variable maxdelta
    maxdelta=max(max_angle_dev_for_KPI)
    KPI=abs(180-maxdelta)

#if index =0 then this means that the global maximum RA is met between
#SG1 and SG2,
#if index=1 then the global maximum RA is met between SG1 and SG3.
#if index =2 then the global maximum RA is met betwwen SG1 and SG4
#and so on...
    index=max_angle_dev_for_KPI.index(maxdelta)


#this is the index associated with the time that the global
#maximum RA occurs
    index_of_global_time=index_local_maxRA_happens[index]
    time_of_global_max_RA=time_list[index_of_global_time]
#its mentioned that SG1 (in scripting) is SG3 in PowerFactory,
#SG2 (in scripting) is SG5 in PowerFactory,
#SG3 (in scripting) is SG7 in PowerFactory,
#SG4 (in scripting) is SG8 in PowerFactory,
#SG5 (in scripting) is SG10 in PowerFactory,
#SG6 (in scripting) is SG11 in PowerFactory,
#SG7 (in scripting) is SG13 in PowerFactory,
#SG8 (in scripting) is SG15 in PowerFactory,
#SG9 (in scripting) is SG16 in PowerFactory,
#SG10 (in scripting) is SG19 in PowerFactory,
#SG11 (in scripting) is SG20 in PowerFactory,

    if index==0:
        print("KPI is " +str(KPI)+ " and is defined by the deviation
        between SG1 and SG2 at " +str(time_of_global_max_RA)+ " seconds")
    if index==1:
        print("KPI is " +str(KPI)+ " and is defined by the deviation
        between SG1 and SG3 at " +str(time_of_global_max_RA)+ " seconds")
    if index==2:
        print("KPI is " +str(KPI)+ " and is defined by the deviation
        between SG1 and SG4 at " +str(time_of_global_max_RA)+ " seconds")
    if index==3:
        print("KPI is " +str(KPI)+ " and is defined by the deviation
        between SG1 and SG5 at " +str(time_of_global_max_RA)+ " seconds")
    if index==4:
        print("KPI is " +str(KPI)+ " and is defined by the deviation
        between SG1 and SG6 at " +str(time_of_global_max_RA)+ " seconds")
    if index==5:
```

```
        print("KPI is " +str(KPI)+ " and is defined by the deviation
        between SG1 and SG7 at " +str(time_of_global_max_RA)+ " seconds")
    if index==6:
        print("KPI is " +str(KPI)+ " and is defined by the deviation
        between SG1 and SG8 at " +str(time_of_global_max_RA)+ " seconds")
    if index==7:
        print("KPI is " +str(KPI)+ " and is defined by the deviation
        between SG1 and SG9 at " +str(time_of_global_max_RA)+ " seconds")
    if index==8:
        print("KPI is " +str(KPI)+ " and is defined by the deviation
        between SG1 and SG10 at " +str(time_of_global_max_RA)+ " seconds")
    if index==9:
        print("KPI is " +str(KPI)+ " and is defined by the deviation
        between SG1 and SG11 at " +str(time_of_global_max_RA)+ " seconds")


    if index==10:
        print("KPI is " +str(KPI)+ " and is defined by the deviation
        between SG2 and SG3 at " +str(time_of_global_max_RA)+ " seconds")
    if index==11:
        print("KPI is " +str(KPI)+ " and is defined by the deviation
        between SG2 and SG4 at " +str(time_of_global_max_RA)+ " seconds")
    if index==12:
        print("KPI is " +str(KPI)+ " and is defined by the deviation
        between SG2 and SG5 at " +str(time_of_global_max_RA)+ " seconds")
    if index==13:
        print("KPI is " +str(KPI)+ " and is defined by the deviation
        between SG2 and SG6 at " +str(time_of_global_max_RA)+ " seconds")
    if index==14:
        print("KPI is " +str(KPI)+ " and is defined by the deviation
        between SG2 and SG7 at " +str(time_of_global_max_RA)+ " seconds")
    if index==15:
        print("KPI is " +str(KPI)+ " and is defined by the deviation
        between SG2 and SG8 at " +str(time_of_global_max_RA)+ " seconds")
    if index==16:
        print("KPI is " +str(KPI)+ " and is defined by the deviation
        between SG2 and SG9 at " +str(time_of_global_max_RA)+ " seconds")
    if index==17:
        print("KPI is " +str(KPI)+ " and is defined by the deviation
        between SG2 and SG10 at " +str(time_of_global_max_RA)+ " seconds")
    if index==18:
        print("KPI is " +str(KPI)+ " and is defined by the deviation
        between SG2 and SG11 at " +str(time_of_global_max_RA)+ " seconds")


    if index==19:
        print("KPI is " +str(KPI)+ " and is defined by the deviation
        between SG3 and SG4 at " +str(time_of_global_max_RA)+ " seconds")
    if index==20:
        print("KPI is " +str(KPI)+ " and is defined by the deviation
        between SG3 and SG5 at " +str(time_of_global_max_RA)+ " seconds")
    if index==21:
        print("KPI is " +str(KPI)+ " and is defined by the deviation
        between SG3 and SG6 at " +str(time_of_global_max_RA)+ " seconds")
    if index==22:
        print("KPI is " +str(KPI)+ " and is defined by the deviation
```

```
    between SG3 and SG7 at " +str(time_of_global_max_RA)+ " seconds")
if index==23:
    print("KPI is " +str(KPI)+ " and is defined by the deviation
    betweenSG3 and SG8 at " +str(time_of_global_max_RA)+ " seconds")
if index==24:
    print("KPI is " +str(KPI)+ " and is defined by the deviation
    between SG3 and SG9 at " +str(time_of_global_max_RA)+ " seconds")
if index==25:
    print("KPI is " +str(KPI)+ " and is defined by the deviation
    between SG3 and SG10 at " +str(time_of_global_max_RA)+ " seconds")
if index==26:
    print("KPI is " +str(KPI)+ " and is defined by the deviation
    between SG3 and SG11 at " +str(time_of_global_max_RA)+ " seconds")


if index==27:
    print("KPI is " +str(KPI)+ " and is defined by the deviation
    between SG4 and SG5 at " +str(time_of_global_max_RA)+ " seconds")
if index==28:
    print("KPI is " +str(KPI)+ " and is defined by the deviation
    between SG4 and SG6 at " +str(time_of_global_max_RA)+ " seconds")
if index==29:
    print("KPI is " +str(KPI)+ " and is defined by the deviation
    between SG4 and SG7 at " +str(time_of_global_max_RA)+ " seconds")
if index==30:
    print("KPI is " +str(KPI)+ " and is defined by the deviation
    between SG4 and SG8 at " +str(time_of_global_max_RA)+ " seconds")
if index==31:
    print("KPI is " +str(KPI)+ " and is defined by the deviation
    between SG4 and SG9 at " +str(time_of_global_max_RA)+ " seconds")
if index==32:
    print("KPI is " +str(KPI)+ " and is defined by the deviation
    betweenSG4 and SG10 at " +str(time_of_global_max_RA)+ " seconds")
if index==33:
    print("KPI is " +str(KPI)+ " and is defined by the deviation
    between SG4 and SG11 at " +str(time_of_global_max_RA)+ " seconds")


if index==34:
    print("KPI is " +str(KPI)+ " and is defined by the deviation
    between SG5 and SG6 at " +str(time_of_global_max_RA)+ " seconds")
if index==35:
    print("KPI is " +str(KPI)+ " and is defined by the deviation
    between SG5 and SG7 at " +str(time_of_global_max_RA)+ " seconds")
if index==36:
    print("KPI is " +str(KPI)+ " and is defined by the deviation
    between SG5 and SG8 at " +str(time_of_global_max_RA)+ " seconds")
if index==37:
    print("KPI is " +str(KPI)+ " and is difined by the deviation
    between SG5 and SG9 at " +str(time_of_global_max_RA)+ " seconds")
if index==38:
    print("KPI is " +str(KPI)+ " and is defined by the deviation
    between SG5 and SG10 at " +str(time_of_global_max_RA)+ " seconds")
if index==39:
    print("KPI is " +str(KPI)+ " and is defined by the deviation
    between SG5 and SG11 at " +str(time_of_global_max_RA)+ " seconds")
```

```
if index==40:
    print("KPI is " +str(KPI)+ " and is defined by the deviation
    between SG6 and SG7 at " +str(time_of_global_max_RA)+ " seconds")
if index==41:
    print("KPI is " +str(KPI)+ " and is defined by the deviation
    between SG6 and SG8 at " +str(time_of_global_max_RA)+ " seconds")
if index==42:
    print("KPI is " +str(KPI)+ " and is defined by the deviation
    between SG6 and SG9 at " +str(time_of_global_max_RA)+ " seconds")
if index==43:
    print("KPI is " +str(KPI)+ " and is defined by the deviation
    between SG6 and SG10 at " +str(time_of_global_max_RA)+ " seconds")
if index==44:
    print("KPI is " +str(KPI)+ " and is defined by the deviation
    between SG6 and SG11 at " +str(time_of_global_max_RA)+ " seconds")



if index==45:
    print("KPI is " +str(KPI)+ " and is defined by the deviation
    between SG7 and SG8 at " +str(time_of_global_max_RA)+ " seconds")
if index==46:
    print("KPI is " +str(KPI)+ " and is defined by the deviation
    between SG7 and SG9 at " +str(time_of_global_max_RA)+ " seconds")
if index==47:
    print("KPI is " +str(KPI)+ " and is defined by the deviation
    between SG7 and SG10 at " +str(time_of_global_max_RA)+ " seconds")
if index==48:
    print("KPI is " +str(KPI)+ " and is defined by the deviation
    between SG7 and SG11 at " +str(time_of_global_max_RA)+ " seconds")



if index==49:
    print("KPI is " +str(KPI)+ " and is defined by the deviation
    between
          SG8 and SG9 at " +str(time_of_global_max_RA)+ " seconds")
if index==50:
    print("KPI is " +str(KPI)+ " and is defined by the deviation
    between SG8 and SG10 at " +str(time_of_global_max_RA)+ " seconds")
if index==51:
    print("KPI is " +str(KPI)+ " and is defined by the deviation
    between SG8 and SG11 at " +str(time_of_global_max_RA)+ " seconds")


if index==52:
    print("KPI is " +str(KPI)+ " and is defined by the deviation
    between SG9 and SG10 at " +str(time_of_global_max_RA)+ " seconds")
if index==53:
    print("KPI is " +str(KPI)+ " and is defined by the deviation
    between SG9 and SG11 at " +str(time_of_global_max_RA)+ " seconds")
```

```
    if index==54:
        print("KPI is " +str(KPI)+ " and is defined by the deviation
        between SG10 and SG11 at " +str(time_of_global_max_RA)+ " seconds")



#returns 1)KPI which is max value from 55 pairs, 2)index which is
#the pair of machines that participate in the maximum oscillation,
# 3) the time that the KPI is observed, 4) max_angle_dev_for_KPIis a list
# with the 55 maximum angles (one for each pair) and 5) maxdelta
#is a number which is the maximum angle of all the 55 pairs
    return (KPI,index,time_of_global_max_RA,max_angle_dev_for_KPI,maxdelta)

#end of KPI computation function
##############################################################

'''
Main Code; updates the PowerFactoryParameters, applies faults,
calls function for KPI computation, stores the result in csv file
'''

#take all the composote models - see extention .ElmDsl and place them
# in a list
DSLs_List = app.GetCalcRelevantObjects("*.ElmDsl")



#lists of parameters that will be traveresed in a nested loop.
t_washout_list=[0.01,0.1,0.5,1,2,2.5,5,7,10,12,15,20,30,40,50,60,70,80]
k_washout_list=[1,5,10,15,20,25,30,35,40,45,50,55,60,65,70,75,80]


KPI_list_from_K_comparison=[]
index_list_from_K_comparison=[]
time_list_from_K_comparison=[]


previousKPI=-100000000000000   #Initialization of KPI

file1=open('3.L69_sensitivity_ultimate.csv','w') #create a csv file



for element_k in range(len(k_washout_list)):
    for element_t in range(len(t_washout_list)):
#take the current iteration's values from the lists and store them
#in the variables as seen
        Twash=t_washout_list[element_t]
        Kwash=k_washout_list[element_k]


        #apply the changes in the power factory model
        PCtrlT34_ObjList = []
        for Element in DSLs_List:
            if Element.loc_name[:23] == 'XP Control Type 3 and 4':
                PCtrlT34_ObjList.append(Element)
```

```
        for DslObj in PCtrlT34_ObjList:
            SpecialCarrier                = DslObj.params
            SpecialCarrier[4]    =Kwash
            SpecialCarrier[5]=Twash
            DslObj.params=SpecialCarrier


#For that pair of washout constants run the fault, create the csv file
#from the angles (test2.csv) computed with respect to the slack machine
#and give it to function computation. this funtion will return a tuple
#with KPI, index-(pair of machines), time of KPI,
#and a list with max angles per pair

        # Time Domain Initial Conditions
        comInc=app.GetFromStudyCase("ComInc")
        # Time Domain(RMS or EMT) Simulations
        comSim=app.GetFromStudyCase("ComSim")
        ##set simulation
        comInc.iopt_sim="rms"
        comInc.tstart = 0 #starts simulation from 0 sec
        comSim.tstop = 8 # total event time =  8 sec


        #execute initial conditions and time domain RMS simulation
        app.EchoOff()
        comInc.Execute()
        app.EchoOn()
        comSim.Execute()

        comRes = app.GetFromStudyCase("ComRes")
        Case = app.GetActiveStudyCase()
        res = Case.GetContents('*.ElmRes')[0]

        ObjG03_Scotland = app.GetCalcRelevantObjects('G03.ElmSym')[0]
        ObjG05_Scotland = app.GetCalcRelevantObjects('G05.ElmSym')[0]
        ObjG07_Scotland = app.GetCalcRelevantObjects('G07.ElmSym')[0]
        ObjG08_Scotland = app.GetCalcRelevantObjects('G08.ElmSym')[0]
        ObjG10_NEngland = app.GetCalcRelevantObjects('G10.ElmSym')[0]
        ObjG11_NEngland = app.GetCalcRelevantObjects('G11.ElmSym')[0]
        ObjG13_WEngland = app.GetCalcRelevantObjects('G13.ElmSym')[0]
        ObjG15_WEngland = app.GetCalcRelevantObjects('G15.ElmSym')[0]
        ObjG16_NEngland = app.GetCalcRelevantObjects('G16.ElmSym')[0]
        ObjG19_EEngland = app.GetCalcRelevantObjects('G19.ElmSym')[0]
        ObjG20_EEngland = app.GetCalcRelevantObjects('G20.ElmSym')[0]

        comRes.pResult = res
        comRes.iopt_exp = 6 # to export as csv
        comRes.f_name ='test2.csv'
        comRes.iopt_sep = 1 # to use the system seperator
        comRes.iopt_honly = 0 # to export data and not only the header
        comRes.iopt_csel = 1 # export only selected variables
        comRes.iopt_tsel = 0 # All time registration active


        resObj = [None, None, None, None, None, None, None, None, None,
                  None,None, None]
```

```
resElms = [res,ObjG03_Scotland,ObjG05_Scotland,ObjG07_Scotland,
           ObjG08_Scotland,ObjG10_NEngland,ObjG11_NEngland,
           ObjG13_WEngland,ObjG15_WEngland,ObjG16_NEngland,
           ObjG19_EEngland,ObjG20_EEngland]
resVars = ["b:tnow","c:firel","c:firel","c:firel","c:firel",
           "c:firel","c:firel","c:firel","c:firel","c:firel",
           "c:firel","c:firel"]

comRes.resultobj = resObj # Export selected
comRes.element = resElms
comRes.variable = resVars
comRes.Execute()

tupla_output=computation()  #Here the function computation
#is being called and the result is stored to the tuple as seen


if tupla_output[0]>previousKPI:
    bestK=Kwash
    bestT=Twash


previousKPI=tupla_output[0] #When all the washout parameters
#are tested this value will be the maximum KPI of all the KPIs
#that have been found


counter_list=[]
for i in range (len(tupla_output[3])):
    counter_list.append(i)

#write the csv file
file1.write('Kwash: ' + ',' )
file1.write(str(Kwash) +'\n')
file1.write('Twash: ' + ',' )
file1.write(str(Twash)+ '\n')
file1.write('SG pair number: ' + ',' )
file1.write(str(counter_list)+ '\n')
file1.write('max angle dif per pairs: ' + ',' )
file1.write(str(tupla_output[3])+ '\n')
file1.write('global max angle of all pairs: ' + ',' )
file1.write(str(tupla_output[4])+ '\n')
file1.write('KPI: ' + ',' )
file1.write(str(tupla_output[0])+ '\n')
file1.write('SGs pair causing KPI: ' + ',' )
file1.write(str(tupla_output[1])+ '\n')
file1.write('time KPI computed: ' + ',' )
file1.write(str(tupla_output[2])+ '\n')

file1.write('\n')
file1.write('\n')

KPI_list_from_K_comparison.append(tupla_output[0])
index_list_from_K_comparison.append(tupla_output[1])
time_list_from_K_comparison.append(tupla_output[2])
```

```
#store after all the parameters are tested, the maximum KPI result
#in the csv file, also the Gain and the Time constants that lead to
#that best KPI
maximumKPI=max(KPI_list_from_K_comparison)
index_in_KPI_list_from_K_comparison=
KPI_list_from_K_comparison.index(maximumKPI)

koptimal=k_washout_list[index_in_KPI_list_from_K_comparison]


file1.write('\n')
file1.write('\n')
file1.write('----------------------------------------')

file1.write('\n')
file1.write('the best washout constants are found to be: Kgain= '
            +str(bestK)+ ' , T=' +str(bestT)+
            ' and this combination gives KPI='
            +str(maximumKPI))
file1.close()


#Appear the same message in PowerFactory command window
app.PrintPlain('the best washout constants are found to be: Kgain='
               +str(bestK)+' , T=' +str(bestT)+
               ' and this combination gives KPI='
               +str(maximumKPI))
```

I.4. Results for 75% GB - Grid Following

The following tables illustrate the effect of different washout tuning for grid following technology, when different faults are applied. Two critical faults are examined, i.e. Fault at Node 9 and Fault at Line 6-9. The criticality of these faults can be observed by the relatively low CCTs, as seen in Figure 4.14.

Table I.1: Grid Following SDC in all (HYBRID) GB zones & Bus 9 Fault

G	$T_1 = 0.01$	$T_2 = 0.1$	$T_3 = 0.5$	$T_4 = 1$	$T_5 = 2$	$T_6 = 5$	$T_7 = 10$	$T_8 = 15$	$T_9 = 20$	$T_{10} = 30$
5	113.53463	110.674413	105.897568	105.587435	108.172636	114.278888	112.252947	110.541437	110.022861	109.214313
10	114.860283	110.807246	107.012132	106.93245	107.621879	112.651505	111.057309	110.341931	109.082987	108.155376
15	115.394329	111.37368	108.107103	107.863156	106.64909	107.140884	110.807365	110.761829	109.611157	108.446807
20	115.493	111.823481	108.881336	108.264405	105.882363	108.70016	111.603505	111.375186	110.310347	109.153076
30	115.535962	112.007617	109.342356	108.825767	105.617499	109.051786	112.526336	110.267892	111.176049	109.535335
40	115.460431	111.740973	109.753576	109.047025	105.301875	109.747751	112.673103	110.886875	111.103206	109.990321
50	115.315796	110.77684	109.679004	109.145425	105.141108	109.563144	112.981402	111.10011	110.962389	109.593539
60	115.155058	108.106008	109.617062	108.971849	105.118648	109.347899	112.663199	111.506438	110.817529	109.686968
70	115.085662	105.907966	109.486491	108.973112	105.129785	109.169687	112.676091	111.454882	109.389978	109.604724
80	114.964486	104.060474	109.154028	108.985465	105.038226	109.098045	112.379366	111.270793	109.358297	107.78699

Table I.2: Grid Following SDC in East and Scottish zones & Bus 9 Fault

G	$T_1 = 0.01$	$T_2 = 0.1$	$T_3 = 0.5$	$T_4 = 1$	$T_5 = 2$	$T_6 = 5$	$T_7 = 10$	$T_8 = 15$	$T_9 = 20$	$T_{10} = 30$
5	113.124617	111.633161	106.168684	105.183581	105.282104	108.907795	110.902982	111.604497	111.939048	112.312407
10	114.867384	111.356932	107.156081	106.045584	105.041709	108.101875	109.517847	110.670336	111.140688	111.591073
15	115.485343	111.442359	108.220137	106.848919	104.52122	107.389881	109.315881	109.893002	110.723963	111.139125
20	115.631964	109.785864	109.09239	107.343572	104.445685	106.788223	108.922684	109.70805	110.209783	110.781608
30	115.329738	108.47329	108.443918	107.90021	103.016369	105.982981	108.426752	109.326945	109.679358	110.22435
40	114.810282	107.672602	107.821197	108.412915	103.212561	105.773109	108.129332	108.862105	109.653443	109.90669
50	114.388503	107.093717	107.351644	108.618637	102.896975	105.447898	107.872492	108.94985	109.527211	109.805048
60	113.964096	106.518584	106.637608	108.775586	103.391857	105.310159	107.779646	108.537707	109.359782	109.693161
70	113.651236	106.242915	106.450374	108.793501	103.380992	105.355294	107.806126	108.834955	109.324995	109.615954
80	113.338792	105.981256	106.518583	109.104015	103.460827	105.30395	107.739985	108.757333	109.360577	109.559492

Table I.3: Grid Following SDC in all (Hybrid) zones & Line 6-9 Fault

G	$T_1 = 0.01$	$T_2 = 0.1$	$T_3 = 0.5$	$T_4 = 1$	$T_5 = 2$	$T_6 = 5$	$T_7 = 10$	$T_8 = 15$	$T_9 = 20$	$T_{10} = 30$
5	113.573924	110.993499	106.889155	106.82208	109.983239	115.647302	117.957223	118.383558	118.377524	118.338636
10	114.194974	110.533619	106.49231	106.549299	109.138616	114.367904	117.690441	117.938285	118.171006	118.197504
15	114.33812	110.401192	106.874311	106.77717	107.551964	113.317241	117.320749	117.969843	118.11257	118.030676
20	114.46991	110.8884	107.795573	107.658466	107.040612	112.876868	117.205229	117.777617	117.819387	117.915326
30	114.47489	111.32369	107.782444	108.517307	106.607745	111.986688	116.801031	117.676609	117.686613	117.78563
40	114.60601	111.33531	107.972349	108.555885	106.040406	111.237888	116.514946	117.539487	117.66883	117.7141
50	114.555886	110.48688	107.86319	108.535094	106.362925	111.203611	116.449847	117.428931	117.607970	117.682684
60	114.644445	108.825084	107.82782	108.679708	105.885481	110.879694	116.266973	117.331730	117.548898	117.672722
70	114.596488	107.124135	107.462067	108.7965	105.865487	110.970944	116.304634	117.320616	117.463811	117.572373
80	114.561704	106.133411	107.47635	108.743309	105.960977	110.74057	116.198995	117.208961	117.36017	117.614624

Table I.4: Grid Following SDC in East and Scottish zones & Line 6-9 Fault

G	$T_1 = 0.01$	$T_2 = 0.1$	$T_3 = 0.5$	$T_4 = 1$	$T_5 = 2$	$T_6 = 5$	$T_7 = 10$	$T_8 = 15$	$T_9 = 20$	$T_{10} = 30$
5	113.506038	112.202281	107.280399	106.430021	107.182941	110.445606	112.034852	112.885416	113.256451	113.643413
10	114.713016	111.552634	107.060063	106.130683	106.109568	109.595574	111.337726	112.584385	113.120642	113.720893
15	115.293671	111.548128	107.138951	106.168796	105.383416	108.951764	110.978987	112.144026	112.872754	113.640862
20	115.561781	111.814646	108.444834	106.889918	104.746018	108.610522	110.476456	111.868841	112.787953	113.635431
30	115.584122	111.388822	108.637001	107.512586	104.521005	107.829599	109.950912	111.425168	112.44259	113.623364
40	115.493637	110.353747	108.663499	108.023695	104.881181	107.763252	109.678905	111.240789	112.233629	113.668786
50	115.307198	110.004847	108.553855	108.086725	104.894988	107.601238	109.457154	111.076283	112.125095	113.659782
60	115.061105	109.791193	108.394092	108.232166	104.80205	107.45749	109.318435	110.792208	112.046441	113.651349
70	114.874636	109.435329	108.225673	108.338556	105.122736	107.363441	109.108284	110.551626	111.853029	113.643706
80	114.643	109.215459	108.132333	108.722645	105.09497	107.341537	109.093084	110.633087	111.710059	113.636735

It can be observed, that for the Line 6-9 Fault, there are some KPIs that are high (see Table I.3, when:

- SDCs are used in all the Hybrid GB zones which include both Wind Generation and Synchronous Generation Production
- the Time Constants in the SDCs controllers are high (and not necessarily very low in which the KPI is also high)

However, high time constant gains can maybe slightly decrease the first swing of the mostly affected SGs' pair during this specific fault, but time - domain simulations, indicate that high values of time constants, can decrease the damping torques of the machines, due to the interactions with the SGs' governors, as mentioned in [44]. Figures I.4 and I.5 illustrate this observation.

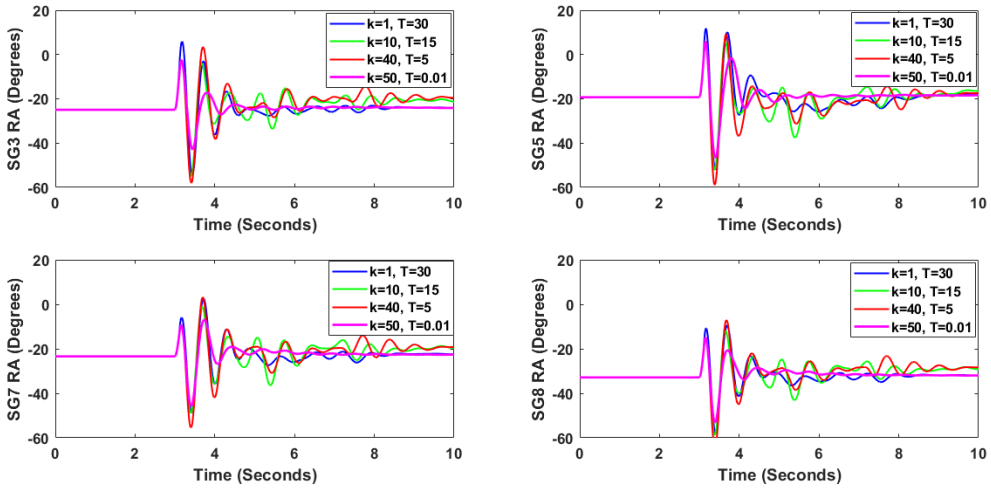

Figure I.4: Scottish SGs rotor angles when a three phase fault at Bus 9 is performed (FCT=120ms), for different SDC washout gains - SDC Technology used in all the hybrid GB zones

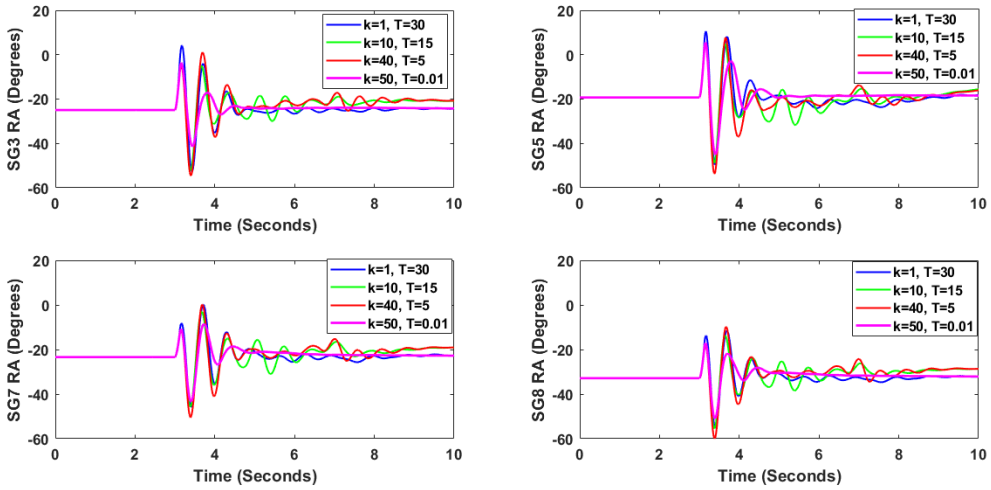

Figure I.5: Scottish SGs rotor angles when a three phase fault at Line 6-9 is performed (FCT=120ms), for different SDC washout gains - SDC Technology used in all the hybrid GB zones

I.5. Results for 75% GB - Grid Forming

The same faults (test cases) were performed for the tuning of washout filters in the P and Q loops of the grid forming controllers. As seen in Table I.5, it was found that gains in the washout filters higher than 0.15, deteriorate the transient stability of the system.

As seen in Figures I.6 and I.7, the rotor angle responses are very similar no matter of the washout parameters, since the permitted range is small. It is mentioned that the bad damping response of the washout filters when their gain is high, could be an initialization problem of the simulation itself. To this end, in order not to enhance the high frequency oscillations with the washout filters, a timer was introduced, so as to start the simulations with a small washout gain, then wait until the system, is fully well initialized, then the washout gains can be increased. However, it was observed that even like this way, the oscillations are not damped with high gains.

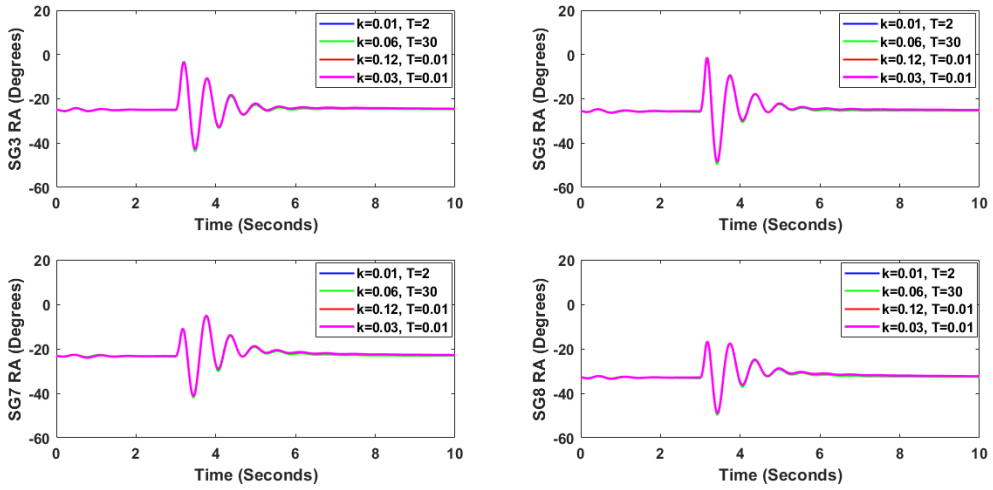

Figure I.6: Scottish SGs rotor angles when a three phase fault at Bus 9 is performed (FCT=120ms), for different grid forming washout gains - SDC Technology used in all the hybrid GB zones

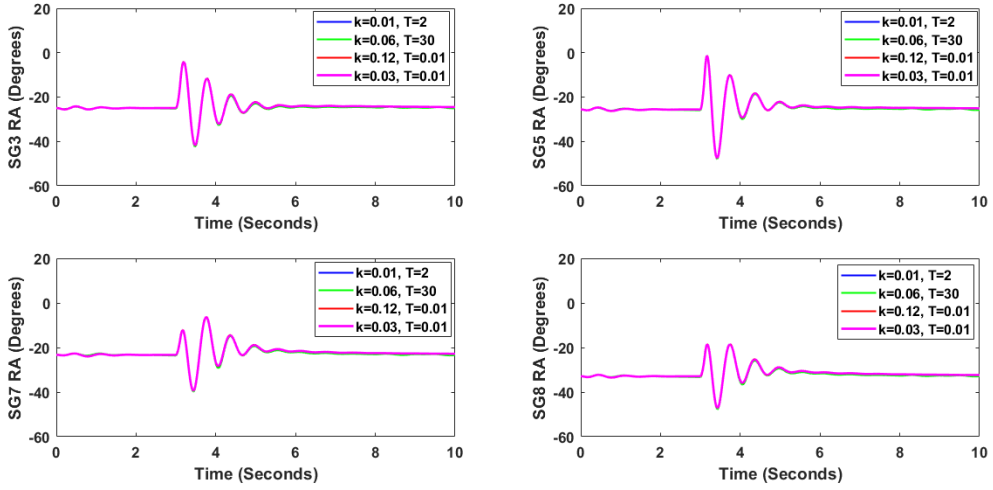

Figure I.7: Scottish SGs rotor angles when a three phase fault at Line 6-9 is performed (FCT=120ms), for different gridforming washout gains- SDC Technology used in all the hybrid GB zones

As a last experiment, rotor angle deviations between SGs (the same exactly synchronous machines' angles as in the grid following configuration for each wind generator) are used. However, as seen in I.8,

not any difference is observed between the default case in which the inputs in the washout filters are currents. This may be due to the small permitted gains that can be used in the washout filters. Further investigation needs to be done in the future, maybe even with one other power system, in which the permitted range of washout parameters is more vast.

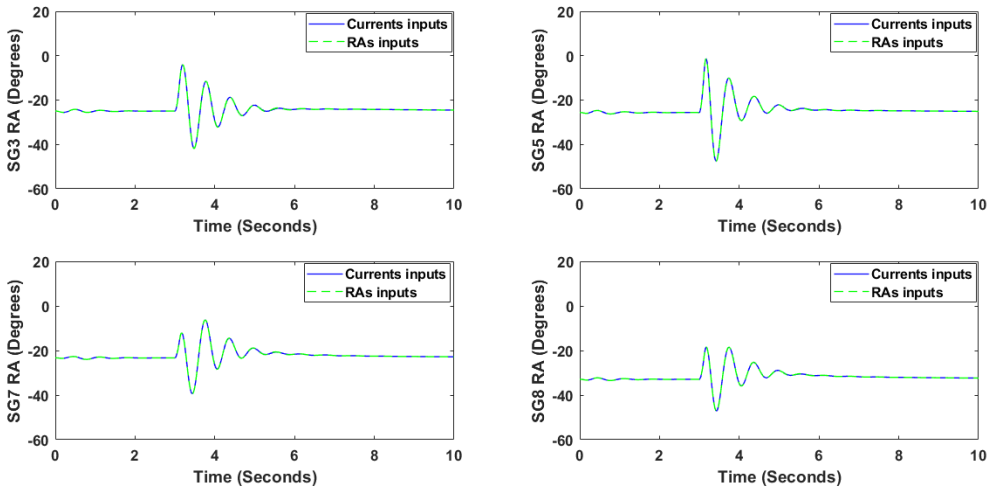

Figure I.8: Scottish SGs rotor angles when a three phase fault at Line 6-9 is performed (FCT=120ms), for different grid forming washout input signals - Grid Forming Technology used in all the hybrid GB zones

Table I.5: Grid Forming WGs in all (HYBRID) GB zones & Line 6-9 Fault

G	$T_1 = 0.01$	$T_2 = 0.1$	$T_3 = 0.5$	$T_4 = 1$	$T_5 = 2$	$T_6 = 5$	$T_7 = 10$	$T_8 = 15$	$T_9 = 20$	$T_{10} = 30$
0.01	116.764009	116.740816	116.732117	116.726369	116.768093	116.734451	116.726934	116.761811	116.763478	116.765418
0.03	116.710271	116.69212	116.682921	116.68814	116.700344	116.650845	116.655564	116.644083	116.633759	116.623893
0.06	116.705135	116.63646	116.528762	116.51443	116.495143	116.469783	116.344011	116.400331	116.375906	116.381424
0.09	116.673304	116.549523	116.160469	116.079402	116.088324	116.077653	116.013932	115.957159	115.997354	116.123961
0.12	116.632554	109.881039	105.5759	106.079699	113.508529	104.292043	115.90196	115.522981	113.290465	116.396385
0.15	116.656753	83.722557	100.674551	83.588175	98.72954	96.459007	81.491928	104.132935	96.738501	88.881097
0.2	111.403347	76.145396	72.293358	71.37069	71.656834	72.077286	70.550424	73.076589	74.79569	71.356849
0.25	61.237631	75.672211	73.583924	71.742324	71.298735	71.557919	71.399464	72.160487	71.802961	71.670355
1	54.433136	63.914148	53.563227	51.301188	63.508494	57.175287	56.762039	54.103046	59.591719	51.19835

J

Great Britain System with 66% WG share Dispatches - Modification to 75% WG Share

Table J.1: 75% GB- shift from %66

Region	Substation	Synchronous Gen (MVA)	Wind Gen (MVA)
Scotland	3	-88.2	+88.2
Scotland	5	-170	+170
N.England	16	-798	+798
W.England	13	-534	+534
W.England	15	-748	+748
E.England	19	-617	+617
E.England	20	-922	+922

Table J.2: GB 66% Dispatches

Region	Substation	Sync Gen (GW)	PEIG (GW)	Load (GW)	Reactive load (MVAr)	Syn.Dispatch + 5% Losses (GW)	Dispatch PEIG (GW)
Scotland	1	0	1.85033	0.55	115.5	0	1.83183
	2	0	1.85	0.55	115.5	0	0
	3	0.864	0.85	0.55	115.5	0.7056	0.8415
	4	0	0	0.55	115.5	0	0
	5	1.08	1.85	0.55	115.5	0.8505	1.8315
	6	0	2.218	0.55	115.5	0	2.19582
	7	1.08	0	0.55	115.5	0.8505	0
	8	1.08	2.291	0.55	115.5	0.9072	0
North England	9	0	2.658	3.13	656.25	0	2.63142
	10	1.512	3.35	3.13	656.25	1.11132	3.3165
	11	3.78	2.56	3.13	656.25	2.69892	0
	16	3.78	2.332	3.13	656.25	2.65923	2.30868
West England	12	0	1.9	2.17	455	0	1.881
	13	2.18	1	2.17	455	1.6023	0.99
	14	0	1.2	2.17	455	0	1.188
	15	4.158	0.95	2.17	455	4.118205	0.9405
	17		0.2	2.17	455	0	0.198
	18	4.536	0.95	2.17	455	0	0.9405
East England	19	2.34	4.1	2	420	1.23375	4.059
	20	3.12	6.4	2	420	1.638	6.336
South England	21	0	0.4	2.11	443.33	0	0.396
	22	0	0.53	2.11	443.33	0	0.5247
	23	1	0.497	2.11	443.33	0	0.49203
	24	1	0	2.11	443.33	0	0
	25	1	0	2.11	443.33	0	0
	26	1	0.504	2.11	443.33	0	0.49896
	27	1	0.53	2.11	443.33	0	0.5247
	28	1	0.53	2.11	443.33	0	0.5247
	29	1	0.4995	2.11	443.33	0	0.49451
						Tot: 18.375525	34.9458
							WG share=66%

K

Great Britain System (75% WG) – Transient stability performance with supplementary damping control in selected wind generators

As indicated in Section 4.4.2, increasing the number of WGs with SDC should be done only if significantly higher FCT values are of interest. Figure K.1 - Figure K.4 illustrate simulation outcomes concerning the transient stability performance observed in the synthetic model of the GB system, when two selected faults occur, one close location (line 6-9), and one distant location (Bus 15), from the (Scotland and East England) areas of the GB system that are prone to transient instability. Note in the Figures that the achievable reduction of amplitude of the first swing of rotor angle oscillations and the increase of damping is nearly the same if the fault occurs close (FCT = 420 ms for fault at line 6-9) to the Scotland and East England areas, considering that only WGs of these areas perform SDC vs the case when all WGs perform SDC. Similar finding is obtained, but with slightly higher FCT value, if the fault occurs in a distant location (FCT= 490 ms for fault at bus 15).

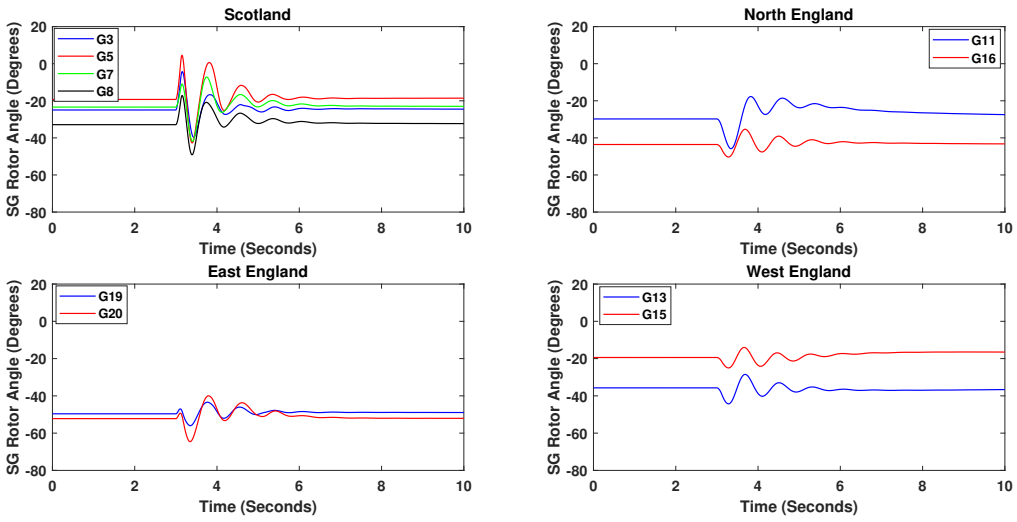

Figure K.1: Three phase fault at line 6-9, FCT = 120ms. WGs with SDC only in Scotland and East England areas

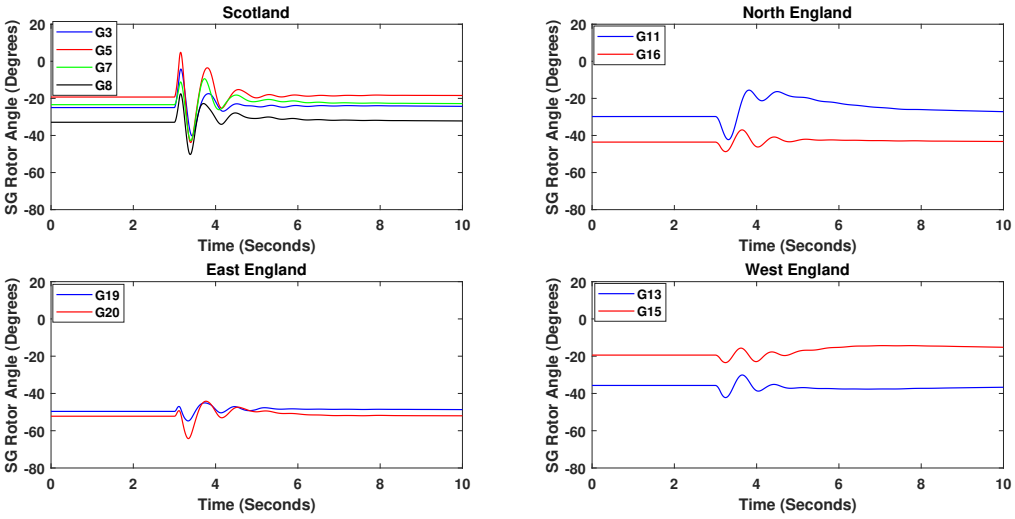

Figure K.2: Three phase fault at line 6-9, FCT = 120ms. All WGs equipped with SDC.

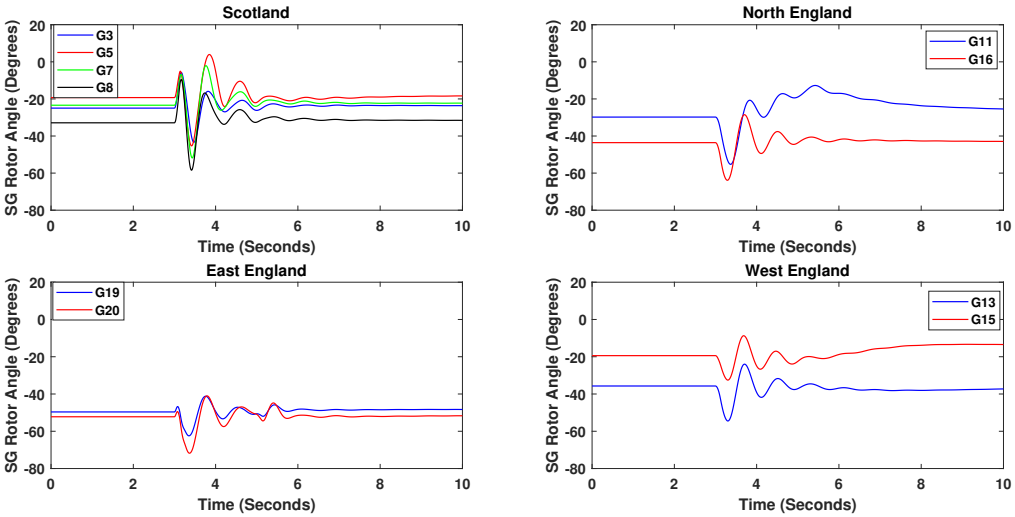

Figure K.3: Three phase fault at node 15, FCT = 120ms. WGs with SDC only in Scotland and East England areas.

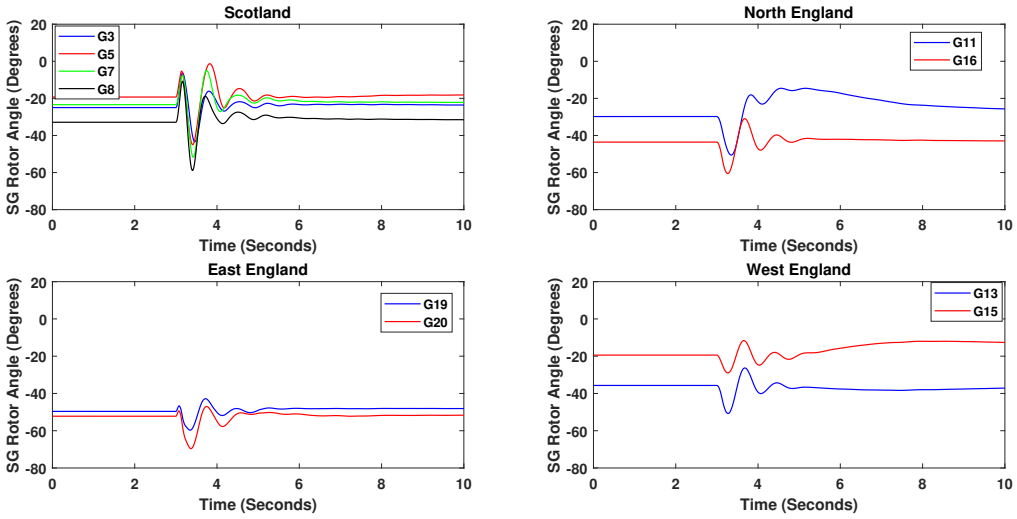

Figure K.4: Three phase fault at node 15, FCT = 120 ms. All WGs equipped with SDC.

L

User Manual for RMS models

L.1. Grid Following Model Description

The aim of the particular section is to examine the modifications applied in the existing RMS type IV wind generator model provided by Energynautics gmbh.

In Figure L.1, the composite frame as used in DigSILENT PowerFactory of the type IV wind generator controllers is presented. Inside the purple graphic box, the composite frame of the Network generators is comprised. This frame, as seen in Figure L.2, as expected retrieves the SGs pair's rotor angles and subtracts them. Then, as seen in Figure L.1 (i.e. purple line), this rotor angle difference (i.e. ad10), will be fed to the P - controller model definition. As observed in Figure L.3, and in particular in the red box diagram, the SDC controller will act when:

- The LVRT flag will be activated (i.e. when voltage in the PCC of the WG drops below 0.8 pu due to a fault)
- The user has selected the corresponding control mode that enables this new controller and differentiates it from the default one, as implemented by Energynautics gmbh. To this end, parameter C is exists in the P-loop controller which is determined by the user (i.e. C=0: default controller mode enabled / C=1: SDC mode enabled).

The SDC controller itself is illustrated in Figure L.4. As can be seen, it comprises a washout- filter, a lead lag compensator and also the two additional blocks, which represent two different ways to represent data latencies that inherently are presented, as signals coming from the power systems need to be fed to the WG locations. The description of the time-delay blocks is done in the first section of the main text. Moreover as mentioned before, the lead-lag filter even modelled, is not used.

As stated before, two different types of transfer function were added separately to the SDC to represent the delays.

Figure L.5 illustrates the way in which the user can select the SGs that will act in the WG SDC controller. Last, Figure L.6 presents all the new parameters that are associated to the SDC controller.

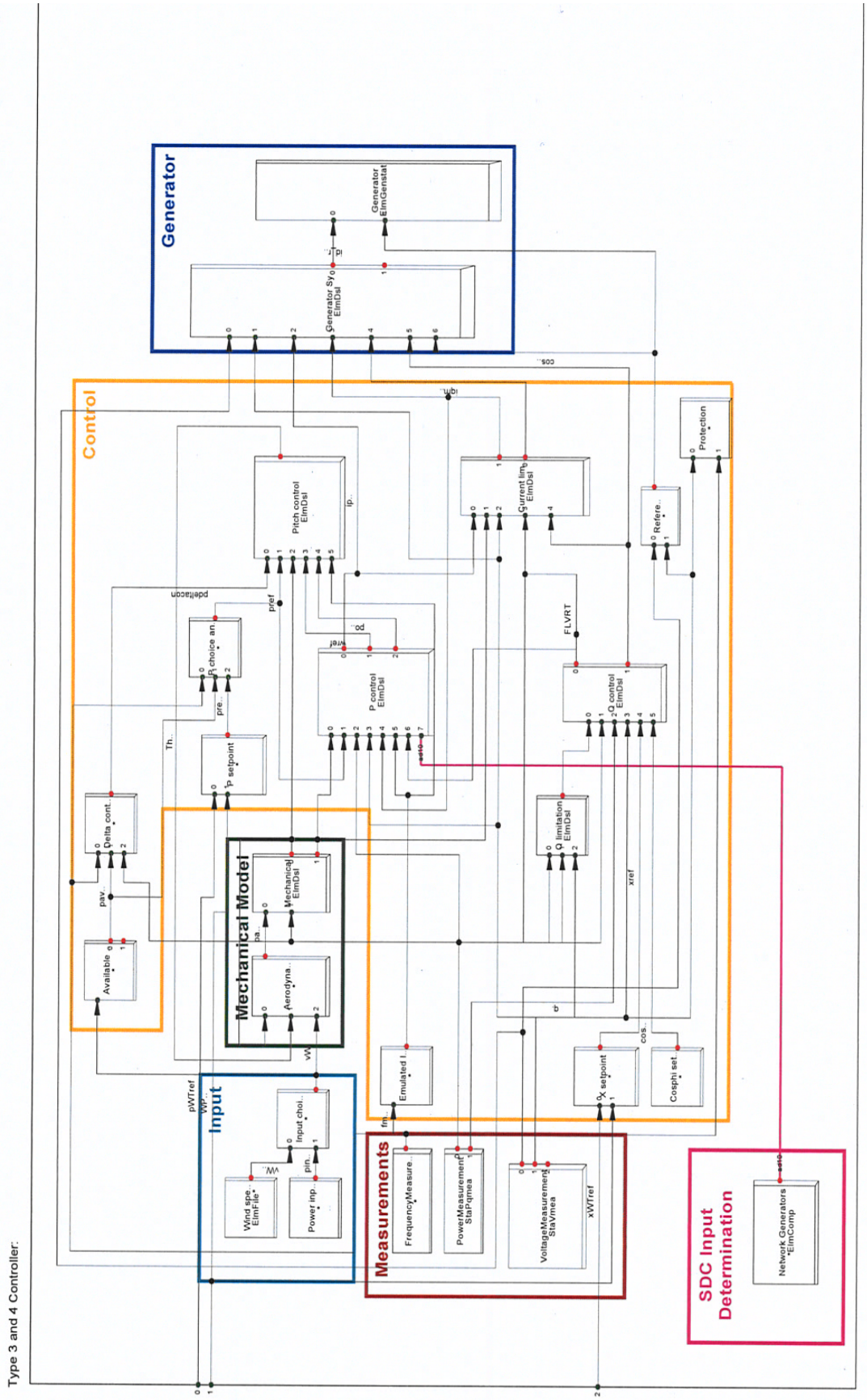

Figure L.1: DigSILENT PowerFactory Modified Type IV WG Composite Frame for SDC accommodation

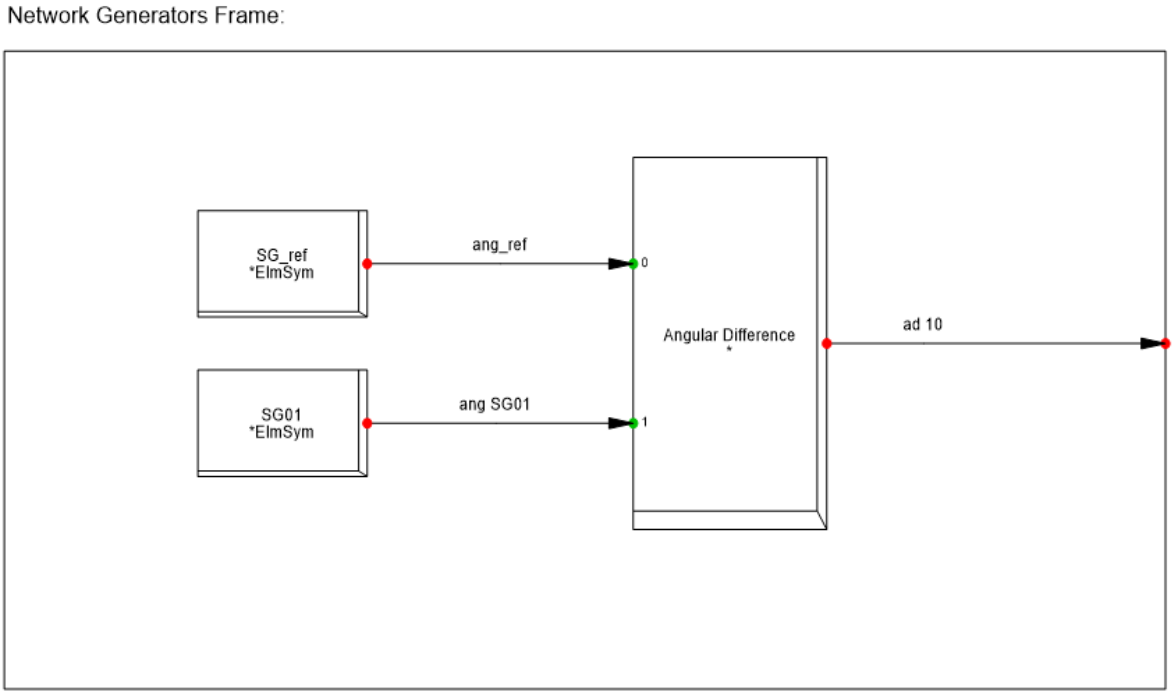

Figure L.2: DigSILENT PowerFactory Network Generators' Composite Frame added for SDC input

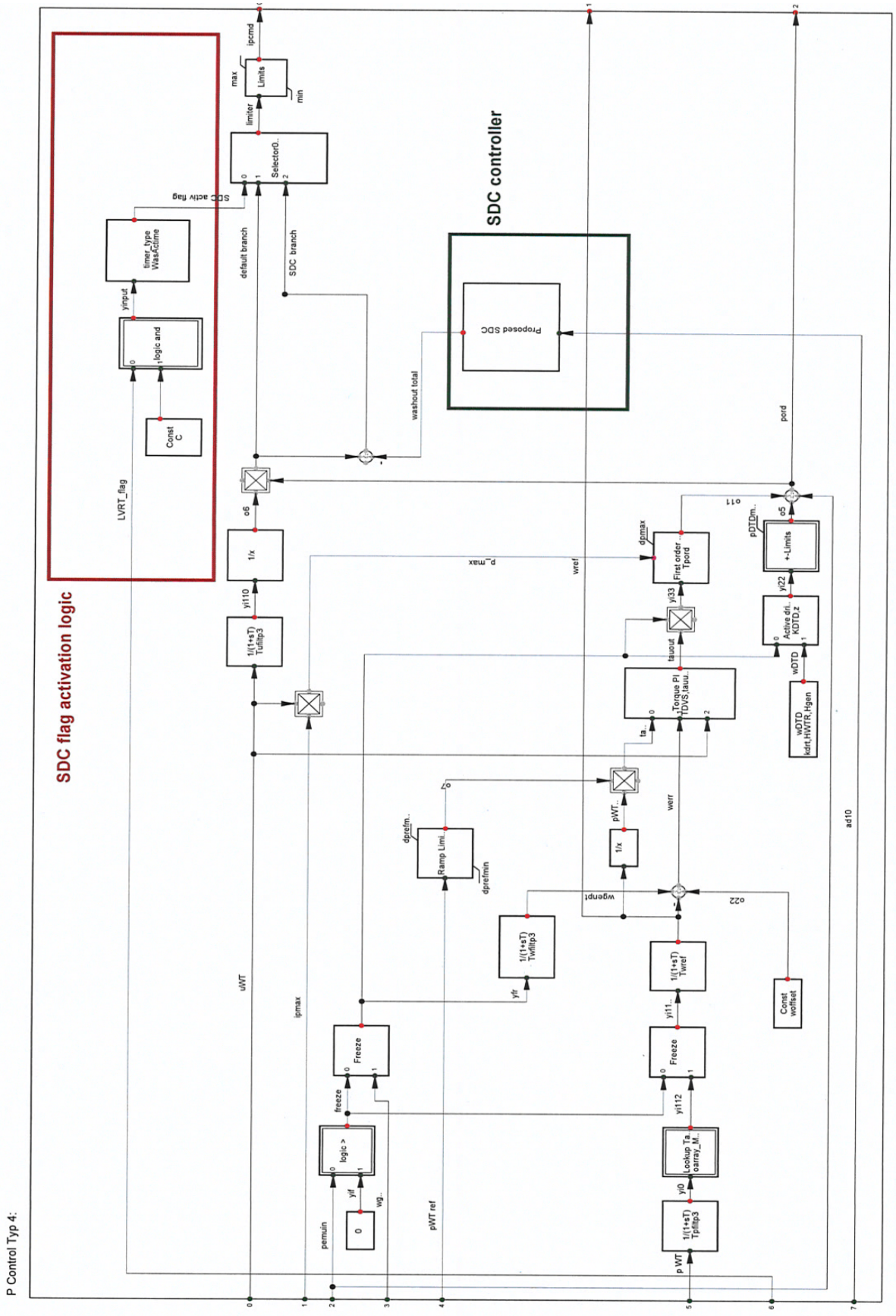

Figure L.3: DigSILENT PowerFactory modified P - controller model definition

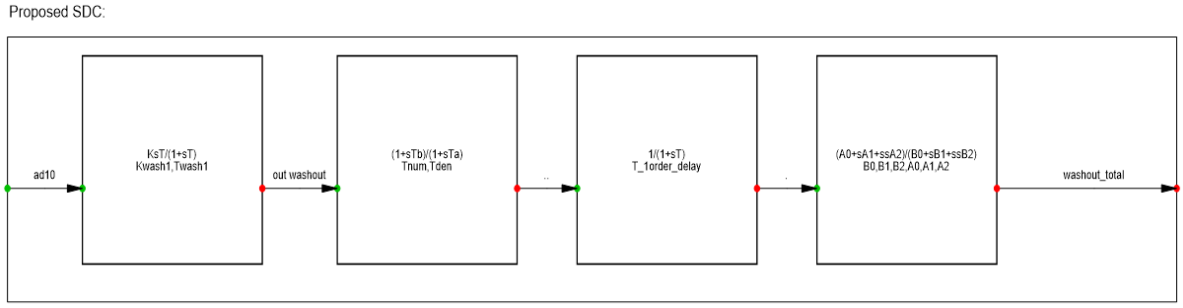

Figure L.4: DigSILENT PowerFactory Supplementary Damping Controller (SDC) - model definition employed

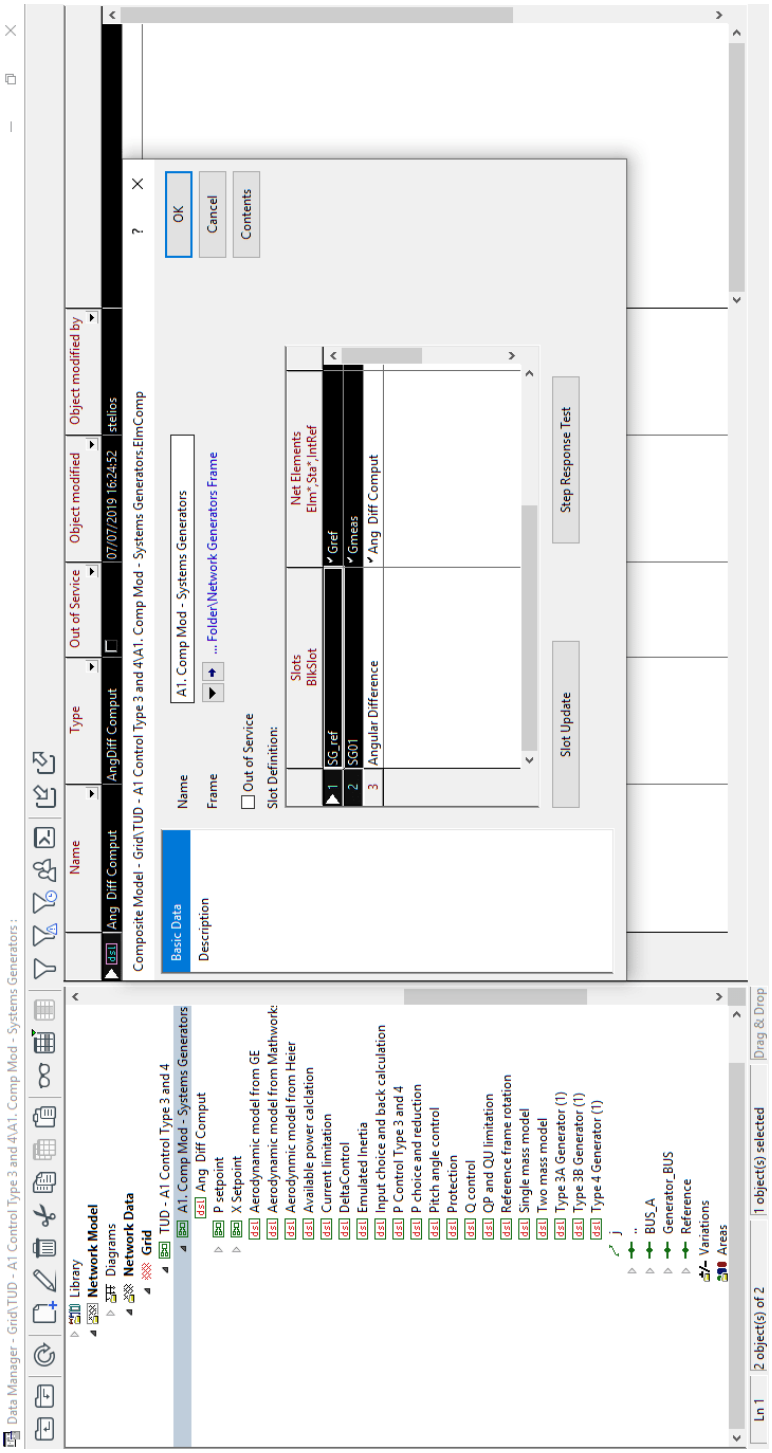

Figure L.5: DigSILENT PowerFactory Synchronous generators' rotor angles selection for feeding specific WG's SDC mechanism

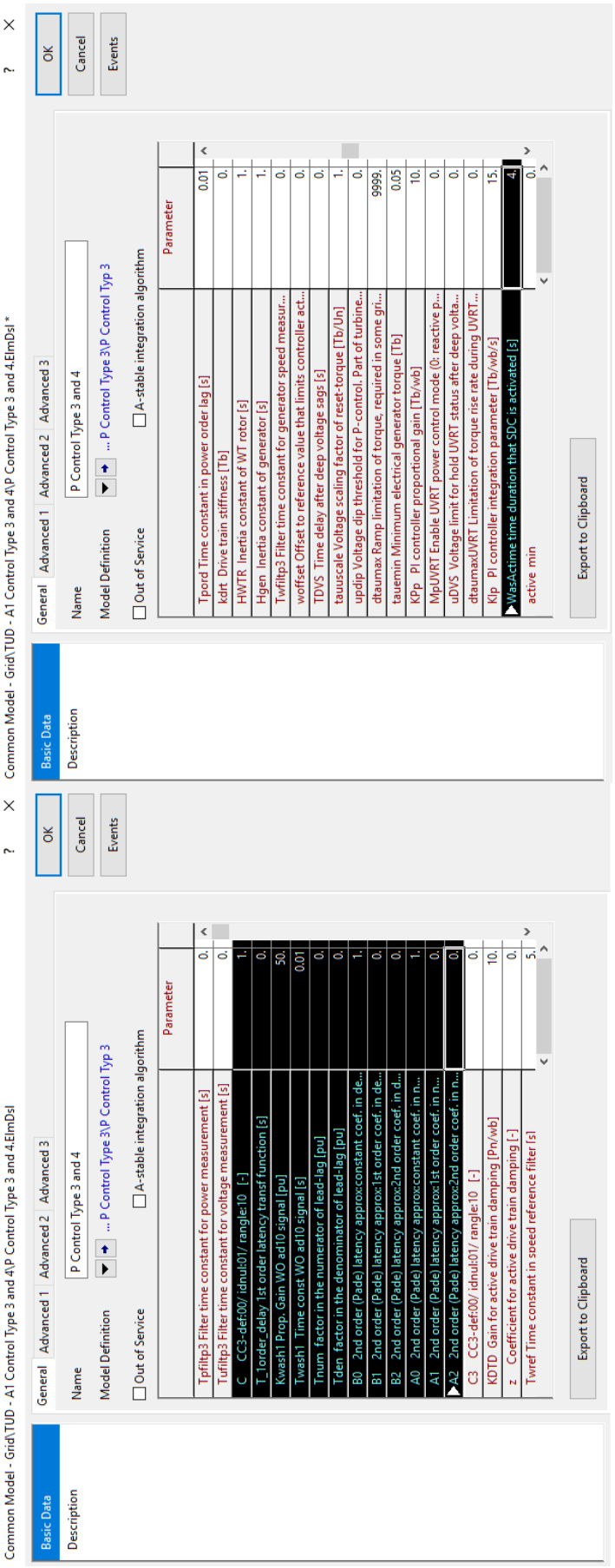

Figure L.6: DigSILENT PowerFactory Supplementary Damping Controller (SDC) related parameters, as located in P-loop common model

L.2. How grid following WG templates can be integrated in different RMS power system grids?

The following steps have to be followed if the user, needs to take the wind generator model (grid following/grid forming technology), proposed in this report, and wants to integrate it into his own power system, for performance testing, or for further modifications of the existing controller:

1. Copy the libraries from the existing RMS power system models (IEEE 9 BUS, SMIB, GB), that are used in the current report, in the RMS system that the user desires. In particular, the user should copy all the elements that are located in the folders: "Equipment Type Library", "User Defined Models" and "Templates" to the new project library of the user. The template consists of the static generator (i.e. wind generator), the controllers that are described in Section 4.1, and also the interface transformer. The template interface is illustrated in Figure L.7. It is mentioned, that the user, can create his own template (with the corresponding composite models and model definitions of the wind generators' controls automatically integrated). To this aim, the user has to select one randomly chosen wind generator in it's own system (i.e. select the whole interface as seen in Figure L.7), then right click and select the option "Define Template".

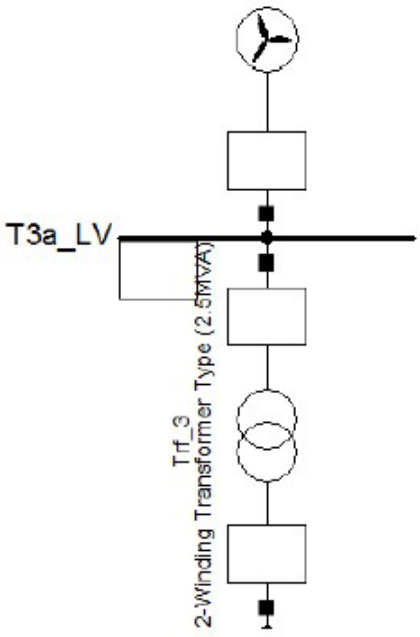

Figure L.7: Wind Generator Template in RMS models

2. The user, then needs to integrate the wind generator and it's inter-phase to his grid model. For this purpose, in the tab related to the Grid configuration, in the Annotation Layers, the user has to select "General Template",as seen in Figure L.8, and then drag the template in the location he wants. When the template is placed in the Grid, it can be observed that the common and composite models of the specific wind generator, are automatically connected.The frequency and voltage measurements, are based on local signals in the template busbar of the wind generator; the terminal busbar is already included in the template, so no extra action is needed by the user, when he uses the same template in different grid locations. This comes, in contrast with the grid forming model, in which remote signals are utilized, therefore additional workload is added for the user. The steps for integrating grid forming models in different locations are described in the following section.

3. Scaling Factors of the static generator and the interface transformer should be adjusted according to the user's needs. The scaling factor is controlled, by choosing properly the number of parallel

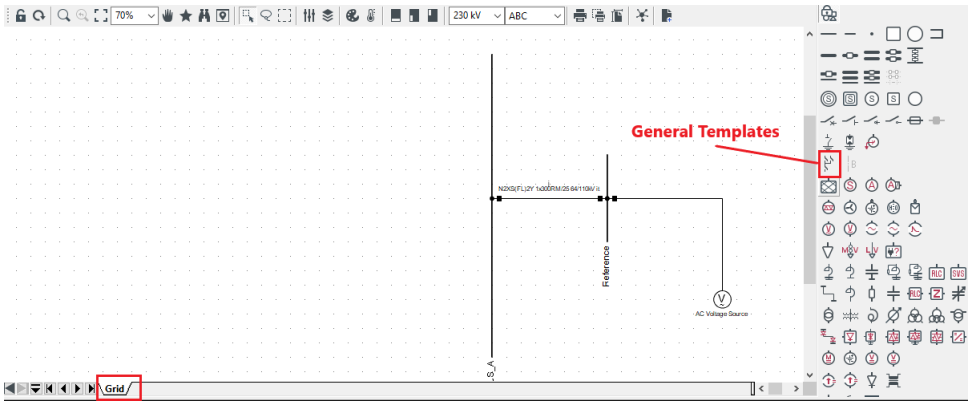

Figure L.8: Placing the template in the Grid

units. Moreover, the secondary winding of the transformer, that is connected to the rest grid, needs to have the same nominal voltage as the voltage of the terminal bus that is connected to.

4. Depending on the template used and in particular depending on the input of the SDC controller, the slots of the composite model of the wind generators should be updated accordingly. For instance, when the speed or the active power of a synchronous generator are used as inputs, the the slot of the wind generators, should be updated with the specific synchronous generator. Additionally, when rotor angle difference between two machines is used, then the two machines should also be defined in the composite model of the machine. Last, if terminal angle of the synchronous machine is used as input, a new PLL block has to be created which will incorporate the specific electrical angle.

5. An external data file, with the wind speeds, the active and reactive power set-points has also to be added. To this aim,the user has to select in the main window Edit →Project Data →Project Settings →External Data and select the path of the directory the external file is located.

Steps 1-4 have to be performed for each single wind generator interface that is placed in the system. Following the described procedure, load flow and RMS simulations can be executed successively.

L.3. How grid forming WG templates can be integrated in different RMS power system grids?

The documentation related to the grid forming model used, can be found in [88], and the purpose of this section is not to analyze the model but to provide some hints on how the user can use the model, to adjust it at his own needs. Steps on how to create the template, how to copy-paste the libraries in any new project and how to place it in the new grid are the same as in the grid following topology and not repeated here. The following additional steps (comparing to the grid following model, previously examined), need to be followed if the grid forming wind generator RMS model, is to be transferred to one other grid system.

1. The wind generator, is modelled not by having several parallel units (in contrast to the grid following configuration), but as a unified aggregated power plant. To this end, the user has to define in the static generator common model the rated MVA of the whole plant, while the number of parallel units is set at one.

2. In the ”DC Busbar and Capacitor” common model and the WG one, the rated active power and the base of the apparent power have to be inserted. These two numbers are the same, assuming that zero reactive power is injected in the pre-fault state of the wind generator. For zero reactive power injection, the user in the load flow tab of the static generator common model, has to select ”Local Controller: Const. Q”) and at the same time insert zero MVARs, in the dispatch of the model.

3. In the ”Full_Scale_Converter” composite frame of the wind generator’s, the measurement point of the voltage terminal of the grid has to be defined in the ”AC Voltage Measurement point” block. This is the remote voltage signal that is used in Figure 4.22.

4. The terminal ac nominal voltage of the wind generator’s model should be also set in the ”Modulation Limitation” common model of the wind generator. This voltage, should be the same with the terminal voltage defined in the static generator’s block.

M

User Manual for MVMO related models

M.1. Python Script for Objective Function Calculation

M.1.1. Step 1: Area Computation Function

The first step is to define the a function that takes as arguments 3 lists (i.e the time, and 2 curves) and returns the area created by these two curves. Two cases are needed, for a correct area computation of the two graphs. As seen in the script followed, there is a difference for the area computation formula between two consecutive points in the starting and ending time step of the PowerFactory Simulation (i.e. 0.01s). The difference in the formula used, depends on whether the two are changing their relative position (cross each other or not). If the two graphs cross each other, then the crossing time instant has to be found, and then the two areas formed (triangles) have to be added. The function with the corresponding comments, are presented as following:

```
def Area_computation(x,y1,y2):
    x = np.array(x) # create array x from list x

    y1=[abs(x) for x in y1]
    y1 = np.array(y1) # create array y1 from list y1
    y2=[abs(x) for x in y2]
    y2 = np.array(y2) # create array y2 from list y2
    z = y1-y2
    dx = x[1:] - x[:-1] #array with elements, the x step integration
    #area calculation. In our case, this is the time step of time
    #integration step size used in PowerFactory simulations

    cross_test = np.sign(z[:-1] * z[1:]) #array with elements -1 whenever
    #the curves y1 and y2 change their relevant position
    #(cross each other)

    #having indetified between which two time steps of PowerFactory
    # the two curves are crossed, now it is needed to identify the
    #exact crossing point. Assumming small time step, solver, then
    #linear approximaiton can be used to find the x insersection point
```

```
    #i.e. Suppose we have z1 and z2 at x1 and x2, then we are solving
    #for x0 such that z = 0:
    # (z2 - z1)/(x2 - x1) = (z0 - z1) / (x0 - x1) = -z1/(x0 - x1)
    # x0 = x1 - (x2 - x1) / (z2 - z1) * z1
    #Therefore dx_intersect= x1-x0 =..
    dx_intersect = - dx / (z[1:] - z[:-1]) * z[:-1]
    areas_pos = abs(z[:-1] + z[1:]) * 0.5 * dx # signs of both z,
    #z[:-1] and z[1:], are same inside the specified time step dx
    areas_neg = 0.5 * dx_intersect * abs(z[:-1]) + 0.5 *
    (dx - dx_intersect) * abs(z[1:]) #signs of both z are different
    #inside the time step dx, so the area will be a summation of
    #the two triangles formed
    areas = np.where(cross_test < 0, areas_neg, areas_pos) #select
    #area formula to use according to the relative position of the 2
    #curves inside the dx time step
    total_area = np.sum(areas)
    return (total_area)
```

M.1.2. Step 2: Function for .csv Creation of the 55 angle-pairs

As shown in Appendix I, 55 SGs pairs are formed, when 11 SGs are operating in the power system. However, PowerFactory, presents only the angles of the SGs with respect to the slack machine. Therefore, there is a need to create a .csv file with time-data of all the 55 pairs. The following function, takes as input the .csv file with the rotor angles of the 10 synchronous machines with respect to the slack machine, (defined in the arguments as 'a') and returns the .csv file (i.e. 'newfilecreated.csv') with the 55 angles. The piece of code is followed.

```
def pairs_creation_csv(a):
    csv_f=csv.reader(a)


    columns = zip(*csv_f)
    my_list=[]   #my_list is a list of lists. The inner lists are
    #the columns (rotor angle of each machine wrt to time)
    for column in columns:
            c=list(column)
            c=c[2:]   #if you see the csv file from powerfactory has
            #the 2 first row without any data.In the lists above we
            #want only numbers
            my_list.append(c)

    #In the following, the lists of time and of the 11 rotor angles
    #wrt slack are formed
    time_list=[float(i) for i in my_list[0]]
    a_list= [float(i) for i in my_list[1]]
    b_list= [float(i) for i in my_list[2]]
    c_list= [float(i) for i in my_list[3]]
    d_list= [float(i) for i in my_list[4]]
    e_list= [float(i) for i in my_list[5]]
    f_list= [float(i) for i in my_list[6]]
    g_list= [float(i) for i in my_list[7]]
    h_list= [float(i) for i in my_list[8]]
    i_list= [float(i) for i in my_list[9]]
    j_list= [float(i) for i in my_list[10]]
    k_list= [float(i) for i in my_list[11]]
```

```
#1-2
ra12=[]
#list that represents the angular difference between
#G1 and G2 in time
ra12=list(np.subtract(a_list,b_list))


#1-3
ra13=[]
#list that represents the angular difference between
#G1 and G3 in time
ra13=list(np.subtract(a_list,c_list))


...

#1-11
ra111=[]
#list that represents the angular difference between
#G1 and G3 in time
ra111=list(np.subtract(a_list,k_list))

#end of first
#####################################################################

#2-3
ra23=[]
ra23=list(np.subtract(b_list,c_list))



#2-4
ra24=[]
ra24=list(np.subtract(b_list,d_list))



#2-11
ra211=[]
ra211=list(np.subtract(b_list,k_list))

#end of second
#####################################################################

# code missing because is repetitive
......
......
......

#####################################################################
#9-10
ra910=[]
ra910=list(np.subtract(i_list,j_list))
```

```
#9-11
ra911=[]
ra911=list(np.subtract(i_list,k_list))


#end of eninth
#################################################################

#10-11
ra1011=[]
ra1011=list(np.subtract(j_list,k_list))


#end of tenth
#################################################################

#create the csv file with the 55 angles lists & time list
rows = zip(time_list,ra12,ra13,ra14,ra15,ra16,ra17,ra18,ra19,
ra110,ra111,ra23,ra24,ra25,ra26,ra27,ra28,ra29,ra210,ra211,
ra34,ra35,ra36,ra37,ra38,ra39,ra310,ra311,ra45,ra46,ra47,
ra48,ra49,ra410,ra411,ra56,ra57,ra58,ra59,ra510,ra511,ra67,
ra68,ra69,ra610,ra611,ra78,ra79,ra710,ra711,ra89,ra810,ra811,
ra910,ra911,ra1011)
with open('newfilecreated.csv', 'w', newline='') as myfile:
    wr = csv.writer(myfile)
    rcount = 0
    for row in time_list:
        wr.writerow((time[rcount], ra12[rcount],ra13[rcount],
        ra14[rcount],ra15[rcount],ra16[rcount],ra17[rcount],
        ra18[rcount],ra19[rcount],ra110[rcount],ra111[rcount],
        ra23[rcount],ra24[rcount],ra25[rcount],ra26[rcount],
        ra27[rcount],ra28[rcount],ra29[rcount],ra210[rcount],
        ra211[rcount],ra34[rcount],ra35[rcount],ra36[rcount],
        ra37[rcount],ra38[rcount],ra39[rcount],ra310[rcount],
        ra311[rcount],ra45[rcount],ra46[rcount],ra47[rcount],
        ra48[rcount],ra49[rcount],ra410[rcount],ra411[rcount],
        ra56[rcount],ra57[rcount],ra58[rcount],ra59[rcount],
        ra510[rcount],ra511[rcount],ra67[rcount],ra68[rcount],
        ra69[rcount],ra610[rcount],ra611[rcount],ra78[rcount],
        ra79[rcount],ra710[rcount],ra711[rcount],ra89[rcount],
        ra810[rcount],ra811[rcount],ra910[rcount],ra911[rcount],
        ra1011[rcount]))
        rcount = rcount + 1
myfile.close()
```

M.1.3. Step 3: Function for Computation of 55 angle Areas & their Summation

This function uses the generic function described in subsection M.1.1, and as input, receives the .csv file of the 55 rotor angle pairs created from the function described in subsection M.1.2. It returns a tuple with a list of the 55 areas derived from the comparison of the 55 rotor angles curves from their initial angle values. Moreover, the total area which is the summation of the 55 areas computed, is returned in the tuple. Part of the code follows.:

```
def Total_Area_computation_for_all_SG_machines(a):

    csv_f=csv.reader(a)

    columns = zip(*csv_f)
    my_list=[]
    for column in columns:
        c=list(column)
        my_list.append(c)


    #In the following, the lists of time and of the 55 rotor angles
    # are formed
    time_list=[float(i) for i in my_list[0]]
    ra12_list= [float(i) for i in my_list[1]]
    ra13_list= [float(i) for i in my_list[2]]
    ra14_list= [float(i) for i in my_list[3]]
    ra15_list= [float(i) for i in my_list[4]]
    ra16_list= [float(i) for i in my_list[5]]
    ra17_list= [float(i) for i in my_list[6]]
    ra18_list= [float(i) for i in my_list[7]]
    ra19_list= [float(i) for i in my_list[8]]
    ra110_list= [float(i) for i in my_list[9]]
    ra111_list= [float(i) for i in my_list[10]]

    ra23_list= [float(i) for i in my_list[11]]
    ra24_list= [float(i) for i in my_list[12]]
    .....
    .....
    .....
    ra211_list= [float(i) for i in my_list[19]]

    .....
    .....
    .....
    ra89_list= [float(i) for i in my_list[50]]
    ra810_list= [float(i) for i in my_list[51]]
    ra811_list= [float(i) for i in my_list[52]]

    ra910_list= [float(i) for i in my_list[53]]
    ra911_list= [float(i) for i in my_list[54]]

    ra1011_list= [float(i) for i in my_list[55]]


    #In the following, the 55 lists of their initial angle values
    #are formed. The size of the new lists equals the size of the
    #initial angle lists that they are created from.
    reference_list0=[ra12_list[0]]*len(time_list)
    .....
    .....
    .....
    reference_list50=[ra810_list[0]]*len(time_list)
    reference_list51=[ra811_list[0]]*len(time_list)
    reference_list52=[ra910_list[0]]*len(time_list)
    reference_list53=[ra911_list[0]]*len(time_list)
```

```
reference_list54=[ra1011_list[0]]*len(time_list)


#In the following, find the 55 areas of the 55 angles
#from their initial values in a specific time - window
#store the 55 areas in the list "areas_list"
areas_list=[]
areas_list.append(Area_computation(time_list,ra12_list,
                                   reference_list0))
areas_list.append(Area_computation(time_list,ra13_list,
                                    reference_list1))
areas_list.append(Area_computation(time_list,ra14_list,
                                    reference_list2))
.....
.....
.....
areas_list.append(Area_computation(time_list,ra1011_list,
                                    reference_list54))


#In the following the total (aggragated) area of the
#55 areas, is computed
total_area_for_all_machines=sum(areas_list)
#the function returns a tuple with elemets a list of the
#55 individual areas, as well as the number of their
#summation
return (areas_list,total_area_for_all_machines)
```

M.1.4. Step 4: Main Code for the Objective Function Computation

In this section, the main part of the python script that controls the Power-Factory model, calls the aforementioned functions and communicates with the Matlab code (in which the MVMO algorithm is built), is displayed. Before analyzing the code, it is better to describe how the communication between Python and Matlab is achieved. For communication purposes between the two different tools, specific .csv / .txt files are used.

In particular, the output files from Python, and equivalently, the input files to MATLAB (MVMO), are:

1. *"OFvalue_to_Matlab_Iteration_i.txt"*: This is a file not for communication with Matlab, but for the user to interpret the results. This file has the areas of each study case for all the machines and also the summation of the study areas (which is the Objective Function VALUE). In other words, if three faults are considered per MVMO iteration (e.g. the most critical ones), then this file has three numbers (each number represents the total area obtained from the 55 pairs for the specific fault out of the three performed) plus the summation of this 3 numbers which is the final Objective Function value that is wanted to be minimized. Moreover, the number of such .txt files will be the same as the number of iterations.

2. *"Flag_to_Matlab.txt"*: This file initially, before the MVMO algorithm is executed, has "0" value. Then, when Python has computed the Objective Function value, this flag goes to "1", so as MATLAB will understand that Python has computed it. Then, the flag is set (after some seconds to avoid conflicts with MATLAB - note that any .txt can not be read from MATLAB and writen from Python at the same time) to "0" again for the next Python/PowerFactory iteration, with the new solution vectors that MVMO provides.

3. *"For_user_area_of_each_generator_per_fault&iteration.txt"*: This is a .txt file (only for the user- is not exchanged between Matlab and Python). The user can see at the end of the

MVMO procedure, what is the area of each single machine, for each iteration and for each one of the study cases (i.e.different study case means different location examined fault). For instance, the user can see the area of SG2 w.r.t SG3 in the second MVMO iteration and when the fault is happening at Line 6-9 in the GB system.

4. *"OFvalue.txt"*: This is the .txt that will be given to Matlab MVMO when python will finish all the study cases/faults for the current iteration. For the next MVMO iteration the same .txt file will be sent to MATLAB with the new updated OF value. It can be understood, that this file dynamically will have the same value of the last number that is written (for the user needs) in file *"OFvalue_to_Matlab_Iteration_i.txt"*.

Additionally, the output files from MATLAB (MVMO), and equivalently, the input files to Python, are:

1. *"Flag_from_Matlab.txt"*: This file is generated from Matlab MVMO. Initially, before the MVMO algorithm ignition, this flag has value of "1". When MATLAB has computed a new offspring, then this flag becomes "0" and Python/PowerFactory can start performing the dynamic simulations so as to compute the new Objective Function value.

2. *"offspring_vector.csv"*: This is the vector sent by MVMO algorithm, with the solution vector after each MATLAB iteration is finished. The solution vector, comprises washout gains and time constants, as well as lead-lag time constants.

The previous files, and the way they are created/processed are illustrated in the following Python code:

```
#path address
Pathtowrite = r'D:\spapadakis\Desktop\mvmo_algorithm'

#Calling powerfactory app object and the folders of the
#active project
app = powerfactory.GetApplication()
FolderWhereStudyCasesAreSaved = app.GetProjectFolder('study')
AllStudyCasesInProject = FolderWhereStudyCasesAreSaved.
                         GetContents('*.IntCase',1)

Simulation_Time =10 #simulation time window
iteration=1 #iteration of MVMO algorithm


#this is the initial number of the study case for the specific
#MVMO iteration. If 3 faults are done per iteration, the maximum
#value that variable "counter" will take is 3.
counter=1
area_per_iteration_for_three_faults=[]

maximum_MVMO_iteration=100 #



while iteration<=maximum_MVMO_iteration:
#we need to wait until the mvmo algorithm in matlab will compute
#the offsprings and will send the vector x.
# when matlab will finish the computation and give the x vector
#it will make the "flag_from_Matlab.txt " at "1"; it sais to
#PowerFactory:"HERE ARE THE NEW X VALUES,YOU CAN NOW RUN THE
```

```
#DUNAMIC SIMULATION"

# In other words we have a delay, so as to wait for matlab to compute
#the x vector and update the :flag_from_Matlab.txt" and then, after
#Matlab finishes processing this flag, we can start #reading the .txt
#file from Python
    time=0
    while time<150000:
        time=time+1

    #read the .txt file and wait until the flag from matlab is "1"
    file4 = open("Flag_from_Matlab.txt","r")
    flag=file4.read()
    flag2=int(flag)
    file4.close
    while flag2!=1:
        file4 = open("Flag_from_Matlab.txt","r")
        app.PrintPlain('Waiting to read Flag=1 coming from MatLab')
        flag=file4.read()
        flag2=int(flag)
        file4.close
    app.PrintPlain('Finally we can start')

#In this point Matlab is responsibe to do the Flag in the
#"Flag_from_Matlab.txt", zero again



#We are going to set the gains and time constants of the washout
#filters and lead-lags To this end, we are going to read
#"offspring_vector.csv" which is created by matlab MVMO after each
# iteration.


    #load the DSL elements of the active project
    DSLs_List = app.GetCalcRelevantObjects("*.ElmDsl")

    #read the .csv file created by MATLAB MVMO
    f = open('offspring_vector.csv')


#this is a file that we create only for the user needs,
#and is not  needed for the communication with Matlab.
#In this file we store all the times of the day, that we
#update the PowerFactory Models with the new x values, coming
#from MATLAB. In general, this file was created for verifica-
#tion reason, that Python reads the updated new offsprings from
#The user can see the time instant(e.g.t1) that the solution vector
#is created by matlab, and the time (e.g.t2) that Python updates
#PowerFactory parameters. It can be seen, that (t2)>(t1), so the
#communication between Matlab & Python is correct

    now = datetime.datetime.now()
    file1 = open("timespythonreadsnewx.txt","a")
    file1.write(str(now))
    file1.write('\n')
```

```
file1.close()

csv_f = csv.reader(f)
a = []
for row in csv_f:
    #a is a list but it's a list of lists with one only element
    a.append(row[:])
c=a[0] # c is a list of stings
d=[float(i) for i in c] #d is a list of float numbers

#Update the parameters for the wind generators in zones
#3,5,10,13,15,16,19,20
#Its stated that each zone has several WGs (A,B,C,e.t.c)
for Element in DSLs_List:

    if Element.loc_name[:27] == '3A_ XP Control Type 3 and 4':
        SpecialCarrier=Element.params
        SpecialCarrier[6]=d[0] #Kwash
        SpecialCarrier[7]=d[1] #Twash
        SpecialCarrier[4]=d[2] #T(lead-lag)numerator
        SpecialCarrier[5]=d[3] #T(lead-lag)denominator
        Element.params=SpecialCarrier


    if Element.loc_name[:27] == '3B_ XP Control Type 3 and 4':
        SpecialCarrier=Element.params
        SpecialCarrier[6]=d[0]
        SpecialCarrier[7]=d[1]
        SpecialCarrier[4]=d[2]
        SpecialCarrier[5]=d[3]
        Element.params=SpecialCarrier


    if Element.loc_name[:27] == '5A_ XP Control Type 3 and 4':
        SpecialCarrier=Element.params
        SpecialCarrier[6]=d[4]
        SpecialCarrier[7]=d[5]
        SpecialCarrier[4]=d[6]
        SpecialCarrier[5]=d[7]
        Element.params=SpecialCarrier

    if Element.loc_name[:27] == '5B_ XP Control Type 3 and 4':
        SpecialCarrier=Element.params
        SpecialCarrier[6]=d[4]
        SpecialCarrier[7]=d[5]
        SpecialCarrier[4]=d[6]
        SpecialCarrier[5]=d[7]
        Element.params=SpecialCarrier

    if Element.loc_name[:27] == '5C_ XP Control Type 3 and 4':
        SpecialCarrier=Element.params
        SpecialCarrier[6]=d[4]
        SpecialCarrier[7]=d[5]
        SpecialCarrier[4]=d[6]
        SpecialCarrier[5]=d[7]
        Element.params=SpecialCarrier
```

```
        if Element.loc_name[:27] == '5D_ XP Control Type 3 and 4':
            SpecialCarrier=Element.params
            SpecialCarrier[6]=d[4]
            SpecialCarrier[7]=d[5]
            SpecialCarrier[4]=d[6]
            SpecialCarrier[5]=d[7]
            Element.params=SpecialCarrier

        .....
        .....
        Same for 10A,10B,10C,10D,10E,10F
        Same for 13A,13B,13C
        Same for 15A,15B
        Same for 16A,16B,16C,16D
        Same for 19A,19B,19C,19D,19E,19F,19G
        Same for 20A,20B,20C,20D,20E,20F,20G,20H
        .....
        .....

        if Element.loc_name[:28] == '20H_ XP Control Type 3 and 4':
            SpecialCarrier=Element.params
            SpecialCarrier[6]=d[28]
            SpecialCarrier[7]=d[29]
            SpecialCarrier[4]=d[30]
            SpecialCarrier[5]=d[31]
            Element.params=SpecialCarrier



#Having set the parameters, we are ready to make the faults
#in PowerFactory


#the study-cases are the different faults applied in PowerFactory
    for StudyCase in AllStudyCasesInProject:

        StudyCase.Activate()
        comSim = app.GetFromStudyCase("ComSim")
        comSim.tstop = Simulation_Time
        NameFault = StudyCase.loc_name[0:12]
        app.PrintPlain(NameFault)
        comSim.Execute()
        comRes = app.GetFromStudyCase("ComRes")#csv window in PF
        Case = app.GetActiveStudyCase()
        res = Case.GetContents('*.ElmRes')[0]

        ObjG03_Scotland = app.GetCalcRelevantObjects('G03.ElmSym')[0]
        ObjG05_Scotland = app.GetCalcRelevantObjects('G05.ElmSym')[0]
        ObjG07_Scotland = app.GetCalcRelevantObjects('G07.ElmSym')[0]
        ObjG08_Scotland = app.GetCalcRelevantObjects('G08.ElmSym')[0]
        ObjG10_NEngland = app.GetCalcRelevantObjects('G10.ElmSym')[0]
        ObjG11_NEngland = app.GetCalcRelevantObjects('G11.ElmSym')[0]
        ObjG13_WEngland = app.GetCalcRelevantObjects('G13.ElmSym')[0]
        ObjG15_WEngland = app.GetCalcRelevantObjects('G15.ElmSym')[0]
```

```
        ObjG16_NEngland = app.GetCalcRelevantObjects('G16.ElmSym')[0]
        ObjG19_EEngland = app.GetCalcRelevantObjects('G19.ElmSym')[0]
        ObjG20_EEngland = app.GetCalcRelevantObjects('G20.ElmSym')[0]

        comRes.pResult = res
        comRes.iopt_exp = 6 # to export as csv
        comRes.f_name = Pathtowrite + '\\' + NameFault +'iteration_'
                        + str(iteration) + '.csv'
        comRes.iopt_sep = 1 # to use the system seperator
        comRes.iopt_honly = 0 # to export data and not only the header
        comRes.iopt_csel = 1 # export only selected variables
        comRes.iopt_tsel = 0 # All time registration active


        resObj = [None, None, None, None, None, None, None, None,
                  None, None, None]
        resElms = [res,ObjG03_Scotland,ObjG05_Scotland,ObjG07_Scotland,
                   ObjG08_Scotland,ObjG10_NEngland,ObjG11_NEngland,
                   ObjG13_WEngland,ObjG15_WEngland,ObjG16_NEngland,
                   ObjG19_EEngland,ObjG20_EEngland]
        resVars = ["b:tnow","c:firel","c:firel","c:firel","c:firel",
                   "c:firel","c:firel","c:firel","c:firel","c:firel",
                   "c:firel","c:firel"]

        comRes.resultobj = resObj# Export selected
        comRes.element = resElms
        comRes.variable = resVars
        comRes.Execute()

#In the "Namefault""iteration".csv file, now we have the 11 w.r.t time
#angles of the machines, with respect to the slack

#But, I am not giving this csv file to the
#"Total_Area_computation_for_all_SG_machines" function directly,
#because this .csv file, as created by PowerFactory, has some headers
#in the first 2 lines. What I am doing is that I take out the two
#first rows of the .csv file, then I take the columns of the csv file
#in lists and I am writing againg the same csv file, without
#the headers

        b = open(NameFault +'iteration_'+ str(iteration) + '.csv',
                 errors='ignore')
        csv_f=csv.reader(b)
        columns = zip(*csv_f)
        my_list=[]
        for column in columns:
                c=list(column)
                c=c[2:]  #get rid of the first 2 rows in each column
                my_list.append(c)

        time=[float(i) for i in my_list[0]]
        a_list= [float(i) for i in my_list[1]]
        b_list= [float(i) for i in my_list[2]]
        c_list= [float(i) for i in my_list[3]]
        d_list= [float(i) for i in my_list[4]]
        e_list= [float(i) for i in my_list[5]]
```

```
        f_list= [float(i) for i in my_list[6]]
        g_list= [float(i) for i in my_list[7]]
        h_list= [float(i) for i in my_list[8]]
        i_list= [float(i) for i in my_list[9]]
        j_list= [float(i) for i in my_list[10]]
        k_list= [float(i) for i in my_list[11]]



        rows = zip(time,a_list,b_list,c_list,d_list,e_list,f_list,
                   g_list,h_list,i_list,j_list,k_list)
        with open(NameFault +'iteration_'+ str(iteration) + '.csv',
                  'w', newline='') as myfile:
            wr = csv.writer(myfile)
            rcount = 0
            for row in time:
                wr.writerow((time[rcount],a_list[rcount],b_list[rcount],
                        c_list[rcount],d_list[rcount],e_list[rcount],
                        f_list[rcount],g_list[rcount],h_list[rcount],
                        i_list[rcount], j_list[rcount], k_list[rcount]))
                rcount = rcount + 1
            myfile.close()

#as descibed, in this point, the csv file without the headers is ready

#call "pairs_creation_csv" for creation of the 55 angles
        b = open(NameFault +'iteration_'+ str(iteration) + '.csv',
                 errors='ignore')
        pairs_creation_csv(b)
        b.close()


        #open .csv file created with the 55 angles and process it
        q = open('newfilecreated.csv',errors='ignore')

        #this is a list with the 55 areas for the current study case
        #and for the current iteration
        new_list_per_fault_per_iteration=
        Total_Area_computation_for_all_SG_machines(q)[0]

        #and in the first index of the list we insert also the iteration
        #number that the MVMO algorithm runs
        new_list_per_fault_per_iteration.insert(0, iteration)

#for only the first time of the first iteration during the
#MVMO algorithm duration run, we need to store the list but
#before, we need to create the headers

        if (counter==1 and iteration==1):
            file3 = open("For_user_area_of_each_generator_per_
                         fault&iteration.txt","w")
            file3.write("[i,SG12 RA area from nom,SG13 RA area from nom,
                         ,..,SG1011 RA area from nom]")
            file3.write('\n')
            file3.write(str(new_list_per_fault_per_iteration))
            file3.write('\n')
```

```
            file3.close()
#for the rest study cases of all the iterations we need to update only
#the list in the txt file; not the headers
        else:
            file3 = open("For_user_area_of_each_generator_per_
                        fault&iteration.txt","a")
            file3.write(str(new_list_per_fault_per_iteration))
            file3.write('\n')
            file3.close()
        q.close()



        q = open('newfilecreated.csv',errors='ignore')
 #for the current study case find the total area numbers
 #of all the SGs pairs
        total_area=Total_Area_computation_for_all_SG_machines(q)[1]
#and place this number in the list "area_per_iteration_for_three_faults"
        area_per_iteration_for_three_faults.append(total_area)
        file1 = open("OFvalue_to_Matlab_Iteration_"+
                     str(iteration)+".txt","a")
#for the user needs, write the total area of the specific study case
#and the specific iteration in the .txt file as seen above.
        file1.write(str(total_area))
        file1.write('\n')
        file1.close()
        q.close()

#If we consider 3 faults per MVMO iteration, then %3 is needed below
#If we consider 1 fault per MVMO iteration, then %1 is needed below
#This means, that only when all the study cases are tested per iter
#then the final objective function (which is the summation of the areas
#found for each study case), will be written in the
#"OFvalue_to_Matlab_Iteration_iteration".txt file
        if counter%3==0: #

            objective_function=sum(area_per_iteration_for_three_faults)

#this is a .txt file that we create only for the user,
#no for MVMO (Matlab) needed
            file1 = open("OFvalue_to_Matlab_Iteration_"+str(iteration)+
                        ".txt","a")
            file1.write(str(objective_function))
            file1.write('\n')
            file1.close()

#THIS IS A FLAG THAT GOES TO MVMO. IT SAIS:
#"HEY MATLAB, I HAVE THE OF COMPUTED; TAKE THE RESULT AND PROCESS
#IT TO FIND A NEW SOLUTION VECTOR
            file2.write(str(1))
            file2 = open("Flag_to_Matlab.txt","w")
            file2.close()
```

```
#this is the file that the MVMO algorithm will finally take with the
#objective function after the study cases are finished for the current
#MVMO iteration
            file5 = open("OFvalue.txt","w")
            file5.write('\n')
            file5.close()


#Python SAIS: "HEY MATLAB, YOU TOOK YOUR OF VALUE THAT YOU NEEDED.
#OUR COMMUNICATION WILL TERMINATE NOW

            file2 = open("Flag_to_Matlab.txt","w")
            file2.write(str(0))
            file2.close()



#we have to empty the list for the next iteration
            area_per_iteration_for_three_faults=[]

#after the final study case tested for any MVMO iteration
#the counter should be 0
            counter=0

#after the final study case tested for any MVMO iteration
#the MVMO iteration number, should increase by one
            iteration=iteration+1

#counter is increased after each study case is tested.
#For the first fault tested in any MVMO iteration,
#the counter has value one
#For the second fault (if) tested in any MVMO iteration,
#the counter has value two
#For the third fault (if) tested in any MVMO iteration,
#the counter has value three

        counter=counter+1
```

M.2. Matlab MVMO Script- Basic Points

In the following three subsections, the reader can see how the communication with Python is set from the side of Matlab tool. It is mentioned that focus is given mainly in the integration between Python and Matlab, therefore, the main part of the MVMO optimization is neglected.

M.2.1. Main Code

```
% ================================================================
%                          MVMO- MAIN
% ================================================================
%

close all
clear all
clc
```

```
%=========================================================================
%                        Setting global variables and Flags
%=========================================================================
global ps of_val opt_var
global xvectorstoredinTable


%=========================================================================
%                              Define MVO parameters
%=========================================================================
%For the 75% GB share in total 8 WGs appear in zones
%(3,5,10,13,15,16,19,20). The variables associated to each one
%of the WG are the washout gain & time constant and the lead-lag
%gain and time constants. So in total the optimization problem is
%32 dimensions problem
ps.D=32;

%Min and max limits of control variables
%the variables are in the form of:
%[washout gain, washout time constant, lead-lag gain,
%lead-lag time constant]

%as seen the time constants for the washout filter and the
%lead-lag filter are not allowed to be zero
low_limits = [0,0.003,0,0.01];
b=repmat(low_limits',8,1) % have the previous vector 8 times;
ps.x_min=b.' %row vector

upper_limits = [200,10,0.5,1.5]; %row vector
a=repmat(upper_limits',8,1) % have the previous vector 8 times;
ps.x_max=a.' %row vector

algorithm_name='mvmo_ceno2018';
algorithm_hd=str2func(algorithm_name); %Function hanlde of MVMO
of_apg_hd=str2func('test_func2'); %Function hanlde of m-file for
%obj function calculation
args{1}=0; %Print in Matlab command window (1 means yes, 0 means No)
args{2}=1; %Printing step; 1 means printing each iteration results
args{3}=100;%Maximum function evaluations

%=========================================================================
%                        Performing MVMO-based optimization
%=========================================================================

%Recorded values of best Objective Function so far
of_val=zeros(args{3},1);
%Corresponding best optimization variable values
%that lead to minimum Objective Function values
opt_var=zeros(args{3},ps.D);

%=========================================================================
%                        MVMO function call
%=========================================================================
op_runs=1;%In case we want to run the whole optimization several times
%(i.e. number of optimization runs)
```

```
for iii=1:op_runs
    feval(algorithm_hd,of_apg_hd,iii,args);
end

%=========================================================================
%                      Visualization and Storage of Results
%=========================================================================
figure (1)
plot(of_val);
xlabel('No. of objective function evaluations');
ylabel('Fitness value');


figure(2)
for i=1:ps.D
    plot(opt_var(:,i));
    hold on
end

%Save results in .mat file
Results_mvmo_SDC_tuning.of_val=of_val;
Results_mvmo_SDC_tuning.opt_var=opt_var;
Results_mvmo_SDC_tuning.xvectorstoredinTable=xvectorstoredinTable;
save Results_mvmo_SDC_tuning
```

M.2.2. MVMO algorithm - (Function)

```
function mvmo_ceno2018(fhd,iii,args)

        global proc
    global ps
    global parameter
    global x_normalized_save
    global DD
    global ipp
    global xvectorstoredinTable
    proc.i_eval=0;
    proc.finish=0;
    D=ps.D;
    DD=1:D;
    proc.n_eval=args{3};
    n_eval =proc.n_eval;

%%%%%%%%%%%%%%%%%%%%%%%%%%%%%%%%%%%%%%%%%%%%%%%%%%%%%%%%%%%%%%%%%%%%%%%%%%%%
    parameter.n_par=1;   %Number of particles
    parameter.n_tosave=5 ; % Archive size
    parameter.fs_factor_start=1 % Initial fs-factor
    parameter.fs_factor_end=1 % Final fs-factor
    % initial number of variables selected for mutation ;
    parameter.n_random_ini =round(ps.D/2.0) ;
    % final number of variables selected for mutation
    parameter.n_random_last=round(ps.D/1.0 ) ;


    %%------ Create initial random population ------
```

```
    for iijj=1:parameter.n_par %Start initialization: x_normalized
          for jjkk=DD
              xx(iijj,jjkk)=ps.x_min(jjkk) + rand(1)*(ps.x_max(jjkk)-
              ps.x_min(jjkk));

          end
        x_norm(iijj,:)=(xx(iijj,:)-ps.x_min)./parameter.scaling;

    end % End initialization
    x_normalized_save=x_norm;

    .....
    .....

    %write this file with the denormalized random x values
    %coming for the first MVMO iteration.
    %In the meantime python is in a wait loop so no conflicts
    %exist with the processing of the csv file
    xfile= fopen('offspring_vector.csv','w');
    csvwrite('offspring_vector.csv',xx(1,:));
    fclose(xfile);

    .......
    .......

  while 1

      %read the flag file coming from python. When this flag
      %is one,then it means that python has computed the Objective
      %Function and matlab is ready for taking the .txt file with
      %the Objective Function.Otherwise we have to wait until this
      %flag will be one.

            time=0
            while time<600000
                time=time+1
            end


            file_to_Python= fopen('Flag_from_Matlab.txt','w');
            csvwrite('Flag_from_Matlab.txt',0);
            fclose(file_to_Python);

            file_flag_from_python = fopen('Flag_to_Matlab.txt','r');
            formatSpec = '%d'
            flag_to_matlab=fscanf(file_flag_from_python,formatSpec)
            while flag_to_matlab ==0
                fclose(file_flag_from_python);
                disp('Python has not computed yet the OF')
                file_flag_from_python = fopen('Flag_to_Matlab.txt','r');
                flag_to_matlab=fscanf(file_flag_from_python,formatSpec)
            end
            fclose(file_flag_from_python);
            disp('Continue: Python has computed the OF')
```

```
        %give some time for python to store the OF to
        %a .txt file before matlab will process it in test_func2.m
        time=0
        while time<20000
            time=time+1
        end

        .......
        ........
        ........

        %this is a denormalized solution vector
        x_normalized(ipp,:) = ps.x_min+parameter.scaling.*
        x_normalized(ipp,:);

        %calling fitness evaluation function
        [ffx,~,~,~]=feval(fhd,iii,args,x_normalized (ipp,:));

        %this is a normalized solution vector
        x_normalized(ipp,:) = (x_normalized(ipp,:)-ps.x_min)./
        parameter.scaling;


        %terminate when iterations reach the
        %predefined by the user number
        if proc.finish
            return;
        end

       .....
       .....#code related to mutation of solution vector
       .....#storing & sorting FitnessEvaluation in achieve


    %this is a new normalized vector of D elements
    stored_denormalized_offspring=x_normalized(ipp,:)

    %this is a new denormalized vector of D elements
    stored_denormalized_offspring = ps.x_min+parameter.scaling.*
    stored_denormalized_offspring;


    %store the denormalized offspring
    xfile= fopen('offspring_vector.csv','w');
    csvwrite('offspring_vector.csv',stored_denormalized_offspring);
    fclose(xfile);


    %flag from matlab set at 1, so as Python
    %to read the offspring file
    file_to_Python= fopen('Flag_from_Matlab.txt','w');
    csvwrite('Flag_from_Matlab.txt',1);
    fclose(file_to_Python);

end %End while loop
```

M.2.3. Function Evaluations Minimization - (Function)

```
function [f,g,g_sum,xn_out] = test_func2(iii,args,xx_yy)

global of_val opt_var
global proc
global xvectorstoredinTable
global ps

%store the first (denormalized) offspring as randomly seleceted
if proc.i_eval==0
    xvectorstoredinTable=zeros(args{3},ps.D)
end

%increment of the iteration
proc.i_eval=proc.i_eval+1;

%store the denormalized offsping of each iteration that
%created the OF value and will be given in the mvmo algorithm
%to store them in the achieve and find the new offspring
xvectorstoredinTable(proc.i_eval,:)=xx_yy

%%%%%%%%%%%%%%%%%%%%%%%%%%%%%%%%%%%%%%%%%%%%%%%%%%%%%%%%%%%%%%%%%%%%%%%%%%%%%%%
%the objective function value from the txt file is read so as to
%form the fithess evaluation value f
fileID = fopen('OFvalue.txt','r');
formatSpec = '%f';
sum=fscanf(fileID,formatSpec)
fclose(fileID);
f=sum; % fitness evaluation is the same as the OF
g=0; % No constraints considered
g_sum %

if proc.i_eval>=args{3} %Maximum function evaluations reached
    proc.finish=1;
end


%it is a minimization problem, so store for each iteration,
%the minimum function evaluation achieved so far with the solution
%vector as well
if proc.i_eval==1
    of_val(proc.i_eval)=f;
    opt_var (proc.i_eval,:)=xn_out;
else
    if f<of_val(proc.i_eval-1)
        of_val(proc.i_eval)=f;
        opt_var (proc.i_eval,:)=xn_out;
    else
        of_val(proc.i_eval)=of_val(proc.i_eval-1);
        opt_var (proc.i_eval,:)=opt_var (proc.i_eval-1,:);
    end
end

%print in the command window the number of
```

```
if ((proc.i_eval==1)||(mod(proc.i_eval,args{2})==0))& args{1}
    fprintf('Trial: %5d,    i_eval: %7d,    f_best: %12.7E \n',...
        iii,proc.i_eval,of_val(proc.i_eval));
end
end
```

M.3. How to run the MVMO simulations

M.3.1. Actions for performing MVMO simulations

The user before starting performing the MVMO algorithm, has first to import the numpy and date time packages, in the Python version that PowerFactory utilizes. The packages can easily be imported with the aid of the command prompt, by typing the commands ”pip install numpy” and ”pip install DateTime”. After importing the packages the procedure can start as seen below.

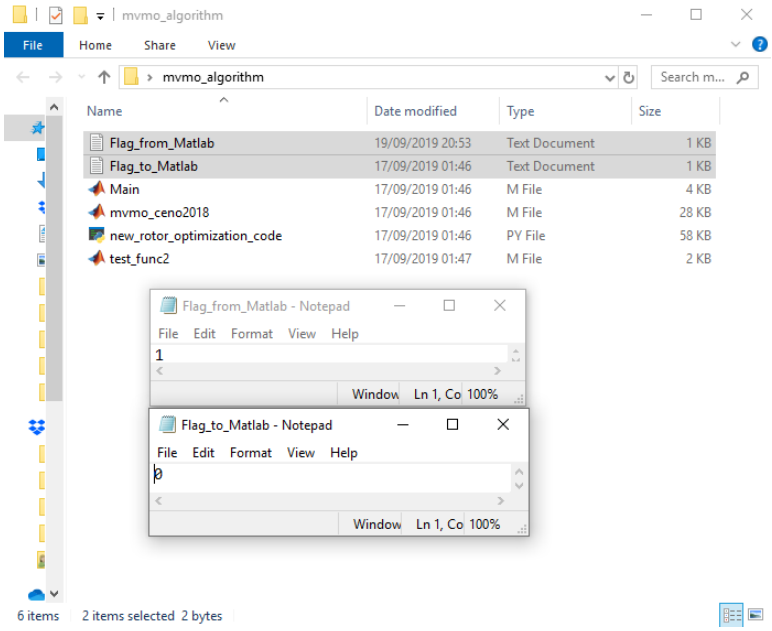

Figure M.1: Initial Files needed for MVMO execution Initial Flags' Values for Communication between Matlab and Python

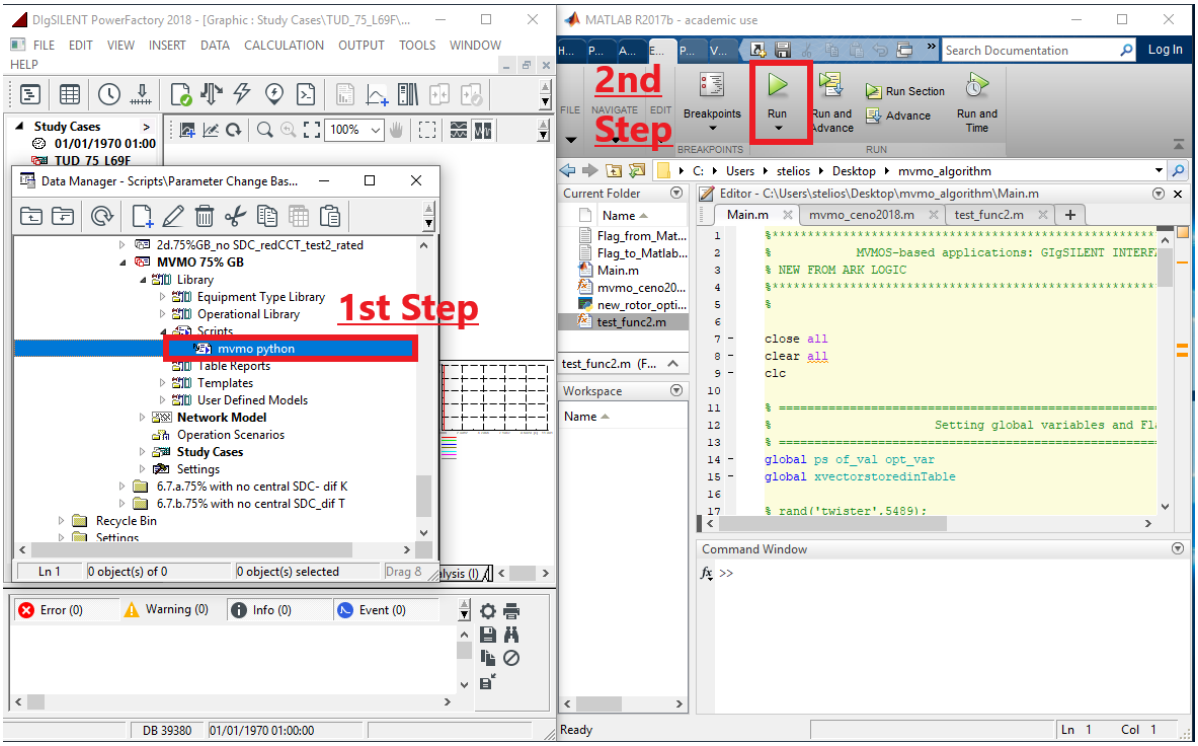

Figure M.2: Steps for MVMO execution. First Python script should be executed and right after Matlab script should start. The two tools are running at the same time

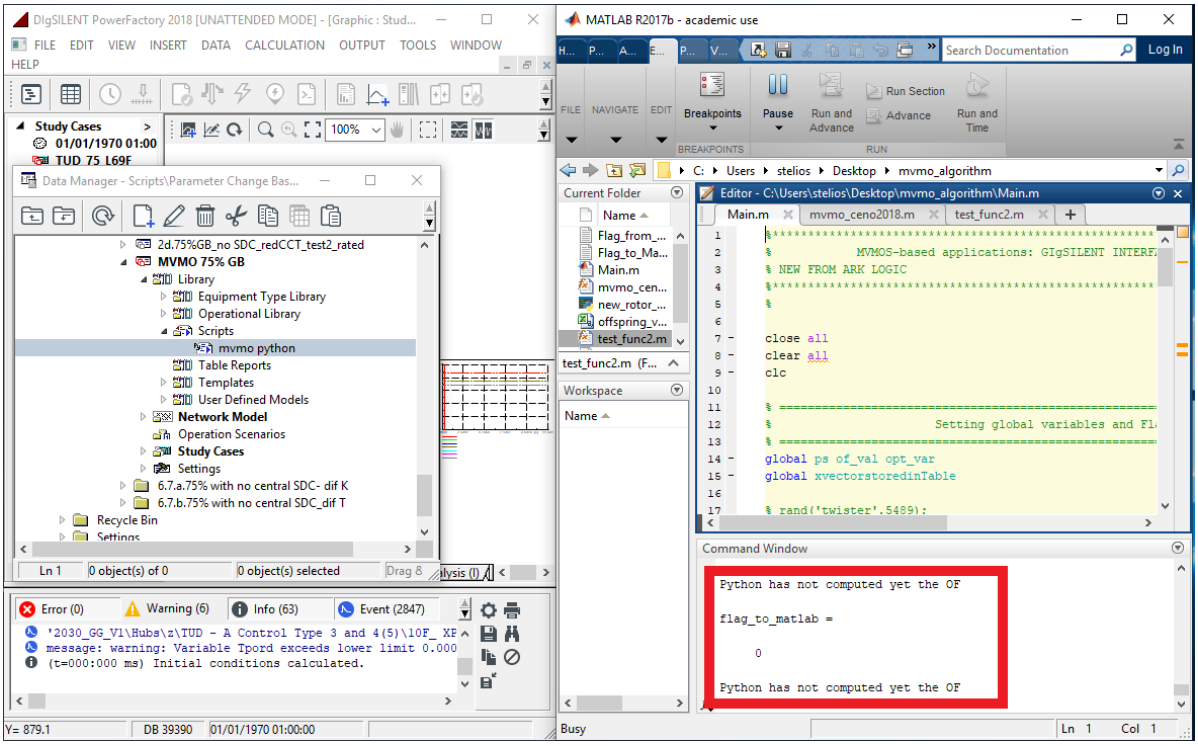

Figure M.3: Matlab in idle mode, waiting for OF value from PowerFactory, which in parallel is performing the RMS simulations

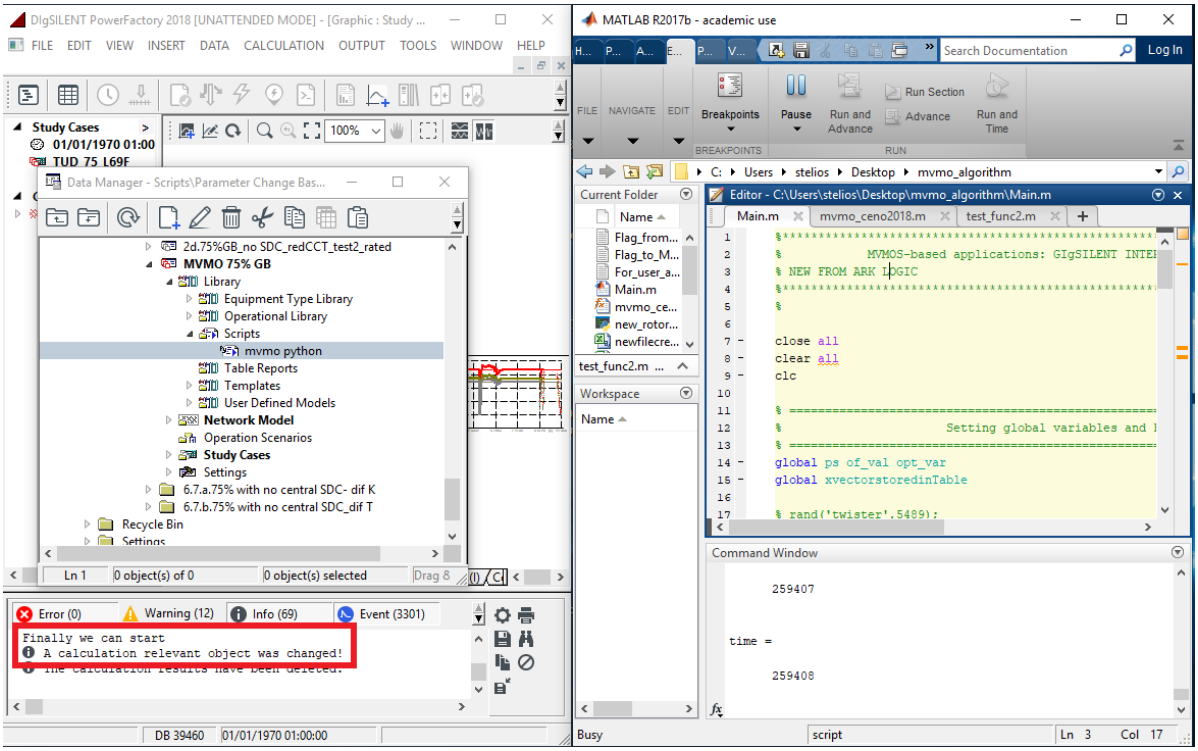

Figure M.4: Matlab MVMO, received the OF value & returned the new offspring. PowerFactory has updated the new variable values & is ready for the new iteration

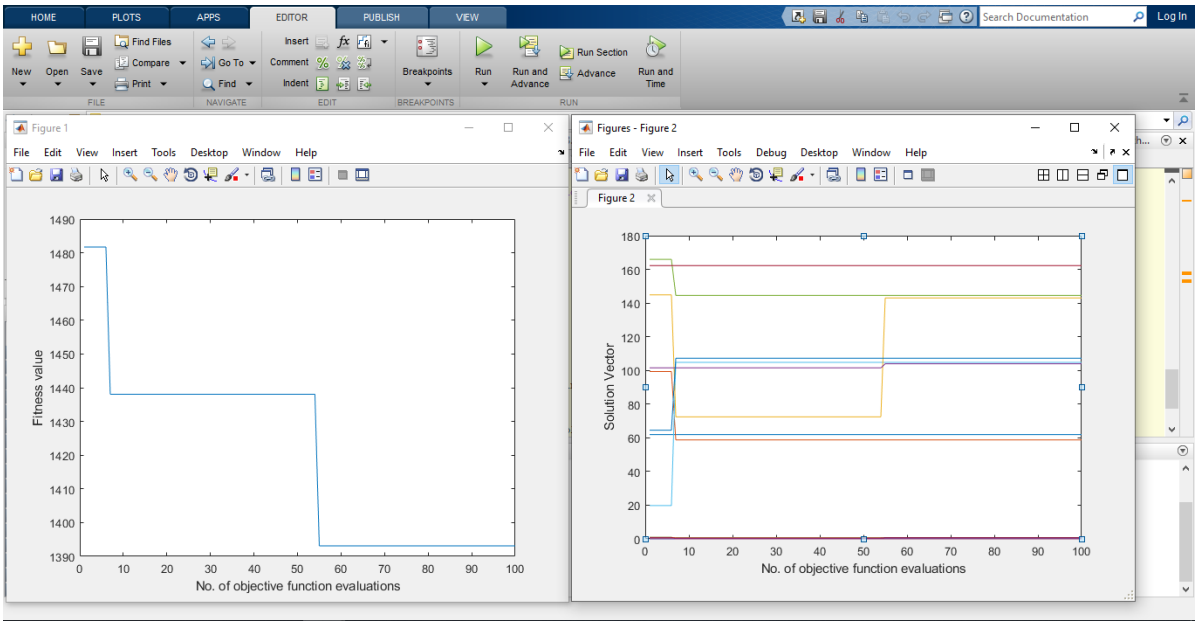

Figure M.5: When MVMO is executed, in Matlab the user can see the fitness evaluations and the optimal parameters over iterations. The user should then update manually the parameters in PowerFactory controllers with the last iterations' optimal variables as indicated

M.3.2. Files' elaboration created during MVMO execution

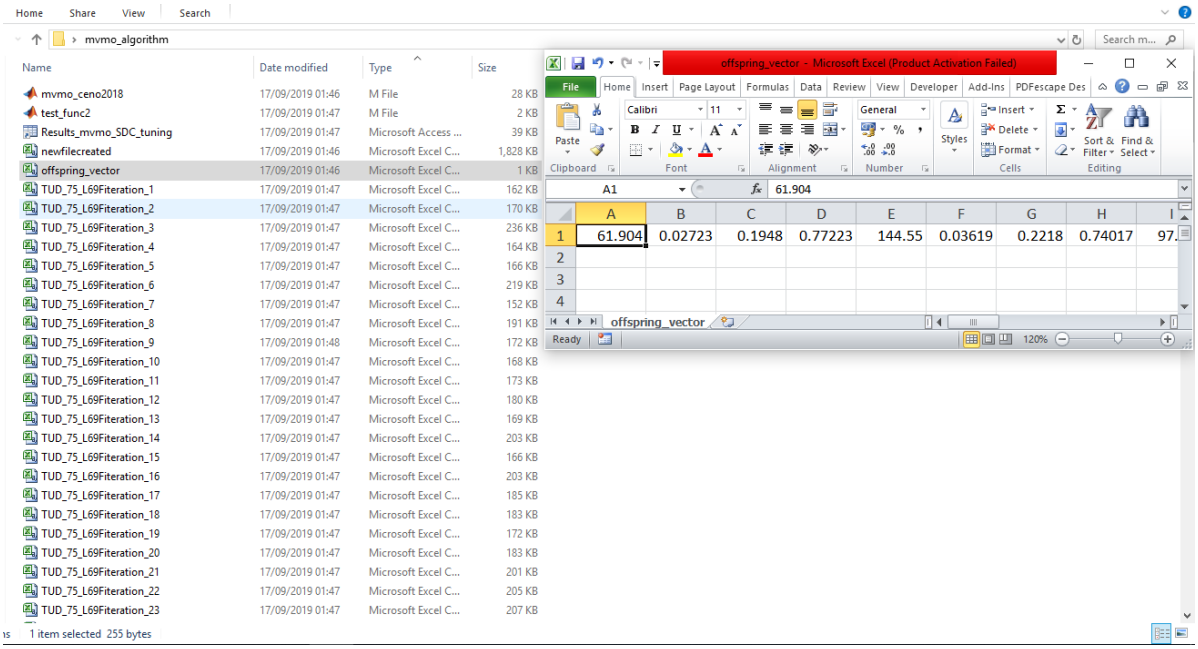

Figure M.6: "offspring_vector":.csv file that Matlab creates dynamically and Python reads in every iteration. At the end of each MVMO iteration Matlab writes the gains and time constants of washout filters and lead-lag compensators

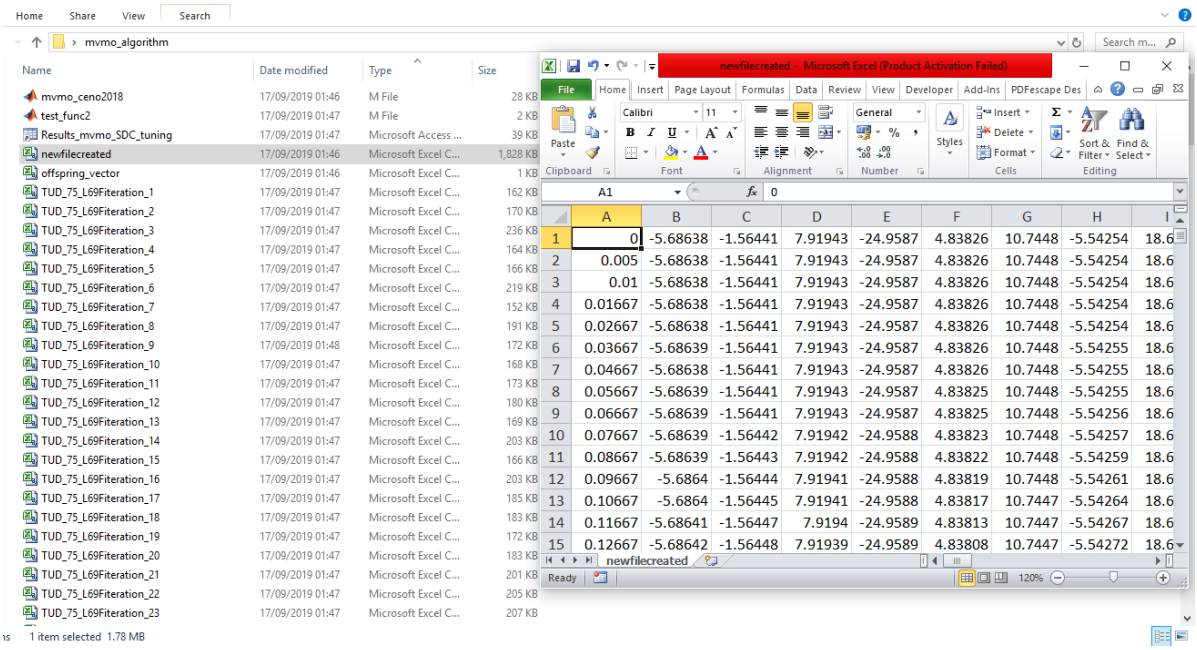

Figure M.7: "newfilecreated":.csv file that Python creates as described with the aid of the function in Section M.1.2. The first column is the time duration of the simulations performed and the rest columns are the 55 angles of the SGs pairs created.

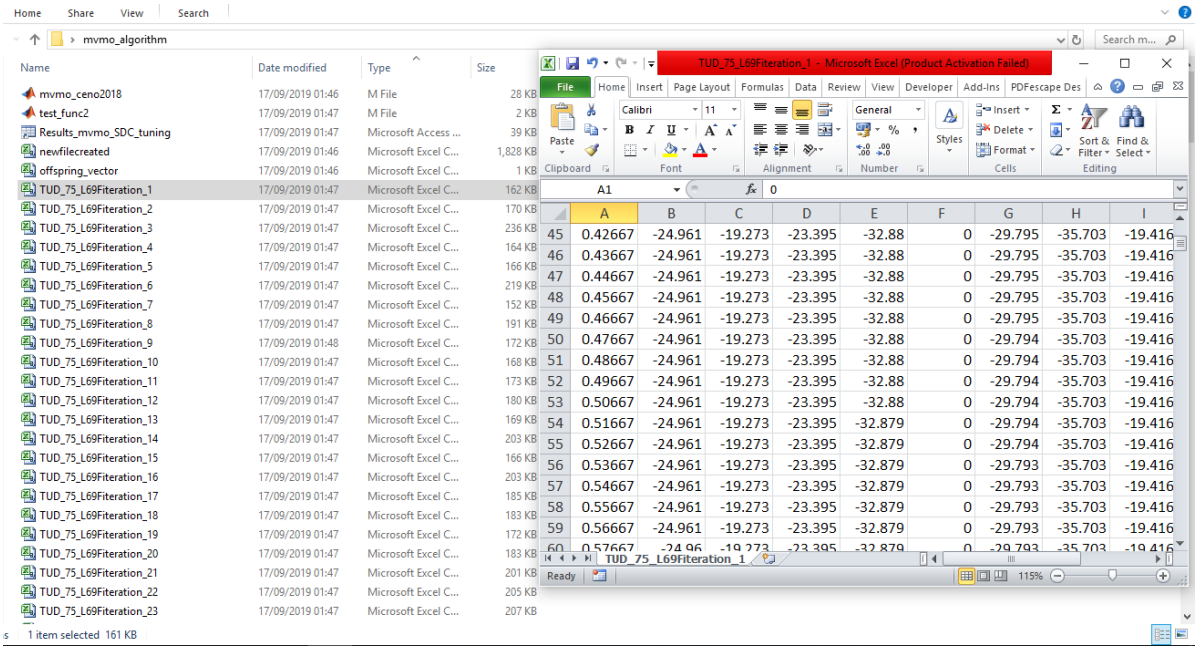

Figure M.8: "*TUD_75_L69Fiteration_1*":.csv file that Python uses as input in the function described in Section M.1.2. The first column is the time duration of the simulations performed and the rest columns are the 11 angles of the SGs machines w.r.t the slack machine SG11.

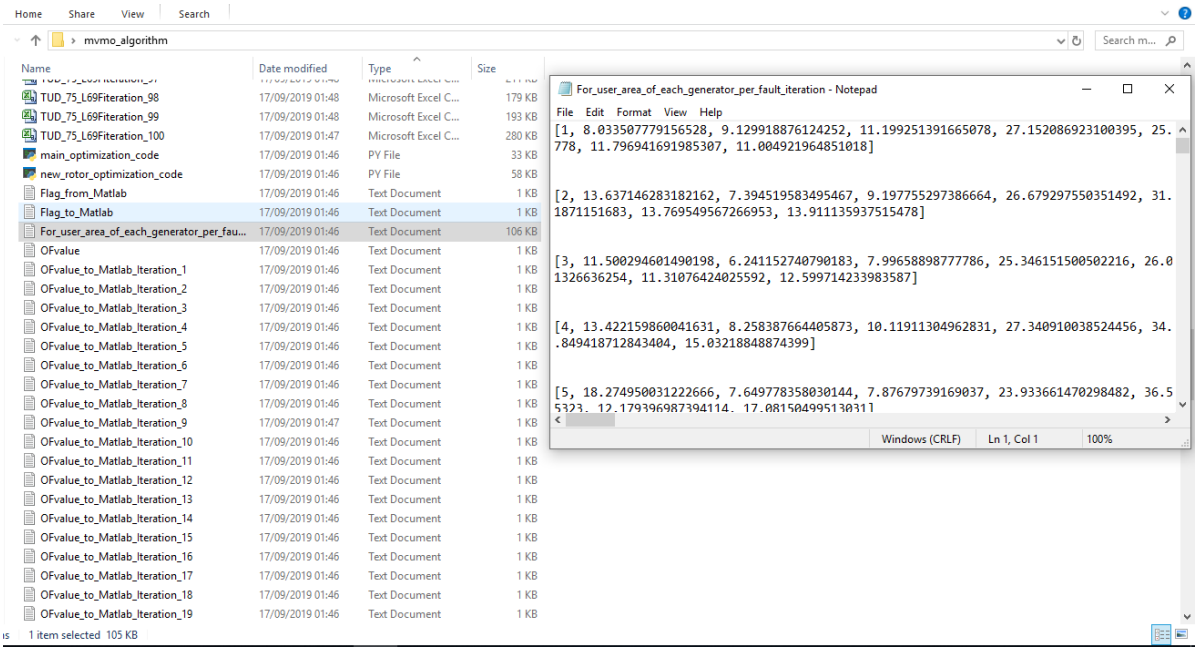

Figure M.9: "*For_user_area_of_each_generator_per_fault_iteration*:.txt file that has per MVMO iteration the areas formed between each one of the 55 SGs formed.

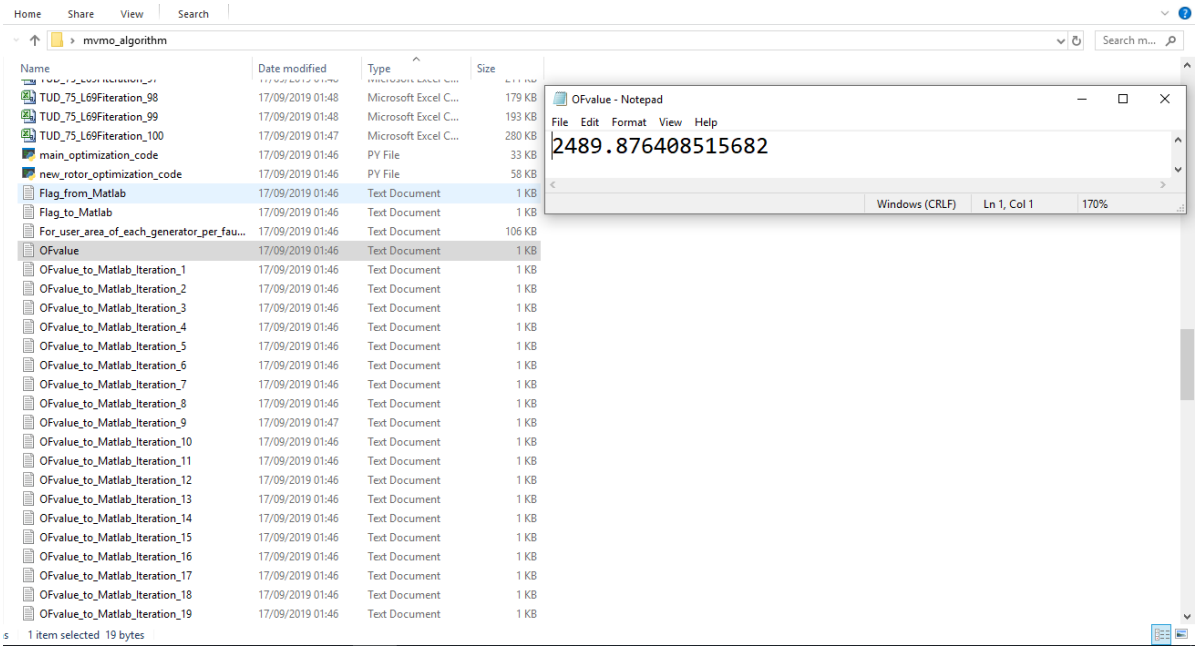

Figure M.10: "OFvalue":.txt file that Python writes in each MVMO iteration and Matlab MVMO reads, in order to compute the new solution vector

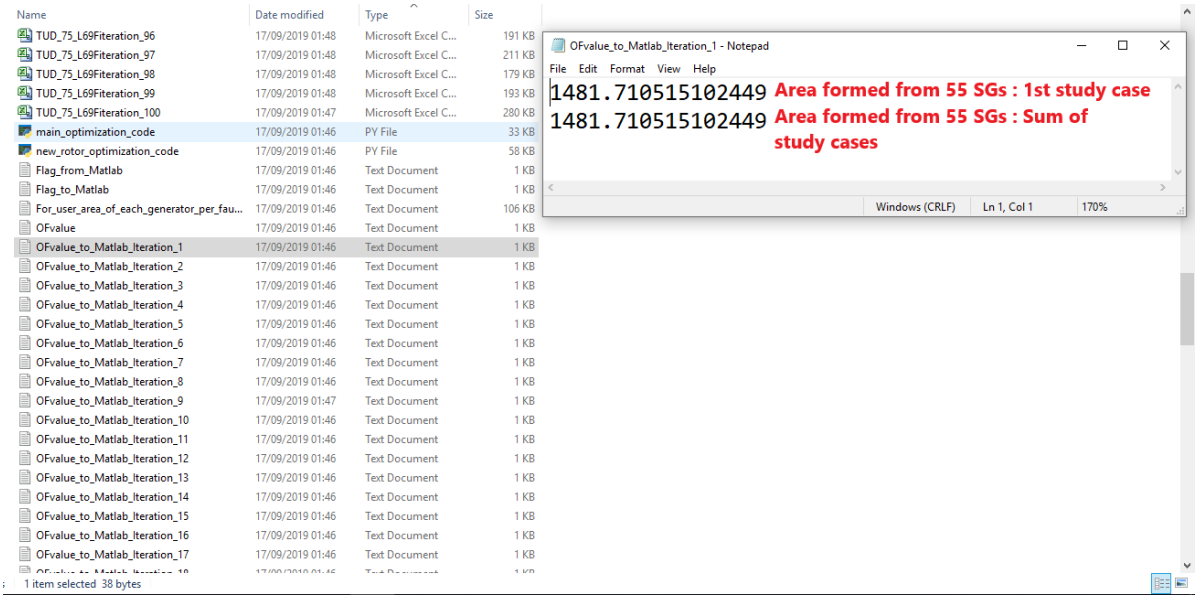

Figure M.11: "*OFvalue_to_Matlab_Iteration_1*":.txt file that has the area of the total 55 SGs pairs formed. Each line represents area computed under a different fault. The last line is the total objective function value which is the summation of the areas of all the faults created. In the examined case, only one Fault is performed; the fault at Line 6-9

M.3.3. Updating the MVMO ”best” parameters in the PowerFactory model

After executing the MVMO algorithm in Matlab, the user has to take the optimal parameters and update the washout filter model parameters. In order to avoid the tedious task of manually updating 32 parameters in the system, Python Scripting can be used so as to facilitate the parameters' writing in PowerFactory. Figures M.12 - M.15 , illustrate the *"opt_var"* table which is stored in the *"Results_mvmo_SDC_tuning".mat* file.

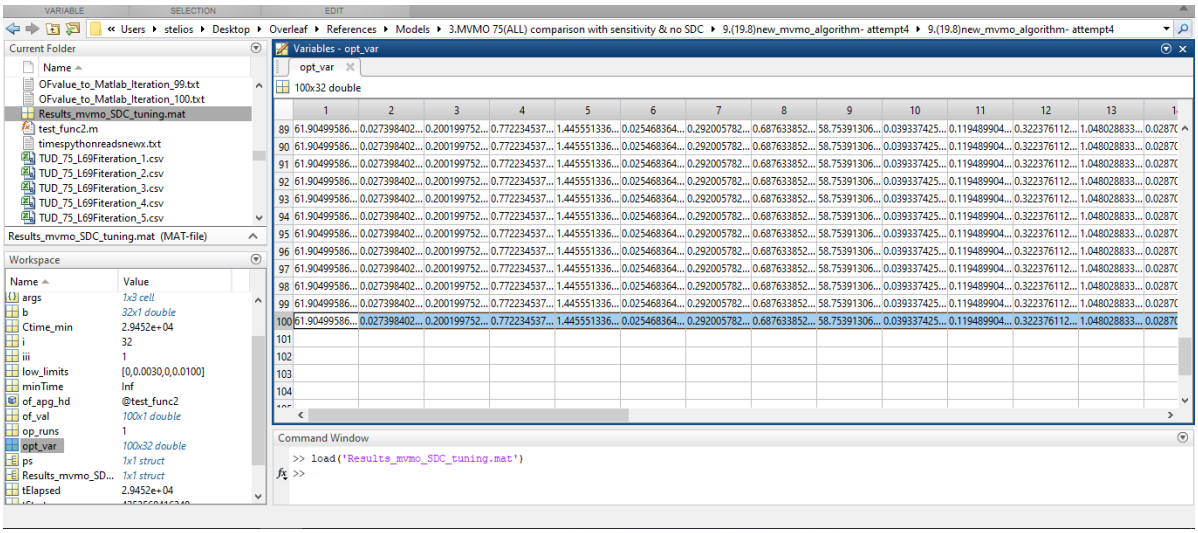

Figure M.12: *"opt_var"* table, the last line of which needs to be accessed by Python. The python file, as desctibed below has to be imported and executed from PowerFactory

```
3 from scipy.io import loadmat
4
5 data=loadmat('Results_mvmo_SDC_tuning.mat') #this is a dictionary
6 table=data['opt_var'] #this is an array
7 d=table.tolist() #this is a list of lists
8 d=d[99] #take the last list
```

Figure M.13: In order to access the data from matlab, a python script is created, in which the module scipy has to be imported. Then the last line, is imported in a list d[]

```
for Element in DSLs_List:

    if Element.loc_name[:27] == '3A_ XP Control Type 3 and 4':
        SpecialCarrier=Element.params
        SpecialCarrier[6]=d[0]
        SpecialCarrier[7]=d[1]
        SpecialCarrier[4]=d[2]
        SpecialCarrier[5]=d[3]
        Element.params=SpecialCarrier


    if Element.loc_name[:27] == '3B_ XP Control Type 3 and 4':

        SpecialCarrier=Element.params
        SpecialCarrier[6]=d[0]
        SpecialCarrier[7]=d[1]
        SpecialCarrier[4]=d[2]
        SpecialCarrier[5]=d[3]
        Element.params=SpecialCarrier
```

Figure M.14: For all the WGs in the system the parameters in d are imported. d[0] is the washout gain, d[1] is the washout time constant, and d[2], d[3] are the numerator and denominator values of the lead-lag compensator which in that case they are zero (defined in Matlab MVMO)

```
for Element in DSLs_List:

        if Element.loc_name[:27] == '3A_ XP Control Type 3 and 4':
            SpecialCarrier=Element.params
            SpecialCarrier[6]=d[0]
            SpecialCarrier[7]=d[1]
            SpecialCarrier[4]=d[2]
            SpecialCarrier[5]=d[2]/d[3]
            Element.params=SpecialCarrier


        if Element.loc_name[:27] == '3B_ XP Control Type 3 and 4':
            SpecialCarrier=Element.params
            SpecialCarrier[6]=d[0]
            SpecialCarrier[7]=d[1]
            SpecialCarrier[4]=d[2]
            SpecialCarrier[5]=d[2]/d[3]
            Element.params=SpecialCarrier
```

Figure M.15: In case lead- lag compensator needs to be taken into consideration, then d[3] coming from the Matlab MVMO represents the factor that the denominator is smaller than the numerator, therefore the value applied in the denominator is the ratio between the lead-lag numerator and this factor

Bibliography

[1] K. Cory, T. Couture, and Claire Kreycik, Feed-in Tariff Policy: Design, Implementation, and RPS Policy Interactions, NREL Technical Report, NREL/TP-6A2-45549, 2009.

[2] Renewables 2016: Global Status Report (GSR) Technical report, 2017.

[3] P. Kundur, Power System Stability and Control, McGraw-Hill Professional, 1st Edition, 1994.

[4] G. Trudel, J. Gingras, and J. Pierre, Designing a Reliable Power System: Hydro- Quebec's Integrated Approach, Proc. of the IEEE,vol. 93, pp. 907-917, 2005.

[5] M. H. Ali, Wind Energy Systems: Solutions for Power Quality and Stabilization, CRC Press, 2012.

[6] P. Kundur et al., Definition and Classification of Power System Stability, IEEE Trans. Power Syst.,vol. 19, no. 3, pp. 1387–1401, 2004.

[7] C. Huang, F. Li, and Z. Jin, Maximum Power Point Tracking Strategy for Large-Scale Wind Generation Systems Considering Wind Turbine Dynamics, IEEE Trans. Ind. Electron.,vol. 62, no. 4, pp. 2530–2539, 2015.

[8] M. Cirrincione, S. Member, M. Pucci, and S. Member, Neural MPPT of Variable-Pitch Wind Generators With Induction Machines in a Wide Wind Speed Range, IEEE Trans. Ind. Appl.,vol. 49, no. 2, pp. 942–953, 2013.

[9] L. Shi, S. Sun, L. Yao, Y. Ni, and M. Bazargan, Effects of wind generation intermittency and volatility on power system transient stability, IET Renew. Power Gener.,vol. 8, no. 5, pp. 509–521, 2014.

[10] L. Lin, H. Zhao, T. Lan, Q. Wang, and J. Zeng, Transient stability mechanism of DFIG wind farm and grid-connected power system, in 2013 IEEE Grenoble Conference,Grenoble, 2013.

[11] S. Liu, G. Li, and M. Zhou, Power System Transient Stability Analysis with Integration of DFIGs Based on Center of Inertia, CSEE J. Power Energy Syst.,vol. 2, no. 2, pp. 20–29, 2016.

[12] S. M. Muyeen, R. Takahashi, and T. Murata, Integration of an Energy Capacitor System With a Variable-Speed Wind Generator, IEEE Trans. Energy Convers., vol. 24, no. 3, pp. 740–749, 2009.

[13] L. Wang, S. Member, and D. Truong, Dynamic Stability Improvement of Four Wind Turbine Generators Fed to a Power System Using a STATCOM, IEEE Trans. Power Deliv., vol. 28, no. 1, pp. 111–119, 2013.

[14] H. Geng and D. Xu, Stability Analysis and Improvements for Variable-Speed Multipole Permanent Magnet Synchronous Generator-Based Wind Energy Conversion System, IEEE Trans. Sustain. Energy,, vol. 2, no. 4, pp. 459–467, 2011.

[15] A. Egea-alvarez, G. S. Member, and S. Fekriasl, Advanced Vector Control for Voltage Source Converters Connected to Weak Grids, IEEE Trans. Power Syst.,vol. 30, no. 6, pp. 3072–3081, 2015.

[16] B. Weise, Impact of K-factor and active current reduction during fault-ride-through of generating units connected via voltage-sourced converters on power system stability, IET Renew. Power Gener., vol. 9, no. 1, pp. 25–36, 2015.

[17] A. E. Leon, G. Revel, D. M. Alonso, and G. E. Alonso, Wind power converters improving the power system stability, IET Gener. Transm. Distrib., vol. 10, no. 7, pp. 1622–1633, 2016.

[18] A. Mohanty, An adaptive fuzzy sliding mode controller for reactive power transient stability management, in 2016 IEEE Region 10 Conference (TENCON), Singapore, pp. 3195–3199, 2016.

[19] V. Yaramasu and B. Wu, Predictive Control of a Three-Level Boost Converter and an NPC Inverter for High-Power PMSG-Based Medium Voltage Wind Energy Conversion Systems, in IEEE Trans. Power Electron., vol. 29, no. 10, pp. 5308–5322, 2014.

[20] M. Q. Duong et al., Improving LVRT Characteristics in Variable-speed Wind Power Generation by means of Fuzzy Logic, in 2014 IEEE International Conference on Fuzzy Systems (FUZZ-IEEE),pp. 332-337, Beijing, 2014.

[21] H. M. Yassin, H. H. Hanafy, and M. M. Hallouda, Enhancement low-voltage ride through capability of permanent magnet synchronous generator-based wind turbines using interval type-2 fuzzy control, IET Renew. Power Gener.,vol. 10, no. 3, pp. 339–348, 2015.

[22] M. A. Soliman, H. M. Hasanien, H. Z. Azazi, E. E. El-kholy, and S. A. Mahmoud, Hybrid ANFIS-GA-based control scheme for performance enhancement of a grid- connected wind generator, IET Renew. Power Gener.,vol. 12, no. 7, pp. 832–843, 2018.

[23] The MIGRATE Project, AN EU-FUNDED PROJECT UNDER THE FRAMEWORK OF EUROPEAN UNION'S HORIZON 2020, [Online] Available: https://www.h2020-migrate.eu, [Accessed: 25- Sep- 2019].

[24] S. M. Muyeen, J. Tamura Stability Augmentation of a Grid-connected Wind Farm, Springer, 2009.

[25] B. Wu, Y. Lang, N. Zargari, S. Kouro, Power Conversion and Control of Wind Energy Systems, WILEY IEEE PRESS, 2011.

[26] H. A. L. Carballido, Control of a wind turbine equipped with a variable rotor resistance, Master's thesis, Chalmers University of Technology, Goteborg, Sweden, 2009.

[27] R Nalawade. P. Joshi, Study of circulating current phenomena in multiple parallel inverters operating in microgrid, in International Journal Of Electrical, Electronics And Data Communication, Vol. 3, no. 11, 2015.

[28] ENTSO-E. Network code for requirements for grid connection applicable to all generators (NG RFG). Technical report, March 2013.

[29] M. Ndreko. Offshore wind power plants with VSC-HVDC transmission: Grid code compliance optimization and the effect on high voltage ac transmission system. PhD thesis, Delft University of Technology, 2017.

[30] Shewarega. F., Erlich I., Rueda J.L., Impact of large offshore wind farms on power system transient stability, Power Systems Conference and Exposition, PSCE '09. IEEE/PES , pp. 1-8. doi: 10.1109/PSCE.2009.4840006.

[31] L. Meegahapola and D. Flynn, Impact on transient and frequency stability for a power system at very high wind penetration, in Proc. IEEE Power Eng. Soc. Gen. Meeting, pp. 1-8, 2010.

[32] J. Basler, C. Schaefer, Understanding Power-System Stability, in Proc. IEEE Trans. on Industry Applications,vol. 44, no. 2, 2008.

[33] A. Abdelaziz1, A. Ibrahim , G. Hasan Transient stability analysis with equal-area criterion for out of step detection using phasor measurement units, in International Journal of Engineering, Science and Technology ,Vol. 5, No. 1, pp. 1-17,2013.

[34] D. Aguilar et. al , Simulation of Wound Rotor Synchronous Machine under Voltage Sags, in IEEE International Symposium on Industrial Electronics ,Bari, pp. 2626-2631, 2010.

[35] P. Kumar, D. Fredrickson,K. Chanda, Stability Studies For System Dependent Generator Protection Functions , in 57th IEEE Pulp and Paper Industry Conference , Nashville, 2011.

[36] S. Paudyal,G.Ramakrishna, M. Sachdev, Application of Equal Area Criterion Conditions in the Time Domain for Out-of-Step Protection, in IEEE Transactions On Power Delivery, vol. 25, no. 2, 2010.

[37] Mitsubishi, Electric Power System Stabilizer (PSS), Technical report, 2010.

[38] F. Dib et al., Sliding mode control without reaching phase for multimachine power system combined with fuzzy PID based on PSS, in WSEAS Transactions on Systems and Control, vol. 10, pp 206-214, 2015.

[39] Deliverable D1.2 Power System Analysis and Key Performance Indicators, Technical Report, MIGRATE - Massive InteGRATion of power Electronic devices, Grant Agreement Number: 691800, 31.01.2018.

[40] Ullah, N. R. and T. Thiringer Effect of Operational Modes of a Wind Farm on the Transient Stability of Nearby Generators and on Power Oscillations: A Nordic Grid Study, Research Article, Wind Energy 11, pp 63-73, 2018.

[41] J. Clemens et. al. Design of a wind turbine pitch angle controller for power system stabilisation, Research Article, Renewable Energy. 32, pp 2334-2349, 2007.

[42] D. Garcıa JL et. al.. Power system stabilizer control for wind power to enhance power system stability stabilisation, in Proceedings of 5th international scientific conference on physics and control, pp 1-6, 2011.

[43] G. Tsourakis, S. Nanou, and C. Vournas, A power system stabilizer for variable-speed wind generators, IFAC Proc. Vol., vol. 44, no. 1, pp. 11713–11719, 2011.

[44] Tsourakis and C. Vournas, A controller for wind generators to increase damping of power oscillations, in Proceedings of 2010 IEEE International Symposium on Circuits and Systems, pp. 2195-2198, 2010.

[45] Z. Miao, L. Fan, D. Osborn ans S. Yuvarajan, Control of DFIG based wind generation to improve inter-area oscillations damping, in IEEE transactions on energy conversion, vol. 24, no. 2, 2009

[46] H. Geng, D. Xu, B. Wu and G. Yang, Comparison of oscillation damping capability in three power control strategies for PMSG-based WECS, in Wind Energ. 2011, vol. 14, No. 3,pp.389- 406., 2011

[47] T. Smed, G. Andersson Utilising HVDC to Damp Power Oscillations, in IEEE Transactions on Power Delivery, Vol. 8, No. 2, 1993

[48] RTDS Technologies Inc., The simulator-Hardware, [Online] Available: https://www.rtds.com/the-simulator/our-hardware/, [Accessed: 26- Aug- 2019].

[49] RTDS Technologies Inc., RSCAD modules, [Online] Available: https://www.rtds.com/the-simulator/our-software/rscad-modules/, [Accessed: 26- Aug- 2019].

[50] M. Ndreko. Type-3 and Type-4 Wind Turbine Models in RSCAD for Real Time Power System Stability Studies. Technical Report of MIGRATE – Massive InteGRATion of power Electronic devices,Tennet TSO GmbH, 2018.

[51] F. Shewarega, I. Erlich, and J. L. Rueda, Impact of large offshore wind farms on power system transient stability, in 2009 IEEE/PES Power Systems Conference and Exposition, Seattle, WA, pp. 1–8, 2009.

[52] Mohan N, Undeland TM, Robbins WP, Power Electronics: Converters, Applications, and Design, 3rd ed. John Wiley Sons, 2002.

[53] C. Martinez, G. Joos, and B. T. Ooi, Power system stabilizers in variable speed wind farms, in 2009 IEEE Power Energy Society General Meeting, Calgary, AB, pp. 1–7, 2009

[54] T. Knüppel, J. N. Nielsen, K. H. Jensen, A. Dixon, and J. Østergaard, Power oscillation damping capabilities of wind power plant with full converter wind turbines considering its distributed and modular characteristics, in IET Renew. Power Gener., vol. 7, no. 5, pp. 431–442, 2013.

[55] I. Erlich et al. New Control of Wind Turbines Ensuring Stable and Secure Operation Following Islanding of Wind Farms, in IEEE Transactions on Energy Conversion, vol. 32, no. 3, pp. 1263-1271, 2017.

[56] K. Clark, N. Miller, and J. Sanchez- Gasca, Modeling of GE wind turbine-generators for grid studies, in GE Energy, no. 4, pp. 13-17, 2010.

[57] M. J. Gibbard, P. Pourbeik, and D. J. Vowels, Small-signal stability, control and dynamic performance of power systems, Adelaide: University of Adelaide Press, 2015.

[58] D. E. Echeverría, J. L. Rueda, J. C. Cepeda, D. G. Colomé, and I. Erlich, Comprehensive approach for prediction and assessment of power system transient stability in real-time, in IEEE PES ISGT Europe 2013, Lyngby, pp. 1–5, 2013.

[59] A. Karaolanis, A. Perilla Guerra, J. L. Rueda Torres, M. A. A. M. van der Meijden, and A. Alefragkis, Generic model of a VSC-based HVDC link for RMS simulations in PSS/E, in IFAC-PapersOnLine, vol. 51, no. 28, pp. 303–308, 2018.

[60] Shih-Yu Yang, Yuan-Kang Wu, Huei-Jeng Lin, The direct torque control of the PMSG based wind turbine with two level voltage source converter, in Automatic Control Conference (CACS) 2014 CACS International, pp. 39-44, 2014.

[61] N. Fazli, and J. Siahbalaee, Direct torque control of a wind energy conversion system with permanent magnet synchronous generator and matrix converter, in Proc.2017 8th Power Electronics, Drive Systems & Technologies Conference (PEDSTC), 2017.

[62] N.Maleki, M. Pahlavani, I. Soltani, A Detailed Comparison Between FOC and DTC Methods of a Permanent Magnet Synchronous Motor Drive in The Open Electrical Electronic Engineering Journal, Vol. 3, No. 2-1, 2015.

[63] M. Chinchilla, S. Arnaltes, J.C. Burgos, Control of Permanent−Magnet Generators Applied to Variable−SpeedWind−Energy Systems Connected to the Grid in IEEE Transactions on Energy Conversion , Vol. 21, No.1, pp. 130−135, 2006.

[64] N.P.W. Strachan, D. Jovcic, Stability of a Variable−Speed Permanent Magnet Wind Generator With Weak AC Grids, in IEEE TPD , vol.25, no.4, pp. 2779−2788, 2010.

[65] L. Zeni et al., Power oscillation damping from VSC-HVDC connected offshore wind power plants, in IEEE Transactions on Energy Conversion ,IEEE Trans. Power Deliv., vol. 31, no. 2, pp. 829–838, 2016.

[66] A. Adamczyk, R. Teodorescu, and P. Rodriguez, Control of full-scale converter based wind power plants for damping of low frequency system oscillations, in 2011 IEEE Trondheim PowerTech ,pp. 1–7,Trondheim, 2011.

[67] Energynautics, MIGRATE Project, Type-3 and Type-4 EMT – Model Documentation, Tecnical Report,Darmstadt, Germany, 2017.

[68] IEC 61400-27-1, Wind turbines – Part 27-1: Electrical simulation models – Wind turbines, Technical Report,IEC, Edition 1, 2015.

[69] N. T. Anh, L. Vanfretti, J. Driesen, and D. Van Hertem, A Quantitative Method to Determine ICT Delay Requirements for Wide-Area Power System Damping Controllers, in IEEE Trans. Power Syst., vol. 30, no. 4, pp. 2023–2030, 2015.

[70] A. Heniche and I. Kamwa, Assessment of two methods to select wide-area signals for power system damping control, in IEEE Trans. Power Syst.,vol. 23, no. 2, pp. 572–581, 2008.

[71] C. A. Juárez, J. L. Rueda, I. Erlich, and D. G. Colomé, Probabilistic approach-based wide-area damping controller for small-signal stability enhancement of wind-thermal power systems, in 2011 IEEE Power and Energy Society General Meeting,San Diego, CA, pp. 1–4, 2011.

[72] Q. Yang, T. Bi, and J. Wu, WAMS implementation in China and the challenges for bulk power system protection, in 2007 IEEE Power Engineering Society General Meeting,Tampa, FL, pp. 1–6, 2007.

[73] Center for Intelligent Systems Networks, Dynamic IEEE Test Systems, [Online] Available: [Accessed: 03- Sep- 2019].

[74] F. Sanchez, J. Cayenne, F. Gonzalez-Longatt, and J. L. Rueda, Controller to enable the enhanced frequency response services from a multi-electrical energy storage system, in IET Gener. Transm. Distrib., vol. 13, no. 2, pp. 258–265, 2018.

[75] P. Dattaray, D. Chakravorty, J. Bos, C. Mishra, and A. Rampokanyo, M Atallah, FFR from Offshore Wind Farms connected through HVDC links: Control Philosophies and Challenges, in CIGRE Symposium Aalborg, Denmark 2019.

[76] A. Nikolopoulou, Wind Turbine Contribution to Ancillary Services under Increased Renewable Penetration levels, MSc thesis dissertation, Delft University of Technology, 2018.

[77] ENTSO-E, Frequency ranges ENTSO-E guidance document for national implementation for network codes on grid connection, Technical report, Brussels, 2018.

[78] T. Knüppel, J. N. Nielsen, K. H. Jensen, A. Dixon, and J. Ostergaard, Small-signal stability of wind power system with full-load converter interfaced wind turbines, in IET Renew. Power Gener., vol. 6, no. 2, p. 79, 2012.

[79] X. Feng, S. Yuanzhang, and Y. Fang, Inter-area damping controller design based on mode controllability and observability, in 2007 International Power Enginnering Conference (IPEC 2007), 2007.

[80] K. Elkington, The Dynamic Impact of Large Wind Farms on Power System Stability, Doctoral Thesis,KTH Royal Institute of Technology, 2012.

[81] V. G. Rau, Power Systems Dynamics, New Academic Science, 2011.

[82] J. L. Dominguez-Garcia, O. Gomis-Bellmunt, F. D. Bianchi, and A. Sumper, Power system stabilizer control for wind power to enhance power system stability, in 5th International Scientific Conference on Physics and Control (Physcon 2011), 2011.

[83] Y. Chompoobutrgool and L. Vanfretti, Analysis of time delay effects for wide-area damping control design using dominant path signals, in 2014 IEEE PES General Meeting Conference Exposition,pp. 1–5, 2014.

[84] C. A. Juárez, J. L. Rueda, I. Erlich, and D. G. Colomé, Probabilistic approach-based wide-area damping controller for small-signal stability enhancement of wind-thermal power systems, in 2011 IEEE Power and Energy Society General Meeting, San Diego, CA, pp. 1–4, 2011.

[85] J. L. Rueda and F. Gonzalez-Longatt, Dynamic Vulnerability assessment and intelligent control: For Sustainable Power Systems, Wiley-IEEE Press, 2018.

[86] Intelligent Energy Europe - Wind Energy the FACTS, [Online] Available: https://www.wind-energy-the-facts.org/the-cost-of-energy-generated-by-wind-power.html, [Accessed: 09- Sep- 2019].

[87] I. Erlich, A. Korai et al., New Control of Wind Turbines Ensuring Stable and Secure Operation Following Islanding of Wind Farms, in IEEE Transactions on Energy Conversion,vol. 32, no. 3, pp. 1263-1271, Sept. 2017.

[88] I. Erlich, A. Korai, Description, Modelling and Simulation of a Benchmark System for Converter Dominated Grdis (Part I) Technical report, 2018.

[89] F. Wu, X. P. Zhang, K. Godfrey and P. Ju, Small signal stability analysis and optimal control of a wind turbine with doubly fed induction generator, in IET Generation, Transmission Distribution, vol.1, no.5, pp. 751-760, 2007.

[90] A. Mendonca and J. A. P. Lopes, Simultaneous Tuning of Power System Stabilizers Installed in DFIG-Based Wind Generation, in IEEE Lausanne Power Tech, pp. 219-224, Lausanne, 2007.

[91] D. Simon, Evolutionary optimization algorithms: biiologically inspired and population - based approaches to computer intelligence, Wiley, 2013.

[92] E. Talbi, Metaheuristics: from design to implementation Wiley, 2009.

[93] J. L. Rueda and I. Erlich, Hybrid Single Parent-Offspring MVMO for Solving CEC2018 Computationally Expensive Problems, in 2018 IEEE Congress on Evolutionary Computation (CEC), pp. 1-8, 2018.

[94] I. Erlich, G. K. Venayagamoorthy and N. Worawat, A Mean-Variance Optimization algorithm, in IEEE Congress on Evolutionary Computation, pp. 1-6, 2010.

[95] I. Kamwa, R. Grondin, and G. Trudel, IEEE PSS2B versus PSS4B: The limits of performance of modern power system stabilizers, in IEEE Transactions on Power Systems, vol. 20, no. 2, pp. 903–915, 2005.

[96] J. L. Rueda, J. C. Cepeda and I. Erlich, Probabilistic approach for optimal placement and tuning of power system supplementary damping controllers, in IET Generation, Transmission Distribution, vol. 8, no. 11, pp. 1831-1842, 2014.